

Modelling of Ship-Bank Interaction and Ship Squat for Ship-Handling Simulation

by


Jonathan Duffy, B.Eng. (Hons)

Submitted in fulfilment of the
requirements for the degree of
Doctor of Philosophy

University of Tasmania
September 2008

Signed Statement


This thesis contains no material which has been accepted for a degree or diploma by the University or any other institution, except by way of background information and duly acknowledged in the thesis, and to the best of my knowledge and belief no material previously published or written by another person except where due acknowledgement is made in the text of the thesis, nor does the thesis contain any material that infringes copyright.

.....

Jonathan Duffy
September 2008

Authority of Access

This thesis may be made available for loan and limited copying in accordance with the Copyright Act 1968.

A handwritten signature in black ink, appearing to read 'J. Duffy', is written over a horizontal dotted line.

Jonathan Duffy
September 2008

Abstract

This thesis reports on an investigation into the simulation of ship manoeuvring in restricted waters; in particular ship squat and ship-bank interaction.

A time-domain mathematical model has been developed to predict unsteady squat and dynamic acceleration effects for a vessel travelling in non-uniform water depth. A quasi-steady approach was adopted, where the prediction at each time step is based on steady-state heave force and pitch moment in uniform water depth. A comprehensive set of model scale experiments was conducted to investigate squat in both uniform and non-uniform water depth. Regression analysis was performed on the uniform water depth test data to develop empirical equations for steady-state squat, which were used as input to the mathematical model. The equations apply to a full form vessel and are dependent on under keel clearance parameters, channel width parameters and depth Froude number. Empirical correction factors were also developed to estimate the effect of propulsion on squat.

Good correlation was observed between predictions from the squat mathematical model and steady-state sinkage measurements for a wide range of water depth to draught ratios. Predictions from the mathematical model were also compared with unsteady sinkage measurements on a ship model travelling over a simplified ramp bank. The general trend of the predicted unsteady sinkage was reasonable, improving the realism of simulation for abrupt changes in water depth compared to predictions where acceleration effects in the vertical plane are neglected. However, the maximum unsteady sinkage was not always predicted accurately, which may be attributable to limitations and assumptions associated with the technique.

A comprehensive model scale experiment program was conducted to investigate ship-bank interaction. The following parameters were systematically varied for three different hull forms: flooded bank height, water depth, bank slope, lateral ship to bank distance, vessel speed and vessel draught. The results from these experiments were used to develop a bank parameter to estimate the effects of lateral surface piercing and flooded banks. This parameter was utilised in regression analyses to develop empirical formulae for steady-state bank induced sway force and yaw moment.

The empirical formulae were validated against independent model scale measurements from literature and showed reasonable agreement for a range of cases. The formulae were then incorporated into the existing mathematical model of the AMC ship-handling simulator. The quasi-steady technique was used to predict the path of a vessel for a real-life manoeuvre where bank induced yaw moment is used to aid a turn. The proposed bank effect simulation method was found to provide a satisfactory solution to the problem of ship-bank interaction simulation.

Acknowledgements

My supervisors, Dr Giles Thomas and Professor Martin Renilson, have provided a wealth of information concerning the project, along with valuable guidance and support. I would like to thank them for their enthusiasm and for always making time to answer my questions.

During the course of this work I conducted model scale experiments using the towing tank facility at the Australian Maritime College. Many thanks to towing tank staff who provided valuable assistance during the conduct of the experiments. Thanks particularly to Gregor Macfarlane and Richard Young.

Throughout this project I have worked with a number of staff and students from the Department of Maritime Engineering at the Australian Maritime College and the Department of Applied Mathematics at the University of Adelaide. In particular, I would like to thank Professor Ernie Tuck and Dr Tim Gourlay for their valuable assistance and fruitful discussions and to Roger Duffield and Gillian Carter for their assistance with model scale experiments.

I wish to thank the Australian Research Council and STN Atlas for partly funding this project.

Sincere thanks to my family and close friends for their support and encouragement during the project.

Table of Contents

| | |
|--|-------------|
| Signed Statement..... | ii |
| Authority of Access | iii |
| Abstract..... | iv |
| Acknowledgements | v |
| Table of Contents | vi |
| List of Figures..... | xi |
| List of Tables | xvii |
| Nomenclature | xix |
| Co-ordinate System..... | xxiv |
| 1 Introduction..... | 1 |
| 1.1 Background | 1 |
| 1.2 Objectives..... | 2 |
| 1.3 Methodology | 3 |
| 1.4 Overview of thesis structure | 4 |
| 2 Squat and Ship-Bank Interaction Prediction Techniques | 5 |
| 2.1 Introduction..... | 5 |
| 2.2 Background | 5 |
| 2.2.1 Steady-state prediction | 5 |
| Squat..... | 5 |
| Ship-bank interaction | 8 |
| 2.2.2 Unsteady prediction..... | 9 |
| Squat..... | 9 |
| Ship-bank interaction | 10 |
| 2.2.3 Review of prediction techniques | 11 |

| | | |
|----------|---|-----------|
| 2.3 | Steady-state prediction | 12 |
| 2.3.1 | Regression analysis: squat and ship-bank interaction..... | 12 |
| | Statistical terminology..... | 12 |
| | Multiple linear regression analysis | 13 |
| | Non-linear regression analysis | 14 |
| 2.3.2 | Three-dimensional panel method | 14 |
| | Squat and ship-bank interaction | 14 |
| 2.4 | Unsteady prediction | 20 |
| 2.4.1 | Squat..... | 20 |
| 2.4.2 | Ship-bank interaction | 22 |
| 3 | Squat Experiments..... | 24 |
| 3.1 | Introduction..... | 24 |
| 3.2 | Ship models..... | 24 |
| 3.3 | Bank models..... | 25 |
| 3.4 | Test rigs..... | 26 |
| 3.4.1 | Test rig to measure sinkage, trim and surge force..... | 26 |
| 3.4.2 | Test rigs to measure forces and moments | 27 |
| 3.5 | Instrumentation | 28 |
| 3.6 | Test procedure and data acquisition..... | 29 |
| 3.7 | Effect of model scale on squat measurements | 29 |
| 3.7.1 | Introduction | 29 |
| 3.7.2 | Test program..... | 30 |
| 3.7.3 | Results and discussion..... | 30 |
| 3.8 | Effect of channel dimensions and vessel draught on squat..... | 35 |
| 3.8.1 | Introduction | 35 |
| 3.8.2 | Test program..... | 36 |
| 3.8.3 | Results and discussion..... | 36 |
| 3.9 | Effect of propulsion on squat..... | 44 |
| 3.9.1 | Introduction | 44 |
| 3.9.2 | Test method for propulsion tests | 45 |
| 3.9.3 | Test program..... | 45 |
| 3.9.4 | Results and discussion..... | 46 |

| | | |
|----------|---|-----------|
| 3.10 | Unsteady squat | 53 |
| 3.10.1 | Introduction | 53 |
| 3.10.2 | Test program..... | 54 |
| 3.10.3 | Results and discussion..... | 54 |
| 3.11 | Assessment of three-dimensional panel method | 61 |
| 3.12 | Concluding remarks..... | 63 |
| 4 | Modelling of Unsteady Squat for Ship-Handling Simulation..... | 64 |
| 4.1 | Introduction..... | 64 |
| 4.2 | Prediction of steady-state heave force and pitch moment for an unpropelled hull | 64 |
| 4.2.1 | Regression parameters..... | 64 |
| | Vessel speed parameter | 64 |
| | Under keel clearance parameter | 65 |
| | Channel width parameter | 66 |
| 4.2.2 | Empirical formulae for heave force and pitch moment on an unpropelled hull | 68 |
| 4.3 | Prediction of steady-state heave force and pitch moment due to propulsion..... | 69 |
| 4.3.1 | Regression parameters..... | 69 |
| | Vessel speed parameter | 70 |
| | Effective thrust parameter | 70 |
| | Under keel clearance parameter | 70 |
| 4.3.2 | Empirical formulae for heave force and pitch moment correction due to propulsion..... | 71 |
| 4.4 | Prediction of unsteady squat | 74 |
| 4.5 | Concluding remarks | 84 |
| 5 | Ship-Bank Interaction Experiments | 85 |
| 5.1 | Introduction..... | 85 |
| 5.2 | Ship models..... | 86 |
| 5.3 | Bank models..... | 87 |
| 5.4 | Test rig | 87 |
| 5.5 | Instrumentation | 88 |
| 5.6 | Test procedure and data acquisition..... | 88 |
| 5.7 | Test program | 88 |
| 5.8 | Results and discussion | 89 |

| | | |
|----------|--|------------|
| 5.8.1 | General | 89 |
| 5.8.2 | Depth Froude number..... | 90 |
| 5.8.3 | Draught to under keel clearance ratio | 95 |
| 5.8.4 | Ship to bank distance..... | 97 |
| 5.8.5 | Bank flooding | 100 |
| 5.8.6 | Bank slope | 103 |
| 5.8.7 | Hull form | 106 |
| 5.8.8 | Discussion | 110 |
| 5.9 | Assessment of three-dimensional panel method..... | 111 |
| 5.10 | Concluding remarks | 114 |
| 6 | Modelling of Ship-Bank Interaction for Ship-Handling Simulation | 116 |
| 6.1 | Introduction | 116 |
| 6.2 | Prediction of bank induced sway force and yaw moment..... | 116 |
| 6.2.1 | Regression parameters..... | 116 |
| | Vessel speed parameter | 116 |
| | Under keel clearance parameter | 117 |
| | Ship to bank distance parameter..... | 119 |
| | Bank slope parameter | 123 |
| | Bank parameter..... | 129 |
| | Hull form parameter | 136 |
| 6.2.2 | Regression formulae for bank induced sway force and yaw moment..... | 138 |
| 6.3 | Validation of prediction technique | 142 |
| 6.3.1 | Comparison with experimental data - sway force and yaw moment..... | 142 |
| 6.3.2 | Comparison with known real-life manoeuvre - sway and yaw motion..... | 146 |
| 7 | Concluding Remarks and Recommendations | 149 |
| 7.1 | Concluding remarks | 149 |
| 7.2 | Recommendations for future research | 151 |
| | References | 153 |
| | Appendix A | 161 |
| | Australian Maritime College towing tank details..... | 161 |

| | |
|---|------------|
| Appendix B | 162 |
| Ship model details..... | 162 |
| Appendix C | 164 |
| Model bank details..... | 164 |
| Appendix D | 167 |
| Uncertainty analysis..... | 167 |
| Measurement of vertical displacement | 167 |
| Measurement of sway force and yaw moment | 169 |
| Appendix E | 173 |
| Comparison between sway force and yaw moment measurements from the present study and Ch'ng (1991)..... | 173 |

List of Figures

| | |
|---|------|
| Figure 0.1 Co-ordinate system | xxiv |
| Figure 2.1 Shipflow co-ordinate system, Larsson <i>et al.</i> (1989) | 19 |
| Figure 2.2 Flow zones used in Shipflow, Larsson (1993) | 19 |
| Figure 2.3 Squat mathematical model flow chart | 20 |
| Figure 3.1 Schematic of simplified bank geometries for unsteady squat tests | 26 |
| Figure 3.2 Schematic of model setup for measurement of sinkage, trim and surge force | 26 |
| Figure 3.3 Schematic of model setup for measurement of heave force and pitch moment for unsteady squat tests..... | 27 |
| Figure 3.4 Schematic of model setup for measurement of forces and moments | 28 |
| Figure 3.5 Midship sinkage coefficient as a function of F_{nh} , $h_l/d=1.2$, $W/B=4.8$ | 32 |
| Figure 3.6 Midship sinkage coefficient as a function of F_{nh} , $h_l/d=1.3$, $W/B=4.8$ | 32 |
| Figure 3.7 Midship sinkage coefficient as a function of F_{nh} , $h_l/d=1.4$, $W/B=4.8$ | 33 |
| Figure 3.8 Bow sinkage coefficient as a function of F_{nh} , $h_l/d=1.2$, $W/B=4.8$ | 33 |
| Figure 3.9 Bow sinkage coefficient as a function of F_{nh} , $h_l/d=1.3$, $W/B=4.8$ | 34 |
| Figure 3.10 Bow sinkage coefficient as a function of F_{nh} , $h_l/d=1.4$, $W/B=4.8$ | 34 |
| Figure 3.11 Non-dimensional heave force as a function of F_{nh} , varying h_l/d , $W/B=5.0$ | 39 |
| Figure 3.12 Non-dimensional pitch moment as a function of F_{nh} , varying h_l/d , $W/B=10.3$ | 39 |
| Figure 3.13 Non-dimensional pitch moment as a function of F_{nh} , varying h_l/d , $W/B=3.0$ | 40 |
| Figure 3.14 Non-dimensional heave force (using the Bis system) as a function of F_{nh} , varying h_l/d , $W/B=5.0$ | 40 |
| Figure 3.15 Non-dimensional pitch moment (using the Bis system) as a function of F_{nh} , varying h_l/d , $W/B=10.3$ | 41 |
| Figure 3.16 Non-dimensional heave force as a function of F_{nh} , varying W/B , $h_l/d=1.2$ | 41 |
| Figure 3.17 Non-dimensional pitch moment as a function of F_{nh} , varying W/B , $h_l/d=1.7$ | 42 |
| Figure 3.18 Centre of pressure location as a function of F_{nh} , varying W/B , $h_l/d=1.7$ | 42 |
| Figure 3.19 Predicted sinkage at forward perpendicular as a function of F_{nh} , varying W/B , $h_l/d=1.7$ | 43 |
| Figure 3.20 Non-dimensional heave force as a function of F_{nh} , varying d | 43 |
| Figure 3.21 Non-dimensional pitch moment as a function of F_{nh} , varying d | 44 |
| Figure 3.22 Non-dimensional heave force as a function of T'' , varying F_{nh} , $h_l/d=1.1$ | 48 |
| Figure 3.23 Non-dimensional heave force as a function of T'' , varying F_{nh} , $h_l/d=1.2$ | 48 |
| Figure 3.24 Non-dimensional pitch moment as a function of T'' , varying F_{nh} , $h_l/d=1.1$ | 49 |
| Figure 3.25 Non-dimensional pitch moment as a function of T'' , varying F_{nh} , $h_l/d=1.2$ | 49 |

| | |
|--|----|
| Figure 3.26 Schematic of additional heave force due to propulsion..... | 50 |
| Figure 3.27 Additional heave force due to propulsion as a function of F_{nh} , varying T'' , $h_l/d=1.1$ | 50 |
| Figure 3.28 Additional pitch moment due to propulsion as a function of F_{nh} , varying T'' , $h_l/d=1.1$ | 51 |
| Figure 3.29 Additional heave force due to propulsion as a function of h_l/d , varying T'' and F_{nL} | 51 |
| Figure 3.30 Additional pitch moment due to propulsion as a function of h_l/d , varying T'' and F_{nL} | 52 |
| Figure 3.31 Longitudinal position of additional heave force due to propulsion as a function of F_{nh} , varying T'' , $h_l/d=1.1$ | 52 |
| Figure 3.32 Longitudinal position of additional heave force due to propulsion as a function of F_{nh} , varying T'' , $h_l/d=1.2$ | 53 |
| Figure 3.33 Sinkage over ramp bank, $F_{nh}=0.30-0.55$, $h_l/d=4.3-1.3$ | 57 |
| Figure 3.34 Trim over ramp bank, $F_{nh}=0.30-0.55$, $h_l/d=4.3-1.3$ | 57 |
| Figure 3.35 Midship sinkage over ramp bank for different water depths..... | 58 |
| Figure 3.36 Bow sinkage over ramp bank for different water depths..... | 58 |
| Figure 3.37 Midship sinkage over ramp bank for different vessel speeds..... | 59 |
| Figure 3.38 Bow sinkage over ramp bank for different vessel speeds..... | 59 |
| Figure 3.39 Heave force over ramp bank and step bank, $h_l/d=4.3-1.3$, $F_{nh}=0.35-0.63$ | 60 |
| Figure 3.40 Pitch moment over ramp bank and step bank, $h_l/d=4.3-1.3$, $F_{nh}=0.35-0.63$ | 60 |
| Figure 3.41 Comparison between measured heave force and Shipflow predictions, $W/B=10.3$ | 62 |
| Figure 3.42 Comparison between measured pitch moment and Shipflow predictions, $W/B=10.3$ | 62 |
| Figure 4.1 Non-dimensional additional heave force due to propulsion as a function of T'' , varying h_l/d | 73 |
| Figure 4.2 Non-dimensional additional pitch moment due to propulsion as a function of T'' , varying h_l/d | 73 |
| Figure 4.3 Comparison of midship sinkage measured from semi-captive experiments and quasi-steady mathematical model predictions | 76 |
| Figure 4.4 Comparison of bow sinkage measured from semi-captive experiments and quasi- steady mathematical model predictions..... | 76 |
| Figure 4.5 Midship sinkage over ramp bank, $F_{nh}=0.25-0.47$, $h_l/d=4.2-1.2$ | 77 |
| Figure 4.6 Bow sinkage over ramp bank, $F_{nh}=0.25-0.47$, $h_l/d=4.2-1.2$ | 77 |
| Figure 4.7 Midship sinkage over ramp bank, $F_{nh}=0.25-0.45$, $h_l/d=4.3-1.3$ | 78 |
| Figure 4.8 Bow sinkage over ramp bank, $F_{nh}=0.25-0.45$, $h_l/d=4.3-1.3$ | 78 |

| | |
|--|-----|
| Figure 4.9 Midship sinkage over ramp bank, $F_{nh}=0.25-0.43$, $h_1/d=4.51-1.51$ | 79 |
| Figure 4.10 Bow sinkage over ramp bank, $F_{nh}=0.25-0.43$, $h_1/d=4.51-1.51$ | 79 |
| Figure 4.11 Midship sinkage over ramp bank, $F_{nh}=0.20-0.36$, $h_1/d=4.3-1.3$ | 80 |
| Figure 4.12 Bow sinkage over ramp bank, $F_{nh}=0.20-0.36$, $h_1/d=4.3-1.3$ | 80 |
| Figure 4.13 Midship sinkage over ramp bank, $F_{nh}=0.25-0.45$, $h_1/d=4.3-1.3$ | 81 |
| Figure 4.14 Bow sinkage over ramp bank, $F_{nh}=0.25-0.45$, $h_1/d=4.3-1.3$ | 81 |
| Figure 4.15 Midship sinkage over ramp bank, $F_{nh}=0.30-0.55$, $h_1/d=4.3-1.3$ | 82 |
| Figure 4.16 Bow sinkage over ramp bank, $F_{nh}=0.30-0.55$, $h_1/d=4.3-1.3$ | 82 |
| Figure 4.17 Midship sinkage over ramp bank, $F_{nh}=0.25-0.47$, $h_1/d=4.2-1.2$ | 83 |
| Figure 4.18 Bow sinkage over ramp bank, $F_{nh}=0.25-0.47$, $h_1/d=4.2-1.2$ | 83 |
| Figure 5.1 Schematic of model set up for sway force and yaw moment tests | 88 |
| Figure 5.2 Parameters defining bank geometry | 90 |
| Figure 5.3 Non-dimensional sway force as a function of F_{nh} , MarAd L series model | 92 |
| Figure 5.4 Non-dimensional yaw moment as a function of F_{nh} , MarAd L series model | 92 |
| Figure 5.5 Non-dimensional sway force as a function of F_{nh} | 93 |
| Figure 5.6 Non-dimensional yaw moment as a function of F_{nh} | 93 |
| Figure 5.7 Non-dimensional sway force as a function of F_{nh} , MarAd L series model | 94 |
| Figure 5.8 Non-dimensional yaw moment as a function of F_{nh} , MarAd L series model | 94 |
| Figure 5.9 Non-dimensional sway force as a function of $d/(h_1-d)$ | 96 |
| Figure 5.10 Non-dimensional yaw moment as a function of $d/(h_1-d)$ | 96 |
| Figure 5.11 Non-dimensional sway force as a function of y_{Bt} for surface piercing banks | 98 |
| Figure 5.12 Non-dimensional yaw moment as a function of y_{Bt} for surface piercing banks | 98 |
| Figure 5.13 Non-dimensional sway force as a function of y_{Bt} for flooded banks, MarAd L series model | 99 |
| Figure 5.14 Non-dimensional yaw moment as a function of y_{Bt} for flooded banks, MarAd L series model | 99 |
| Figure 5.15 Non-dimensional sway force as a function of $1-(h_{2p}/h_1)$ | 101 |
| Figure 5.16 Non-dimensional yaw moment as a function of $1-(h_{2p}/h_1)$ | 101 |
| Figure 5.17 Non-dimensional sway force as a function of $1-(h_{2p}/h_1)$ | 102 |
| Figure 5.18 Non-dimensional yaw moment as a function of $1-(h_{2p}/h_1)$ | 102 |
| Figure 5.19 Non-dimensional sway force as a function of F_{nL} , varying α_p , $d/(h_1-d)=3.35$, $y_{pt}/B=1.00$, $1-(h_{2p}/h_1)=1.00$, MarAd L series model..... | 104 |
| Figure 5.20 Non-dimensional yaw moment as a function of F_{nL} , varying α_p , $d/(h_1-d)=3.35$, $y_{pt}/B=1.00$, $1-(h_{2p}/h_1)=1.00$, MarAd L series model | 104 |

| | |
|--|-----|
| Figure 5.21 Non-dimensional sway force as a function of α_p | 105 |
| Figure 5.22 Non-dimensional yaw moment as a function of α_p | 105 |
| Figure 5.23 Non-dimensional sway force as a function of F_{nh} , $y_{pt}/W=0.162$, $d/(h_1-d)=9.63$, $1-(h_{2p}/h_1)=1.00$, $\alpha_p=90^\circ$ | 107 |
| Figure 5.24 Non-dimensional yaw moment as a function of F_{nh} , $y_{pt}/W=0.162$, $d/(h_1-d)=9.63$, $1-(h_{2p}/h_1)=1.00$, $\alpha_p=90^\circ$ | 107 |
| Figure 5.25 Non-dimensional sway force as a function of F_{nh} for bulk carrier and containership models..... | 108 |
| Figure 5.26 Non-dimensional yaw moment as a function of F_{nh} for bulk carrier and containership models..... | 108 |
| Figure 5.27 Non-dimensional sway force as a function of F_{nh} for bulk carrier and containership models, $y_{pt}/W=0.118$, $d/(h_1-d)=5.13$, $1-(h_{2p}/h_1)=1.00$, $\alpha_p=90^\circ$ | 109 |
| Figure 5.28 Non-dimensional yaw moment as a function of F_{nh} for bulk carrier and containership models, $y_{pt}/W=0.118$, $d/(h_1-d)=5.13$, $1-(h_{2p}/h_1)=1.00$, $\alpha_p=90^\circ$ | 109 |
| Figure 5.29 Comparison between measured sway force and Shipflow predictions, $y_{Bt}=-0.403$, $1-(h_{2p}/h_1)=1$, $1-(h_{2s}/h_1)=1$, $\alpha_p=90^\circ$, MarAd L series model..... | 113 |
| Figure 5.30 Comparison between measured yaw moment and Shipflow predictions, $y_{Bt}=-0.403$, $1-(h_{2p}/h_1)=1$, $1-(h_{2s}/h_1)=1$, $\alpha_p=90^\circ$, MarAd L series model..... | 113 |
| Figure 6.1 Non-dimensional sway force as a function of $d/(h_1-d)$ | 118 |
| Figure 6.2 Non-dimensional yaw moment as a function of $d/(h_1-d)$ | 118 |
| Figure 6.3 Lateral ship to bank distances for surface piercing banks, Ch'ng (1991)..... | 124 |
| Figure 6.4 Lateral ship to bank distances for flooded and surface piercing banks..... | 125 |
| Figure 6.5 Non-dimensional sway force as a function of y_{Bt} , varying α_p , $d/(h_1-d)=9.63$, MarAd L series..... | 125 |
| Figure 6.6 Non-dimensional sway force as a function of y_{B5} , varying α_p , $d/(h_1-d)=9.63$, MarAd L series..... | 126 |
| Figure 6.7 Non-dimensional sway force as a function of y_{B6} , varying α_p , $d/(h_1-d)=9.63$, MarAd L series..... | 126 |
| Figure 6.8 Non-dimensional sway force as a function of y_{B7} , varying α_p , $d/(h_1-d)=9.63$, MarAd L series..... | 127 |
| Figure 6.9 Non-dimensional yaw moment as a function of y_{Bt} , varying α_p , $d/(h_1-d)=9.63$, MarAd L series..... | 127 |
| Figure 6.10 Non-dimensional yaw moment as a function of y_{B5} , varying α_p , $d/(h_1-d)=9.63$, MarAd L series | 128 |
| Figure 6.11 Non-dimensional yaw moment as a function of y_{B6} , varying α_p , $d/(h_1-d)=9.63$, MarAd L series | 128 |
| Figure 6.12 Non-dimensional yaw moment as a function of y_{B7} , varying α_p , $d/(h_1-d)=9.63$, MarAd L series | 129 |
| Figure 6.13 c_y as a function of F_{nh} , MarAd L series model..... | 132 |

| | |
|---|-----|
| Figure 6.14 c_n as a function of F_{nh} , MarAd L series model..... | 132 |
| Figure 6.15 c_y as a function of $d/(h_1-d)$ | 133 |
| Figure 6.16 c_n as a function of $d/(h_1-d)$ | 133 |
| Figure 6.17 Non-dimensional sway force as a function of $1-(h_{2p}/h_1)$, MarAd L series model .. | 134 |
| Figure 6.18 Non-dimensional yaw moment as a function of $1-(h_{2p}/h_1)$, MarAd L series model | 134 |
| Figure 6.19 Non-dimensional sway force as a function of BP_{Y6} for varying bank submergence, $y_{pt}/B=0.69$, MarAd L series..... | 135 |
| Figure 6.20 Non-dimensional yaw moment as a function of BP_{N6} for varying bank submergence, $y_{pt}/B=0.69$, MarAd L series..... | 135 |
| Figure 6.21 Non-linear relationship between non-dimensional sway force and yaw moment with C_B , $d/(h_1-d)=9.63$, $y_{pt}/W=0.097$, $1-(h_{2p}/h_1)=1.00$, $\alpha_p=90^\circ$, MarAd L series, MarAd F series, S-175 containership..... | 138 |
| Figure 6.22 Sample of a test conducted to assess the accuracy of regression equations, $y_{pt}/B=1.00$, $y_{st}/B=5.15$, $d/(h_1-d)=2.00$, $1-(h_{2p}/h_1)=0.47$, $1-(h_{2s}/h_1)=1.00$, $\alpha_p=90^\circ$, MarAd L..... | 140 |
| Figure 6.23 Comparison between regression prediction and non-dimensional sway force measured by Dand (1981), Cases 1 - 4..... | 144 |
| Figure 6.24 Comparison between regression prediction and non-dimensional sway force measured by Dand (1981), Cases 5 - 8..... | 144 |
| Figure 6.25 Comparison between regression prediction and non-dimensional yaw moment measured by Dand (1981), Cases 1 - 4..... | 145 |
| Figure 6.26 Comparison between regression prediction and non-dimensional yaw moment measured by Dand (1981), Cases 5 - 8..... | 145 |
| Figure 6.27 Predicted ship path using empirical equations from the present study in the AMC ship-handling simulator for the Port of Weipa..... | 147 |
| Figure 6.28 Predicted bank induced sway force and yaw moment for the simulation of a manoeuvre at the Port of Weipa (output from AMC ship-handling simulator) | 148 |
| Figure B1 Body plan of MarAd L series model (Roseman 1987) | 162 |
| Figure B2 Body plan of MarAd F series model (Roseman 1987) | 162 |
| Figure B3 Body plan of S-175 containership (ITTC 1987)..... | 163 |
| Figure B4 MarAd L series model with propeller fitted | 163 |
| Figure C1 Channel walls constructed in towing tank for squat tests..... | 164 |
| Figure C2 Photograph showing steel port wall set up in the towing tank | 165 |
| Figure C3 Flooded bank assembly prior to water fill | 166 |
| Figure E1 Non-dimensional sway force as a function of F_{nL} , $y_{Bt}=-0.629$, $d/(h_1-d)=5.13$, $1-(h_{2p}/h_1)=1.00$, $1-(h_{2s}/h_1)=1.00$, $\alpha_p=90^\circ$, $\alpha_s=90^\circ$, MarAd L..... | 174 |

Figure E2 Non-dimensional yaw moment as a function of F_{nL} , $y_{Bt}=-0.629$, $d/(h_1-d)=5.13$,
 $1-(h_{2p}/h_1)=1.00$, $1-(h_{2s}/h_1)=1.00$, $\alpha_p=90^\circ$, $\alpha_s=90^\circ$, MarAd L.....174

Figure E3 Non-dimensional sway force as a function of F_{nL} , $y_{Bt}=-0.629$, $d/(h_1-d)=2.00$,
 $1-(h_{2p}/h_1)=1.00$, $1-(h_{2s}/h_1)=1.00$, $\alpha_p=90^\circ$, $\alpha_s=90^\circ$, MarAd L.....175

Figure E4 Non-dimensional yaw moment as a function of F_{nL} , $y_{Bt}=-0.629$, $d/(h_1-d)=2.00$,
 $1-(h_{2p}/h_1)=1.00$, $1-(h_{2s}/h_1)=1.00$, $\alpha_p=90^\circ$, $\alpha_s=90^\circ$, MarAd L.....175

List of Tables

| | |
|---|-----|
| Table 2.1 Number of panels for a Shipflow mesh, $W/B=3$, $h_1/d=1.4$ | 18 |
| Table 3.1 Principal particulars of models | 25 |
| Table 3.2 Test program: effect of scale on squat measurement using MarAd F series | 30 |
| Table 3.3 Test program: effect of vessel speed, water depth and channel width on heave force and pitch moment due to squat, $B/d=4.42$ | 36 |
| Table 3.4 Test program: effect of vessel speed, water depth and vessel draught on heave force and pitch moment due to squat, $W/B=10.3$ | 36 |
| Table 3.5 Test program to investigate the influence of propulsion on squat..... | 46 |
| Table 3.6 Test program for unsteady squat tests..... | 54 |
| Table 4.1 Statistical fit for under keel clearance parameters for heave force for three sample cases | 66 |
| Table 4.2 Statistical fit for under keel clearance parameters for pitch moment for three sample cases | 66 |
| Table 4.3 Statistical fit for channel width parameters for heave force for sample cases | 67 |
| Table 4.4 Statistical fit for channel width parameters for pitch moment for sample cases..... | 68 |
| Table 4.5 Statistical fit for under keel clearance parameters for additional heave force due to propulsion for two sample cases | 71 |
| Table 4.6 Statistical fit for under keel clearance parameters for additional pitch moment due to propulsion for two sample cases | 71 |
| Table 6.1 Statistical fit for under keel clearance parameters for sway force for three sample cases | 119 |
| Table 6.2 Statistical fit for under keel clearance parameters for yaw moment for three sample cases | 119 |
| Table 6.3 Statistical fit for ship to bank distance parameters for a sample of surface piercing bank cases for sway force | 121 |
| Table 6.4 Statistical fit for ship to bank distance parameters for a sample of surface piercing bank cases for yaw moment | 121 |
| Table 6.5 Statistical fit for ship to bank distance parameters for a sample of flooded bank cases for sway force..... | 122 |
| Table 6.6 Statistical fit for ship to bank distance parameters for a sample of flooded bank cases for yaw moment..... | 123 |
| Table 6.7 Analysis of hull form parameters for non-dimensional sway force, $F_{nh}=0.176$, 0.194 , 0.219 , $d/(h_1-d)=9.63$, $y_{pt}/W=0.097$, $1-(h_{2p}/h_1)=1.00$, $\alpha_p=90^\circ$, MarAd L series, MarAd F series, S-175 containership | 137 |

| | |
|--|-----|
| Table 6.8 Analysis of hull form parameters for non-dimensional yaw moment, $F_{nh}=0.176$, 0.194, 0.219, $d/(h_1-d)=9.63$, $y_{pt}/W=0.097$, $1-(h_{2p}/h_1)=1.00$, $\alpha_p=90^\circ$, MarAd L series, MarAd F series, S-175 containership | 137 |
| Table 6.9 Analysis of hull form parameters for non-dimensional sway force, $F_{nh}=0.269$, 0.296, $d/(h_1-d)=9.63$, $1-(h_{2p}/h_1)=0.65$, $y_{pt}/W=0.097$, $\alpha_p=90^\circ$, MarAd L series, MarAd F series, S-175 containership | 137 |
| Table 6.10 Analysis of hull form parameters for non-dimensional yaw moment, $F_{nh}=0.269$, 0.296, 0.219, $d/(h_1-d)=9.63$, $y_{pt}/W=0.097$, $1-(h_{2p}/h_1)=0.65$, $\alpha_p=90^\circ$, MarAd L series, MarAd F series, S-175 containership | 138 |
| Table 6.11 Principal particulars of the bulk carrier, Kumasachi Maru | 146 |

Nomenclature

| | |
|-------------------|---|
| A | Panel area |
| B | Vessel beam |
| C_B | Block coefficient |
| C_p | Pressure coefficient |
| d | Vessel draught |
| D_B | Bank height |
| F_{nh} | Depth Froude number, $\frac{U}{\sqrt{gh_1}}$ |
| F_{nL} | Length Froude number, $\frac{U}{\sqrt{gL_{PP}}}$ |
| g | Acceleration due to gravity |
| h_1 | Water depth in channel |
| h_{2p} | Depth of water over port bank |
| h_{2s} | Depth of water over starboard bank |
| I_{yy} | Pitch mass moment of inertia |
| δI_{yy} | Added pitch mass moment of inertia |
| I_{zz} | Yaw mass moment of inertia |
| L_{PP} | Length between perpendiculars |
| M | Pitch moment due to squat |
| M' | Non-dimensional pitch moment, $\frac{M}{\frac{1}{2}\rho U^2 L_{PP}^3}$ |
| M'' | Non-dimensional pitch moment, $\frac{M}{\rho g \nabla_o L_{PP}}$ |
| M_{ADD} | Additional pitch moment due to propulsion |
| M_{ADD}'' | Non-dimensional additional pitch moment due to propulsion, $\frac{M_{ADD}}{\rho g \nabla_o L_{PP}}$ |
| $M_{damping}$ | Damping pitch moment |
| $M_{hydrostatic}$ | Hydrostatic pitch moment |
| $M_{propelled}$ | Pitch moment on propelled hull |
| $M_{unpropelled}$ | Pitch moment on unpropelled hull |

| | |
|-------------------------|--|
| n | Outward normal |
| N | Yaw moment |
| N' | Non-dimensional yaw moment, $\frac{N}{\frac{1}{2}\rho U^2 L_{PP}^2 d}$ |
| N'' | Non-dimensional yaw moment, $\frac{N}{\rho g \nabla_o L_{PP}}$ |
| p | Pressure |
| p_∞ | Free stream pressure |
| p_d | Dynamic pressure |
| R^2 | Coefficient of determination |
| R^2_{adjusted} | Adjusted coefficient of determination |
| S_{bow} | Bow sinkage (at forward perpendicular) |
| S_{midships} | Midship sinkage |
| S_{stern} | Stern sinkage (at aft perpendicular) |
| S_s | Ship cross-sectional area |
| SC_{bow} | Bow sinkage coefficient |
| SC_{midships} | Midship sinkage coefficient |
| SS | Sum of squares |
| S_o | Channel cross sectional area |
| t | Time |
| T | Effective thrust ($X_{\text{propelled}} - X_{\text{unpropelled}}$) |
| T'' | Non-dimensional effective thrust, $\frac{T}{\rho g \nabla_o}$ |
| U | Velocity |
| \bar{U} | Velocity vector |
| U_∞ | Free stream velocity |
| \bar{U}_∞ | Free stream velocity vector |
| u | Component of U along x ship body axis |
| v | Component of U along y ship body axis |
| \dot{v} | Velocity along y ship body axis |
| W | Channel width |

| | |
|--------------------------|---|
| X | Surge force |
| $X_{\text{propelled}}$ | Surge force on propelled hull |
| $X_{\text{unpropelled}}$ | Surge force on unpropelled hull |
| x_{ADD} | Longitudinal position of additional heave force due to propulsion |
| $x_{\text{LCF-FP}}$ | Distance from static LCF to forward perpendicular |
| x_m | Non-dimensional distance along channel centreline (x^*/L_{PP}) |
| x^* | Distance along channel centreline relative to an earth fixed point |
| $x_{\text{mid-LCF}}$ | Distance from midships to static LCF |
| Y | Sway force |
| Y' | Non-dimensional sway force, $\frac{Y}{\frac{1}{2}\rho U^2 L_{\text{PP}} d}$ |
| Y'' | Non-dimensional sway force, $\frac{Y}{\rho g \nabla_o}$ |
| y_{Bt} | Ship to bank distance parameter, $\left(\frac{1}{y_{\text{pt}}} + \frac{1}{y_{\text{st}}}\right) \frac{B}{2}$ |
| y_{Bi} | Ship to bank distance parameter, $\left(\frac{1}{y_{\text{pi}}} + \frac{1}{y_{\text{si}}}\right) \frac{B}{2}$ |
| y_{pi} | Distance from ship's centreline to port bank on different vertical planes |
| y_{pw} | Width of port flooded bank |
| y_{pt} | Distance from ship's centreline to toe of bank on port side |
| y_{si} | Distance from ship's centreline to starboard bank on different vertical planes |
| y_{st} | Distance from ship's centreline to toe of starboard bank |
| z_{LCF} | Sinkage at LCF |
| z_{LCF0} | Sinkage at LCF (initial condition) |
| \dot{z}_{LCF} | Heave velocity at LCF |
| \dot{z}_{LCF0} | Heave velocity at LCF (initial condition) |
| \ddot{z}_{LCF} | Heave acceleration at LCF |
| z_{FP} | Sinkage at forward perpendicular due to pitch |
| z_{FP0} | Sinkage at forward perpendicular due to pitch (initial condition) |
| \dot{z}_{FP} | Linear heave velocity at forward perpendicular due to pitch |

| | |
|-------------------|---|
| Z | Heave force due to squat |
| Z' | Non-dimensional heave force due to squat, $\frac{Z}{\frac{1}{2}\rho U^2 L_{PP}^2}$ |
| Z'' | Non-dimensional heave force, $\frac{Z}{\rho g \nabla_o}$ |
| Z_{ADD} | Additional heave force due to propulsion |
| Z_{ADD}'' | Non-dimensional additional heave force due to propulsion, $\frac{Z_{ADD}}{\rho g \nabla_o}$ |
| $Z_{damping}$ | Damping heave force |
| $Z_{hydrostatic}$ | Hydrostatic heave force |
| $Z_{propelled}$ | Heave force on propelled hull |
| $Z_{unpropelled}$ | Heave force on unpropelled hull |
| ρ | Water density |
| ∇_o | Volumetric displacement at rest |
| ∇ | Del operator |
| α_p | Port bank angle with respect to the horizontal plane |
| α_s | Starboard bank angle with respect to the horizontal plane |
| σ | Source strength |
| Δ | Ship displacement |
| $\delta\Delta$ | Heave added mass |
| θ | Pitch |
| $\dot{\theta}$ | Pitch velocity |
| $\dot{\theta}_0$ | Pitch velocity (initial condition) |
| $\ddot{\theta}$ | Pitch acceleration |
| Φ | Velocity potential |
| Φ^o | Double body velocity potential |
| η | Free surface elevation |
| η^o | Double body free surface elevation |
| γ_{heave} | Heave damping coefficient |
| γ_{pitch} | Pitch damping coefficient |
| ψ | Yaw angle in the horizontal plane measured from the x axis of the ship |

| | |
|---------------|------------------|
| $\dot{\psi}$ | Yaw velocity |
| $\ddot{\psi}$ | Yaw acceleration |

Abbreviations

| | |
|-------|--|
| AMC | Australian Maritime College |
| AP | Aft perpendicular |
| FP | Forward perpendicular |
| ITTC | International Towing Tank Conference |
| LCB | Longitudinal centre of buoyancy |
| LCF | Longitudinal centre of floatation |
| LVDT | Linear variable differential transformer |
| MCTC | Moment to change trim one centimetre |
| NTSB | National Transportation Safety Board |
| PIANC | Permanent International Association of Navigation Congresses |
| TPC | Tonnes per centimetre |
| UKC | Under keel clearance |

Co-ordinate System

The co-ordinate system used in the present study is shown in Figure 0.1, unless stated otherwise. The origin is situated at midships on the static waterline.

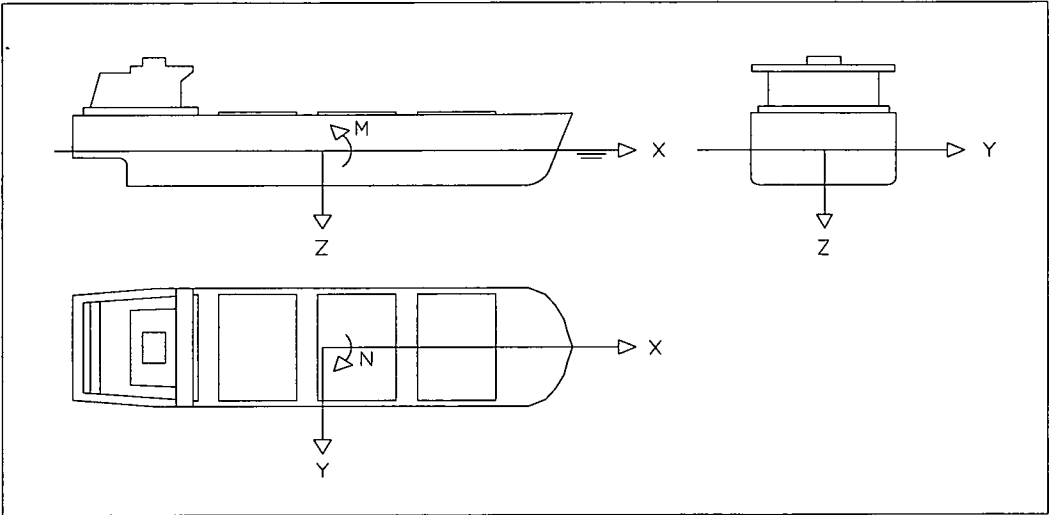


Figure 0.1 Co-ordinate system

Chapter 1

Introduction

1.1 Background

A ship operating within a port environment is likely to travel in close proximity to waterway boundaries. The change in flow due to interaction with these restrictions influences the manoeuvring behaviour of a ship. These interactions are exacerbated by the fact that ship size is steadily increasing to cope with productivity demands. Real-time simulation of ship manoeuvring is widely used to predict the path of a ship within restricted water to assist with tasks such as channel design, developing safe port operating procedures and conducting ship operation training. This thesis reports on a study into the modelling of the interaction between a ship and waterway boundaries, i.e. the sea floor and lateral banks.

As a vessel moves through water the change in flow around the hull causes a vertical displacement of the ship, called sinkage, and a pitch angle, known as trim. The combined effect of this sinkage and trim is known as ship squat. Squat occurs in both unrestricted and restricted water; however squat is accentuated in restricted water and becomes more important to ship operators. There are three distinct flow regimes for ships operating in restricted water: sub-critical, trans-critical and super-critical (Constantine 1961). These regimes are dependent upon blockage and depth Froude number. Attention is focussed on the sub-critical and trans-critical regimes in the present study. Flow is steady for the sub-critical regime where, in general, squat can be considered as a simple Bernoulli effect. Due to the flow contraction beneath the hull the fluid velocity is increased in this region, which results in a reduction in pressure. Therefore the vertical displacement of the ship is usually downward for such cases. The pitch angle may be either bow or stern down depending on factors such as propeller loading, hull form and channel dimensions. In the trans-critical regime the flow is unsteady and water piles up at the bow until a solitary wave is produced forward of the ship, which can have a significant impact on the trim. Flow will also be unsteady when a vessel moves through water of non-uniform depth; this is defined as unsteady squat in the present study. For such cases the time varying forces and moments acting on the hull in the vertical plane lead to acceleration effects, which may cause an overshoot of sinkage (Ferguson *et al.* 1982). The change in under keel clearance due to squat can affect the directional stability and turning properties of a ship. Also, a ship may actually ground on the sea floor, despite the fact that the under keel clearance was sufficient at rest.

In the super-critical regime the ship speed exceeds the natural speed of a shallow water wave, corresponding to the water depth in which the ship is operating. The cases investigated in the present study fall either into the sub-critical or trans-critical regimes due to the combination of depth Froude number and blockage ratio, hence super-critical flow is not discussed further.

When operating in restricted water the behaviour of a ship can be significantly influenced by the presence of lateral banks. Such lateral restrictions can cause an asymmetrical pressure distribution on the submerged portion of the hull, which gives rise to a net sway force and yaw moment. The classical bank effect experienced by a ship offset from the centreline of a long canal is an attraction to the near wall and a bow away yaw moment, both proportional to the

square of the ship speed in the sub-critical flow regime (Norrbin 1978). The attraction sway force can also be described, in general, as a simple Bernoulli effect due to the flow contraction between the ship and near bank. The sway force generally changes to repulsion from the near bank when the blockage is increased and/or when the vessel speed is sufficiently high. The bank induced sway force and yaw moment can influence the manoeuvring properties of a ship, which may lead to potentially dangerous situations, such as collisions with other ships or with waterway boundaries.

Accurate prediction of squat and ship-bank interaction is crucial for realistic real-time simulation of the manoeuvring behaviour of a ship in restricted water. If squat can be predicted accurately, ship-handling simulators may be used to determine the optimum under keel clearance so that the payload can be maximised whilst minimising the risk of grounding. Accurate prediction of ship-bank interaction will enable simulators to be used to determine optimum channel widths and/or to determine if vessels can safely manoeuvre within proposed or existing channel geometries. Such predictions will allow accurate assessment of dredging requirements, potentially reducing dredging expenses. Also, safe operating ship speeds can be determined for specific operating conditions in relation to squat and ship-bank interaction.

Numerous prediction techniques exist to predict squat in uniform depth. In comparison, the prediction of squat in non-uniform depth has received little attention to date (Gourlay 2003). Previous predictions of squat in non-uniform depth have generally been undertaken using constant depth formulae based on the average depth under the ship, assuming that the ship speed and water depth are both sufficiently slowly varying functions of time to neglect unsteadiness (NTSB (1993)). It is uncertain whether this approach will under or over predict unsteady squat. Hatch (1996) developed a mathematical model to predict unsteady squat, but poor correlation was observed with model scale measurements.

In recent years a number of studies have been conducted to predict the interaction between ships and lateral surface piercing banks for the purpose of ship-handling simulation, for example Ch'ng *et al.* (1993) and Vantorre (1995). However, experimental data and prediction methods for the interaction between ships and flooded banks for ship-handling simulation are scarce, limiting the applicability of most simulators to surface piercing bank cases.

1.2 Objectives

As identified in Section 1.1, there is a need for a practical prediction technique for unsteady squat including dynamic acceleration effects and for the quantification of interaction between a ship and flooded lateral banks.

Therefore, the objectives of this work are:

- to develop and validate a practical technique for predicting vessel motion in the vertical plane due to unsteady squat for use in real-time ship-handling simulators, and
- to develop and validate a practical technique for predicting bank induced sway force and yaw moment for use in real-time ship-handling simulators.

1.3 Methodology

The simulation of both squat and ship-bank interaction was undertaken in two steps; the first was the prediction of steady-state forces and moments in the horizontal and vertical planes, and the second was the prediction of real-time motions using quasi-steady mathematical models.

The requirement was to develop techniques to predict steady-state squat and ship-bank interaction in real-time simulation, whilst achieving sufficient accuracy. Developing empirical formulae by performing regression analysis on model scale measurements is an effective method to accurately account for the complex restricted water flow phenomena, whilst satisfying the real-time computation condition. Therefore, model scale experiments were conducted to measure steady-state forces in the horizontal and vertical planes on different ship models for a wide range of channel geometries and waterway parameters. The number of model scale experiments that could be conducted was limited by the resources and time required to perform them. Steady-state heave force and pitch moment due to squat and bank induced sway force and yaw moment were also predicted using a three-dimensional panel method. The aim was to compare the predictions to model scale experiment results to assess if the method was sufficiently accurate to be used to extend the steady-state experimental data matrix for the regression analysis.

Using regression analysis techniques empirical formulae were developed for steady-state heave force and pitch moment due to squat for an unpropelled bulk carrier hull form and a correction was generated for the effect of propulsion. The ship-bank interaction experiments were used to develop a bank parameter to allow approximation of the effects of lateral surface piercing and flooded banks. This parameter was utilised in regression analyses to develop the empirical formulae for steady-state bank induced sway force and yaw moment.

A mathematical model was developed to predict squat and associated acceleration effects for a vessel travelling in water of non-uniform depth. The empirical formulae to predict steady-state heave force and pitch moment due to squat were used as input to the real-time, two degree of freedom mathematical model. Predictions from the quasi-steady model were assessed against model scale steady-state sinkage measurements and unsteady sinkage measurements on a vessel travelling over a simplified ramp bank.

The empirical formulae to predict steady-state bank induced sway force and yaw moment were validated against independent model scale measurements from literature. The formulae were incorporated into an existing mathematical model to predict vessel motions in the horizontal plane. The quasi-steady technique was used to predict the path of a vessel for a manoeuvre where ship-bank interaction is used to aid a turn and the predicted path was compared to that known to occur in the real-life manoeuvre.

The novel components of the work and contributions to knowledge in the field of ship-handling simulation include:

- A comprehensive set of model scale experiments has been conducted for a wide range of conditions, enhancing the understanding of vessel squat and ship-bank interaction.
- Empirical equations have been developed to predict the steady-state heave force and pitch moment due to squat for a range of vessel speeds, water depth to draught ratios

and channel widths. Correction factors for the influence of propulsion have also been presented.

- A mathematical model has been developed to estimate unsteady squat and dynamic acceleration effects in the vertical plane, which is applicable to a wide range of bathymetries.
- Empirical formulae have been developed through the use of a bank parameter that enables estimation of the influence of port and starboard surface piercing and flooded banks. With the capability to predict the influence of flooded banks for such a wide range of cases the proposed prediction technique is applicable to a broader range of port geometries, when compared to previous prediction techniques.
- The empirical formulae to predict steady-state ship-bank interaction have been incorporated into an existing mathematical model to predict the real-time manoeuvring behaviour of a ship travelling in close proximity to lateral flooded and surface piercing banks.

1.4 Overview of thesis structure

A review of previous work on the prediction of squat and ship-bank interaction is given in Chapter 2, together with mathematical details concerning the prediction techniques used in the present study.

Chapters 3 and 4 relate exclusively to ship squat. Both steady and unsteady model scale experimental results are presented and discussed in Chapter 3, whilst in Chapter 4 empirical equations are developed to predict steady-state heave force and pitch moment in the squat mathematical model. Unsteady squat predictions using the mathematical model are compared with unsteady squat measurements from model scale experiments in Chapter 4.

Ship-bank interaction is addressed in Chapters 5 and 6. Model scale experiment results for bank induced sway force and yaw moment are presented in Chapter 5. In Chapter 6 empirical equations are developed to predict steady-state bank induced sway force and yaw moment and are validated against independent results from literature. These equations are incorporated into an existing mathematical model to predict the path of a ship for a manoeuvre that is performed in an Australian port, where bank effect is utilised to aid a turn. The predictions are compared to the ship path that is known to occur in the real-life manoeuvre.

Finally, conclusions and recommendations for further work for both squat and ship-bank interaction are presented in Chapter 7.

Parts of the present study have been summarised in publications during the course of the work: Duffy and Renilson (2000), Duffy *et al.* (2000), Duffy and Renilson (2001), Duffy (2002), Maio *et al.* (2003) and Duffy (2005).

Chapter 2

Squat and Ship-Bank Interaction Prediction Techniques

2.1 Introduction

Existing prediction techniques for ship squat and ship-bank interaction are reviewed in Section 2.2.

The aim of the present study was to develop real-time simulation models for ship squat and ship-bank interaction. Due to the complex flow phenomena associated with vessel transit in restricted water the proposed methodology for real-time simulation was to use regression analysis techniques to develop empirical equations to predict steady-state forces and moments for use as input to quasi-steady mathematical models. However, predictions were also performed for steady-state cases using a three-dimensional panel method with the aim to determine if the method is sufficiently accurate to complement experimental measurements for input data to the regression analyses. In Section 2.3 background on the three-dimensional panel method is given along with details concerning the regression techniques used to develop the empirical equations.

A quasi-steady mathematical model has been developed to predict unsteady squat and associated acceleration effects in the vertical plane. An existing mathematical model was used to predict sway and yaw motions due to ship-bank interaction. Both models are outlined in Section 2.4.

2.2 Background

2.2.1 Steady-state prediction

A steady-state case is defined as a ship moving at constant speed in water of uniform depth, travelling parallel to straight uniform lateral banks.

Squat

Numerous techniques exist to predict steady-state vessel squat. These can be broadly classified into the following categories: prediction of water level depression, theoretically based prediction of sinkage and trim, semi-empirical prediction of sinkage and trim, and empirically based prediction of sinkage and trim.

Prediction of a uniform water level depression can be achieved through applying the continuity equation in conjunction with the conservation of energy (Bernoulli's equation) or conservation of momentum. The ship is replaced by a fixed obstacle whose cross section is uniform over its entire length; hence end effects are ignored. This is a simplified approach where the water level

depression is assumed to be equal to the ship sinkage, ignoring the trim of the vessel. This approach assumes that the flow is one-dimensional and the velocities of the water particles in any channel cross section are constant over that cross section. This technique is useful near the ship where the lengthwise-averaged water-level depression and ship's sinkage are similar. However, this assumption breaks down as the channel width becomes large with respect to the vessel beam.

The prediction of water level depression and back flow velocity using the momentum approach was undertaken by Sharp and Fenton (1968) and Bouwmeester (1977). The latter author accounted for the water level rise in front of the bow and made use of an empirical correction factor to improve the accuracy of the technique. Blaauw and Van Der Knaap (1983) compared predictions from the Bouwmeester method against model scale experiment sinkage results. The correlation was reasonable for channel width to vessel beam ratios between 5 and 8. They found that sinkage predictions from Sharp and Fenton's method were around 20% less than those of Bouwmeester.

Ship sinkage has been predicted by the water level depression technique using the continuity equation in conjunction with the conservation of energy by many authors, such as Balanin and Bykov (1965), Constantine (1961), Tothill (1967), McNown (1976) and Gates and Herbich (1977). These methods all yielded similar results, which showed reasonable correlation with measured sinkage values for channel width to vessel beam ratios less than 5. Vessel sinkage was under predicted using this prediction technique for greater channel width to beam ratios (Blaauw and Van Der Knaap 1983).

Tuck (1966) used slender body theory to predict vertical forces on slender ships in shallow water at both sub-critical and super-critical speeds, sinkage and trim were then calculated using ship hydrostatic particulars. The predictions showed reasonable correlation with scale model experiment results presented by Graff *et al.* (1964) for low water depth to ship length ratios and low depth Froude numbers. However, the correlation deteriorated for larger water depths and as the depth Froude number approached 1.0. Blaauw and Van Der Knaap (1983) found that Tuck's theory gave reasonable agreement with experimental results for channel width to vessel beam ratios between 6 and 13. It was found that trim correlated reasonably well with model experiment results, except for some cases with an LNG carrier model, where the wrong trim direction was predicted. Hooft (1974) proposed a modified version of Tuck's formula to compute bow squat and Huuska (1976) proposed new coefficients, for Hooft's formulae, and introduced a blockage correction factor. Vermeer (1977) proposed approximations to the coefficients in Tuck's formulae to predict sinkage and trim for ships in narrow canals. Tuck (1967) extended his earlier work to account for the presence of vertical side walls, but only for sub-critical flow, with the assumption that the channel width is comparable with the ship length. The work was extended further by Tuck and Taylor (1970) to a three-dimensional squat theory for water of finite depth and width. Slender body theory was further utilised to predict squat for the case of a ship travelling in a dredged channel (Beck *et al.* 1975).

Further theoretical approaches have followed the work based on Tuck's theory. For example, Pettersen (1982) presented a numerical method for computing steady-state potential flow past an arbitrary body moving horizontally in shallow water with the free surface replaced by a rigid wall. The flow around the middle of the ship was treated as two-dimensional and around the bow and stern as three-dimensional. Results from the method were found to, generally, be in good agreement with experimental data for the Tokyo Maru from Fujino (1972). Naghdi and

Rubin (1984) used a two-dimensional theory to predict steady-state squat in shallow water based on non-linear directed sheet theory. Good agreement was found with data from Graff *et al.* (1964) for ship length to water depth ratios of 3 and 4.8, but poorer correlation was observed when the ship length to water depth ratio was increased to 8. Kijima and Higashi (1996) presented a prediction method for ship squat considering non-linear terms on the effect of the free surface using slender body theory. The results of the numerical calculation on sinkage agreed well with model experiment results but showed an over estimation of trim. A simpler prediction method based on principal ship particulars was also presented by Kijima and Higashi (1996). The predictions using this simple prediction were reasonable when compared to model experiment results; however, it was concluded that further work is required to include the influence of a working propeller. Gourlay (2000) applied slender body theory to predict squat in open water of finite depth.

Semi-empirical techniques have been used to predict squat, where empirical correction factors were used in conjunction with numerical methods, for example Dand and Ferguson (1973), Fuehrer and Romisch (1977) and Ankudinov and Jakobsen (1996). Dand and Ferguson (1973) and Fuehrer and Romisch (1977) developed empirical correction factors to be used in conjunction with a one-dimensional theory based on the continuity equation and conservation of energy. Dand and Ferguson (1973) made use of an effective width parameter developed by Tuck (1967) and also developed propulsion correction factors. They obtained full-scale measurements from a number of ships and compared the results to their predictions. The comparisons were encouraging given the practical limitations of the accuracy of the full-scale results. Blaauw and Van Der Knaap (1983) compared the predictions from Dand and Ferguson and Fuehrer and Romisch with measured squat values. They found that the predictions using the method proposed by Dand and Ferguson showed reasonable correlation with model experiment results for channel width to vessel beam ratios between 7 and 13. The predictions were found to underestimate squat for channel width to beam ratios less than 7. The Fuehrer and Romisch approach was found to generally over predict squat. However, Millward (1990), on comparing Fuehrer and Romisch's prediction to model scale experiments found that it underestimated bow squat by up to 50%, but was more accurate for midship sinkage.

Model scale experiments have been used extensively to develop empirical equations for the prediction of ship squat in laterally unrestricted water (Soukhomel and Zass 1958; Eryuzlu and Hausser 1978; Barrass 1979; Millward 1990). Blaauw and Van Der Knaap (1983) compared the prediction methods of Soukhomel and Zass (1958), Eryuzlu and Hausser (1978) and Barrass (1979) to experimental results for self-propelled models of a VLCC ($C_B=0.85$) and an LNG carrier ($C_B=0.74$). It was found that results from Soukhomel and Zass's method over predicted measured squat. The Eryuzlu and Hausser prediction technique correlated satisfactorily with model scale results for channel width to vessel beam ratios between 6 and 13. For the Barrass method it was found that the predictions correlated reasonably well for a VLCC where the bow squat dominated, but the correlation was poor for an LNG carrier. Millward (1990) found that Soukhomel and Zass's method was reasonably accurate for full form vessels but overestimated squat for fine form vessels, whilst Millward found that Eryuzlu and Hausser's method was reasonably accurate for full form vessels but overestimated squat for fine form vessels. Millward's (1990) formulae predictions were compared to published data for the ferry Herald of Free Enterprise; good agreement was observed, with a tendency to overestimate the squat at high depth Froude numbers.

Model scale experiments have also been used to develop empirical equations for ship squat in laterally restricted water. For example, Blaauw and Van Der Knaap (1983) conducted experiments in a flume tank with self-propelled scale models of a VLCC and an LNG carrier for a number of different channel widths and water depths. They measured the water-level depression near the model and near the lateral bank, and developed an empirical equation to describe the relationship between the water-level depression at the ship and the lateral bank. Barrass (1979), Millward (1992), and Eryuzlu *et al.* (1994) developed empirical formulae to predict squat in laterally restricted water of finite depth.

Collinson (1994) compared the results from well known published sinkage and trim prediction techniques against experimental results from Millward (1990, 1992) and found that the predictions produced a large divergence of results and that no single prediction technique provided the best correlation for all cases. He stated that no single method accurately predicted squat for all ships and conditions. Dand (1996) compared squat prediction methods for typical ships. It was found that there was a wide scatter in the results, although there was some evidence of 'common ground' near the centre of the scatter.

Ship-bank interaction

There have been a number of simplified bank effect prediction techniques developed based upon model scale investigations. For example, Schoenherr (1960) used model scale experiment results to develop design charts, from which bank induced sway force and yaw moment could be determined for a range of channel parameters. Fuehrer and Romisch (1983) conducted a comprehensive set of model scale experiments on models fitted with propellers and rudders. An empirical equation for the prediction of rudder force was developed along with a series of diagrams for calculating lateral forces and yaw moment acting on a ship for different channel widths at various drift angles. The diagrams were based on the equilibrium of lateral hydrodynamic forces acting on a ship and can be used to determine optimum channel profiles. The predictions were found to correlate well with experiment results published by Gates and Herbich (1977).

Several empirical equations have been developed to predict bank induced sway force and yaw moment utilising linear superposition of the effect of port and starboard banks. Norrbin (1985) presented empirical equations to predict bank induced sway force and yaw moment valid for water depth to draught ratios as low as 1.1 for surface piercing banks, which included the effect of ship speed, ship to bank distance, draught to water depth ratio and bank slope. Ch'ng (1991) developed empirical equations for the prediction of steady-state bank induced sway force and yaw moment for surface piercing banks down to a water depth to draught ratio of 1.2. These formulae accounted for the same variables as Norrbin's equations, and included the effect of hull form and propulsion. Vantorre (1995) found that Ch'ng's empirical formulae significantly over predicted bank induced sway force and yaw moment when extrapolated to a water depth to draught ratio of 1.1. Vantorre (1995) proposed empirical mathematical models for surface piercing banks for a number of different water depth to draught ratios for bank induced sway force and yaw moment.

A number of potential flow solutions have been developed to predict steady-state bank induced forces. For example, Hess and Smith (1962) developed a potential flow solution, ignoring free surface effects to predict bank induced force. Newman (1965), using slender body theory, presented a technique to predict bank induced sway force for a slender body of revolution in

deep water near an infinitely long wall. Newman (1972) developed a numerical technique using an approximate method of source images to predict the non-circulatory force on slender ships moving alongside vertical surface piercing side banks or between parallel walls in shallow water. Norrbin (1974) compared model experiment results to Newman's approximate method for an ore/oil carrier. It was found that the predictions underestimated the lateral force by approximately 40%. Tuck and Newman (1974) developed a numerical prediction technique for interaction forces between two slender ships by extending the work of Newman (1972) to include the presence of a large circulatory force in compliance with the requirements of the Kutta trailing edge condition. Predictions from this method were found to be in better agreement with experimental results. This theory was applied to the case of a ship travelling alongside a lateral bank by Beck (1977) and Hess (1978). Chen and Sharma (1994) used slender body theory in the near field and a non-linear shallow water wave theory in the far field to investigate the general problem of a ship moving off the centreline of a shallow channel at sub-, trans- and super-critical speeds. The theory was based on the technique of matched asymptotic expansions. Numerical examples were conducted for the case of a ship travelling off the centreline of a channel without drift angle and for the case of a ship travelling in oblique motion along the channel centreline. The computed longitudinal force, sinkage, trim, lateral force and yaw moment were found to be in reasonable agreement with experimental results. The flow around a ship operating in water restricted in depth and width was investigated by Xiong and Wu (1996). The free surface wave patterns and bank induced forces on a ship were predicted using a three-dimensional Rankine source method. Miao *et al.* (2003) used a modified version of Dawson's (1977) method to predict bank induced sway force and yaw moment when a ship travels off the centerline of a rectangular channel. Rankine sources were distributed over the vessel and channel boundary surfaces and the free surface condition was linearised in terms of double body model solutions. The correlation with model experiments from Duffy (2002) was reasonable for water depth to draught ratios down to 1.5. However, for lower water depth to draught ratios the correlation was found to be poor.

2.2.2 Unsteady prediction

The following definitions apply to unsteady squat and unsteady ship-bank interaction for the present work. Unsteady squat is the sinkage and trim experienced by a vessel travelling on the centreline of a symmetrical channel that has non-uniform depth along its longitudinal axis. The water depth is considered uniform along the transverse axis of the channel. Unsteady ship-bank interaction is defined as the sway force and yaw moment experienced by a vessel travelling parallel to non-uniform vertical banks, or travelling at an angle to uniform or non-uniform lateral banks.

Squat

Prediction of unsteady squat and the effect of associated vertical plane accelerations have received little attention in previous work in comparison to steady-state squat. A common approach to unsteady squat is to treat it as a steady-state problem and assume that the ship speed and water depth are both sufficiently slowly varying functions of time to neglect unsteadiness (NTSB 1993). This is partly due to the fact that currently the best estimate of squat in non-uniform depth is to use the average water depth under the ship in constant depth formulae (Gourlay 2003). However, if the bottom topography varies rapidly as a function of time the transient behaviour of the vessel must be considered to provide prediction of sufficient accuracy (Hatch 1996; Duffield 1997; Drobyshevskiy 2000; Gourlay 2003). Specific examples of cases

where ship grounding has been partly attributed to unsteady squat include the grounding of the MV Wellpark in 1977 and the grounding of the QE2 in 1992 (Ferguson *et al.* 1982; USCG 1993).

Examples of numerical techniques proposed for the prediction of unsteady squat include Plotkin (1976a, 1976b), Tuck (1976), Mei and Choi (1987), Gourlay and Tuck (1998), Drobyshevskiy (2000) and Gourlay (2000, 2003). Plotkin (1976a, 1976b) presented a technique to predict squat for a slender-ship travelling over a bottom topography that varied sinusoidally with small amplitude in the direction of travel only. Tuck (1976) discussed the extension of variable depth slender body theory to include depth changes transverse to the direction of travel. Mei and Choi (1987) used the technique of matched asymptotics to predict the sinkage and trim of a slender ship near the critical speed in a wide canal for an unsteady case. On comparison with measured values it was found that their predictions overestimated sinkage and trim. Gourlay and Tuck (1998) and Gourlay (2000, 2003) presented one-dimensional theories to predict vessel squat in a channel with non-uniform water depth for simplified bottom topographies, which are valid for cases where the channel width is similar to the vessel beam. Drobyshevskiy (2000) and Gourlay (2000, 2003) applied slender body theory to develop prediction techniques for unsteady heave force and pitch moment due to squat in non-uniform water depth for simplified bottom topographies, which were valid for wider channels and open water. However, both Drobyshevskiy (2000) and Gourlay (2000, 2003) used vessel hydrostatic calculations to predict the sinkage and trim, neglecting dynamic acceleration effects.

Renilson and Hatch (1998) developed a quasi-steady mathematical model, based on Newton's second law of motion, to predict the sinkage and trim and dynamic vertical plane acceleration effects of a vessel travelling over an undulating bottom in the time domain. The steady-state midship sinkage and trim were predicted using empirical formulae from Millward (1990). Renilson and Hatch found that the correlation with experiments was reasonable for steady-state conditions; however, the correlation with model experiments was poor for cases with an undulating bottom.

Ship-bank interaction

As for ship squat, the prediction of ship-bank interaction for unsteady cases has received less attention in previous work compared to steady-state cases. A common treatment for the simulation of unsteady ship-bank interaction is to use a quasi-steady approach, whereby steady-state forces and moments are inputs to a mathematical model to predict sway and yaw motions in the time domain. Norrbin (1971) outlined a ship manoeuvring simulation model with emphasis on the behaviour of large tankers in harbour entrances and canals. The prediction technique was based on that derived for the ship in deep and unrestricted water, adding the effects of shallow water, and of port and starboard lateral restrictions. The model was extended to cases with slowly widening and bending canals. Norrbin (1978) extended the model further for the computer simulation of ship-in-canal handling problems for fast or real-time fairway studies. The method accepted isolated or step-wise offset side banks of finite length for surface piercing banks. Semi-empirical corrections were used to account for the effect of water depth to draught ratio and bank submergence. Predictions from the model for a tanker passing a short bank were verified using measurements on a propelled model with reasonable correlation being observed.

Analytical work on the hydrodynamic interaction of a ship in a restricted waterway with uniform water depth and non-uniform vertical surface piercing banks has been undertaken by several authors. For example, Yeung and Tan (1980) and Hsiung and Gui (1988) presented techniques based on slender body theory using matched asymptotics and a rigid free-surface boundary condition. Neither method was validated with experiment results. The hydrodynamic interaction forces acting on a ship in shallow water in the proximity of a non-uniform bank wall were predicted by Zhang and Wu (1998) using a numerical method based on the boundary element method.

2.2.3 Review of prediction techniques

Numerous techniques exist to predict steady-state squat. However, comparisons conducted by previous authors have revealed a large divergence in predictions and no single prediction technique provides the best correlation with squat measurements for all cases. Hence, empirical equations have been developed in this study from model scale experiments to predict steady-state heave force and pitch moment. These formulae have been used as input to the unsteady squat prediction technique. Background on the regression techniques used to develop the empirical input formulae is given in Section 2.3.1.

In comparison to steady-state squat there has been little previous work undertaken to develop prediction techniques for unsteady squat and the associated acceleration effects in the vertical plane. In existing numerical prediction techniques for unsteady squat in practical channel widths the dynamic acceleration effects in the vertical plane were neglected (Gourlay 2000, 2003; Drobyshevskiy 2000). Also, such techniques provide a solution to specific simplified bottom topographies but are not easily adaptable to more complex cases. Renilson and Hatch (1998) used a quasi-steady mathematical model to predict unsteady squat and dynamic acceleration effects based on the prediction of steady-state sinkage and trim from published empirical formulae. However, the correlation with unsteady model scale measurements was poor. In the present study a more direct approach has been developed than that used by Renilson and Hatch (1998), where the empirical formulae for heave force and pitch moment from the present study are used as inputs for a quasi-steady mathematical model. The proposed mathematical model is outlined in Section 2.4.1.

Norrbin (1985), Ch'ng (1991) and Vantorre (1995) presented empirical formulae for the prediction of steady-state sway force and yaw moment induced by surface piercing banks. In comparison to work conducted on the prediction of interaction with surface piercing banks, little work has been carried out to predict the influence of flooded banks. Norrbin (1978) presented a semi-empirical bank submergence correction factor, however there is a need for a prediction technique that can account for the influence of bank flooding for a wide range of channel geometries. Hence, empirical formulae have been developed to predict steady-state sway force and yaw moment induced by surface piercing and flooded banks.

The steady-state ship-bank interaction formulae have been incorporated into an existing quasi-steady mathematical model, as outlined in Section 2.4.2, to predict sway and yaw motion for a vessel travelling in a restricted waterway. Details concerning the mathematical model are given in Section 2.4.2.

2.3 Steady-state prediction

Methods used in this study to predict steady-state squat and ship-bank interaction are outlined in this section. Firstly, background is given on the regression analysis techniques used to develop empirical equations from model scale experiment results. Secondly, background is provided on a three-dimensional panel method that was assessed for the purpose of predicting steady-state squat and ship-bank interaction to extend the experimental data matrix for the regression analyses.

2.3.1 Regression analysis: squat and ship-bank interaction

The general aim of regression analysis is to evaluate the relationship between independent variables and a dependent variable. Regression analyses were performed on model experiment data to develop prediction techniques for steady-state squat and ship-bank interaction forces and moments to be used as input to quasi-steady mathematical models. The regression analyses were performed using the statistical analysis software package, Statistica for Windows Version 5.0 software (StatSoft 1994).

Statistical terminology

There are a number of statistical measures that are used in the regression process, and to assess the fit of a regression equation. Some of these are introduced in this section and used in following sections. Further information concerning statistical measures can be found in statistics literature or StatSoft (1994).

The relationship between variables has two basic formal properties: magnitude (size), described by correlation coefficient and reliability (truthfulness), described by statistical significance or p-level.

The correlation coefficient measures the magnitude of the relation between variables. It takes on a value of +1 and -1 for perfect positive correlation and positive negative correlation, respectively.

The p-level represents the probability of error that is involved in accepting the observed results as valid, that is, as representative of the population. For example, a p-level of less than 0.05 means that there is less than 5% probability of error, that is, the conclusion is more than 95% reliable. In many areas of research a p-level of 0.05 is customarily treated as a border-line acceptable error (Bojovic 1999).

The difference between a predicted and observed value is defined as the residual. Regression equations are developed by minimising a function of the residuals. Commonly the sum of the squared residuals is minimised, which is known as least squares estimation.

An indicator of how well the regression equation fits the experimental data is the coefficient of determination (R^2). This coefficient describes the variability of the residual values around the regression line relative to the overall variability and can have a value between 0 and 1. A value of 0.9, for example, indicates that the model succeeded in explaining 90% of the original

variability, while 10% variability is left unexplained. The coefficient of determination is given in Equation 2.1.

$$R^2 = 1 - (\text{Residual SS} / \text{Total SS}) \quad (2.1)$$

The adjusted coefficient of determination is obtained by dividing the residual sum of squares and total sum of squares by their respective degrees of freedom, as presented in Equation 2.2.

$$R^2_{\text{adjusted}} = 1 - [(\text{Residual SS} / \text{degree of freedom}) / (\text{Total SS} / \text{degree of freedom})] \quad (2.2)$$

The dispersion of the observed values about the regression line is measured by the standard error of estimate. A small standard error of estimate represents a low dispersion of observed values about the regression line.

Multiple linear regression analysis

In the present study multiple linear regression analysis techniques were used to produce empirical equations. This regression technique assumes a linear relationship between the independent variables, X_i , and the dependent variable W , as shown in Equation 2.3. Another requirement for this regression technique is that the residuals follow a normal distribution.

$$W = b_0 + b_1X_1 + b_2X_2 + \dots + b_pX_p \quad (2.3)$$

Where b_0, b_1, b_2, b_p are constants.

A model known as “non-linear in the variables” is utilised, where transformations of the independent variables are used, i.e. $X_2=X_1^2, X_3=X_1^3, X_4=X_1^4, \dots, X_n=X_1^n$. Such a model is still linear in terms of the unknown coefficients, b_i . The aim of multiple linear regression analysis is to fit the above mathematical model to the experimental data points. The regression coefficients are obtained by minimisation of the square of the residuals, known as least squares estimation. No variable may be linearly (directly) related to another variable, or the sum of the other variables in multiple linear regression analysis.

A forward stepwise regression technique has been used, which starts with a single independent variable in the model. At each succeeding step further independent variables are introduced based on significance testing. The variables with the greatest statistical significance relative to the dependent variable are added first. If a previously added variable becomes insignificant due to the addition of new variables the now statistically insignificant variable is removed from the regression. The above procedure is repeated until no significant independent variables can be found outside the regression model. The acceptance and rejection of variables is based upon statistical tests. The limits for these tests were adjusted to ensure that statistically insignificant variables were omitted from the regression model.

When conducting regression analysis, results could become unstable if highly correlated independent variables were included in the regression model. Setting the tolerance accordingly using the forward stepwise method means that high correlation between the initial set of independent variables can be overcome as the method itself will identify statistically significant independent variables.

The statistical significance of each independent variable in the regression model was assessed using a p-level measure. Limits were set such that the final regression model contained no variables with a p-level greater than 0.05 (5%). The standard error of estimate and the coefficient of determination were used to assess the fit of the regression equations.

Multiple linear regression analysis assumes linear relationships between the variables in the equation and a normal distribution of residuals. The normal probability plot of residuals has been used for each regression model to ensure that the two assumptions above have not been violated excessively. This plot has also been used to ensure that outliers have not seriously biased the regression equations.

Non-linear regression analysis

A non-linear regression technique has been used to establish the relationship between dependent and independent variables to determine the form of the independent parameters for the multiple linear regression analyses. In linear multiple regression analysis it was assumed that the relationship between the independent variables and the dependent variable is linear in nature. However, with the non-linear estimation module the user may specify the nature of the relationship between the independent variables and the dependent variable (for example, exponential or logarithmic relationships). The multiple linear regression model is just one of the possible estimation functions that can be used in non-linear estimation. In multiple linear regression analysis the loss function is set to be the sum of the squared residuals, whereas in the non-linear estimation module the user can specify the loss function.

2.3.2 Three-dimensional panel method

Squat and ship-bank interaction

The number of model scale experiments that could be conducted was limited by the resources and time required to perform them. Steady-state heave force and pitch moment due to squat and bank induced sway force and yaw moment have been predicted using a three-dimensional panel method. The aim was to compare the predictions to model scale experiment results to assess if the method was sufficiently accurate to be used to extend the steady-state experimental data matrix for the regression analyses. The predictions were performed using Shipflow 2.5, which is a three-dimensional panel method software package developed by Flowtech International AB specifically for flow around ship hulls (Larsson 1993).

In this section a brief overview of panel methods and the Shipflow computation methodology is provided. The co-ordinate system and nomenclature relevant to Shipflow are given in Figure 2.1. The Shipflow predictions are compared against model scale squat and ship-bank interaction measurements in Sections 3.11 and 5.9, respectively.

Panel methods may be used to solve potential flow, where arbitrary flow geometry is mathematically generated by distributing singularities over planes (panels) in the field. Sources can be distributed in such a way that a closed streamline is formed. Since there can be no flow over streamlines they can be thought of as boundaries of a body. The only thing that makes these 'streamline bodies' different from real bodies is that they have no boundary layer. It is necessary to determine the specific source distribution that, when combined with a uniform stream, will produce a streamline that coincides with the desired surface.

Panel methods cannot be used to directly account for viscous effects and ‘no slip’ conditions on solid surfaces. Therefore wakes downstream from the body, due to separation and boundary layers have to be computed using other methods. To account for this the flow is divided into three zones in the Shipflow computation method, as shown in Figure 2.2. Zone 1 represents the outer flow where potential flow theory is used with a free surface. The Shipflow potential flow model uses a panel method, where Rankine sources are used on the hull and part of the free surface. The panels are either flat with a constant source distribution or parabolic with a linearly varying source distribution. A momentum integral method is used in Zone II to account for the viscous effects in the boundary layer. A Reynolds-Averaged Navier Stokes model is used in Zone III to account for the viscous effects in the stern/wake flow. Unfortunately the methods in Zones II and III can only be applied to simplified cases where the flow around the ship is symmetrical. Therefore only the potential flow solution was used for the present study. The potential flow solution is valid for cases where the flow is inviscid, incompressible and irrotational. A brief description of the Shipflow computation method follows. A more detailed description can be found in Larsson *et al.* (1989) and Larsson (1993).

The flow field around a ship is described by a velocity potential. The velocities \bar{U} can be found from the velocity potential, Φ , from:

$$\nabla\Phi = \bar{U} \quad (2.4)$$

The continuity equation must be satisfied:

$$\nabla \cdot \bar{U} = 0 \quad (2.5)$$

Substituting the velocity potential into the continuity equation gives Laplace’s equation:

$$\nabla^2\Phi = \frac{\partial^2\Phi}{\partial x^2} + \frac{\partial^2\Phi}{\partial y^2} + \frac{\partial^2\Phi}{\partial z^2} = 0 \quad (2.6)$$

The potential satisfies the regularity condition at infinity, i.e. at infinite distance from the body the flow is undisturbed:

$$\nabla\Phi = \bar{U}_\infty \quad (2.7)$$

To generate a streamline that coincides with the body surface the fluid velocity component normal to the surface, evaluated at the wetted hull surface, must be zero, such that:

$$\frac{\partial\Phi}{\partial n} = 0 \quad (2.8)$$

Where n denotes the outward normal.

The velocity potential is generated by a distribution of sources over a surface S and by the uniform onset flow in the x -direction. The velocity potential at point, p , induced by a distribution of sources on a surface, S , at a distance, $r(p,q)$, for a uniform stream is given by:

$$\Phi(x, y, z) = \iint_S \sigma(q)/r(p, q) ds + \bar{U}_\infty x \quad (2.9)$$

Where $\sigma(q)$ is the source density on the surface element dS and $r(p, q)$ is defined as the distance from point q to the field point p (see Figure 2.1).

Since the sources automatically satisfy the Laplace equation (Equation 2.6) and the condition that the flow is undisturbed as the distance from the body approaches infinity (Equation 2.7), the source strengths are determined using boundary conditions on the hull and free surface. On the wetted portion of the hull the boundary condition specified in Equation 2.8 is enforced. There are two boundary conditions that need to be satisfied on the free surface panels. The first is a kinematic condition that the flow must be tangent to the surface, i.e. zero outflow through the free surface:

$$\frac{\partial \Phi}{\partial x} \frac{\partial \eta}{\partial x} + \frac{\partial \Phi}{\partial y} \frac{\partial \eta}{\partial y} - \frac{\partial \Phi}{\partial z} = 0 \quad (2.10)$$

The second boundary condition is a dynamic condition developed from the Bernoulli equation, which states that the pressure is constant at the free surface:

$$g\eta + \frac{1}{2} \left(\left(\frac{\partial \Phi}{\partial x} \right)^2 + \left(\frac{\partial \Phi}{\partial y} \right)^2 + \left(\frac{\partial \Phi}{\partial z} \right)^2 - U_\infty^2 \right) = 0 \quad (2.11)$$

An additional condition must be satisfied at the free surface, which is a radiation condition that states that no upstream waves must be generated. This is satisfied by using an upstream differencing method to calculate the potential derivatives.

The potential, Φ° , and the free surface elevation, η° , are computed for the double body case and are used as the base solution. The double body free surface elevation is obtained by rearranging Equation 2.11 and neglecting $\frac{\partial \Phi}{\partial z}$ due to symmetry:

$$\eta^\circ = \frac{1}{2g} \left(U_\infty^2 - \left(\frac{\partial \Phi}{\partial x} \right)^2 - \left(\frac{\partial \Phi}{\partial y} \right)^2 \right) \quad (2.12)$$

Small potential and free surface perturbations of the double body solution (based on Φ° and η°) are introduced:

$$\Phi = \Phi^\circ + \delta\Phi \quad (2.13)$$

$$\eta = \eta^\circ + \delta\eta \quad (2.14)$$

A linearisation of the free surface boundary conditions (by neglecting higher order terms) is obtained by introducing Equations 2.13 and 2.14 into 2.10 and 2.11. This gives:

$$\frac{\partial \Phi}{\partial x} \frac{\partial \eta^\circ}{\partial x} + \frac{\partial \Phi}{\partial y} \frac{\partial \eta^\circ}{\partial y} - \frac{\partial \Phi}{\partial z} + \frac{\partial \Phi^\circ}{\partial x} \frac{\partial \delta \eta}{\partial x} + \frac{\partial \Phi^\circ}{\partial y} \frac{\partial \delta \eta}{\partial y} = 0 \quad (2.15)$$

$$\delta \eta = -\left(\frac{1}{g}\right) \left(\frac{\partial \Phi^\circ}{\partial x} \frac{\partial \Phi}{\partial x} + \frac{\partial \Phi^\circ}{\partial y} \frac{\partial \Phi}{\partial y} - \left(\left(\frac{\partial \Phi^\circ}{\partial x} \right)^2 + \left(\frac{\partial \Phi^\circ}{\partial y} \right)^2 \right) \right) \quad (2.16)$$

The derivatives of η° and $\delta \eta$ with respect to x and y are obtained using finite difference formulae. By inserting the derivatives into Equation 2.15 and eliminating terms of $\delta \eta$ from Equation 2.16 the free surface boundary condition is simplified as a set of linear equations. The source strength on all panels (including the free surface) can then be obtained from a set of simultaneous equations. The fluid velocity and pressure at each panel can then be obtained by summing the influence from all panels. The free surface dynamic boundary condition is used to obtain the wave height. The Bernoulli-wave height is obtained from the double body solution (η°) given in Equation 2.12 and $\delta \eta$ is obtained from the linear solution, Equation 2.16. The free surface elevation can then be computed from Equation 2.14.

For the non-linear free surface computation the exact free surface boundary condition, given in Equations 2.10 and 2.11, is satisfied on the wavy surface. To achieve this, an iterative technique is used where the free surface panels in each iteration are moved to the wavy surface from the previous solution. This process is continued, always linearising about the previous solution, until the difference between the previous and new solutions is sufficiently small. At this point the iterations have converged and an exact boundary condition applied at the right position is approached.

Post analysis was performed to compute the sway force and yaw moment acting on the ship from the predicted pressure distribution over the hull surface using Equations 2.17 and 2.18.

$$Y = -\sum_{i=1}^m p_{di} A_i n_i \quad (2.17)$$

$$N = -\sum_{i=1}^m p_{di} A_i n_i x_i \quad (2.18)$$

Where n_i is the normal vector, p_{di} is the dynamic pressure on the i^{th} panel, A_i is the area of the i^{th} panel, m is the number of panels and x_i is the co-ordinate of the i^{th} panel.

The dynamic pressure was predicted in the Shipflow computations from Equation 2.19:

$$p_d = \frac{1}{2} \rho U_\infty^2 C_p \quad (2.19)$$

Where the dynamic pressure coefficient on each hull panel was obtained from the Bernoulli equation in the Shipflow computations:

$$C_p = \frac{p - p_\infty}{\frac{1}{2}\rho U_\infty^2} = 1 - \left(\frac{U}{U_\infty} \right)^2 \quad (2.20)$$

The computations above do not model the influence of lift. In panel methods lift can be introduced into the potential flow by applying the Kutta condition, i.e. developing a circulation of magnitude just sufficient to move the separation point to lie on the trailing edge of the lifting surface. To model circulation vortex distributions are applied to the body surface and the trailing wake. Using the technique developed for Shipflow the Kutta condition can only be applied to lifting surfaces with a defined trailing edge and not for stern geometries such as on the ships tested in the present study. Hence, the effect of lift was not modelled.

There are two ways that the bottom and lateral banks can be modelled: by symmetry or by panelisation. It is better to use symmetry if possible as there may be discretisation errors when using panelisation (Tornblom 2000). In the symmetrical approach the solution is obtained using a method of images, where the flow is computed as if there is a mirror image of the object on the other side of the symmetry plane. This approach can be used for symmetry about the x-z plane, but can only be used for symmetry about the x-y plane if the double-body model solution is used. Symmetry in the x-z plane could not be used for cases where the ship was off the centreline of the channel; therefore, for consistency, the lateral banks were panelised for all cases in the present study. The bottom was also panelised for consistency, since the double-body solution was not valid for all cases.

In the present study the lateral banks and floor of the towing tank were meshed as separate environment groups. The ship hull was meshed in two parts; one for the main hull (bow to 84% L_{OA} aft of bow) and the other for the stern region (84% L_{OA} aft of bow to transom). This improved the panel distribution over the stern part of the ship, which is important for computation of the pressure distribution. The free surface mesh was modelled over the full width of the towing tank with three different sections; upstream (from 0.5 L_{PP} forward of the bow to the bow), adjacent (from bow to stern) and downstream (from the ship stern to 1.9 L_{PP} aft of the ship stern). Panel density studies were conducted to optimise the number of panels and aspect ratio of panels. The meshes were modified in a systematic manner until the solution converged. The final panel density for a case with a channel width to beam ratio of 3 and a water depth to draught ratio of 1.4 is given in Table 2.1. The number of panels on the environment groups was varied according to the channel width and water depth.

| Each channel wall | Channel bottom | Hull main body | Hull stern | Free Surface | | |
|-------------------------|-------------------|----------------------|---------------|--------------|----------|------------|
| | | | | Upstream | Adjacent | Downstream |
| 150 | 800 | 1800 | 450 | 550 | 900 | 1100 |

Table 2.1 Number of panels for a Shipflow mesh, $W/B=3$, $h/d=1.4$

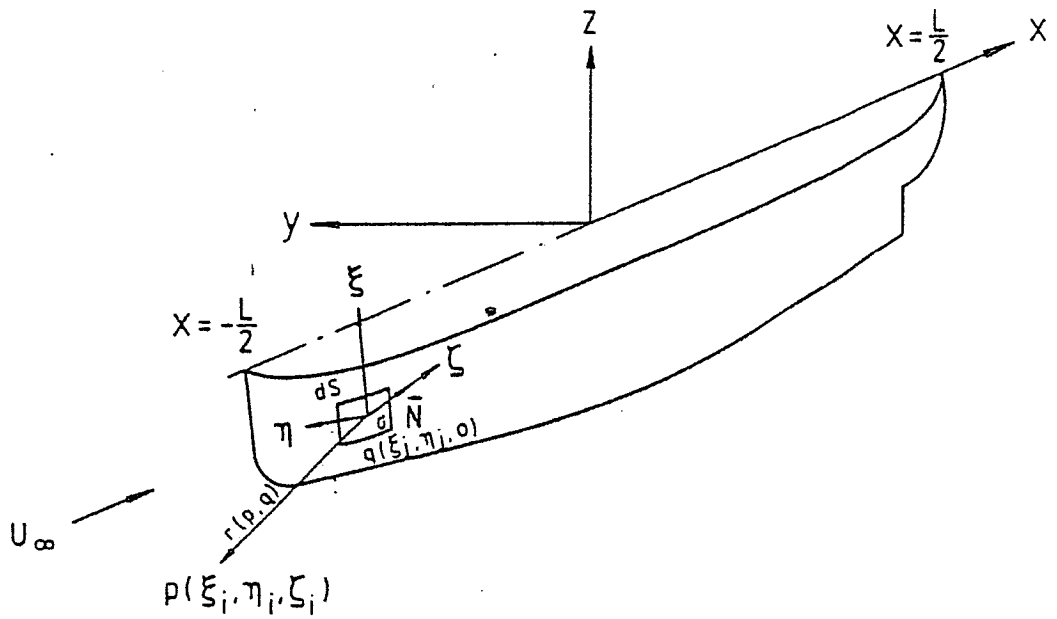


Figure 2.1 Shipflow co-ordinate system (Larsson *et al.* 1989)

ZONE I: PANEL METHOD (FREE SURFACE)

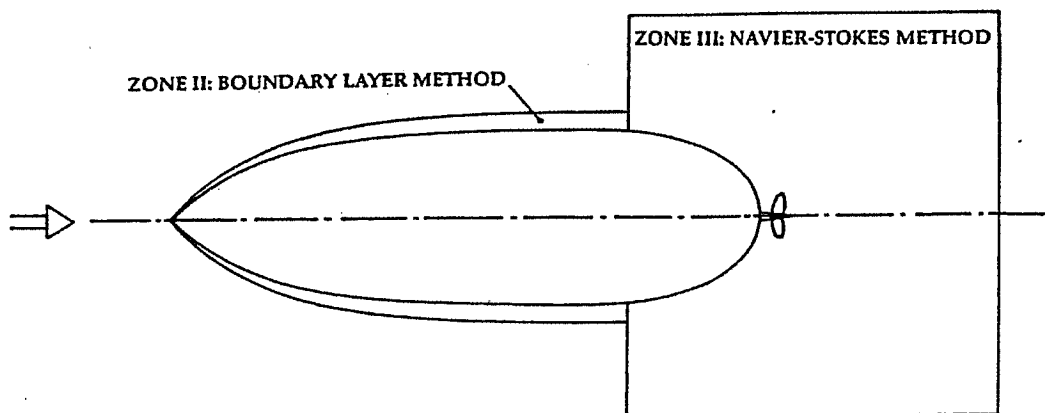


Figure 2.2 Flow zones used in Shipflow (Larsson 1993)

2.4 Unsteady prediction

The quasi-steady squat mathematical model developed in the present study and the existing ship-bank interaction quasi-steady mathematical model used in the present study are both outlined in the following sections.

2.4.1 Squat

One of the aims of the present work was to predict the squat and associated dynamic acceleration effects in the vertical plane on a vessel travelling in water of non-uniform depth. To achieve this a two-degree of freedom time domain mathematical model has been developed based on a quasi-steady approach where steady-state forces and moments are used to predict unsteady sinkage. A flowchart of the mathematical model is given in Figure 2.3.

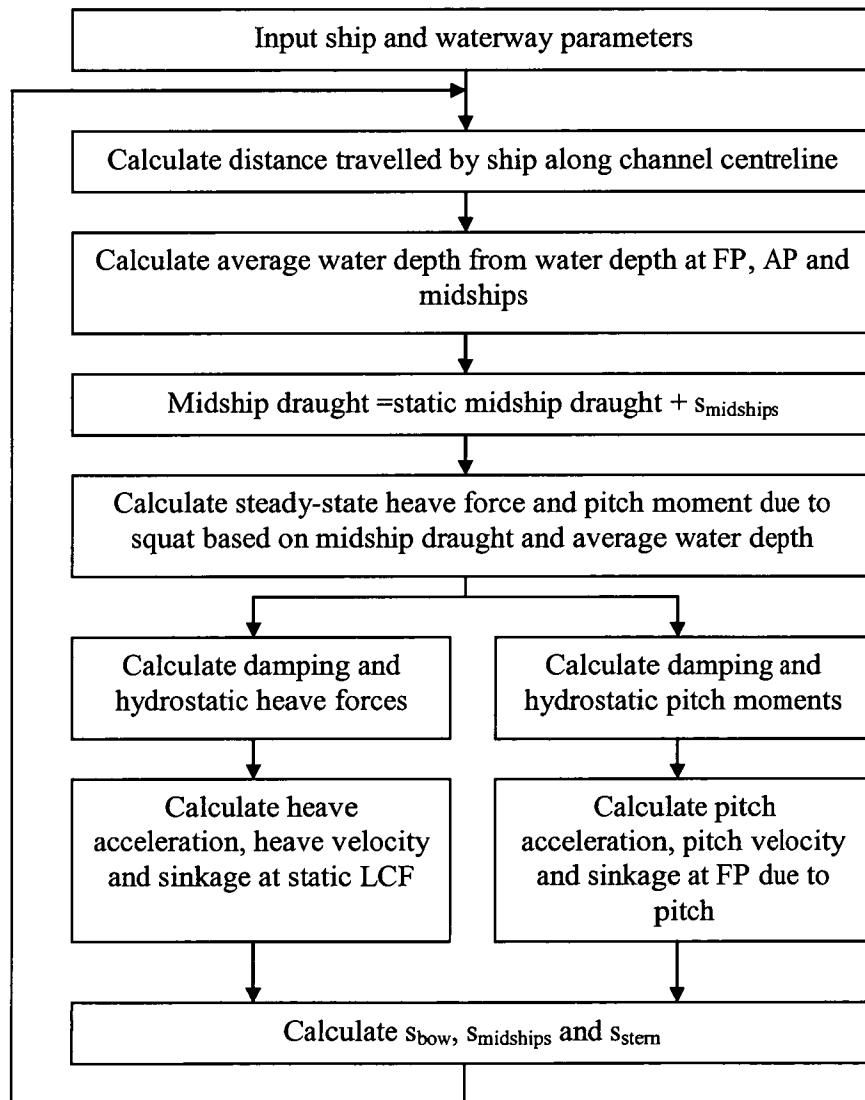


Figure 2.3 Squat mathematical model flow chart

The forces and moments acting on the ship were expressed using Newton's second law of motion:

$$(\Delta + \delta\Delta)\ddot{z}_{LCF} = Z + Z_{hydrostatic} + Z_{damping} \quad (2.21)$$

$$(I_{yy} + \delta I_{yy})\ddot{\theta} = M + M_{hydrostatic} + M_{damping} \quad (2.22)$$

It was assumed that the ship trimmed about the static LCF. This was consistent with the hydrostatic computations and is expected to have little influence on the predicted ship motions as the dynamic acceleration at the centre of gravity is expected to be small and, typically, the longitudinal distance between the static LCF and centre of gravity is small for the type of ships considered. The location of the static LCF was assumed to be constant for small changes in ship draught. At each time step the average water depth was computed based on the water depth at the forward perpendicular, aft perpendicular and midships. The squat at midships was predicted at each time step to give the instantaneous midship draught. The steady-state heave force and pitch moment due to squat (Z and M) were predicted at each time step based on the average water depth, instantaneous midship draught, vessel speed and channel width using empirical formulae developed in Chapter 4.

The hydrostatic heave force and pitch moment were predicted at each time step using Equations 2.23 and 2.24, respectively. Constant values of TPC and MCTC were used, i.e. the variation of TPC and MCTC with vessel draught was neglected.

$$Z_{hydrostatic} = -z_{LCF} \cdot TPC \cdot g \quad (2.23)$$

$$M_{hydrostatic} = -\theta \cdot MCTC \cdot g \quad (2.24)$$

The effects of damping were computed at each time step using Equations 2.25 and 2.26. Heave and pitch damping coefficients, γ_{heave} and γ_{pitch} , were obtained from Vugts (1968).

$$Z_{damping} = -\dot{z}_{LCF} \cdot \gamma_{heave} \quad (2.25)$$

$$M_{damping} = -\dot{\theta} \cdot \gamma_{pitch} \quad (2.26)$$

The heave acceleration at the static LCF was calculated from Equation 2.21. The sinkage at the static LCF was obtained from double integration of the heave acceleration, as shown in Equations 2.27 and 2.28. Since the accuracy of the integration technique used in the mathematical model was sensitive to the magnitude of the time step, a convergence study was performed to determine the optimum time step.

$$\dot{z}_{LCF} = \ddot{z}_{LCF} \cdot dt + \dot{z}_{LCF0} \quad (2.27)$$

$$z_{LCF} = \dot{z}_{LCF} \cdot dt + z_{LCF0} \quad (2.28)$$

The pitch acceleration was obtained from Equation 2.22. Equation 2.29 was used to determine the pitch velocity and the linear heave velocity at the forward perpendicular due to pitch velocity was obtained from Equation 2.30. The sinkage at the forward perpendicular due to pitch was found by integration of the linear heave velocity using Equation 2.31. Sinkage at the bow, stern and midships was calculated using Equations 2.32, 2.33 and 2.34, respectively. The sinkage at the bow and stern was taken at the forward perpendicular and aft perpendicular, respectively.

$$\dot{\theta} = \ddot{\theta}.dt + \dot{\theta}_0 \quad (2.29)$$

$$\dot{Z}_{FP} = x_{LCF-FP} \cdot \dot{\theta} \quad (2.30)$$

$$Z_{FP} = \dot{Z}_{FP}.dt + Z_{FP0} \quad (2.31)$$

$$S_{bow} = Z_{LCF} + Z_{FP} \quad (2.32)$$

$$S_{stern} = S_{bow} + (L_{pp} \cdot \sin(\theta)) \quad (2.33)$$

$$S_{midships} = Z_{LCF} + (x_{mid-LCF} \cdot \sin(\theta)) \quad (2.34)$$

The time domain heave force and pitch moment traces obtained from captive model experiments over simplified bottom topographies have been used as input to the mathematical model, as reported in Chapter 4. For these cases the mathematical model was modified to accommodate the different force and moment input.

2.4.2 Ship-bank interaction

One of the aims of the present study was to develop a technique to simulate the effect of ship-bank interaction for a vessel operating in restricted water. This was achieved by developing equations to predict steady-state ship-bank interaction for input to an existing simulation mathematical model used in the AMC ship-handling simulator based on the method presented by Norrbin (1971), which is briefly outlined in this section.

The balance of all forces and moments acting on the ship's hull at each time instant was used to calculate the appropriate accelerations. The differential equation system was numerically integrated in steps (Euler-Cauchy) to give the instantaneous position and course of the ship. The sway force and yaw moment acting on the ship for the calm water case were provided by Equations 2.35 and 2.36. Note that the origin is taken as the centre of gravity for these equations. The surge force was also modelled, but the equations are not given here.

$$\Delta \left(\dot{v} + u \dot{\psi} \right) = Y_{Hull} + Y_{Rudder} + Y_{Wind} + Y_{Current} + Y_{Bank} \quad (2.35)$$

$$I_{ZZ} \ddot{\psi} = N_{Hull} + N_{Rudder} + N_{Wind} + N_{Current} + N_{Bank} \quad (2.36)$$

The hull forces and moments (Y_{Hull} and N_{Hull}) were calculated on the basis of hydrodynamic coefficients for deep unrestricted water, as shown in Equations 2.37 and 2.38 using notation adopted by Norrbin (1971).

$$Y_{Hull} = \Delta \cdot Y''_{\dot{v}} \dot{v} + \Delta \cdot L_{PP} \cdot Y''_{\ddot{\psi}} \ddot{\psi} + \Delta \cdot Y''_{u\dot{\psi}} u \dot{\psi} + \frac{\Delta}{L_{PP}} Y''_{uv} |u|v + Y''_{non-linear} \quad (2.37)$$

$$N_{Hull} = \Delta \cdot L_{PP}^2 \cdot N''_{\ddot{\psi}} \ddot{\psi} + \Delta \cdot L_{PP} \cdot Y''_{\dot{v}} \dot{v} + \Delta \cdot L_{PP} \cdot N''_{u\dot{\psi}} u \dot{\psi} + \Delta \cdot N''_{uv} uv + N''_{non-linear} \quad (2.38)$$

The non-linear terms ($Y''_{non-linear}$ and $N''_{non-linear}$) were calculated differently depending upon whether the ship turning point was aft, on the ship, or forward (Norrbin 1978).

The coefficients in Equations 2.37 and 2.38 were corrected based on the instantaneous draught to under keel clearance ratio to account for shallow water effects.

The rudder forces and moments (Y_{Rudder} and N_{Rudder}) were calculated using the rudder area, rudder efficiency, lift and drag coefficients and the actual velocity of water flow acting on the rudder, including the propeller induced flow.

The relative wind was calculated from the atmospheric wind and the ship's speed. The forces and moments due to wind acting on the ship (Y_{Wind} and N_{Wind}) were then predicted from the relative wind and the areas of the ship exposed to wind.

A mean current velocity was calculated over the ship hull, which was used to predict the influence of current on the sway force and yaw moment acting on the ship ($Y_{Current}$ and $N_{Current}$).

The sway force and yaw moment induced by lateral banks (Y_{Bank} and N_{Bank}) were developed in the present study. Input of these steady-state predictions to the mathematical model yielded a quasi-steady bank effect prediction approach. This should be reasonably accurate when used to predict bank induced sway force and yaw moment for slow speed cases where a quasi-steady assumption is valid.

The effects of squat will change the instantaneous draught to under keel ratio. The ship-bank interaction was calculated at each time step based on the instantaneous draught to under keel clearance ratio, including the change in draught to under keel ratio due to squat.

Chapter 3

Squat Experiments

3.1 Introduction

Model scale experiments were conducted in the AMC towing tank facility to investigate both motions and forces in the vertical plane due to squat. Details concerning the towing tank facility are given in Appendix A.

A series of steady-state tests were conducted in water of uniform depth. Firstly, the effect of model size on the measurement of squat was investigated to gain a clearer understanding of scale effects and assess whether appropriate model sizes were being utilised. The effect of channel width, water depth, vessel draught and propulsion on heave force and pitch moment was investigated. The aim was to develop empirical formulae for input to the mathematical model outlined in Section 2.4.1 and to assess the accuracy of an existing prediction technique.

Model scale tests were also conducted to measure unsteady squat in non-uniform water depths using simplified two-dimensional bottom topographies, i.e. ramped banks and steps. These tests, conducted in conjunction with an AMC final year naval architecture undergraduate student, Duffield (1997), used both semi-captive and captive models to measure heave force and sinkage, respectively. The force measurements were used as input to the mathematical model outlined in Section 2.4.1, whilst the motion measurements were used to validate the mathematical model.

The measurements obtained using the full towing tank width may not correspond to an infinite width case; these results have not been corrected to correspond to infinite width in this thesis. However, this can be achieved using an effective channel width (Tuck 1967).

3.2 Ship models

Four different ship models were used in the study: three bulk carrier models and a containership model. The bulk carrier models were based on generic bulk carrier hull forms from the MarAd systematic series (Roseman 1987). The majority of the tests were conducted with a MarAd L series bulk carrier, which was tested at a range of draughts. For the scale effect investigation two different size MarAd F series bulk carrier models were tested. The containership hull form was an S-175 containership (ITTC 1987). The principal particulars of the models are given in Table 3.1, with body plans shown in Appendix B. The hull forms chosen for the present work represent large ships and were selected based on ship types that are most commonly used on ship-handling simulators. A greater emphasis was placed on testing large full form ships because squat may have a significant influence on the operation of such ships in restricted water. However, it should be noted that squat may influence the handling characteristics of smaller ships with different hull forms operating in water that is shallow with respect to ship draught. The effect of squat on the handling characteristics of a ship will vary, dependent upon the ship form (Millward 1990).

The MarAd F and S-175 models were not fitted with a rudder or propeller for any tests. The majority of the tests conducted with the MarAd L model were without a propeller and rudder fitted. However, a series of tests was conducted with the MarAd L model with a 0.05 metre diameter propeller to investigate the effect of propulsion on squat (Duffy and Renilson 2000). A photograph of the propeller is shown in Appendix B.

| Ship model particulars | MarAd L | MarAd F (1) | MarAd F (2) | S-175 |
|------------------------|---------------|-------------|-------------|-------|
| L_{pp} (m) | 1.698 | 2.000 | 4.000 | 1.750 |
| B (m) | 0.340 | 0.360 | 0.720 | 0.254 |
| d (m) | 0.077 – 0.094 | 0.121 | 0.242 | 0.077 |
| Δ (kg) | 34.6 – 45.7 | 74.2 | 593.6 | 24.1 |
| C_B | 0.85 | 0.85 | 0.85 | 0.57 |

Table 3.1 Principal particulars of ship models

According to ITTC procedure 7.5-02-05-01 (ITTC 2002), boundary layer turbulence stimulation is recommended when the Reynolds number, based on hull length, is less than 5×10^6 . Given the waterline length of the models and the range of speeds tested, Reynolds numbers below this level were unavoidable. Thus turbulence stimulation studs were attached to the models to induce turbulent flow with their locations based on recommendations outlined in ITTC procedure 7.5-01-01-01 (ITTC 2002).

The Froude law of similitude was used to satisfy geometric and inertia scaling requirements. The model speeds were selected so as to resemble those of full-scale ships manoeuvring in restricted water conditions. The models were towed from the projected thrust line for all tests. The ballasting and trimming of the models was conducted as per ITTC Recommended Procedure 7.5-01-01-01 (ITTC 2002).

3.3 Bank models

Vertical walls were constructed on both the port and starboard sides of the ship model in the AMC towing tank to enable the effect of channel width on vessel squat to be quantified. The vertical walls pierced the free surface and could be moved laterally in the tank to simulate different channel width to vessel beam ratios. The banks were constructed from galvanised steel and stiffened with Dexion frames.

Two-dimensional ramp and step banks were constructed, covering the full width of the towing tank, to investigate unsteady squat. Both banks had vertical trailing edges for simplification and were constructed from galvanised steel. The ratio of bank height to vessel draught was held constant at a value of 3. A schematic of the banks is shown in Figure 3.1.

All banks were sealed at intersections between bank sections and at the intersection of the banks and the towing tank. Further details concerning the banks can be found in Appendix C.

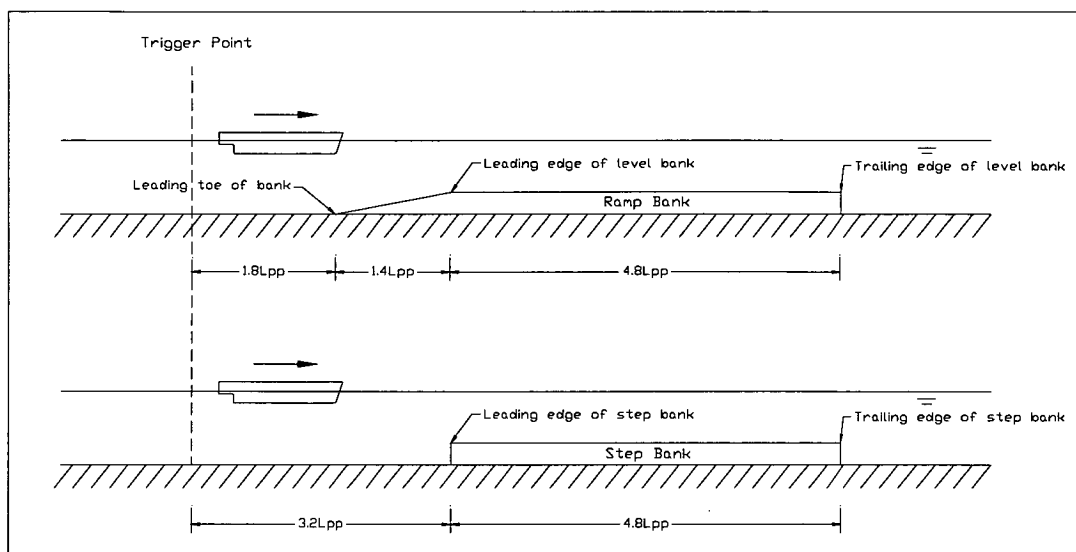


Figure 3.1 Schematic of simplified bank geometries for unsteady squat tests

3.4 Test rigs

3.4.1 Test rig to measure sinkage, trim and surge force

The ship models were constrained in sway, yaw, and surge and were free to heave, pitch and roll. A schematic of the model setup is shown in Figure 3.2. The model was connected to the carriage by counter-balanced forward and aft posts; the forward post was attached to the model using a ball joint and the aft post was attached using a ball joint and slide to prevent it from applying a longitudinal force. The forward post was fitted with a force transducer to measure drag and both counter-balanced posts were fitted with linear variable differential transformers to measure the displacement of the posts in the vertical plane.

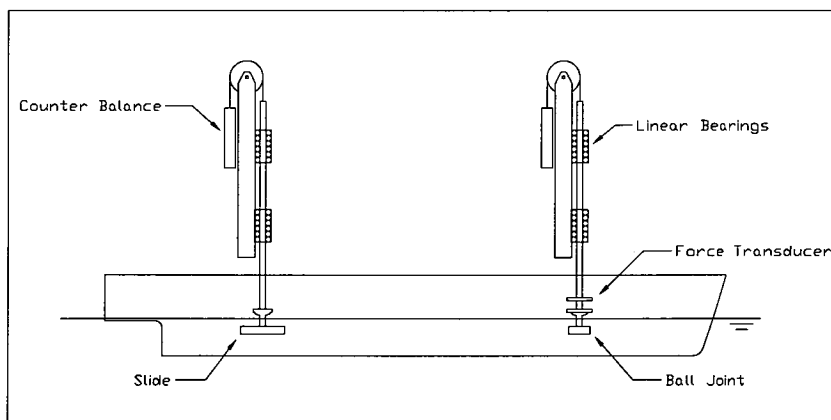


Figure 3.2 Schematic of model setup for measurement of sinkage, trim and surge force

3.4.2 Test rigs to measure forces and moments

Two different test rigs were used to measure the forces on the model in the vertical plane. For both rigs the model was constrained in surge, heave, sway, pitch and yaw and was free to roll, with the models connected to the carriage by forward and aft posts.

The first rig was used only for the unsteady squat tests. Both posts were attached to the model via a slide and were fitted with single axis force transducers to measure the heave force at the posts. The model was towed from a centre post to prevent crosstalk on the single axis force transducers. A schematic of this test rig is shown in Figure 3.3.

The second test rig was used for the remainder of the tests where forces were measured. The forward post was attached to the model using a ball joint and the aft post was attached using a ball joint and slide to prevent it from applying a longitudinal force. Both posts were fitted with multi-axis force transducers to measure the force at the forward and aft posts. A schematic of this test rig is shown in Figure 3.4.

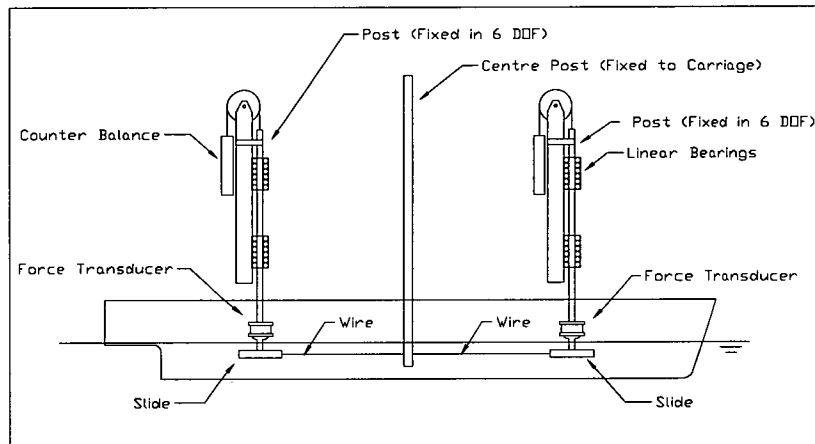


Figure 3.3 Schematic of model setup for measurement of heave force and pitch moment for unsteady squat tests

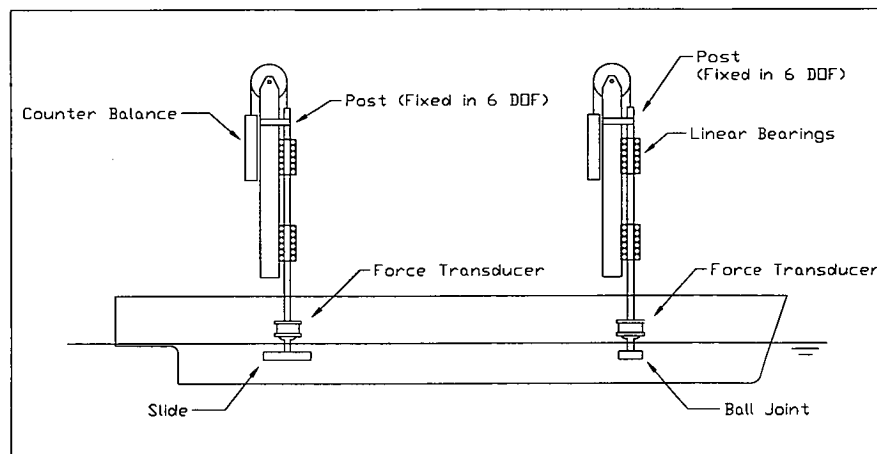


Figure 3.4 Schematic of model setup for measurement of forces and moments

3.5 Instrumentation

The vertical displacement of the forward and aft posts was measured using two Schaevitz 5000 HR linear variable differential transformers (LVDTs). The LVDTs were calibrated on a daily basis and included all items of the measurement chain, including signal conditioner, amplifier, filter and analog to digital converter. For each device the range of calibration exceeded the range of values measured in the experiments and the calibration factors varied less than 0.5% for each test program.

For the unsteady squat tests the heave force at the forward and aft posts was measured using RSC z-type single axis force transducers. For the remainder of the tests the heave force at the forward and aft posts was measured using AMTI MC3A-X-100 multi-component force transducers. The force transducers were calibrated every three to four hours and again included all items of the measurement chain. The range of calibration exceeded the range of values measured in the experiments and the calibration factors varied less than 0.5% over the entire test program. In cases where the force transducers experienced loads in multiple directions tests were conducted to ensure that crosstalk did not adversely affect the force measurements. For example, calibrations were performed for vertical force both with and without a surge force applied to ensure that the calibration factor was not influenced by the vertical load. It was found that the error due to the load in the perpendicular axis was negligible.

The speed of the towing carriage was measured by logging the voltage output from the tachometer of the drive unit and applying a known calibration factor to obtain the carriage speed in metres per second.

The signals from each instrument were recorded using a computer via a National Instruments AT-MIO-16E10 Multifunction Data Acquisition Card, which was controlled by in-house data acquisition software.

3.6 Test procedure and data acquisition

Initial readings of all instruments were taken prior to each run and were checked between runs to ensure that no notable drift had occurred. The model was towed along the centreline of the tank at speeds obtained from Froude scaling. Froude numbers were selected so as to resemble those of full-scale ships manoeuvring in restricted water conditions. The carriage was accelerated to the predetermined speed and the recordings were started at a designated longitudinal location in the tank to maintain consistency in the tank test section. For the unsteady squat tests a trigger switch was incorporated into the data acquisition system to determine the longitudinal location of the model as it travelled over the banks. Data acquisition commenced after a constant speed had been reached and the model was at steady-state. The sample rate was set at 100Hz with the number of samples recorded varying with the speed of the model. For steady-state cases the mean values for each test run were derived afterwards from the time series, selecting a time window where the measurement values had stabilised. Sufficient time was allowed between consecutive runs to achieve calm water conditions.

3.7 Effect of model scale on squat measurements

3.7.1 Introduction

The manoeuvring committee of the 22nd International Towing Tank Conference described the issue of ship-model correlation as one of the key issues related to scale model testing techniques (ITTC 1999). Froude scaling laws are commonly used to satisfy inertia and geometric scaling requirements when conducting model scale experiments to measure squat. However, since the model is tested at a lower Reynolds number to the ship the boundary layer is thicker for the model than the ship (Eryuzlu *et al.* 1994). Hence, Froude scaling laws may not be applicable to scale squat measurements, especially for cases with very low under keel clearance where the model boundary layer may interact with the channel boundary layer induced by backflow (Tothill 1967).

Various aspects of scale effect have been investigated in previous work. For example Gertler (1969) and Edstrand and Norrbin (1978) recommend that models should be greater than 4.5 – 5.0 metres in length to minimise viscous scale effects. Eryuzlu and Hausser (1978) stated that the use of small scale models (e.g. 1/100) to investigate vessel squat is feasible and gives accurate results.

A number of studies have been conducted to assess the correlation between model scale squat results and full scale measurements. One limitation with studies involving full scale/model scale correlation is the fact that full scale tests are conducted in an uncontrolled environment, which is difficult to reproduce in model scale studies. Dand and Ferguson (1973) and Ferguson *et al.* (1983) conducted model scale tests and full scale measurements on a tanker at a water depth to draught ratio of 1.4 and found that the bodily sinkage for the ship marginally exceeded that for the model but the correlation, in general, was reasonable. This was attributed to the fact that the vertical force causing bodily sinkage in shallow water is due almost entirely to the pressure changes over the hull and is probably only slightly affected by viscous forces. Generally, however, it was found that the bow down trim measured on the full scale ship exceeded that measured at model scale. The authors attributed this to the fact that the moment causing running trim, arising from the difference of pressure moments over the fore and aft bodies, may have an

appreciable component of viscous origin giving rise to scaling problems. Seren *et al.* (1981) found that running trim correlated reasonably well but the sinkage was greater for the ship than for the model. It was concluded that, in general, the effect of scale is minimal. Haatainen *et al.* (1978) found that the squat measured from self-propelled model scale tests exceeded that measured from full scale tests for fine form vessels. The author stated that this may be attributed to the higher propeller loading at model scale.

The physical dimensions of the scale models used in the present study were dictated by the size of the AMC towing tank facility, particularly the tank width. In order to maximise the channel width to beam ratio, whilst still measuring forces and motions of sufficient magnitude, the length of the scale models in the present study was restricted to approximately 2m. It was therefore necessary to determine if scale effects had a significant impact on the measured results using models 2m in length, compared to using models around 4m in length. A 2m and 4m model of a MarAd F series bulk carrier (Roseman 1987) were therefore used to investigate the effect of scale when measuring squat for a range of speeds and water depth to draught ratios.

3.7.2 Test program

The model scale tests were conducted with both a 2m and 4m long MarAd F series model travelling in water restricted in width and depth. The models were constrained in surge, sway and yaw to measure the sinkage and trim using the test rig shown in Figure 3.2. Five water depth to draught ratios were tested for each model ranging from 1.2 to 1.7. At least five runs were conducted for each condition. The conditions tested are given in Table 3.2.

| h_1/d | F_{nh} |
|---------|---------------|
| 1.2 | 0.212 - 0.412 |
| 1.3 | 0.254 - 0.491 |
| 1.4 | 0.245 - 0.473 |
| 1.5 | 0.237 - 0.517 |
| 1.7 | 0.220 - 0.481 |

Table 3.2 Test program: effect of scale on squat measurement using MarAd F series

The full width of the towing tank was used for the 4m model giving a channel width to beam ratio of 4.8. Vertical walls were positioned in the towing tank for the 2m model to simulate the same channel width to beam ratio.

Both the 2m and 4m models were tested in the same test session in order to minimise variations in water temperature.

3.7.3 Results and discussion

Midship and bow sinkage coefficients were defined as follows, with the bow sinkage taken at the forward perpendicular:

$$SC_{midships} = \frac{100 \cdot s_{midships}}{F_{nh}^2 L_{pp}} \tag{3.1}$$

$$SC_{\text{bow}} = \frac{100 \cdot s_{\text{bow}}}{F_{\text{nh}}^2 L_{\text{pp}}} \quad (3.2)$$

The midship and bow sinkage coefficients for both the 2m and 4m models are presented as a function of depth Froude number for a selection of typical cases in Figures 3.5 – 3.10. Uncertainty analysis has been conducted on the model scale measurements to determine if the variation in results was within the predicted accuracy. The uncertainty limits have been presented by error bars in Figures 3.5 – 3.10. Full details concerning the uncertainty analysis are given in Appendix D.

It was found that the non-dimensional midship squat for the 2m and 4m models correlated reasonably well, with the results falling within the estimated limits of uncertainty, as illustrated in Figures 3.5 – 3.7. This may be due to the fact that the sinkage is almost entirely due to the predominance of pressure changes over the hull, allowing direct scaling of this component without error of practical significance (Ferguson *et al.* 1983).

The bow sinkage coefficient for the 2 and 4m models was also found to generally lie within the predicted uncertainty limits, as illustrated in Figures 3.8 – 3.10. However, for depth Froude numbers exceeding 0.35 the bow sinkage coefficient for the larger model generally exceeded that for the smaller model. A similar trend was observed by Ferguson *et al.* (1983) when comparing full scale squat results to model test results. The small differences observed between the bow sinkage of the 2m and 4m models may be attributed to viscous effects. Since the Reynolds number is lower for the 2m model the relative boundary layer thickness (boundary layer thickness/UKC) is larger, which will cause greater streamline deflection, impacting on the blockage since the mass flow in the boundary layer is reduced. This may divert more of the fluid flow around the sides of the vessel, resulting in different pressure distributions for the two models. Due to its lower Reynolds number it is possible that the flow separates further forward on the 2m model. This would cause a larger reduction in pressure over its aft section, which would result in a smaller bow down trim.

Since the effect of scale on squat measurements, when using 2m and 4m models, was found to be small, models of the order of 2m in length have been used for the remainder of the present study. However, it would be beneficial to compare model scale measurements to full scale measurements to quantify scale effect when predicting full scale squat from model experiments. The effect of scale should be borne in mind when using experimental results in this study to predict full scale squat.

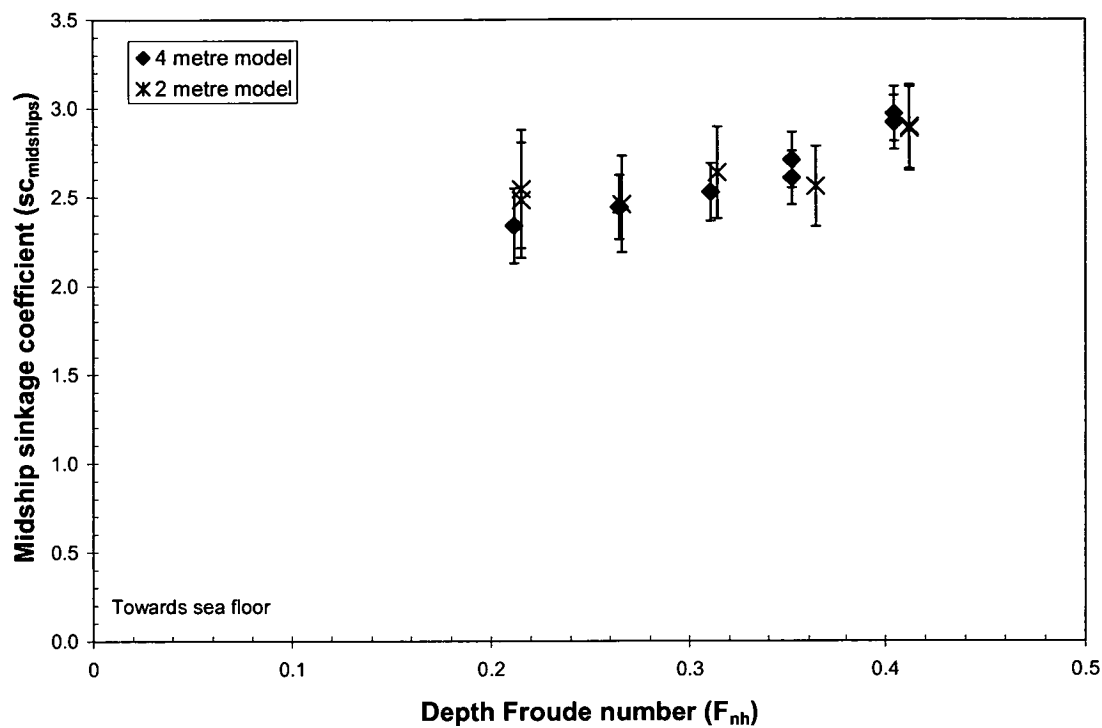


Figure 3.5 Midship sinkage coefficient as a function of F_{nh} , $h_1/d=1.2$, $W/B=4.8$

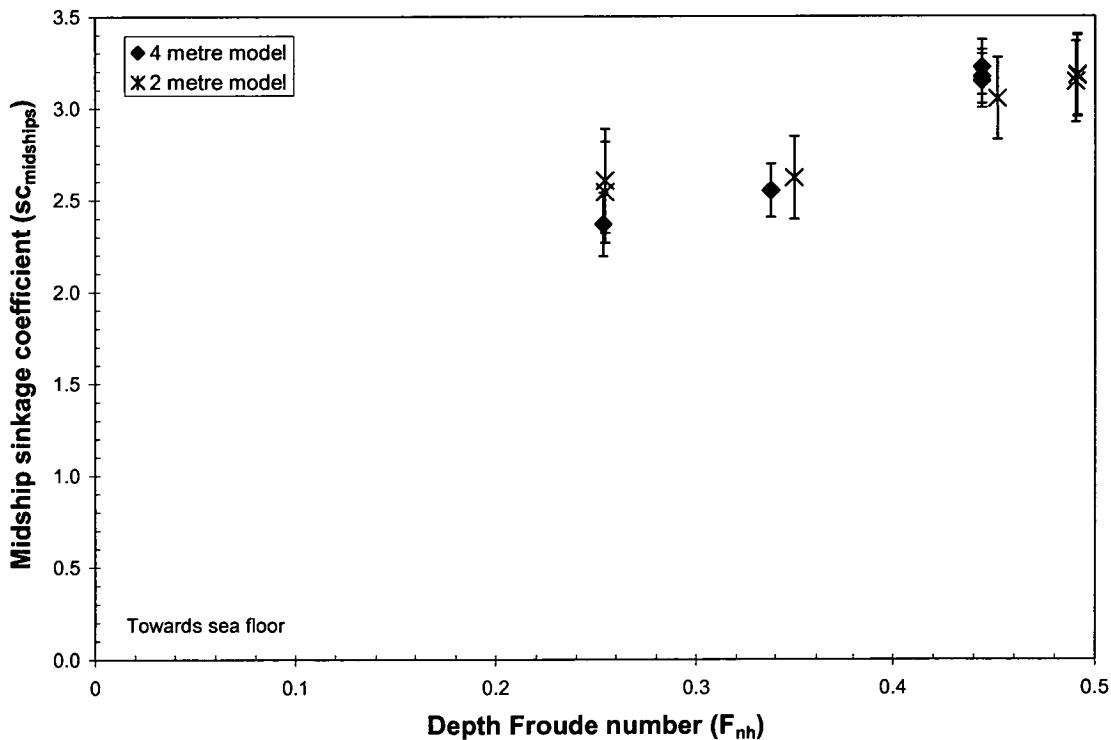


Figure 3.6 Midship sinkage coefficient as a function of F_{nh} , $h_1/d=1.3$, $W/B=4.8$

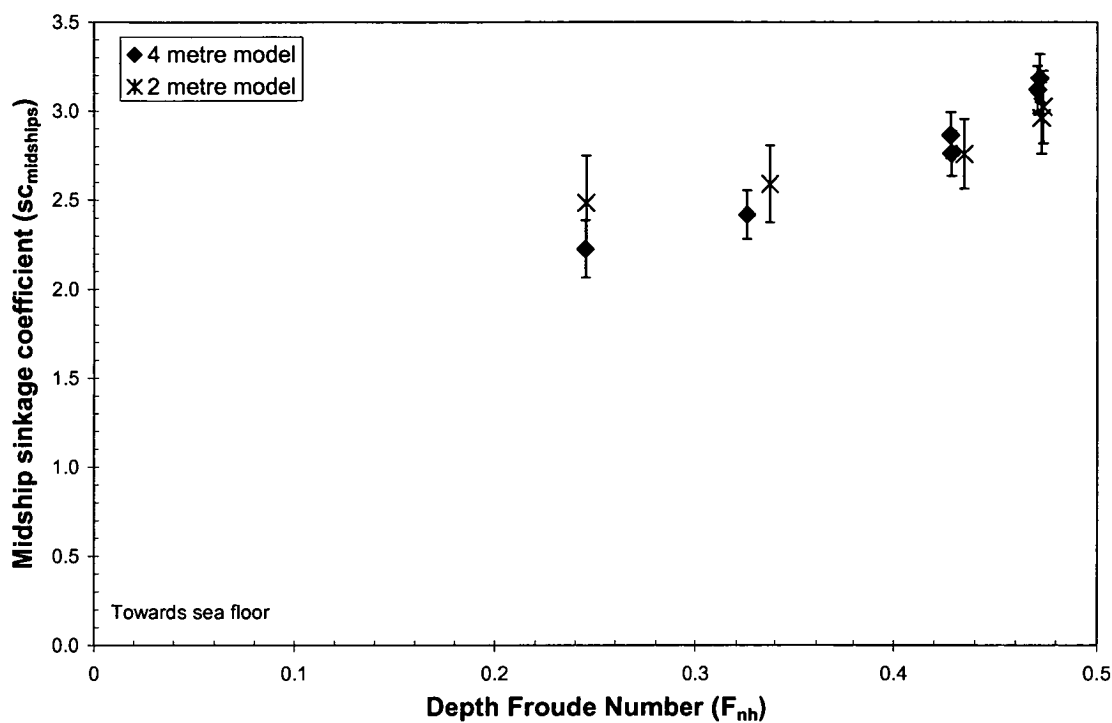


Figure 3.7 Midship sinkage coefficient as a function of F_{nh} , $h_l/d=1.4$, $W/B=4.8$

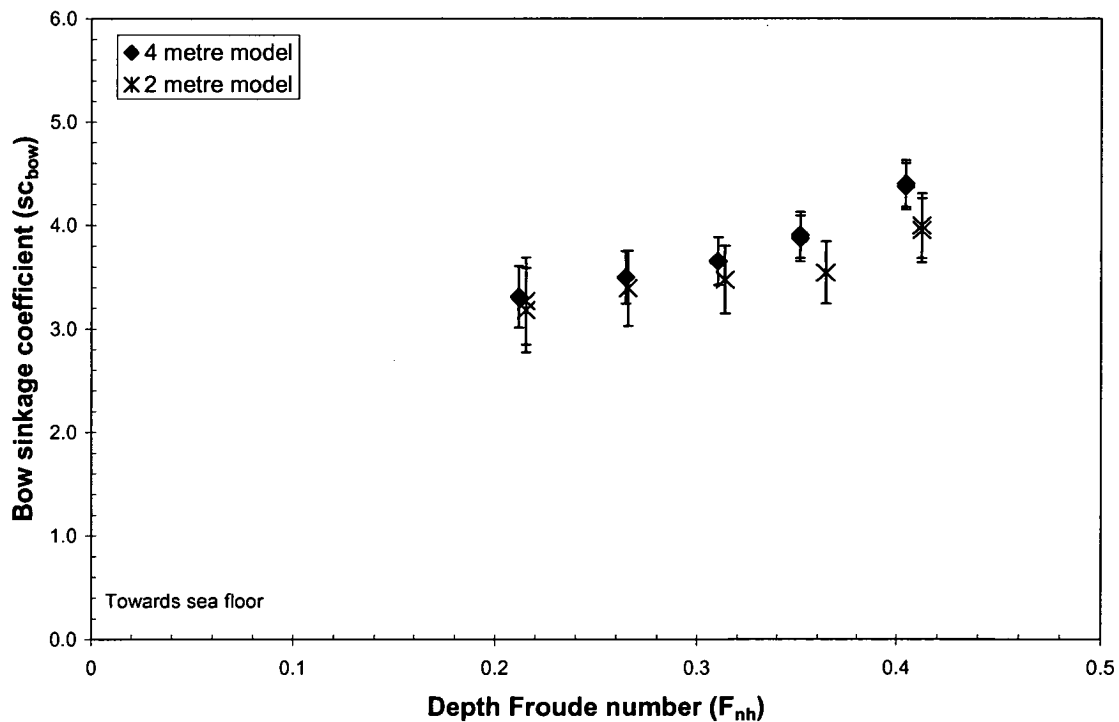


Figure 3.8 Bow sinkage coefficient as a function of F_{nh} , $h_l/d=1.2$, $W/B=4.8$

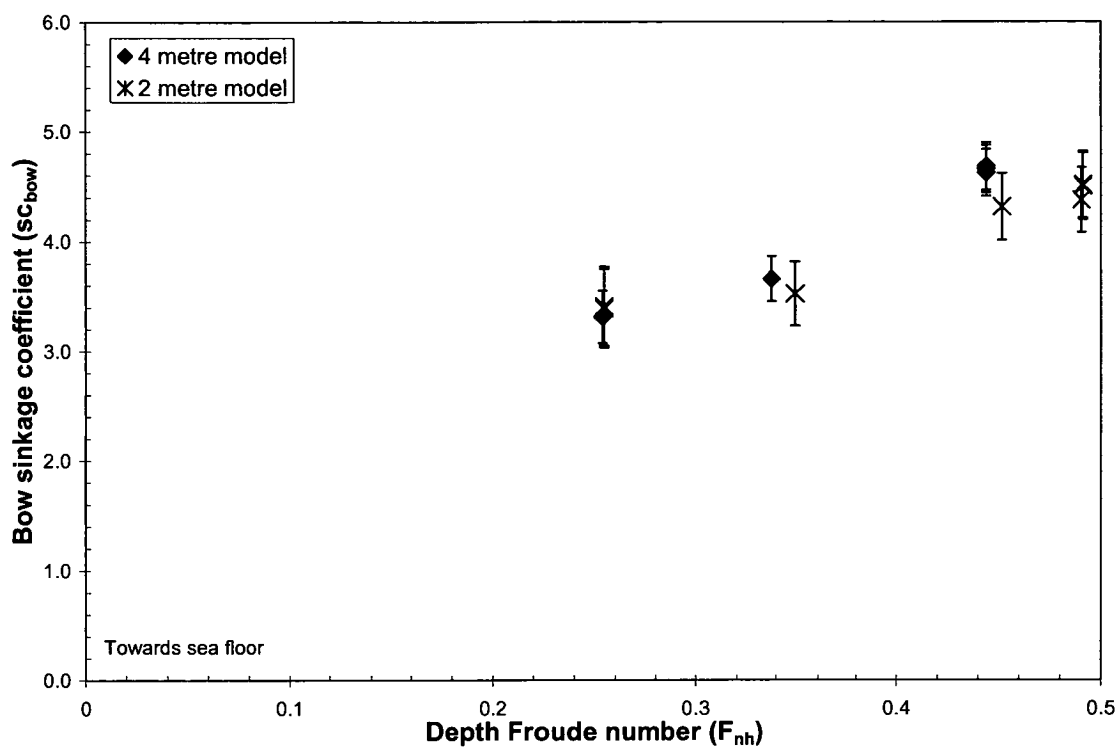


Figure 3.9 Bow sinkage coefficient as a function of F_{nh} , $h_l/d=1.3$, $W/B=4.8$

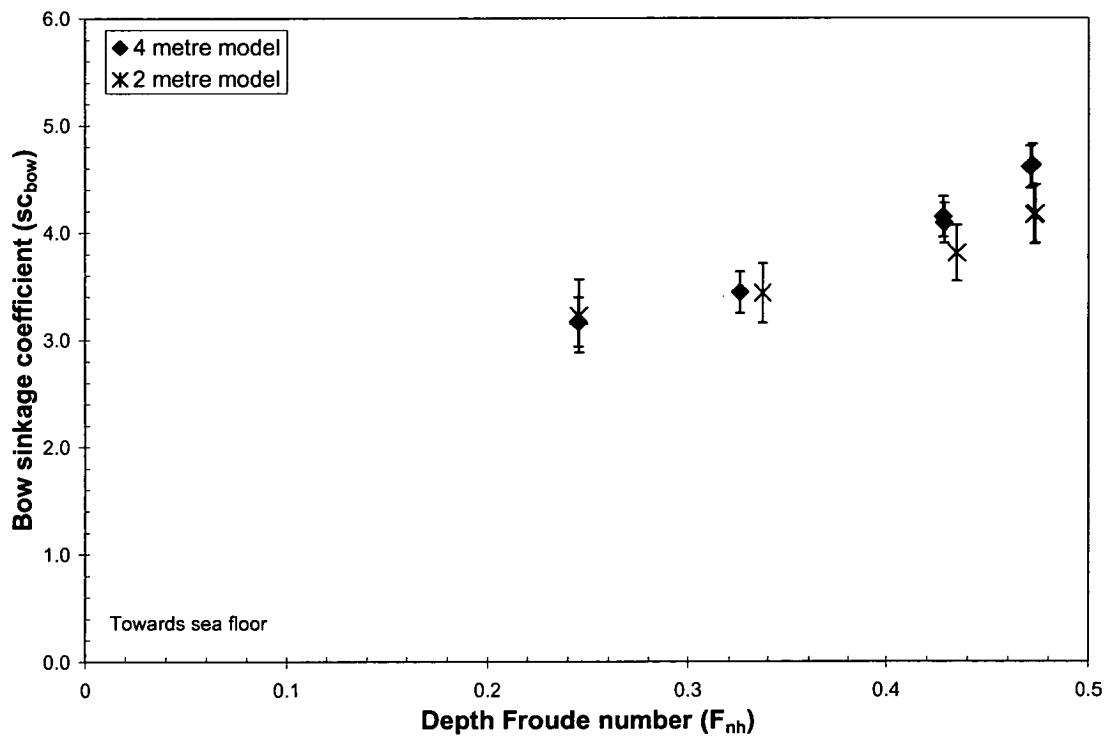


Figure 3.10 Bow sinkage coefficient as a function of F_{nh} , $h_l/d=1.4$, $W/B=4.8$

3.8 Effect of channel dimensions and vessel draught on squat

3.8.1 Introduction

Knowledge of how vessel squat is influenced by water depth, vessel draught and channel width is necessary to ensure vessels can be loaded to the maximum draught to improve their productivity without compromising safety. As ship size steadily increases the effect of water depth to draught ratio and channel width on vessel squat is becoming increasingly more important to ship designers and operators. The blockage ratio, S_v/S_o , has been shown to be a very important parameter in squat investigations (Constantine 1961). Eryuzlu *et al.* (1994) stated that the width of commercial waterways is generally about eight times that of the vessel's beam or wider. However, this may not always be the case; the width of some major waterways can be around six to seven times the beam of the design vessel. In the case of one-way traffic the channel width may be even narrower.

Experiments have been used extensively in previous work to measure the effect of water depth on vessel squat for full form vessels. From the majority of these studies it was found that the maximum sinkage due to squat was larger at low water depth to draught ratios for sub-critical flow (Eryuzlu and Hausser 1978; Barrass 1995). A number of authors found that both the sinkage and trim were larger at low water depth to draught ratios (Dand and Ferguson 1973; Millward 1990; Dand 1996). Millward (1990) determined that the influence of water depth to draught ratio on sinkage and trim due to squat was small for higher water depth to draught ratios for a constant depth Froude number. Dand and Ferguson (1973) tested lower water depth to draught ratios and found small, but measurable, effects on squat due to water depth to draught ratio for a constant depth Froude number. Ankudinov and Jakobsen (1996) found that sinkage due to squat was greater for low water depth to draught ratios but the bow down trim for full form vessels was smaller. Generally the above studies focussed on varying water depth to draught ratio by holding vessel draught constant and varying water depth. An exception is Dand and Ferguson (1973) who tested a fully loaded condition and a light draught condition, and concluded that the sinkage and trim were less for the model with the light draught condition for a constant depth Froude number and water depth to draught ratio.

A number of experimental investigations have been conducted into the effect of channel width on vessel squat motion when the vessel is travelling on the channel centreline. Eryuzlu *et al.* (1994) and Barrass (1995) found that the maximum bow down squat for towed full form vessels was generally greater for small channel widths at a constant vessel speed. Ankudinov and Jakobsen (1996) found the same for sinkage due to channel width but stated that for small channel widths the bow down trim was smaller for full form vessels at a constant speed. It is common for vessels to travel off the channel centreline and it has been found in previous work that the squat of a vessel travelling off the centreline of a channel exceeds that for a vessel travelling on the centreline. For such cases it has been shown that the sinkage due to squat was generally greater for small channel widths (Duncan 1968; Barrass 1989; Ch'ng 1991; Dand 1996).

A major aim of the present study was to further investigate the effect of water depth to draught ratio and channel width on vessel trim and to vary vessel draught to gain a clearer understanding of its effect on vessel squat. Previous work conducted has focussed mainly on the measurement of vessel motions, with little work conducted to measure the heave force and pitch moment

experienced by a ship in restricted waters. In the present study model scale experiments have been conducted to measure the heave force and pitch moment for varying vessel speeds, water depths, channel widths and vessel draughts. The results have been used to develop empirical formulae for input to the mathematical model described in Section 2.4.1, to predict unsteady squat and dynamic acceleration effects on a vessel travelling in non-uniform water depth. The results were also used to assess the accuracy of an existing steady-state prediction technique.

3.8.2 Test program

Model scale tests were conducted with a MarAd L series model constrained in surge, sway, yaw, pitch and heave to measure the heave force and pitch moment experienced by a ship travelling in water restricted in both width and depth. The model setup is shown in Figure 3.4. The test program for varying vessel speed, water depth and channel width is given in Table 3.3, whilst the test program for varying vessel speed, water depth and vessel draught, for a constant channel width to vessel beam ratio, is given in Table 3.4.

| F_{nh} | h_1/d | W/B |
|---------------|-------------|-------|
| 0.282 - 0.612 | 1.10 - 1.40 | 10.3 |
| 0.300 - 0.653 | 1.10 - 1.70 | 5.0 |
| 0.300 - 0.653 | 1.10 - 1.70 | 4.0 |
| 0.300 - 0.653 | 1.10 - 1.70 | 3.0 |

Table 3.3 Test program: effect of vessel speed, water depth and channel width on heave force and pitch moment due to squat, $B/d=4.42$

| F_{nh} | h_1/d | B/d |
|---------------|-------------|-------|
| 0.149 - 0.612 | 1.20 - 4.30 | 4.42 |
| 0.273 - 0.636 | 1.07 - 1.26 | 3.98 |
| 0.197 - 0.609 | 1.06 - 3.61 | 3.62 |

Table 3.4 Test program: effect of vessel speed, water depth and vessel draught on heave force and pitch moment due to squat, $W/B=10.3$

The model speeds were selected so as to resemble those of full-scale ships manoeuvring in restricted water conditions; however speeds exceeding those for typical manoeuvring operations in restricted water were also tested as the model was constrained in the vertical plane.

Large water depth to draught ratios were tested where squat is not typically a concern to ship operators. This was carried out to enable prediction of squat for a vessel travelling from deep water to relatively shallow water.

3.8.3 Results and discussion

Force and moment measurements have been non-dimensionalised using the prime system, unless otherwise stated. The non-dimensional terms are shown in Equations 3.3 and 3.4 for heave force and pitch moment, respectively

$$Z' = \frac{Z}{\frac{1}{2} \rho U^2 L_{PP}^2} \quad (3.3)$$

$$M' = \frac{M}{\frac{1}{2} \rho U^2 L_{PP}^3} \quad (3.4)$$

In practice, a vessel may travel off the centreline of a canal for a number of reasons: for example when two vessels pass in a two-way channel, or when negotiating a channel bend. The sinkage may be increased when a vessel travels off the centreline of a canal (Duncan 1968). Many squat results have been obtained for a vessel travelling off the centreline of a channel as part of the present study to investigate the effect of the following on vessel sinkage: ship to lateral bank distance, bank flooding and bank slope (Duffy 2007). To simplify the present discussions, only results for a vessel travelling on the centreline of a canal are presented.

In Figures 3.11 – 3.17 the influence of channel width, water depth to draught ratio and depth Froude number on heave force and pitch moment is illustrated for a selection of cases. From these figures it can be seen that for a constant channel width and water depth to draught ratio both non-dimensional heave force and pitch moment were found to be larger for higher depth Froude numbers for sub-critical flow.

For sub-critical flow the heave force was found to be towards the sea floor and the pitch moment bow down. This supports sinkage and trim results from other investigations for full form vessels with similar block coefficients to that tested in the present study (Millward 1990; Eryuzlu *et al.* 1994; Dand 1996).

The downward non-dimensional heave force and bow down non-dimensional pitch moment were found to be larger at smaller water depth to draught ratios for sub-critical flows, as illustrated for example cases in Figures 3.11 and 3.12. The moment was bow up for the highest depth Froude numbers tested for a channel width to beam ratio of 3.0, as illustrated in Figure 3.13. Millward and Bevan (1986) also reported bow up trims for speeds near the critical speed. This may be attributed to trans-critical flow, where water is piled up in front of the vessel and a depression of water is present behind the vessel (Tothill 1967). The onset of trans-critical flow is dictated by blockage and depth Froude number (Tuck 1966). From Figure 3.13 it can be seen that the pitch moment changes from bow down to bow up at a lower depth Froude number for cases with higher blockage.

It should be noted that in Figures 3.11 – 3.13 the non-dimensional heave force and pitch moment have a speed squared term in the denominator and the speed is different for a constant depth Froude number since the water depth is different for each series on the graphs. The results given in Figures 3.11 and 3.12 have been re-normalised using the Bis system, Norrbin (1971), in Figures 3.14 and 3.15, for which speed does not appear in the denominator. Figure 3.14 shows that the heave force results generally collapse onto a single line for higher water depth to draught ratios with a slight influence of water depth to draught ratio evident at 1.1. This has been noted by previous authors when presenting sinkage as a function of depth Froude number (Millward 1990). The bow down pitch moment also collapsed onto a single line for different water depth to draught ratios when using the Bis system, as illustrated in Figure 3.15.

The non-dimensional downward heave force was larger for lower channel width to vessel beam ratios, as illustrated in Figure 3.16. The non-dimensional bow down pitch moment, however, showed an opposite trend with channel width to beam ratio for sub-critical flow, see Figure

3.17. This implies that the sinkage of the vessel was larger and the bow down trim of the vessel was smaller for lower channel width to beam ratios, which was also found by Ankudinov and Jakobsen (1996). In order to investigate this further, the centre of pressure location relative to midships has been presented for the same cases in Figure 3.18. As can be seen, the centre of pressure moves aft as the channel width to beam ratio is decreased. In previous work it was found that the bow sinkage was greater for smaller channel width to beam ratios, for example Eryuzlu *et al.* (1994) and Barrass (1995). It is of interest to determine if the reduction in bow down trim due to a reduction in channel width to beam ratio is sufficient to reduce the sinkage at the forward perpendicular. The sinkage at the forward perpendicular has been predicted for the cases shown in Figure 3.17 using the TPC and MCTC and is given in Figure 3.19. As can be seen, the predicted sinkage at the forward perpendicular was generally larger for lower channel width to beam ratios, as was measured by Eryuzlu *et al.* (1994) and Barrass (1995). The reason why the bow down pitch moment was smaller at low channel width to beam ratios is currently unknown. Further research may be undertaken to investigate the wave pattern to gain a clearer understanding of the flow pattern around the vessel.

A selection of results for two vessel displacements is presented in Figure 3.20 and 3.21 for non-dimensional heave force and pitch moment, respectively. The water depth to draught ratio has been held constant for each case to quantify the effect of vessel draught. From Figure 3.20 it can be seen that non-dimensional heave force is generally greatest for the light load condition at a water depth to draught ratio of 1.1. However, the effect of vessel draught on heave force was not as significant at higher water depth to draught ratios. This is illustrated for a water depth to draught ratio of 1.26 in Figure 3.20. An increase in vessel draught generally had a more significant effect on non-dimensional pitch moment than for heave force, as illustrated in Figure 3.21. The magnitude of the non-dimensional pitch moment was generally largest for the light draught condition for each water depth to draught ratio. In general, the effect of vessel draught on pitch moment was smaller for higher water depth to draught ratios. These results appear to contradict the sinkage and trim measurements reported by Dand and Ferguson (1973), who found that the sinkage and running trim were smaller for the model in a light draught condition at a constant depth Froude number and water depth to draught ratio.

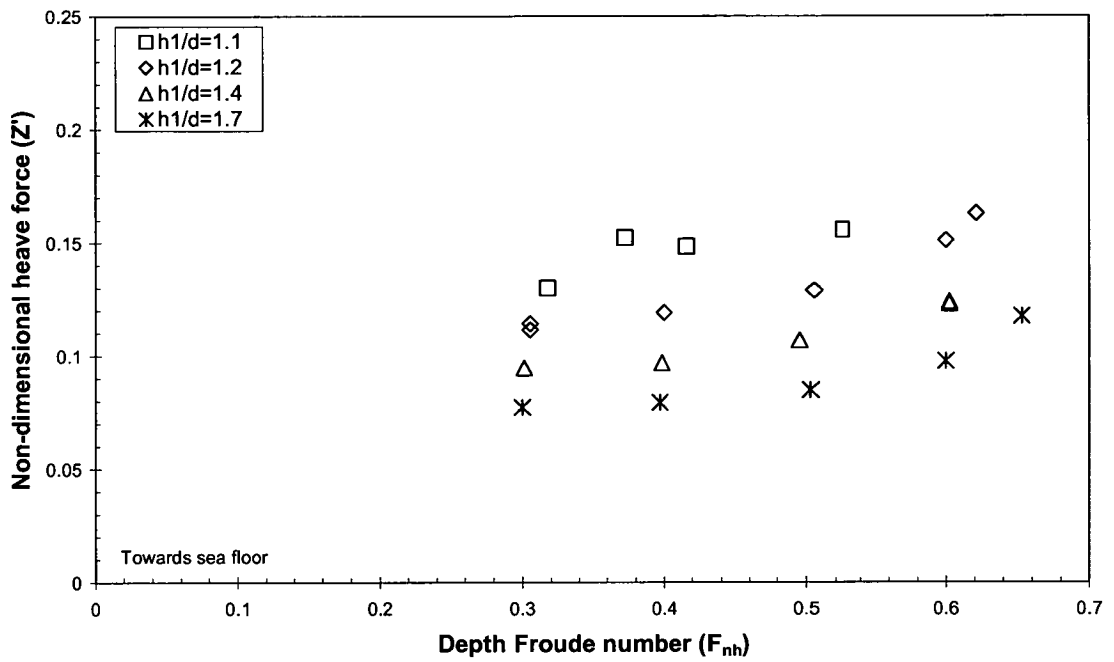


Figure 3.11 Non-dimensional heave force as a function of F_{nh} , varying h_1/d , $W/B=5.0$

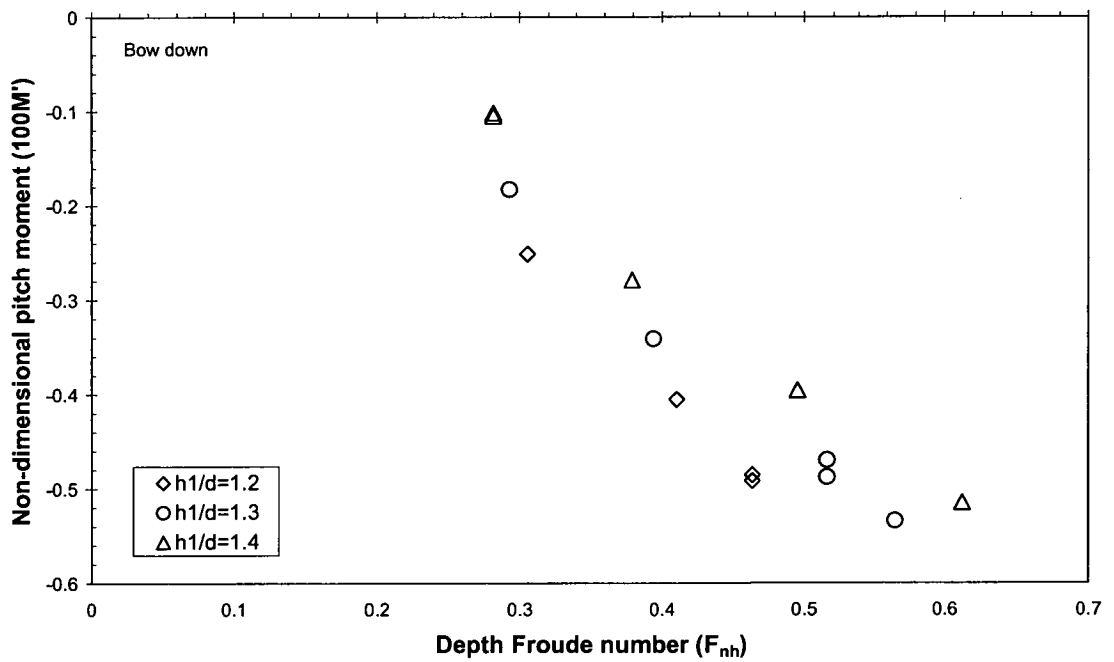


Figure 3.12 Non-dimensional pitch moment as a function of F_{nh} , varying h_1/d , $W/B=10.3$

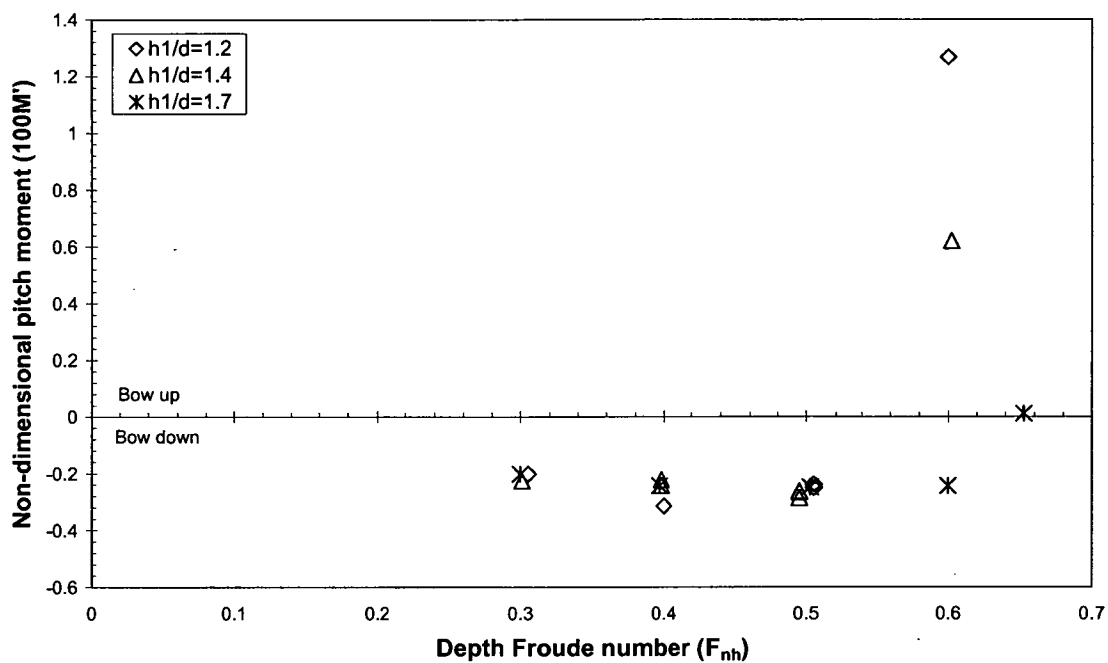


Figure 3.13 Non-dimensional pitch moment as a function of F_{nh} , varying h_1/d , $W/B=3.0$

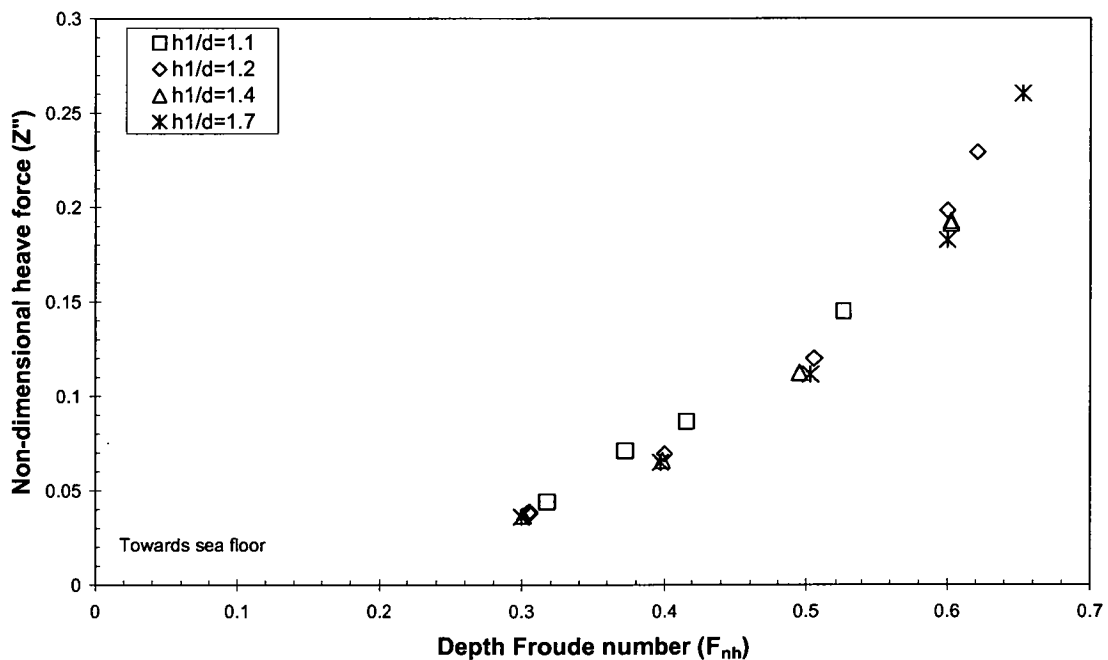


Figure 3.14 Non-dimensional heave force (using the Bis system) as a function of F_{nh} , varying h_1/d , $W/B=5.0$

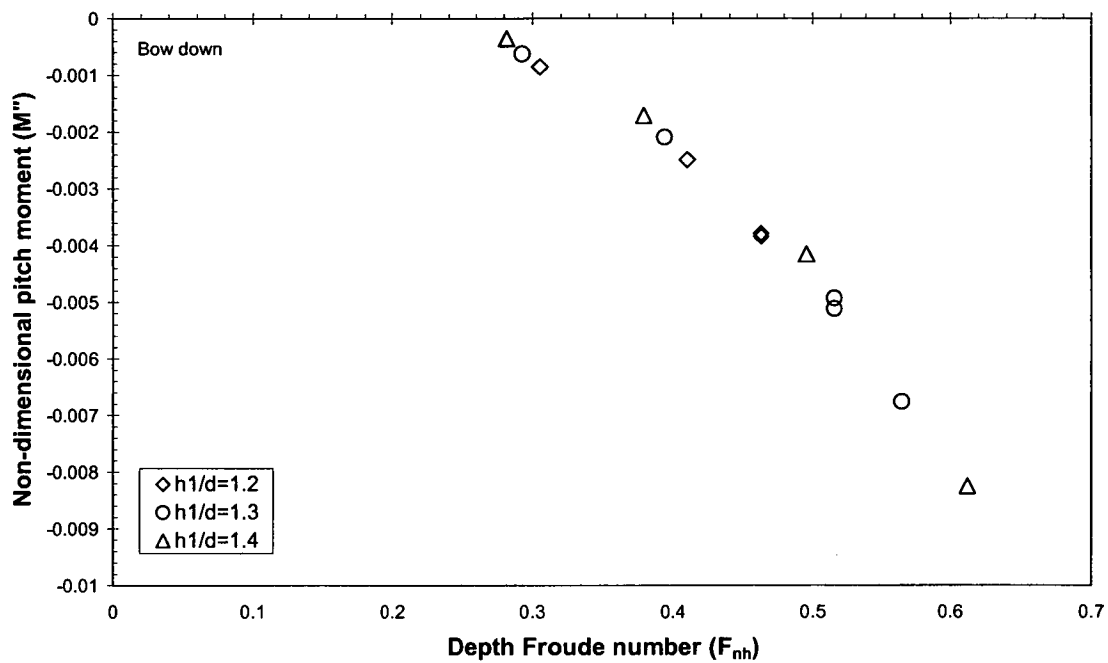


Figure 3.15 Non-dimensional pitch moment (using the Bis system) as a function of F_{nh} , varying h_1/d , $W/B=10.3$

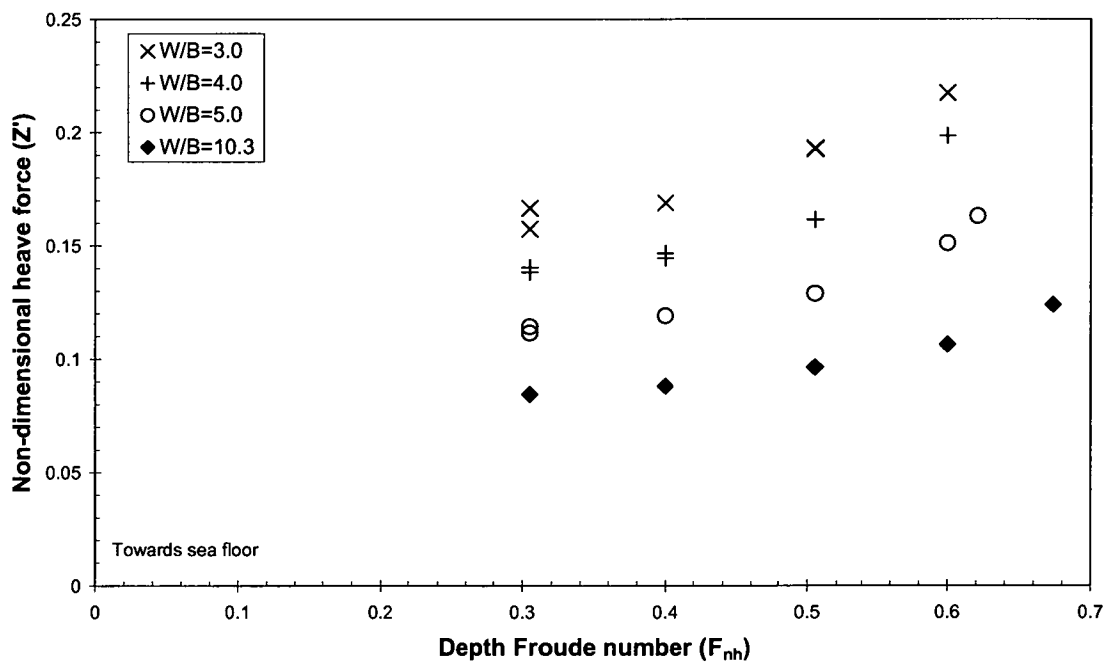


Figure 3.16 Non-dimensional heave force as a function of F_{nh} , varying W/B , $h_1/d=1.2$

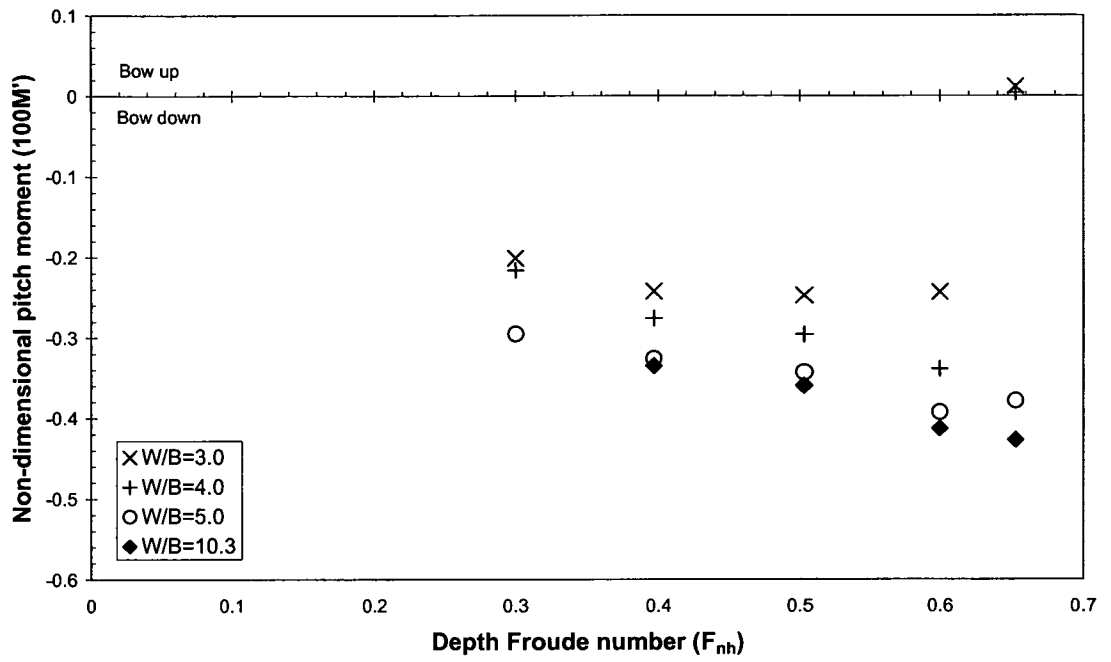


Figure 3.17 Non-dimensional pitch moment as a function of F_{nh} , varying W/B , $h_l/d=1.7$

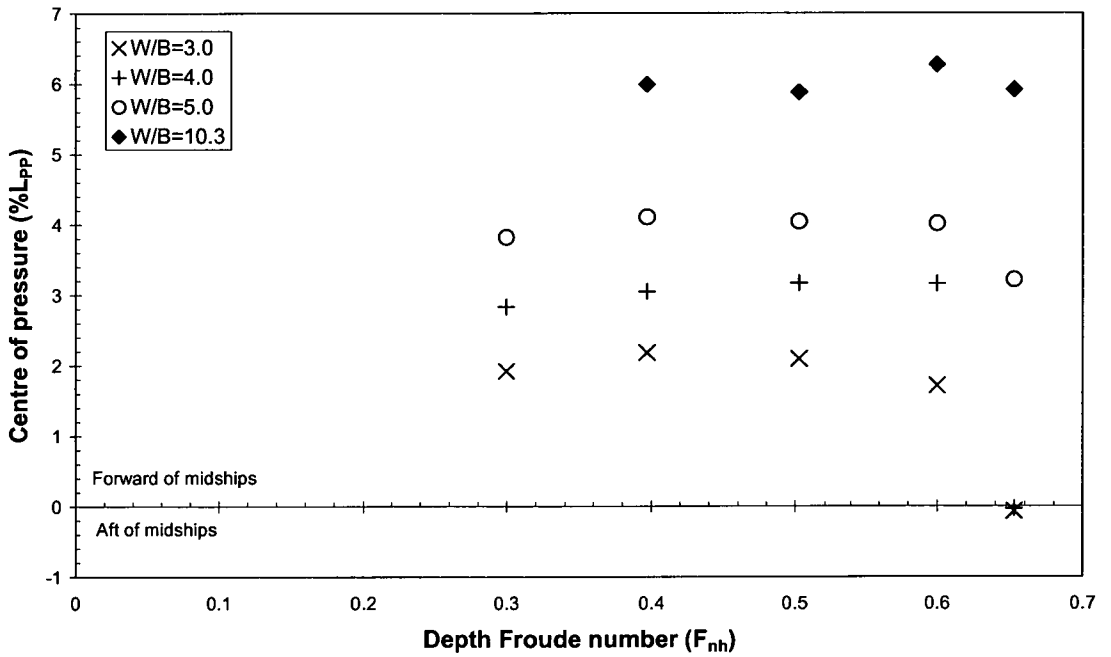


Figure 3.18 Centre of pressure location as a function of F_{nh} , varying W/B , $h_l/d=1.7$

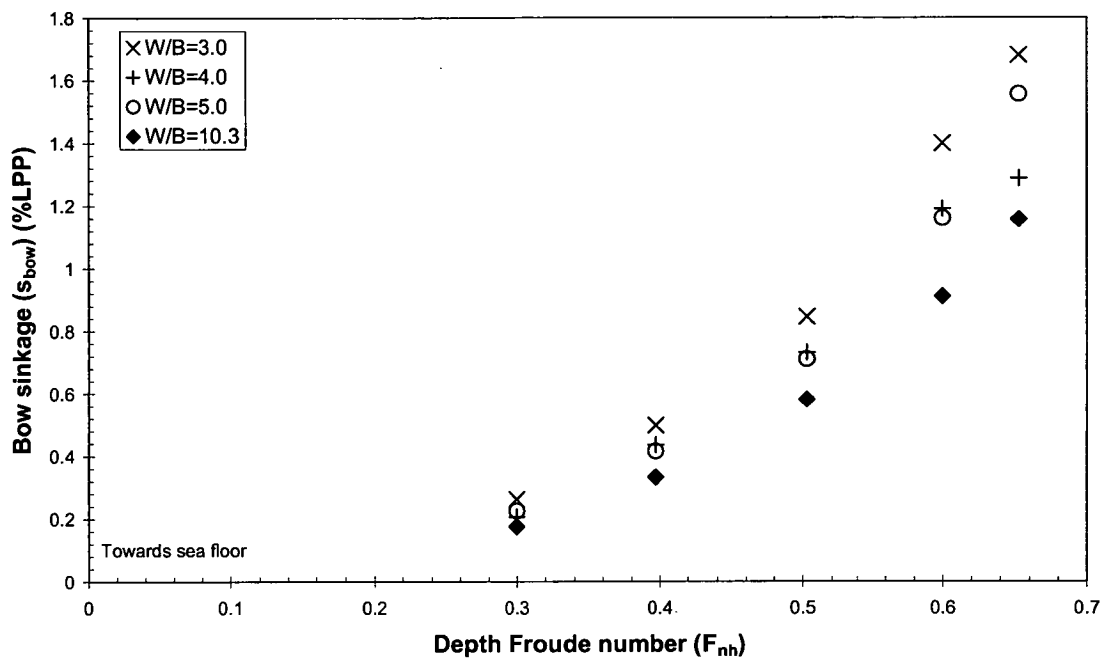


Figure 3.19 Predicted sinkage at forward perpendicular as a function of F_{nh} , varying W/B , $h_1/d=1.7$

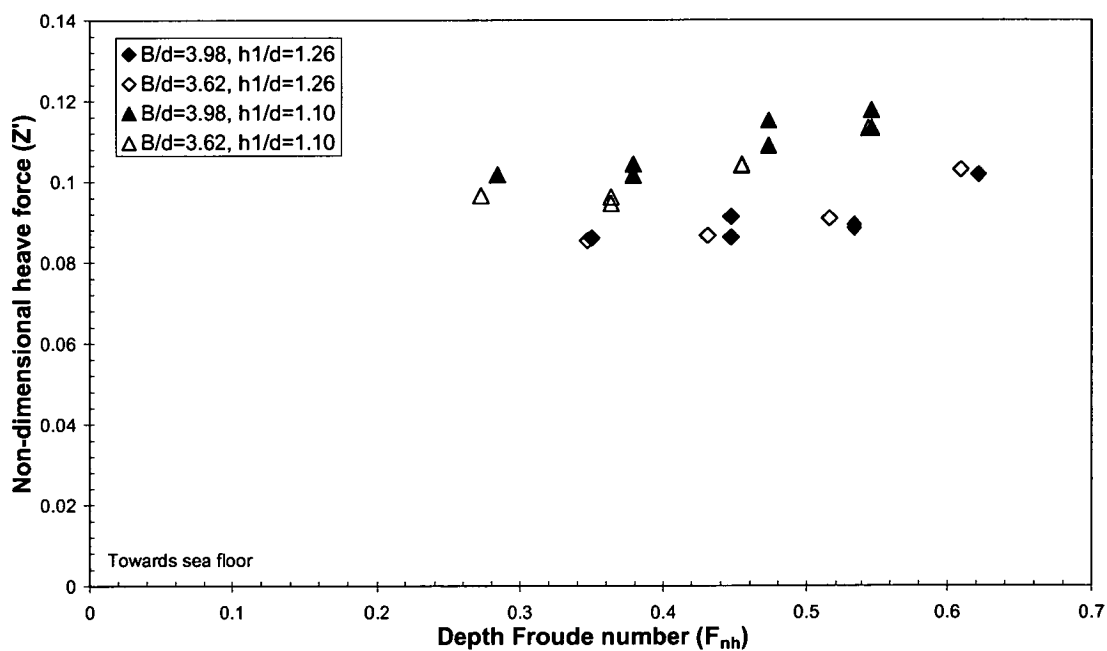


Figure 3.20 Non-dimensional heave force as a function of F_{nh} , varying d

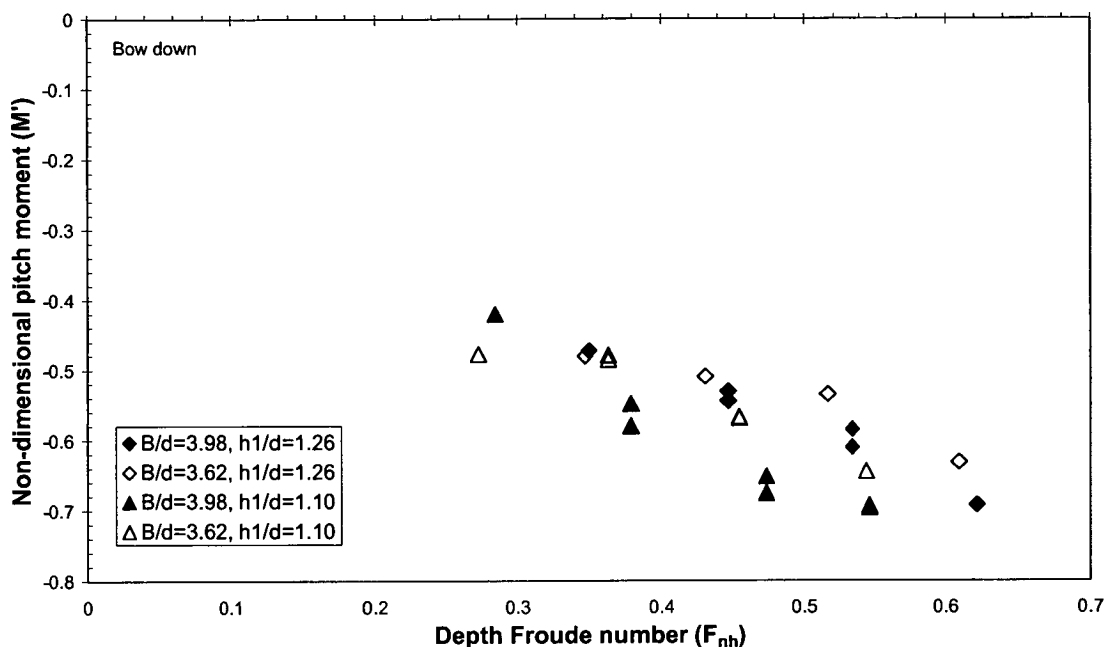


Figure 3.21 Non-dimensional pitch moment as a function of F_{nh} , varying d

3.9 Effect of propulsion on squat

3.9.1 Introduction

A sudden full ahead thrust is often used when a ship is manoeuvring in a confined port situation to improve the turning effect of the rudder. The effect of the operating propeller can influence the sinkage and trim of the vessel (Dand 1996). It is important to accurately predict the effect of propulsion on vertical plane motions when simulating the behaviour of a vessel operating in restricted water (Kijima and Higashi 1996).

Model scale experiments have been used in previous investigations to determine the influence of propulsion on squat. The effect of propeller action has been found to reduce the pressure in the vicinity of the propeller (Haatainen *et al.* 1978; Blaauw and Van Der Knaap 1983). Generally the influence of an operating propeller has been found to increase bodily sinkage (Dand and Ferguson 1973; Ch'ng 1991; Ankudinov and Jakobsen 1996). Whilst propulsion slightly increased bodily sinkage, it has been shown to have a greater influence on running trim. For a full form vessel that trims by the bow, the effect of propulsion reduced the unpropelled hull bow down moment (Dand and Ferguson 1973; Blaauw and Van Der Knaap 1983; Ch'ng 1991; Ankudinov and Jakobsen 1996).

Dand and Ferguson (1973) presented propulsion correction factors for sinkage and running trim, for the self-propulsion point only, to adjust results obtained for unpropelled hulls. The correction factor for sinkage was given as a 10% increase in the unpropelled hull sinkage value and the correction factor for trim was given as a function of depth Froude number and water

depth to draught ratio. Ankudinov and Jakobsen (1996) presented a technique to approximate the vertical force induced by an operating propeller based on the propeller characteristics.

Fuehrer and Romisch (1977) used scale models with and without propulsion to investigate the effect of propulsion on the critical ship speed. The change in critical speed due to the effect of propulsion was quantified for three different blockage ratios.

An investigation into the effect of propulsion on ship squat in shallow water was undertaken in the present study. The surge force, heave force and pitch moment on a MarAd L series model (Roseman 1987) were measured for a range of speeds, at various water depths, with and without propulsion. A range of motor power settings from zero to an equivalent full ahead motor power setting was tested at each length Froude number. This work was also presented in Duffy and Renilson (2001).

3.9.2 Test method for propulsion tests

The model was fitted with an electric motor and propeller for the propulsion tests. Since the influence of propeller loading on squat up to an equivalent full ahead motor power setting was to be investigated, it was necessary to determine the motor power setting for the self-propulsion point at a typical maximum speed for a bulk carrier in deep water. Based on performance data from existing bulk carrier ships a length Froude number of 0.164 was selected. The surge force on the unpropelled hull was measured at this length Froude number in deep water ($h_1/d=19.5$). The surge force acting on the model was then calculated, accounting for the increased viscous effects at model scale compared to full scale, using the ITTC 1957 procedure. With the propeller installed, the electric motor power was adjusted until the surge force was equal to the difference between the model unpropelled hull surge force and the full scale calculated value. Hence, the motor power setting for the full scale self-propulsion point was obtained and was considered to be the equivalent full ahead power setting.

Tests were then conducted in shallow water, where the surge force, heave force and pitch moment on the unpropelled hull were measured at each test speed. With the propeller installed, the surge force, heave force and pitch moment were measured for a series of motor power settings ranging from zero to the full ahead equivalent for each test speed. The effective thrust for each test speed was determined by subtracting the surge force on the unpropelled hull from the surge force on the propelled hull.

3.9.3 Test program

Preliminary tests were conducted with the unpropelled model constrained in surge, sway and yaw to measure the surge force at a full ahead speed in deep water ($h_1/d=19.5$). The model was then fitted with an electric motor and propeller in order to simulate the effect of propulsion. The surge force was measured for the propelled hull to determine the motor power setting for the self-propulsion point at a typical maximum ship speed in deep water.

Tests were then conducted in shallow water with the model constrained in surge, sway, yaw, pitch and heave to measure the surge force, heave force and pitch moment. Tests were firstly conducted on the unpropelled hull for a range of length Froude numbers. With the propeller installed measurements were then performed for four motor power settings at each model speed, up to the maximum motor power setting determined from the deep water tests.

The tests were conducted on a MarAd L series bulk carrier model at a channel width to beam ratio of 10.3. The test program is shown in Table 3.5.

| h_l/d | F_{nL} |
|---------|---------------|
| 1.1 | 0.071 – 0.108 |
| 1.2 | 0.071 – 0.108 |
| 1.3 | 0.071 – 0.137 |
| 1.4 | 0.071 – 0.154 |
| 19.5 | 0.164 |

Table 3.5 Test program to investigate the influence of propulsion on squat

3.9.4 Results and discussion

The heave force, effective thrust and pitch moment have been non-dimensionalised using the Bis system, Norrbin (1971), as shown in Equations 3.5, 3.6 and 3.7. This non-dimensionalisation system was chosen since the heave force, pitch moment and effective thrust can take on a non-zero value at zero vessel speed. The vessel speed has been presented in terms of length Froude number. It should be noted that the effective thrust is the difference between the surge force measured on the propelled hull and the surge force measured on the unpropelled hull.

$$Z'' = \frac{Z}{\rho g \nabla_o} \quad (3.5)$$

$$T'' = \frac{T}{\rho g \nabla_o} \quad (3.6)$$

$$M'' = \frac{M}{\rho g \nabla_o L_{PP}} \quad (3.7)$$

The effect of propulsion on heave force and pitch moment is illustrated in Figures 3.22 - 3.25 for a selection of cases. The cases with zero effective thrust represent the unpropelled hull condition. An increase in effective thrust resulted in a greater downward heave force and a reduction in bow down pitch moment for all water depths and depth Froude numbers tested. The results illustrate that the effect of propulsion had a greater influence on pitch moment than heave force.

From these results it can be deduced that the effect of the operating propeller altered the flow over the stern of the vessel, resulting in an additional heave force, Z_{ADD} , as shown in Figure 3.26. The magnitude of this force was obtained from the results using Equation 3.8 and the additional pitch moment was obtained from Equation 3.9. The longitudinal position of the force was obtained using Equation 3.10.

$$Z_{ADD} = Z_{propelled} - Z_{unpropelled} \quad (3.8)$$

$$M_{ADD} = M_{propelled} - M_{unpropelled} \quad (3.9)$$

$$x_{ADD} = \frac{M_{ADD}}{Z_{ADD}} \quad (3.10)$$

The additional heave force and pitch moment due to propulsion for a selection of cases is shown as a function of depth Froude number in Figures 3.27 and 3.28. The magnitude of the additional heave force and pitch moment due to propulsion increased with effective thrust at all depth Froude numbers and water depth to draught ratios tested. This could be attributed to the acceleration of fluid over the stern increasing with effective thrust. A smaller water depth to draught ratio generally resulted in a greater additional heave force and pitch moment due to propulsion from an increase in blockage, as shown for a selection of cases in Figures 3.29 and 3.30. Generally, the magnitude of the additional heave force and pitch moment increased with vessel speed for a constant effective thrust.

The longitudinal position of the additional heave force due to propulsion is plotted as a function of depth Froude number for a selection of cases in Figures 3.31 and 3.32. It can be seen that this was generally located furthest aft of midships at the lowest speed tested for a constant effective thrust.

In summary, an increase in effective thrust, for a constant water depth to draught ratio and depth Froude number, was found to increase the draught at the stern of the vessel (based on the heave force and pitch moment). Hence, a vessel with an initial trim by the stern may be caused to ground due to an increased propeller loading in very shallow water.

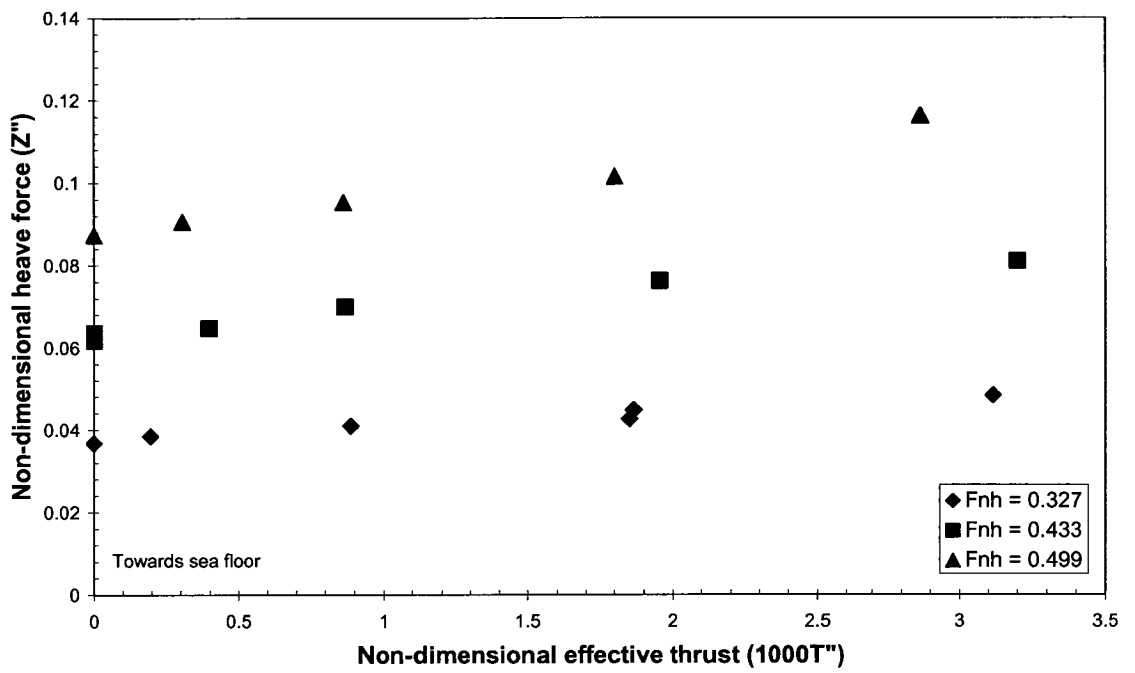


Figure 3.22 Non-dimensional heave force as a function of T'' , varying F_{nh} , $h_1/d=1.1$

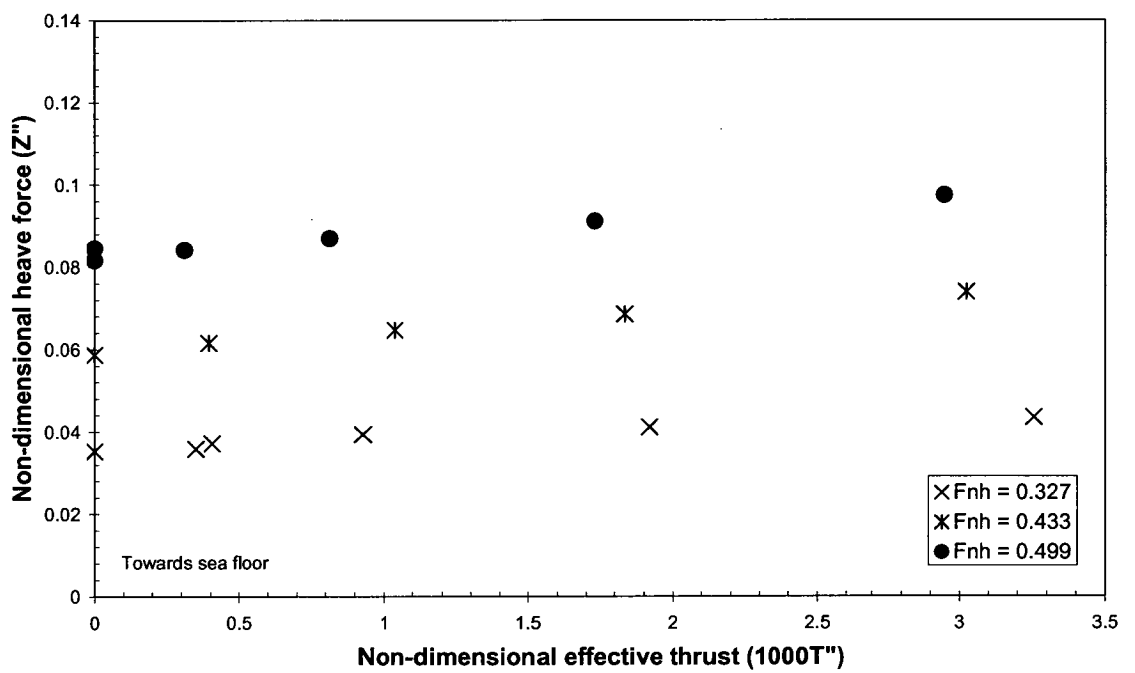


Figure 3.23 Non-dimensional heave force as a function of T'' , varying F_{nh} , $h_1/d=1.2$

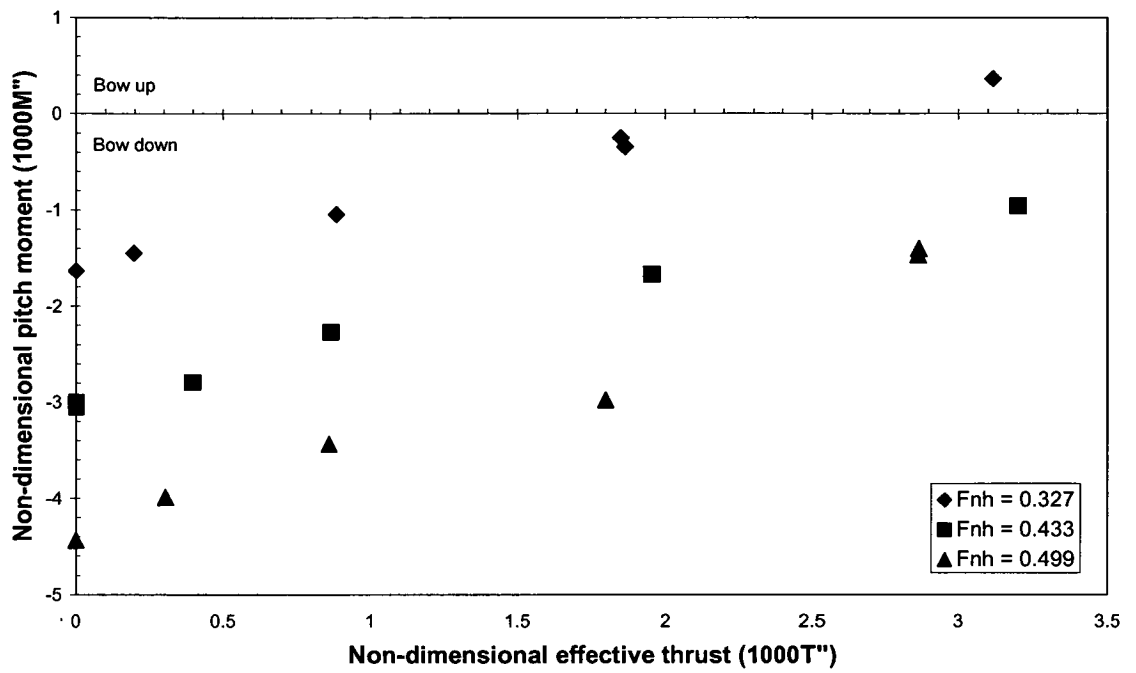


Figure 3.24 Non-dimensional pitch moment as a function of T'' , varying F_{nh} , $h_1/d=1.1$

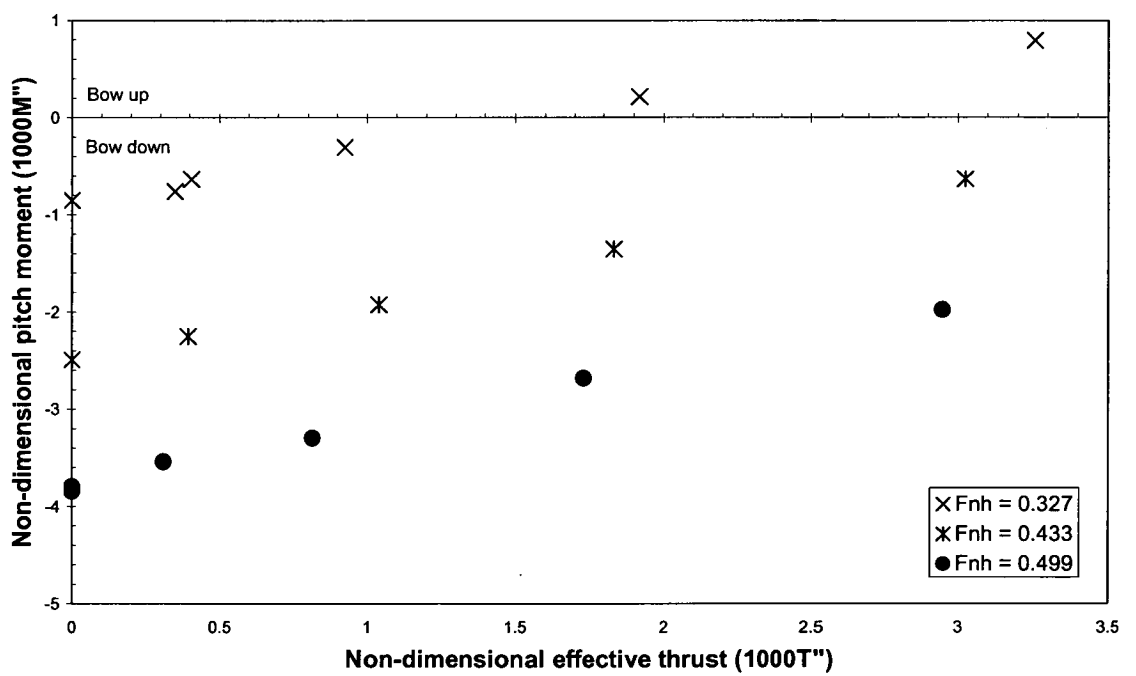


Figure 3.25 Non-dimensional pitch moment as a function of T'' , varying F_{nh} , $h_1/d=1.2$

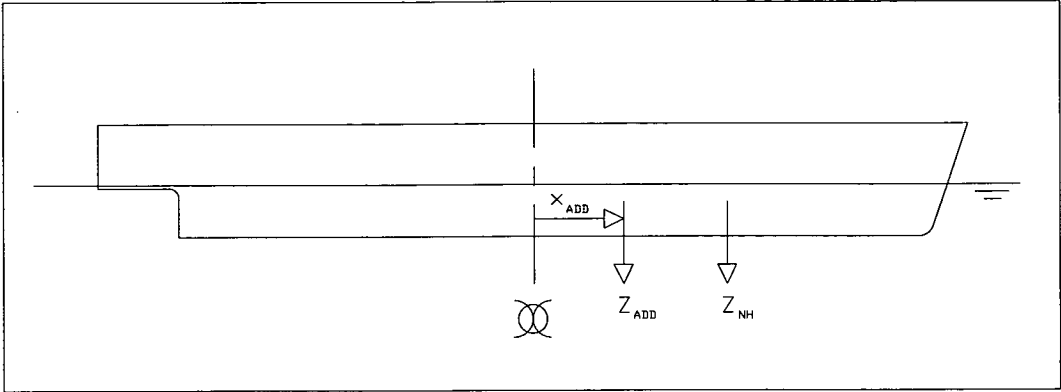


Figure 3.26 Schematic of additional heave force due to propulsion

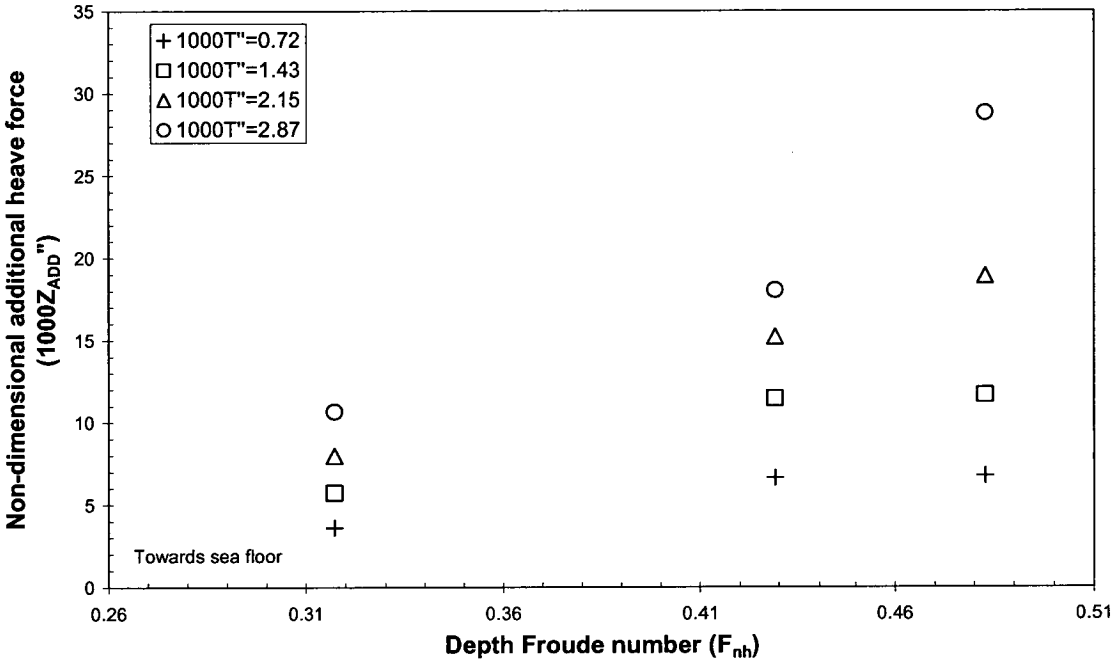


Figure 3.27 Additional heave force due to propulsion as a function of F_{nh} , varying T'' , $h_l/d=1.1$

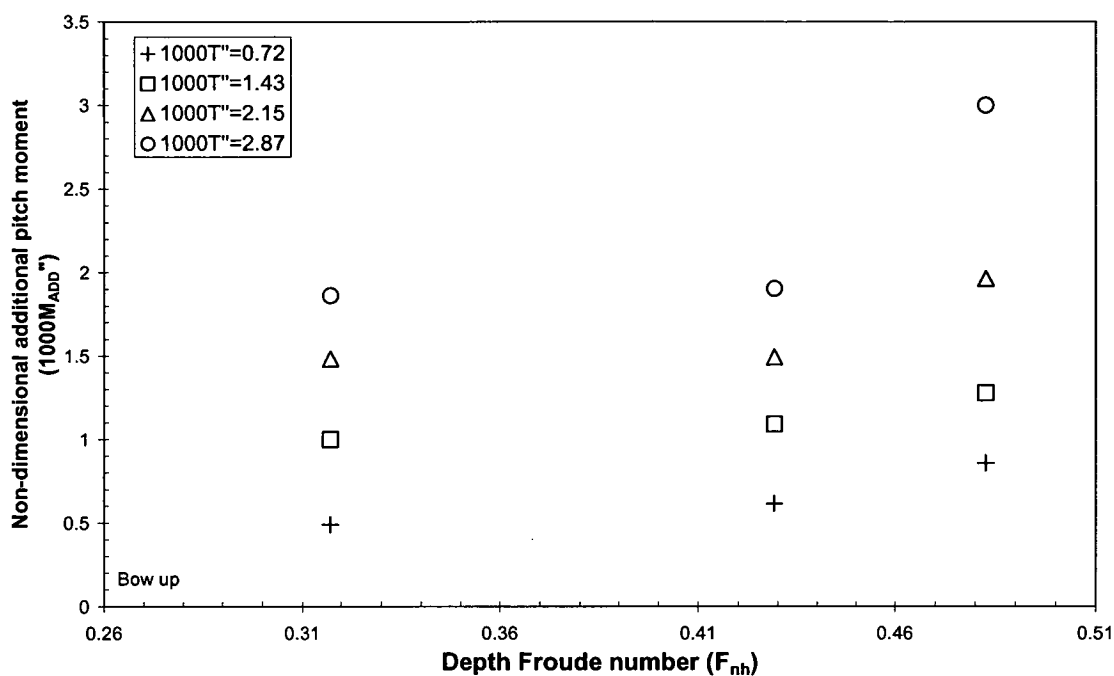


Figure 3.28 Additional pitch moment due to propulsion as a function of F_{nh} , varying T'' , $h_1/d=1.1$

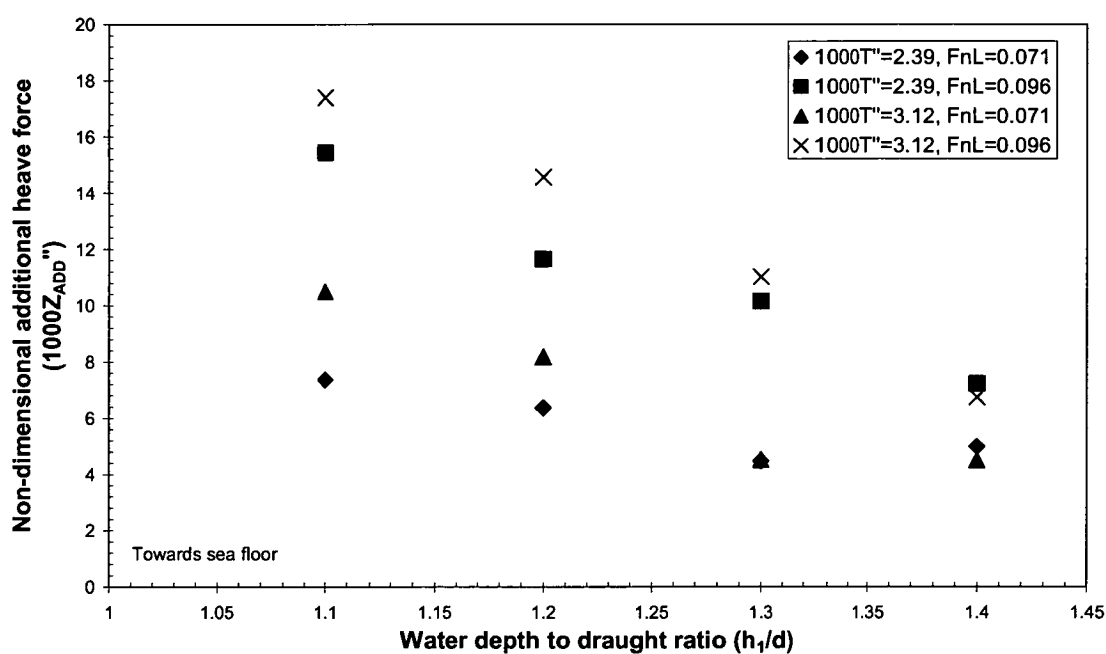


Figure 3.29 Additional heave force due to propulsion as a function of h_1/d , varying T'' and F_{nL}

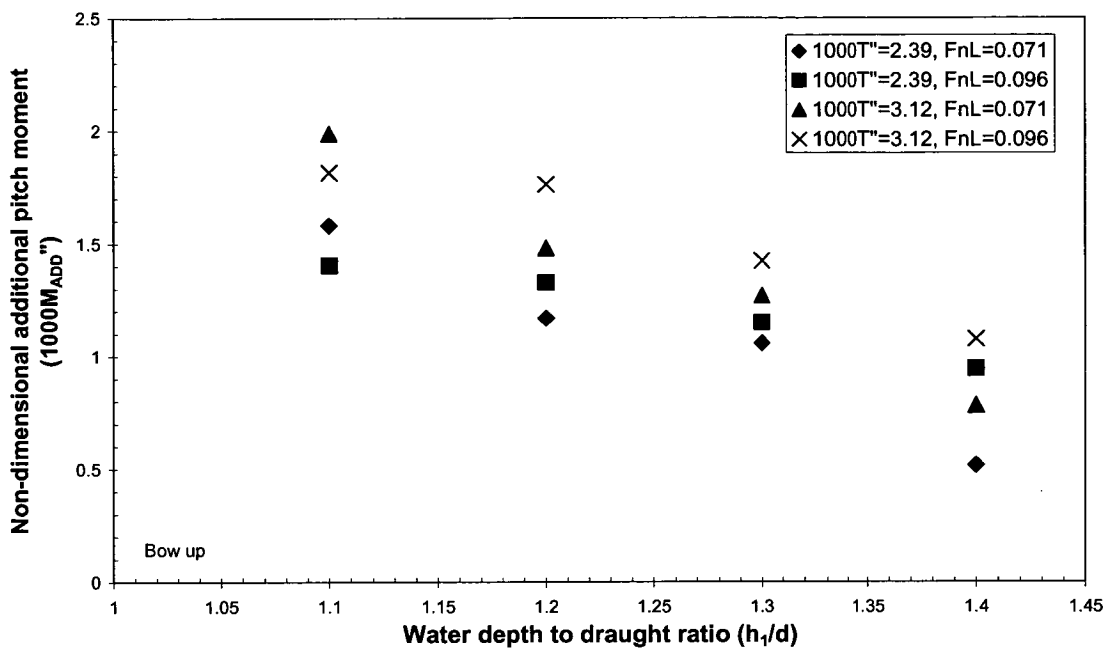


Figure 3.30 Additional pitch moment due to propulsion as a function of h_l/d , varying T'' and F_{nL}

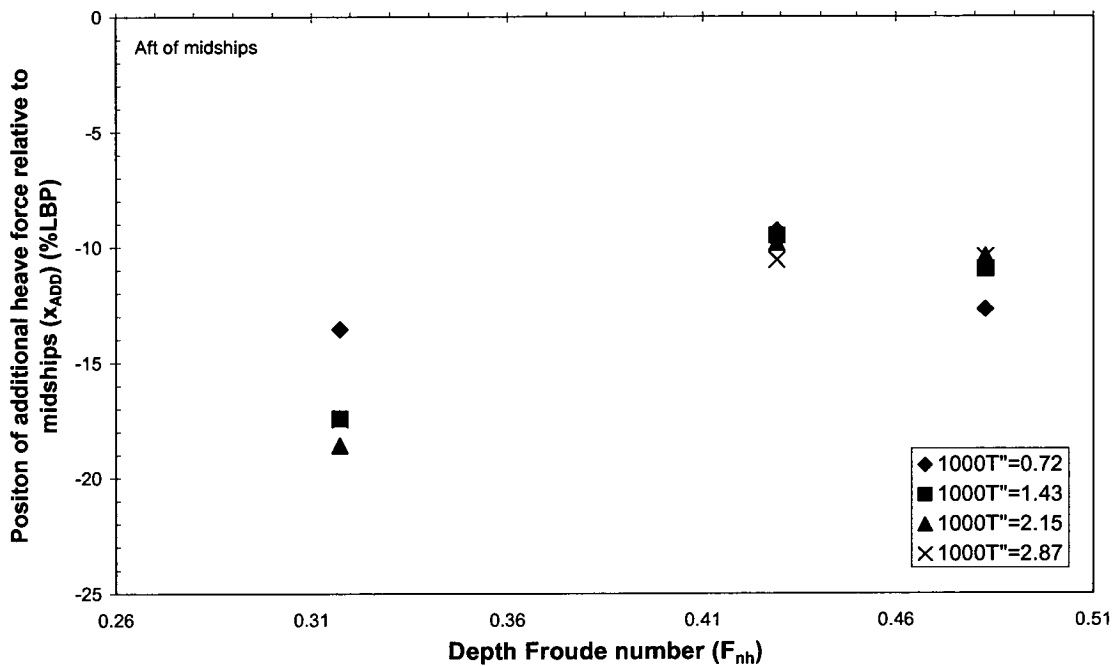


Figure 3.31 Longitudinal position of additional heave force due to propulsion as a function of F_{nh} , varying T'' , $h_l/d=1.1$

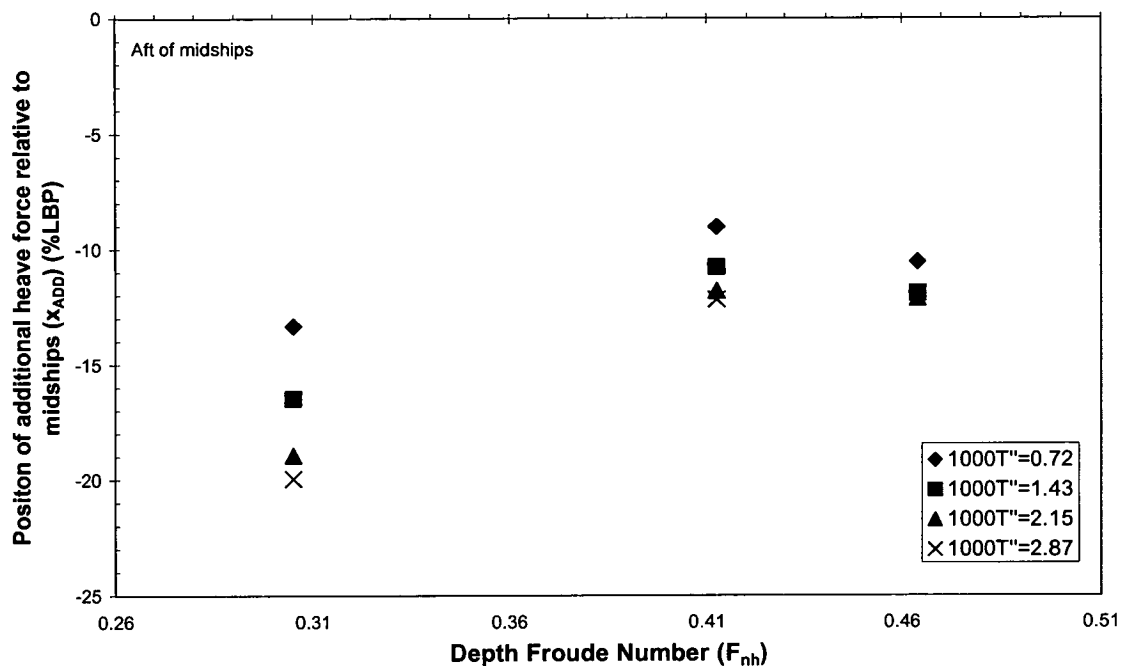


Figure 3.32 Longitudinal position of additional heave force due to propulsion as a function of F_{nh} , varying T , $h_l/d=1.2$

3.10 Unsteady squat

3.10.1 Introduction

Unsteady squat is defined as the sinkage experienced by a vessel travelling in water of non-uniform depth. Several model scale experimental studies have previously been conducted to investigate the phenomenon (Huuska 1976; Edstrand and Norrbin 1978; Haatainen *et al.* 1978; Ferguson *et al.* (1982); Renilson and Hatch 1998).

As a ship moves from one water depth to a more shallow water depth it typically experiences a reduction in speed (Huuska 1976). Edstrand and Norrbin (1978) investigated squat experienced by a ship when travelling over a 'platform type shallow', whereas Ferguson *et al.* (1982) investigated squat over a ramp bank leading to a level platform bank. Both found that the bow dipped towards the bottom as it passed the leading edge of the level platform part of the respective banks. In comparison to the cases tested in the present study, the ramp slope modelled by Ferguson *et al.* was considerably lower and the water depth to draught ratios before the bank were considerably lower, with values less than or equal to 1.7. Ferguson *et al.* found that upon approaching the bank, the transient forces and moments induced an instantaneous 'overshoot' of the steady-state sinkage and trim by bow. This resulted in a maximum instantaneous bow draught greater than the steady-state draught underway, which caused the vessel to ground. This highlights the importance of being able to predict acceleration effects in the vertical plane due to time varying squat force and moment. Edstrand and Norrbin discovered that the bow dip was followed by an increase in bodily sinkage. Ferguson *et al.* found that the bow dip was followed by a sudden bow repulsion that was accompanied by a stern sinkage.

From both studies it was reported that the stern dipped towards the sea floor as the bow passed the end of the level portion of the respective banks.

To a lesser extent unsteady squat has been studied at full scale (Queensland Transport 1996; Hatch 1999). But full scale results are difficult to compare to theoretical predictions due to the complex bottom topography and non-constant ship speed.

In comparison to the number of studies conducted to investigate squat in uniform depth, the paucity of data for unsteady squat is apparent. In addition to this, it was found that the trends from previous studies were not consistent. Hence an experimental investigation was undertaken to study vessel behaviour in the vertical plane when travelling over simplified two-dimensional bottom topographies. The aim of this work was to gain a clearer understanding of squat behaviour in non-uniform depth and to obtain data to validate the mathematical model outlined in Section 2.4.1.

3.10.2 Test program

Model scale tests were conducted in conjunction with Mr. Roger Duffield (Duffield 1997), to determine the sinkage, trim, heave force and pitch moment experienced by a vessel travelling over two simplified bank geometries: a ramp bank and a step bank. The tests were conducted with a MarAd L series model using the set up shown in Figure 3.2 to measure sinkage and trim and the set up shown in Figure 3.3 to measure the heave force and pitch moment. The channel width to vessel beam ratio for all tests was 10.3. The test cases utilised in the present study are presented in Table 3.6.

| F_{nh} before bank | F_{nh} over bank | h_1/d before bank | h_1/d over bank | Bank type | Measurement |
|----------------------|--------------------|---------------------|-------------------|-----------|----------------|
| 0.15-0.45 | 0.26-0.79 | 4.51 | 1.51 | Ramp | Force & motion |
| 0.15-0.45 | 0.27-0.82 | 4.30 | 1.30 | Ramp | Force & motion |
| 0.15-0.40 | 0.40-0.75 | 4.20 | 1.20 | Ramp | Force & motion |
| 0.15-0.45 | 0.26-0.79 | 4.51 | 1.51 | Step | Force |
| 0.15-0.45 | 0.27-0.82 | 4.30 | 1.30 | Step | Force |

Table 3.6 Test program for unsteady squat tests

3.10.3 Results and discussion

It should be noted that vessel speed was held constant during the conduct of these experiments. Therefore the change in speed as the vessel reaches the reduction in depth, as found by Haatainen *et al.* (1978), was not considered. The bow and stern sinkages were taken at the forward perpendicular and aft perpendicular, respectively.

In Figures 3.33 – 3.38 a selection of sinkage and trim results are presented for a vessel travelling over a simplified ramp bank, as described in Section 3.3. For the cases tested it was found that the vessel experienced a bow down trim leading up to the bank and over the flat portion of the bank. For most cases a stern down trim occurred as the bow left the bank; this was also found by Edstrand and Norrbin (1978) and Ferguson *et al.* (1982). This is illustrated in Figure 3.33, where the bow, midship and stern sinkage are presented for a sample case and also in Figure 3.34 where the vessel trim is presented for the same case. As can be seen, for the cases

tested, the bow was more likely to ground than the stern. Therefore the following discussion will focus on the midship sinkage and bow sinkage of the model.

In Figures 3.35 and 3.36 the midship and bow sinkage over the simplified ramp bank are presented for a constant vessel speed and two different water depths: one with a water depth to draught ratio of 1.2 over the bank and the other with a water depth to draught ratio of 1.3 over the bank. Results are also presented for two cases with a water depth to draught ratio of 1.3 but different vessel speeds in Figures 3.37 and 3.38. These cases have been selected as example cases and highlight the general findings from all cases tested. In general, the sinkage was greater for a lower water depth to draught ratio over the bank and at higher vessel speeds. The steady-state sinkage measured from separate tests in water of equivalent depth to that over the bank is also presented in these figures.

The midship sinkage and bow sinkage increased from a steady-state value as the ship travelled over the ramp; however, the increase was not notable until after the ship origin (midships) had travelled past the leading toe of the bank, as illustrated in Figures 3.35 – 3.38. There was not an instantaneous overshoot of midship and bow sinkage upon the bow approaching the leading edge of the level portion of the bank, as measured by Ferguson *et al.* (1982). In fact there was a considerable lag in the distance taken for the midship and bow sinkage to reach the equivalent steady-state sinkage in the same water depth over the bank. The length of the lag was generally larger at higher vessel speeds, as illustrated in Figures 3.37 and 3.38. The lag in the sinkage may be due to viscous effects in the thin layer of fluid between the hull and the sea floor. These viscous effects may influence the time evolution of pressure changes over the hull (Gourlay 2003). Ferguson *et al.* (1982) found that when the bow had passed the leading edge of the level portion of the bank it experienced a sudden repulsion, which was counteracted by an increase in stern sinkage; it was found that the trim changed from bow down to bow up at this point. In the present study there was a reduction in bow down trim when the ship origin was approximately half a ship length past the leading edge of the level portion of the bank, as illustrated in Figure 3.34. However, the trim did not go bow up until the end of the level portion of the bank. This variation in trim behaviour compared to Ferguson *et al.* (1982) may be attributed to the different bank dimensions, vessel particulars and water depth to draught ratios before and over the bank.

Heave and pitch oscillations occurred as the ship passed over the flat portion of the bank, as measured by Edstrand and Norrbin (1978) and Ferguson *et al.* (1982). Generally, the amplitude of these oscillations increased for the lower water depth to draught ratios over the bank and for the higher vessel speeds tested. These oscillations did not decay before the vessel reached the end of the bank when the water depth to draught ratio over the bank was reduced to a value of 1.2, as illustrated by Figures 3.35 and 3.36. For other cases the sinkage was generally found to steady just prior to the vessel reaching the end of the level portion of the bank. For low water depth to draught ratios over the bank the oscillations were more likely to exceed the equivalent steady-state sinkage for the lower speeds tested, as illustrated by Figures 3.37 and 3.38. There was a large reduction in midship sinkage and bow sinkage as the bow passed over the end of the bank, with the trim going stern down for a short distance for most cases, as mentioned earlier. However, despite this stern down trim the stern was not likely to ground in the cases tested.

A number of tests were also performed to measure the heave force and pitch moment over a step bank and ramp bank. Results for the two bank types are compared in Figures 3.39 and 3.40 for heave force and pitch moment, respectively. There is a difference of approximately 20% between the magnitudes of the two squat force measurements in uniform water depth leading up

to the bank in Figure 3.39. This may be due to experimental error, as the magnitude of the forces was small when the model was travelling in deep water. Drobyshevskiy (2000) and Gourlay (2003) stated that it is possible for a ship to 'sense' a sudden change in depth; i.e. the sinkage increases before the ship reaches the bank. Drobyshevskiy (2000) proposed that when a ship is approaching a step decrease in depth the longitudinal fluid velocity decreases around her fore-body, because the fluid meets an obstacle 'reflecting' the flow. Some of the fluid is diverted sideways and the rest goes over the step with an increased velocity, causing an attraction force and hence a pitch moment, so that the ship dips before reaching the step. However, for the cases tested in the present study, the midship and bow sinkage did not begin to increase before the bow reached the step. This may be due to the relatively high water depth to draught ratio before the bank in the present study; therefore the restriction to the flow may not be sufficient for the 'reflected' fluid to cause sufficient pressure changes to influence the sinkage before the vessel reaches the bank. From Figure 3.40 it can be seen that the magnitude of the maximum bow down pitch moment was greater for the step case when the ship origin was in the vicinity of the leading edge of the level/step bank and also there was a much larger reduction in the bow down moment for the step bank case when the origin was located at a non-dimensional distance of approximately 4.5. This may be due to the more rapid movement of fluid associated with transit over the more abrupt depth change for the step bank case.

It has been found that, even at low speeds, the sinkage of a vessel changed in response to variations in the sea-bed profile. The change in pressure distribution over the hull due to forward motion in non-uniform water depth caused time varying sinkage, which can cause additional sinkage due to acceleration effects. Hence, it is important to accurately model these dynamic acceleration effects when simulating the behaviour of a vessel in shallow water. It is possible that viscous effects may make a small contribution to the flow field around a vessel travelling from deep water to shallow water, where the under keel clearance is relatively low. The presence of the bank will modify the boundary layer growth and wake structure aft of the vessel, which will influence the forces and moments acting on the hull.

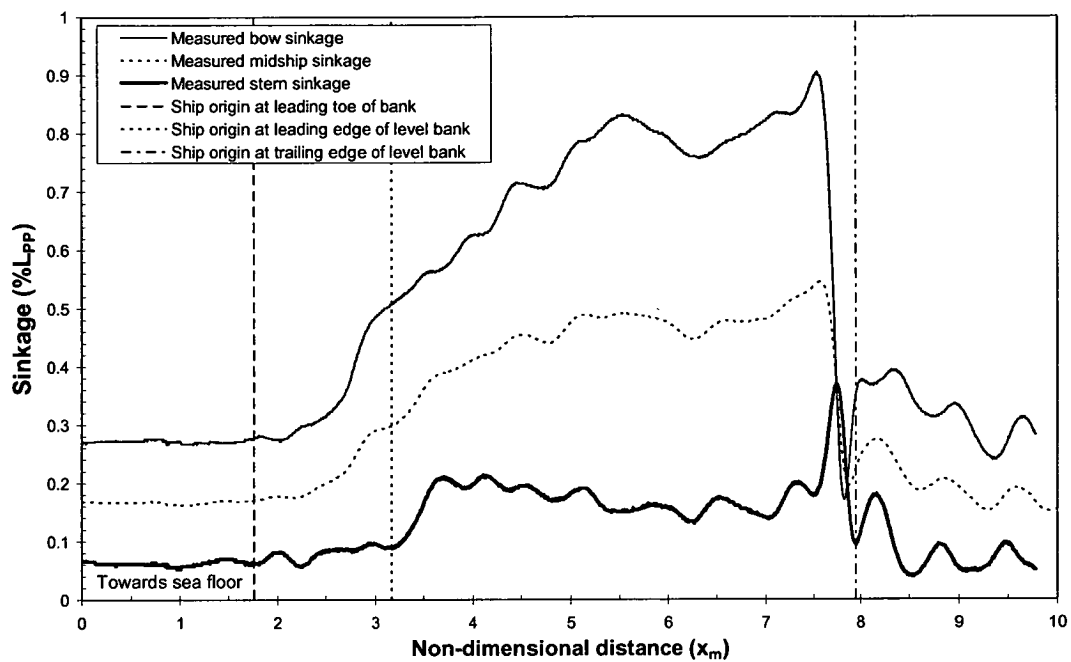


Figure 3.33 Sinkage over ramp bank, $F_{nh}=0.30-0.55$, $h_l/d=4.3-1.3$

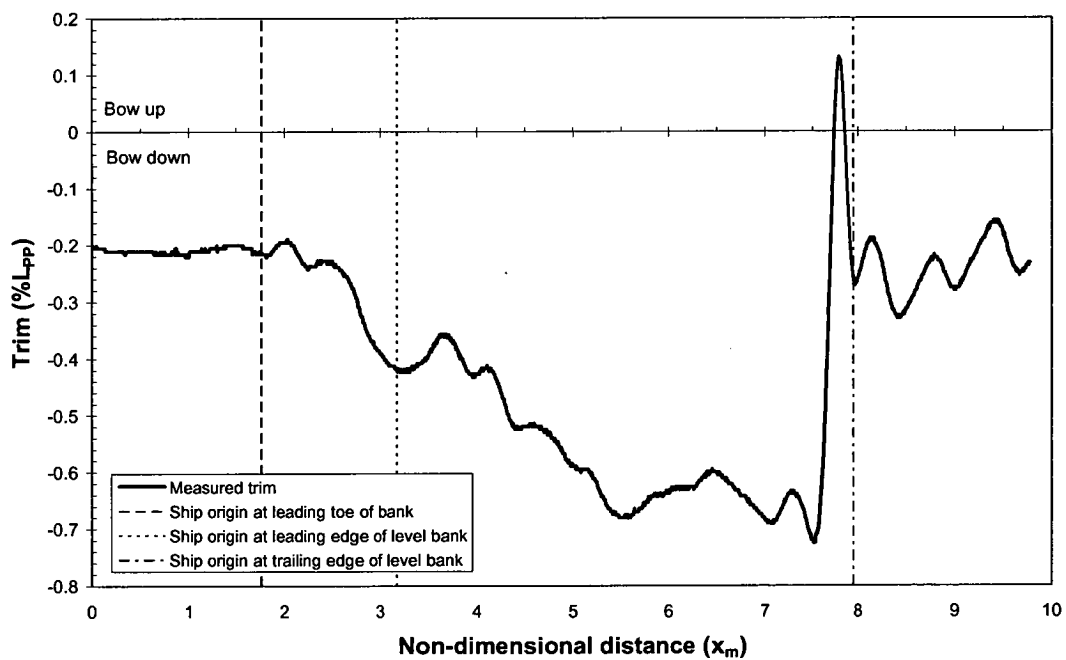


Figure 3.34 Trim over ramp bank, $F_{nh}=0.30-0.55$, $h_l/d=4.3-1.3$

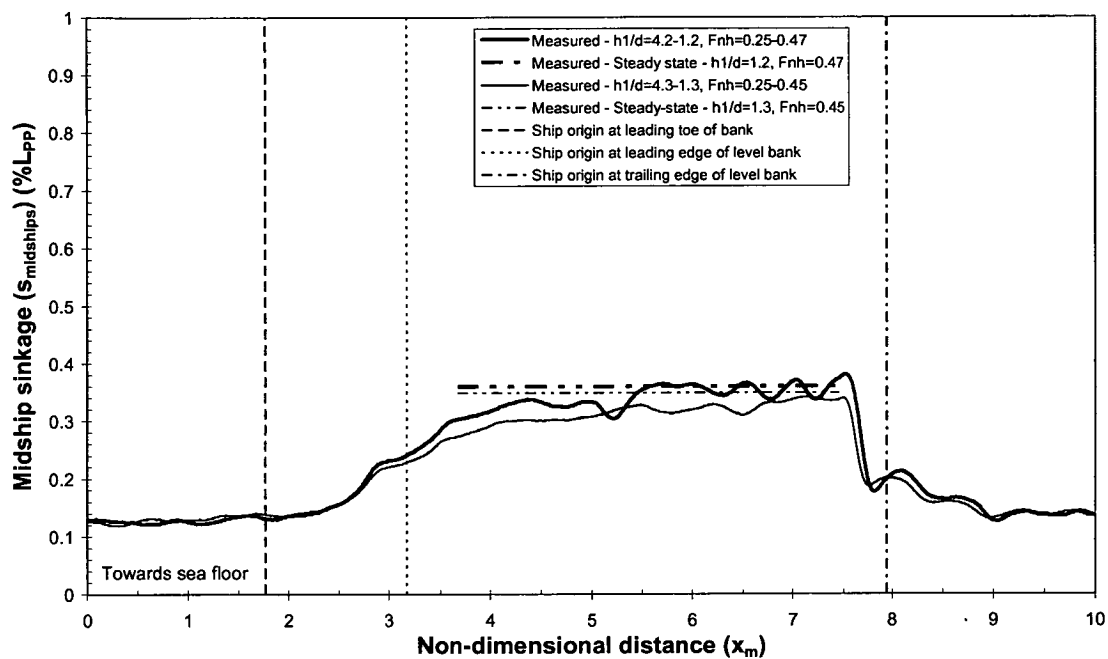


Figure 3.35 Midship sinkage over ramp bank for different water depths

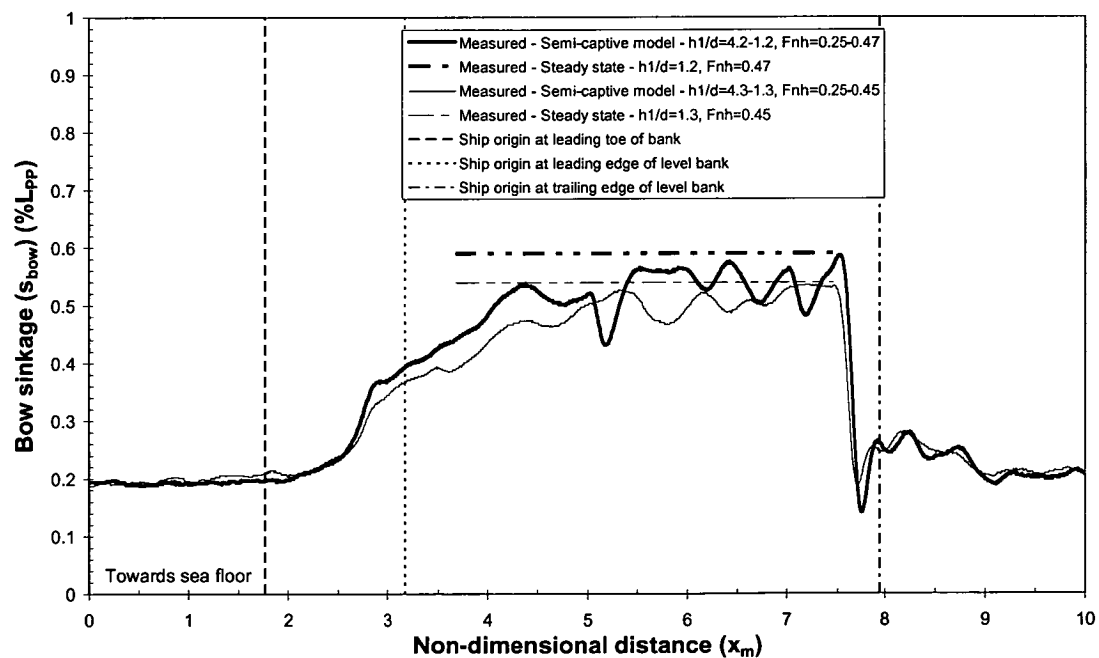


Figure 3.36 Bow sinkage over ramp bank for different water depths

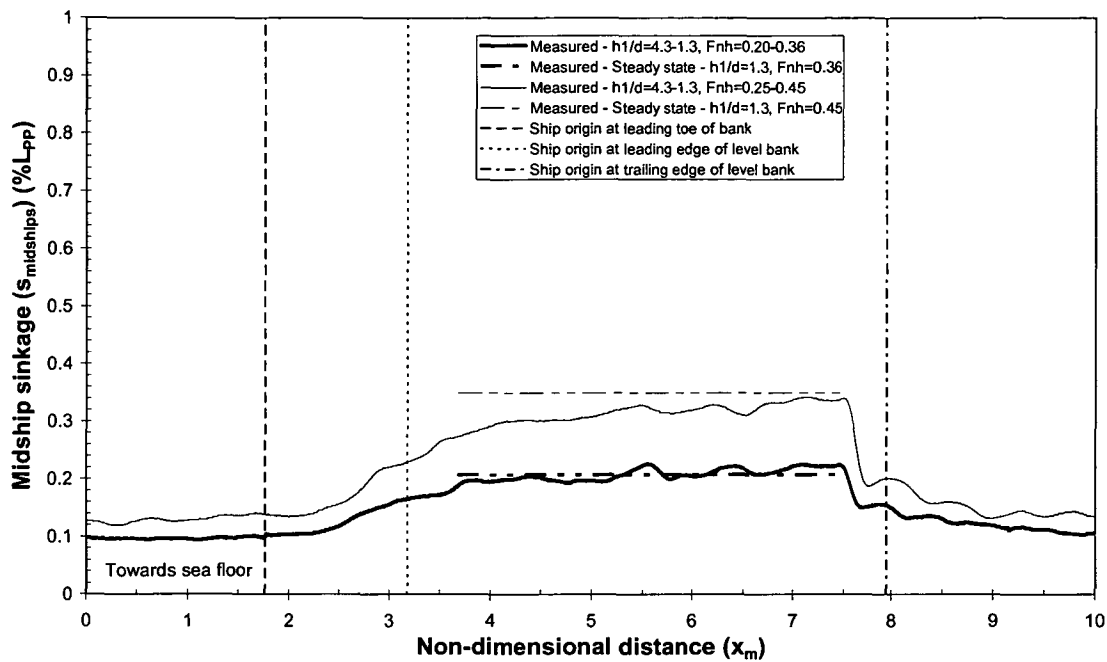


Figure 3.37 Midship sinkage over ramp bank for different vessel speeds

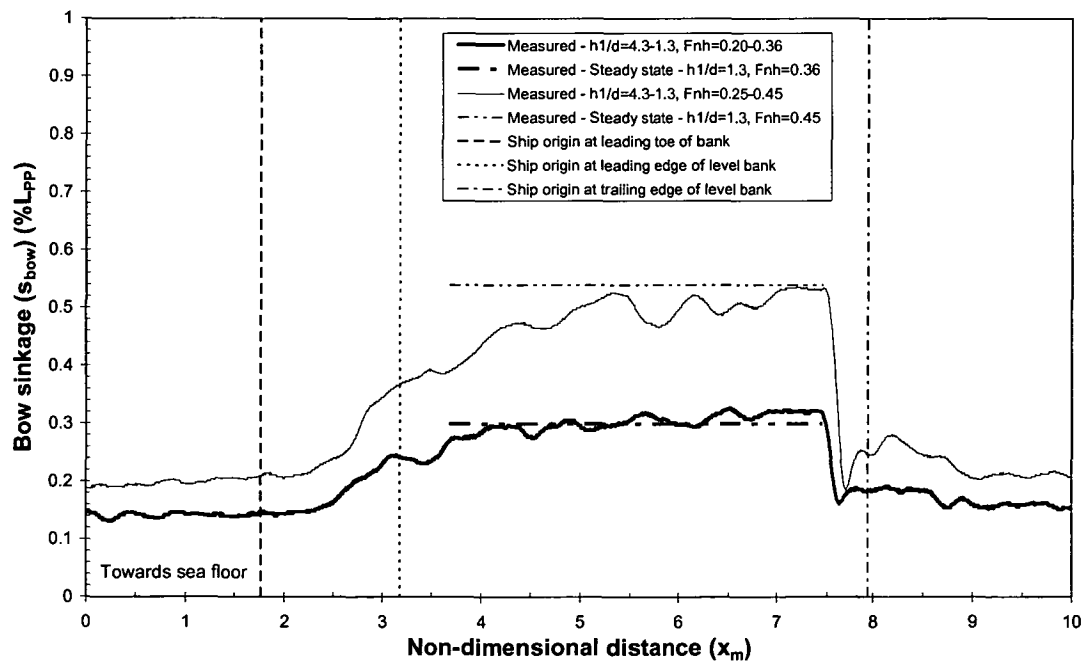


Figure 3.38 Bow sinkage over ramp bank for different vessel speeds

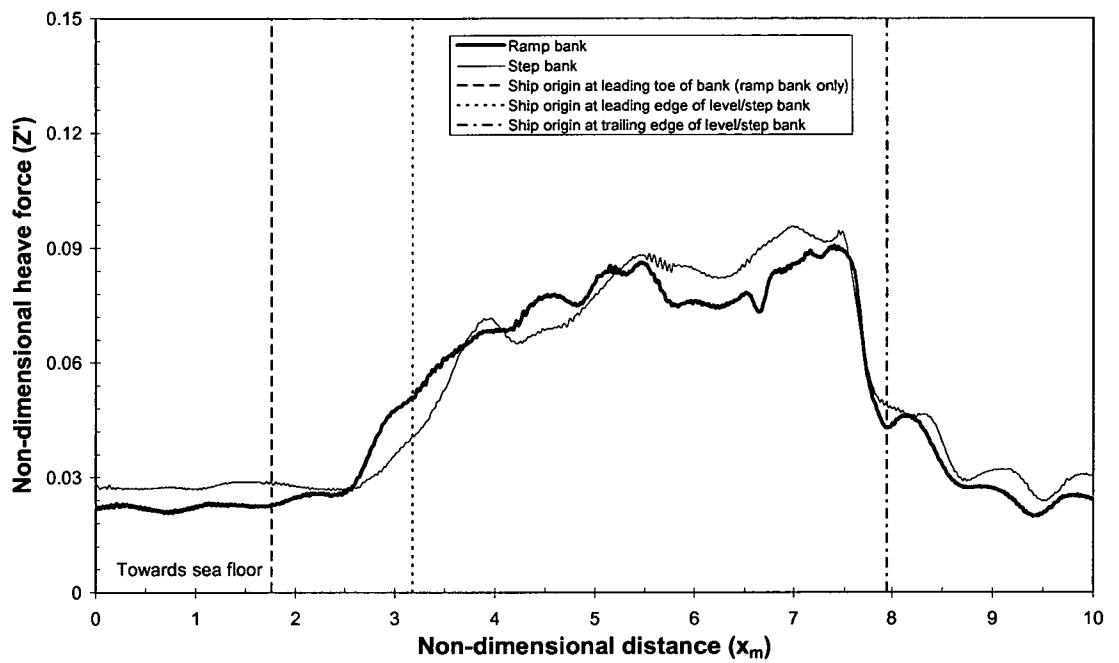


Figure 3.39 Heave force over ramp bank and step bank, $h_1/d=4.3-1.3$, $F_{nh}=0.35-0.63$

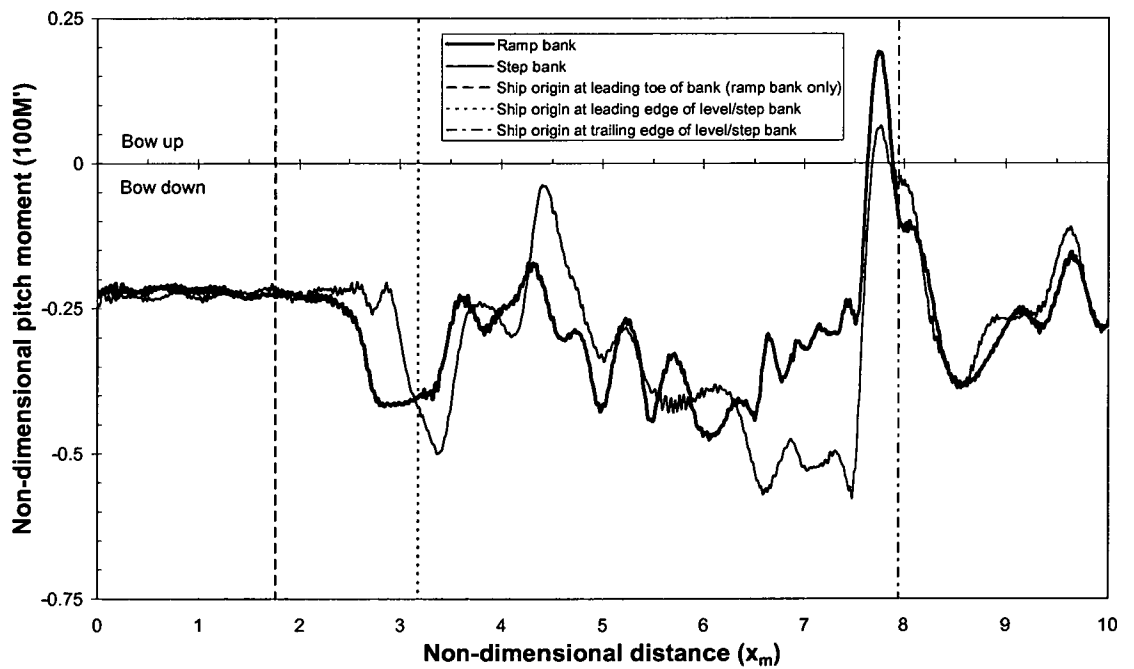


Figure 3.40 Pitch moment over ramp bank and step bank, $h_1/d=4.3-1.3$, $F_{nh}=0.35-0.63$

3.11 Assessment of three-dimensional panel method

The number of model scale experiments that could be conducted was limited by the resources and time required to perform them. Steady-state heave force and pitch moment due to squat in water of uniform depth, with the vessel on the channel centreline, have been predicted using the potential flow module of Shipflow 2.5. Background concerning the computation technique is provided in Section 2.3.2. In the present section the predictions are compared to steady-state model scale experiment results to assess if the prediction technique is sufficiently accurate to be used to extend the steady-state experimental data matrix for the regression analyses.

In general, as blockage and ship speed are increased the flow around a ship becomes more complex (Gourlay 2006). Therefore, in the first instance, predictions were performed for sub-critical cases with a channel width to vessel beam ratio of 10.3, where the general flow properties should be more suited to the Shipflow prediction technique. Computations were performed with both linear and non-linear free surface boundary conditions for cases with the ship fixed in position in the vertical plane. The results from both methods were similar since wave effects were small for the selected sub-critical cases.

Whilst predictions were performed for a large number of cases, only a selection of results that illustrates general trends is presented. Predicted and measured non-dimensional heave force and pitch moment for a range of water depth to draught ratios are presented in Figures 3.41 and 3.42, respectively. Based on the analysis outlined in Appendix D, the uncertainty limits for the model scale measurements in Figures 3.41 and 3.42 will generally be in the order of $\pm 5\%$ to $\pm 10\%$. As can be seen the numerical predictions lie outside these uncertainty limits, with the steady-state heave force underestimated by up to approximately 35%, whilst the pitch moment was underestimated by up to approximately 80% at the higher depth Froude numbers tested. Panel method predictions have previously been found to underestimate squat for fine form hulls at comparable depth Froude numbers to the present study, for example Abbott (1998).

The poor correlation with model scale measurements in the present study may be partly due to the fact that viscous effects were not modelled. A more accurate solution using Shipflow may be achievable by dividing the flow into three zones, as shown in Figure 2.2. The outer flow could be modelled using potential flow theory in Zone I. A momentum integral method could be applied to model the viscous effects in the boundary layer in Zone II and a Reynolds Averaged Navier Stokes solution could be applied over the stern region of the ship in Zone III to account for viscous effects in the stern/wake flow.

Due to the poor correlation with model scale measurements, predictions using the Shipflow 2.5 potential flow method were not included in the steady-state data matrix for the regression analyses. There are a number of alternative prediction techniques that could have been investigated, as described above and as outlined in Section 2.2.1. However, due to the difficulties in accurately predicting the complex nature of the flow around a ship travelling in restricted water, it was decided that empirical equations based on steady-state model scale experimental results would provide the most practical and reliable results for input to the mathematical model.

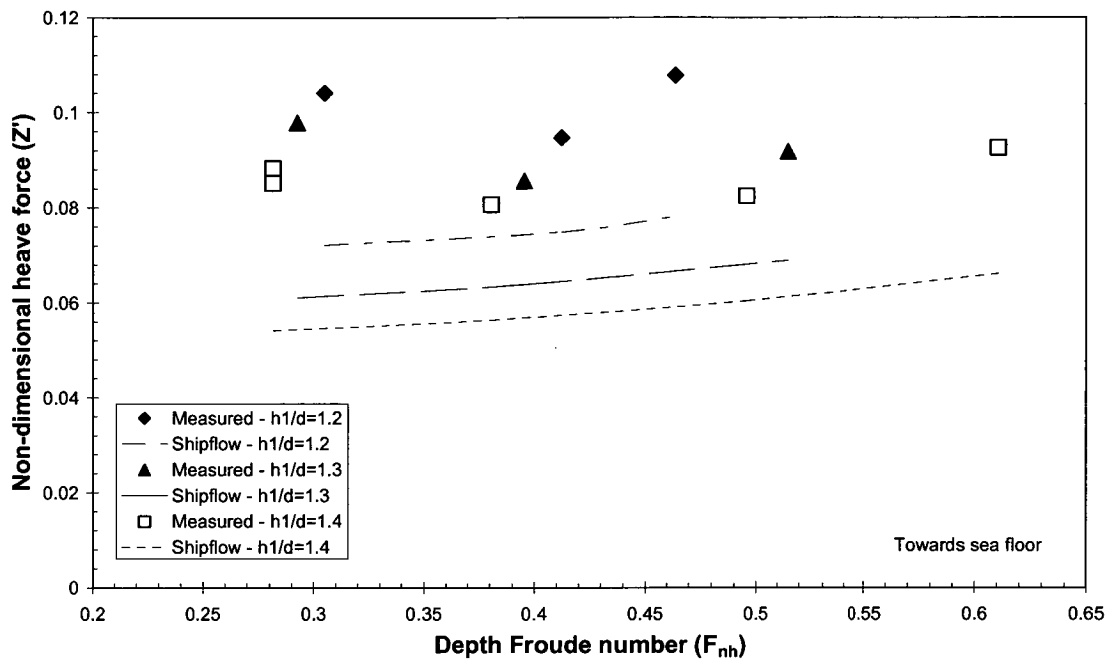


Figure 3.41 Comparison between measured heave force and Shipflow predictions, $W/B=10.3$

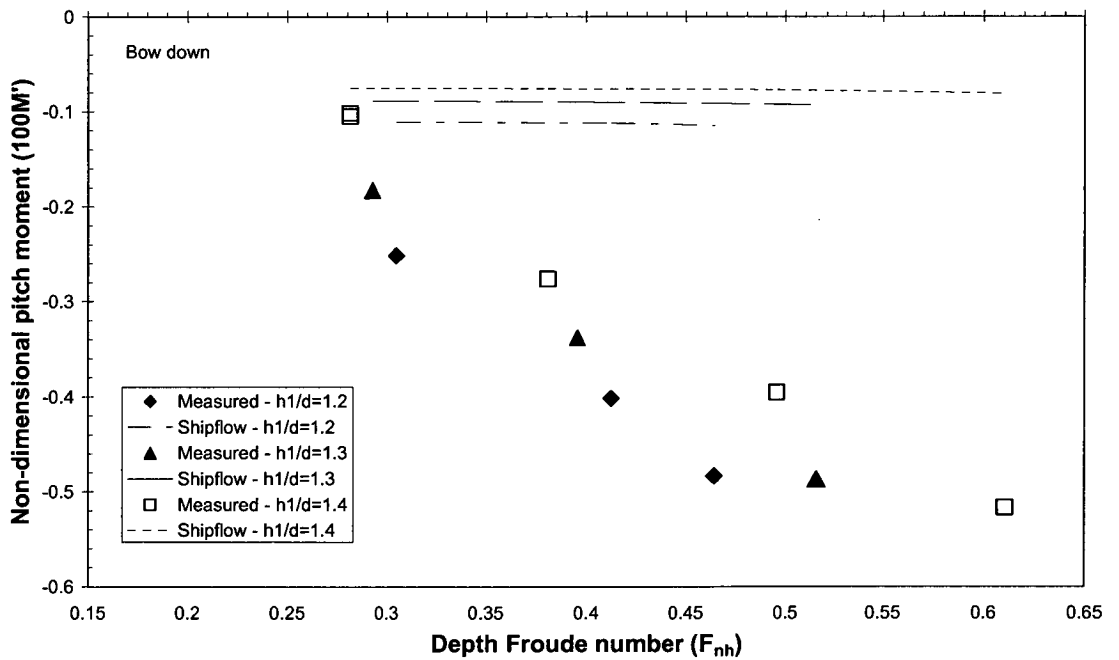


Figure 3.42 Comparison between measured pitch moment and Shipflow predictions, $W/B=10.3$

3.12 Concluding remarks

Model scale investigations have been undertaken to examine steady-state and unsteady squat.

The effect of scale on squat measurements for 2 and 4m bulk carrier models was found to be small. At the higher depth Froude depth numbers tested the bow sinkage coefficient was marginally greater for the 4m model. However, the results were within predicted uncertainty limits.

For a bulk carrier model in sub-critical cases both non-dimensional downward heave force and bow down pitch moment were greater for higher depth Froude numbers and lower water depth to draught ratios. The non-dimensional downward heave force was greater for lower channel width to vessel beam ratios. However, the non-dimensional bow down pitch moment was smaller for low channel width to beam ratios. Sinkage predictions using hydrostatic particulars showed that the sinkage at the forward perpendicular was generally greater for low channel width to beam ratios. The pitch moment was found to be bow up for cases with high blockage and depth Froude numbers where trans-critical flow occurred.

Compared to the unpropelled case, propulsion increased the downwards heave force and reduced the bow down pitch moment for a bulk carrier model. Propulsion was found to have a greater influence on pitch moment than heave force.

Even at low speeds, the sinkage of a vessel changed in response to variations in the sea-bed profile. The change in pressure distribution over the hull due to forward motion in non-uniform water depth caused time varying sinkage, which can cause additional sinkage due to acceleration effects. For the cases tested there was a lag in the distance taken for the midship and bow sinkage to reach the equivalent steady-state sinkage in the same water depth over the bank. It was found that, for a vessel travelling over a ramped bank, the unsteady sinkage over the bank can exceed the equivalent steady-state sinkage in the same water depth.

Steady-state heave force and pitch moment predictions using the potential flow module of Shipflow 2.5 were compared against model scale measurements to assess if the prediction technique is sufficiently accurate to be used to extend the steady-state experimental data matrix for the regression analyses. The steady-state heave force was underestimated by up to approximately 35%, whilst the pitch moment was underestimated by up to approximately 80%. This may be partly due to the fact that viscous effects were not modelled. Hence predictions using the Shipflow 2.5 potential flow method were not included in the steady-state data matrix. Due to the difficulties in accurately predicting the complex nature of the flow around a ship travelling in restricted water, it was decided that empirical equations based on steady-state model scale experimental results would provide the most practical and reliable results for input to the mathematical models.

Chapter 4

Modelling of Unsteady Squat for Ship-Handling Simulation

4.1 Introduction

As discussed in Chapter 3, model scale experiments were conducted to determine the heave force and pitch moment due to squat for a range of vessel speeds, channel widths, water depths and effective thrusts. In this chapter multiple linear regression analysis techniques have been used on the experimental data to develop equations for the prediction of steady-state heave force and pitch moment due to squat for an unpropelled hull. Additional regression analyses were performed to produce correction factors for the effect of propulsion on steady-state heave force and pitch moment. Details concerning multiple linear regression analysis are presented in Section 2.3.1.

The equations to predict steady-state squat for an unpropelled hull have been used as input to a quasi-steady mathematical model to predict unsteady squat and dynamic acceleration effects in the vertical plane. Details concerning the mathematical model can be found in Section 2.4.1. In this chapter the mathematical model has been validated in two steps. Firstly, predictions were performed for cases with uniform water depth and compared against steady-state model scale measurements. Secondly, unsteady squat predictions were performed for a vessel travelling over a simplified two-dimensional ramp bank and compared to unsteady model scale squat measurements for the same bank configuration.

4.2 Prediction of steady-state heave force and pitch moment for an unpropelled hull

4.2.1 Regression parameters

Regression analyses have been conducted to develop equations to predict the steady-state heave force and pitch moment due to squat as a function of vessel speed, channel width, vessel beam and under keel clearance. A number of possible non-dimensional expressions were tested to determine the most suitable regression parameters. The selection of possible parameters was based on the requirements that squat must be non-zero at infinite under keel clearance and infinite channel width and each parameter must be easily attainable for input to ship-handling simulator mathematical models. The selection of the regression parameters is discussed in the following sections.

Vessel speed parameter

Both length Froude number and depth Froude number were considered as possible non-dimensional vessel speed parameters for the regression analyses. Similar data fits were achieved

using either parameter. Since water depth was seen to have a significant influence on the squat force and moment, depth Froude number was chosen as the most suitable parameter.

In Section 3.8.3 it was shown that non-dimensional heave force and pitch moment vary in a non-linear manner with depth Froude number. It was found that a maximum power of 2 was sufficient to account for this non-linearity, whilst still providing accurate prediction between data points.

Under keel clearance parameter

In Section 3.8.3 it was shown that the magnitude of heave force and pitch moment was larger for low water depth to draught ratios. Four possible parameters are presented in Equations 4.1 – 4.4; each are dependent upon the water depth in the channel and vessel draught. These were selected based on the fact that their magnitude is larger for low water depth to draught ratios and they approach zero for the deep water case. In Section 3.8.3 it was shown that the magnitude of heave force and pitch moment can vary for cases with different draughts but having a constant water depth to draught ratio. Due to insufficient data, an additional parameter was not included to account for this.

$$e^{(-h_1/d)} \quad (4.1)$$

$$d/h_1 \quad (4.2)$$

$$e^{(-(h_1/d)-1)} \quad (4.3)$$

$$d/(h_1-d) \quad (4.4)$$

Preliminary multiple regression analyses were performed to identify the parameter with the best statistical fit using Equations 4.5 and 4.6. These analyses were restricted to cases where only the under keel clearance parameters were varied; the values of all other independent variables were held constant. A maximum power of 2 was found to be sufficient to account for the non-linear relationship between the under keel clearance parameters and the heave force and pitch moment, whilst still providing accurate interpolation between observed values.

$$Z' = a_0 + a_1 x + a_2 x^2 \quad (4.5)$$

$$100M' = b_0 + b_1 x + b_2 x^2 \quad (4.6)$$

Where $a_0, a_1, a_2, b_0, b_1, b_2$ are constants and x represents the under keel clearance parameters.

Results from the preliminary regression analyses for a selection of cases are presented in Tables 4.1 and 4.2 for heave force and pitch moment, respectively. It was found that $e^{(-h_1/d)}$ was the most suitable parameter for heave force with the lowest standard error and the largest coefficient of determination for most cases. The parameter $d/(h_1-d)$ was found to generally provide the best statistical fit for pitch moment.

| Parameter | F_{nL} | W/B | Standard error (*1000) | Adjusted R^2 | R^2 |
|--------------------|----------|------|---------------------------|----------------|--------|
| $e^{(-h_1/d)}$ | 0.379 | 10.3 | 2.28 | 0.9903 | 0.9951 |
| $e^{((-h_1/d)-1)}$ | | | 2.28 | 0.9903 | 0.9951 |
| d/h_1 | | | 3.03 | 0.9828 | 0.9914 |
| $d/(h_1-d)$ | | | 3.72 | 0.9741 | 0.9871 |
| $e^{(-h_1/d)}$ | 0.336 | 5.0 | 2.30 | 0.9999 | 0.9999 |
| $e^{((-h_1/d)-1)}$ | | | 2.30 | 0.9999 | 0.9999 |
| d/h_1 | | | 4.80 | 0.9995 | 0.9997 |
| $d/(h_1-d)$ | | | 5.46 | 0.9306 | 0.9653 |
| $e^{(-h_1/d)}$ | 0.336 | 4.0 | 0.31 | 0.9999 | 0.9999 |
| $e^{((-h_1/d)-1)}$ | | | 0.31 | 0.9999 | 0.9999 |
| d/h_1 | | | 1.03 | 0.9990 | 0.9995 |
| $d/(h_1-d)$ | | | 11.40 | 0.8752 | 0.9376 |

Table 4.1 Statistical fit for under keel clearance parameters for heave force for three sample cases

| Parameter | F_{nL} | W/B | Standard error (*1000) | Adjusted R^2 | R^2 |
|--------------------|----------|------|---------------------------|----------------|--------|
| $e^{(-h_1/d)}$ | 0.379 | 10.3 | 5.73 | 0.9968 | 0.9989 |
| $e^{((-h_1/d)-1)}$ | | | 5.73 | 0.9968 | 0.9989 |
| d/h_1 | | | 7.24 | 0.9949 | 0.9983 |
| $d/(h_1-d)$ | | | 14.31 | 0.9801 | 0.9934 |
| $e^{(-h_1/d)}$ | 0.336 | 5.0 | 42.10 | 0.4818 | 0.7409 |
| $e^{((-h_1/d)-1)}$ | | | 42.10 | 0.4818 | 0.7409 |
| d/h_1 | | | 41.50 | 0.4967 | 0.7483 |
| $d/(h_1-d)$ | | | 17.18 | 0.9137 | 0.9569 |
| $e^{(-h_1/d)}$ | 0.336 | 4.0 | 37.39 | 0.7181 | 0.8590 |
| $e^{((-h_1/d)-1)}$ | | | 37.39 | 0.7181 | 0.8590 |
| d/h_1 | | | 36.60 | 0.7299 | 0.8649 |
| $d/(h_1-d)$ | | | 5.98 | 0.9928 | 0.9964 |

Table 4.2 Statistical fit for under keel clearance parameters for pitch moment for three sample cases

Channel width parameter

In Section 3.8.3 it was shown that heave force was larger for low channel width to beam ratios. Two possible parameters were selected for the heave force regression, as shown in Equations 4.7 and 4.8, which take on larger values for low channel widths. However, these parameters provided a poor statistical fit for pitch moment since it went bow up for cases with trans-critical flow. Therefore the additional parameters given in Equations 4.9 and 4.10 were also tested for pitch moment.

$$B/W \tag{4.7}$$

$$e^{(-W/B)} \tag{4.8}$$

W/B

(4.9)

$e^{(-B/W)}$

(4.10)

Preliminary multiple regression analyses were performed to identify the parameter with the best statistical fit using Equations 4.11 and 4.12. This analysis was restricted to cases where only the channel width parameters were varied; the values of all other independent variables were held constant. A maximum power of 2 was found to be sufficient to account for the non-linear relationship between the channel width parameters and the heave force and pitch moment, whilst still providing accurate interpolation between observed values.

$Z''=a_0+a_1x+a_2x^2$

(4.11)

$100M''=b_0+b_1x+b_2x^2$

(4.12)

Where $a_0, a_1, a_2, b_0, b_1, b_2$ were constants and x represents the channel width parameters.

Results from the preliminary regression analyses for sample cases are presented in Tables 4.3 and 4.4 for heave force and pitch moment, respectively. It was found that B/W was generally the parameter that provided the best statistical fit for heave force, with the lowest standard error and the largest coefficient of determination. For the pitch moment it was difficult to clearly identify the parameter with the best statistical fit, as it was very much case dependent. Generally, however, it was found that $e^{(-W/B)}$ provided the best fit.

| Parameter | F_{nh} | h_l/d | Standard error (*1000) | Adjusted R^2 | R^2 |
|--------------|----------|---------|---------------------------|----------------|--------|
| B/W | 0.50 | 1.2 | 1.30 | 0.9993 | 0.9998 |
| $e^{(-W/B)}$ | | | 1.41 | 0.9189 | 0.9730 |
| B/W | 0.50 | 1.4 | 0.64 | 0.9997 | 0.9999 |
| $e^{(-W/B)}$ | | | 10.22 | 0.9109 | 0.9703 |
| B/W | 0.50 | 1.7 | 2.63 | 0.9875 | 0.9958 |
| $e^{(-W/B)}$ | | | 8.34 | 0.8742 | 0.9581 |

Table 4.3 Statistical fit for channel width parameters for heave force for sample cases

| Parameter | F_{nh} | W/B | Standard error (*1000) | Adjusted R^2 | R^2 |
|--------------|----------|-----|---------------------------|----------------|--------|
| B/W | 0.50 | 1.2 | 0.17 | 0.9963 | 0.9988 |
| $e^{(-W/B)}$ | | | 0.16 | 0.9966 | 0.9988 |
| W/B | | | 0.56 | 0.9581 | 0.9860 |
| $e^{(-B/W)}$ | | | 0.10 | 0.9986 | 0.9995 |
| B/W | 0.60 | 1.2 | 0.83 | 0.9940 | 0.9980 |
| $e^{(-W/B)}$ | | | 0.55 | 0.9973 | 0.9991 |
| W/B | | | 2.16 | 0.9593 | 0.9864 |
| $e^{(-B/W)}$ | | | 1.05 | 0.9904 | 0.9968 |
| B/W | 0.50 | 1.4 | 0.11 | 0.9919 | 0.9973 |
| $e^{(-W/B)}$ | | | 0.28 | 0.9496 | 0.9832 |
| W/B | | | 0.33 | 0.9283 | 0.9761 |
| $e^{(-B/W)}$ | | | 0.13 | 0.9893 | 0.9964 |
| B/W | 0.50 | 1.7 | 0.14 | 0.9246 | 0.9749 |
| $e^{(-W/B)}$ | | | 0.07 | 0.9793 | 0.9931 |
| W/B | | | 0.03 | 0.9966 | 0.9989 |
| $e^{(-B/W)}$ | | | 0.13 | 0.9336 | 0.9778 |

Table 4.4 Statistical fit for channel width parameters for pitch moment for sample cases

4.2.2 Empirical formulae for heave force and pitch moment on an unpropelled hull

The general form of the regression equations is given in Equations 4.13 and 4.14 for heave force and pitch moment. The independent variables were created as functions of the chosen parameters.

$$Z' = \sum_{i=0}^2 \sum_{j=0}^2 \sum_{k=0}^2 (F_{nh})^i (e^{(-h_1/d)})^j (B/W)^k \quad (4.13)$$

$$M' = \sum_{i=0}^2 \sum_{j=0}^2 \sum_{k=0}^2 (F_{nh})^i (d/(h_1 - d))^j (e^{(-W/B)})^k \quad (4.14)$$

The final regression equations for heave force and pitch moment due to squat are given in Equations 4.15 and 4.16.

$$Z' = C_z \left(\frac{2.84(e^{(-h_1/d)}) (B/W) + 0.19(1/F_{nh}) + 4.41(B/W)^2}{-(1.06E - 2)(e^{(-h_1/d)})^{-1}} \right) + 3.14E - 2 \quad (4.15)$$

$$\text{Where } C_z = (F_{nh}) (e^{(-h_1/d)})$$

$$100M' = C_M \left(\begin{aligned} &1.81(F_{nh})(d/(h_1 - d))(e^{(-W/B)}) - 0.31(F_{nh})(e^{(-W/B)})^{-1} \\ &+ 1.04(F_{nh})(d/(h_1 - d)) + (1.52E - 2)(F_{nh})(d/(h_1 - d))(e^{(-W/B)})^{-1} \\ &+ 6.03(F_{nh})(h_1 - d)/d - 4.57(d/(h_1 - d))e^{(-W/B)} \end{aligned} \right) - 0.23 \quad (4.16)$$

Where $C_M = (F_{nh})(d/(h_1 - d))(e^{(-W/B)})$

The coefficient of determination (R^2) was 0.976 and 0.853 for the heave force and pitch moment, respectively. This indicates that 97.6% and 85.3% of the original variability has been explained with the variables specified in the models. The fit for the pitch moment was poorer than that for the squat force due to its greater non-linearity with channel width parameters and under keel clearance parameters. This may be partly due to the fact that the pitch moment changes from bow down to bow up when the flow changes from sub-critical to trans-critical. The above formulae have been validated in conjunction with the squat mathematical model in Section 4.4.

A common problem with such equations is that they may not represent the effect of independent variables properly when extrapolated beyond the range of experimental data. Hence, it is important to highlight the limiting conditions, or boundaries of application, of the developed mathematical expressions. The boundaries of application for the above formulae, in terms of extreme values of the varied parameters, are as follows:

- $0.30 < F_{nh} < 0.57$ for $1.1 < h_1/d < 1.3$
- $0.28 < F_{nh} < 0.61$ for $1.4 < h_1/d < 1.7$
- $0.16 < F_{nh} < 0.45$ for $1.5 < h_1/d < 4.5$
- $3.0 < W/B < 10.3$
- $0.208 < d/h_1 < 0.906$

The results for a channel width to vessel beam ratio of 10.3 may not correspond to an infinite width case. These results could be corrected to correspond to infinite width using an effective channel width (Tuck 1967).

4.3 Prediction of steady-state heave force and pitch moment due to propulsion

4.3.1 Regression parameters

Equations were developed through regression analysis to predict the correction to unpropelled steady-state heave force and pitch moment due to propulsion. These formulae are a function of vessel speed, under keel clearance and effective thrust. As with the equations developed for the unpropelled hull case, a number of possible non-dimensional expressions were tested to determine the most suitable regression parameters. The selection of possible parameters was based on the requirements that the additional heave force and pitch moment due to propulsion must be zero for a zero effective thrust and each parameter must be easily attainable for input to ship-handling simulator mathematical models. The selection of the regression parameters is discussed in the following sections.

Vessel speed parameter

As for the unpropelled hull case depth Froude number was found to be the most suitable vessel speed parameter, providing a marginally better statistical fit than length Froude number.

Effective thrust

The non-dimensional additional heave force and pitch moment due to propulsion increased with non-dimensional effective thrust, as shown for example cases in Figures 4.1 and 4.2. Non-dimensional effective thrust was found to provide acceptable statistical fit for both additional heave force and additional pitch moment due to propulsion. Therefore alternative thrust parameters were not investigated.

Under keel clearance parameter

The influence of vessel draught and water depth is represented in the final regression equations by a single parameter. In Section 3.9.4 it was shown that the additional heave force and pitch moment due to propulsion was larger at low water depth to draught ratios. Therefore the same parameters used for the unpropelled hull were investigated. Each of the parameters are dependent upon the water depth in the channel and vessel draught.

Preliminary multiple regression analyses were performed to identify the parameter with the best statistical fit using Equations 4.17 and 4.18. This analysis was restricted to cases where only the under keel clearance parameters were varied; the values of all other independent variables were held constant. A maximum power of 2 was found to be sufficient to account for the non-linear relationship between the under keel clearance parameters and the additional heave force and pitch moment due to propulsion.

$$1000Z_{ADD}'' = a_0 + a_1x + a_2x^2 \quad (4.17)$$

$$1000M_{ADD}'' = b_0 + b_1x + b_2x^2 \quad (4.18)$$

Where $a_0, a_1, a_2, b_0, b_1, b_2$ are constants and x represents the under keel clearance parameters.

Results from the preliminary regression analyses for example cases are presented in Tables 4.5 and 4.6 for additional heave force and pitch moment due to propulsion, respectively. It was found that d/h_1 was the most suitable parameter for additional heave force due to propulsion with the lowest standard error and the largest coefficient of determination. The parameter $e^{(-h_1/d)}$ was found to provide the best statistical fit for the additional pitch moment due to propulsion.

| Parameter | F_{nL} | 1000T'' | Standard error (*1000) | Adjusted R^2 | R^2 |
|--------------------|----------|---------|---------------------------|----------------|--------|
| $e^{(-h_1/d)}$ | 0.096 | 2.24 | 1.95 | 0.9536 | 0.9768 |
| $e^{((-h_1/d)-1)}$ | | | 1.97 | 0.9521 | 0.9761 |
| d/h_1 | | | 1.94 | 0.9537 | 0.9769 |
| $d/(h_1-d)$ | | | 2.16 | 0.9422 | 0.9711 |
| $e^{(-h_1/d)}$ | 0.071 | 2.39 | 0.68 | 0.9869 | 0.9934 |
| $e^{((-h_1/d)-1)}$ | | | 0.69 | 0.9864 | 0.9932 |
| d/h_1 | | | 0.66 | 0.9876 | 0.9938 |
| $d/(h_1-d)$ | | | 0.83 | 0.9801 | 0.9901 |

Table 4.5 Statistical fit for under keel clearance parameters for additional heave force due to propulsion for two sample cases

| Parameter | F_{nL} | 1000T'' | Standard error (*1000) | Adjusted R^2 | R^2 |
|--------------------|----------|---------|---------------------------|----------------|--------|
| $e^{(-h_1/d)}$ | 0.096 | 2.24 | 1.50 | 0.9870 | 0.9935 |
| $e^{((-h_1/d)-1)}$ | | | 1.50 | 0.9870 | 0.9935 |
| d/h_1 | | | 1.60 | 0.9863 | 0.9932 |
| $d/(h_1-d)$ | | | 1.80 | 0.9728 | 0.9864 |
| $e^{(-h_1/d)}$ | 0.071 | 2.39 | 0.69 | 0.9835 | 0.9917 |
| $e^{((-h_1/d)-1)}$ | | | 0.68 | 0.9829 | 0.9914 |
| d/h_1 | | | 0.66 | 0.9819 | 0.9908 |
| $d/(h_1-d)$ | | | 0.83 | 0.9767 | 0.9883 |

Table 4.6 Statistical fit for under keel clearance parameters for additional pitch moment due to propulsion for two sample cases

4.3.2 Empirical formulae for heave force and pitch moment due to propulsion

The additional heave force and pitch moment due to propulsion are given in Equations 4.19 and 4.20.

$$Z_{ADD} = Z_{SP} - Z_{NH} \quad (4.19)$$

$$M_{ADD} = M_{SP} - M_{NH} \quad (4.20)$$

As mentioned in Section 3.9.4, the non-dimensional heave force and pitch moment do not have a speed term in the denominator, since the additional heave force and pitch moment due to propulsion may be non-zero for zero vessel speed.

The general form of the regression equations is given in Equations 4.21 and 4.22 with the independent variables created as functions of the chosen parameters.

$$1000Z_{\text{ADD}}'' = \sum_{i=0}^2 \sum_{j=0}^2 \sum_{k=0}^2 (F_{\text{nh}})^i (d/h_1)^j (1000T'')^k \quad (4.21)$$

$$1000M_{\text{ADD}}'' = \sum_{i=0}^2 \sum_{j=0}^2 \sum_{k=0}^2 (F_{\text{nh}})^i (e^{(-h_1/d)})^j (1000T'')^k \quad (4.22)$$

Regression equations were only developed for water depth to draught ratios between 1.1 and 1.4, since grounding due to propulsion is unlikely at higher water depth to draught ratios. The final regression equations for additional heave force and pitch moment due to propulsion are given in Equations 4.23 and 4.24.

$$1000Z_{\text{ADD}}'' = (1000T'') \left(\begin{aligned} &118.92(d/h_1)^2 (F_{\text{nh}}) - (5.19E - 1)(1000T'') \\ &- 73.02(d/h_1)(F_{\text{nh}}) - 18.80(d/h_1)^2 + 10.19 \end{aligned} \right) \quad (4.23)$$

$$1000M_{\text{ADD}}'' = C_{\text{MADD}} \left(\begin{aligned} &23.00(e^{(-h_1/d)}) - 3.41(F_{\text{nh}}) - 3.10(1000T'') \\ &+ (1.67E - 1)(1000T'') + 11.96(1000T'')(e^{(-h_1/d)})(F_{\text{nh}}) \end{aligned} \right) \quad (4.24)$$

Where $C_{\text{MADD}} = (1000T'')(e^{(-h_1/d)})(F_{\text{nh}})$

The coefficient of determination (R^2) was 0.986 and 0.988 for the additional heave force and pitch moment due to propulsion, respectively. This indicates that 98.6% and 98.8% of the original variability has been explained with the variables specified in the models.

A common problem with such equations is that they may not represent the effect of independent variables properly when extrapolated beyond the range of experimental data. Hence, it is important to highlight the limiting conditions, or boundaries of application, of the developed mathematical expressions. It should be noted that the formulae are based on a channel width to beam ratio of 10.3. Other boundaries of application for the above formulae, in terms of extreme values of the varied parameters, are as follows:

- $0 < 1000T'' < 2.9$
- $1.1 < d/h_1 < 1.4$
- $0.33 < F_{\text{nh}} < 0.50$ for $h_1/d = 1.1$
- $0.31 < F_{\text{nh}} < 0.48$ for $h_1/d = 1.2$
- $0.30 < F_{\text{nh}} < 0.58$ for $h_1/d = 1.3$
- $0.29 < F_{\text{nh}} < 0.62$ for $h_1/d = 1.4$

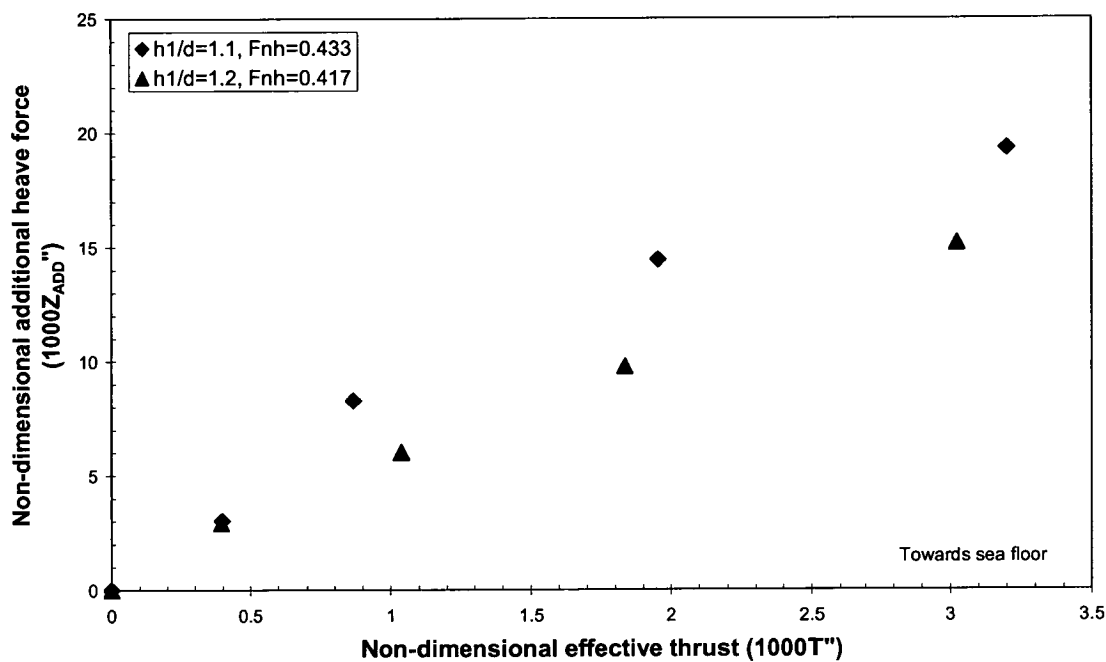


Figure 4.1 Non-dimensional additional heave force due to propulsion as a function of T^* , varying h_1/d

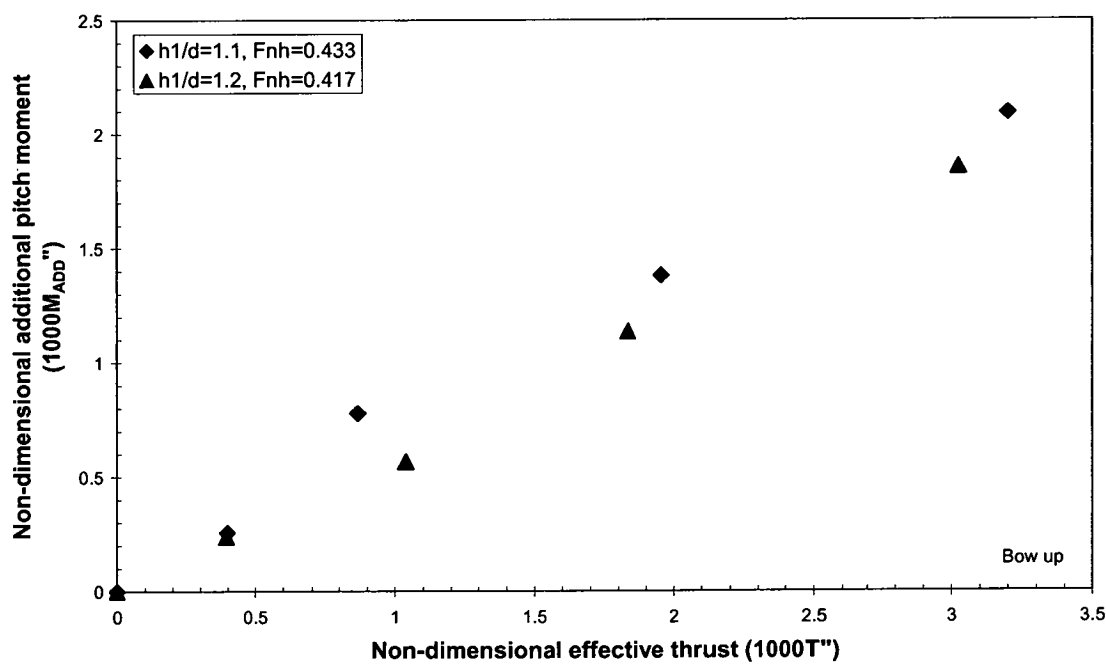


Figure 4.2 Non-dimensional additional pitch moment due to propulsion as a function of T^* , varying h_1/d

4.4 Prediction of unsteady squat

The empirical formulae to predict heave force and pitch moment in uniform water depth have been used as input to the mathematical model outlined in Section 2.4.1 to predict squat in both uniform and non-uniform water depth in the time-domain. Predictions titled ‘quasi-steady’ in this section relate to mathematical model predictions using the empirical formulae as input. The accuracy of these mathematical model predictions have been assessed using a two stage process.

In the first stage, mathematical model predictions were validated against independent steady-state sinkage measurements from tests conducted in uniform water depth to draught ratios of 1.2, 1.3 and 4.3. These results are presented in Figures 4.3 and 4.4 for midship sinkage and bow sinkage. As can be seen the squat generally collapsed onto a single line for water depth to draught ratios of 1.2 and 1.3 when presented as a function of depth Froude number. The predictions were found to be within approximately 15% of the measurements for the majority of depth Froude numbers tested for these water depth to draught ratios. Similar accuracy was observed for the higher depth Froude numbers tested at a water depth to draught ratio of 4.3. However, the midship sinkage was under predicted by up to approximately 45% and the bow sinkage was under predicted by up to approximately 30% for low depth Froude numbers at a water depth to draught ratio of 4.3. This may be partly due to experimental error as the magnitude of the force and sinkage was small for such cases.

The second stage of validation involved comparing mathematical model predictions to sinkage measurements made on a model travelling over a simplified two-dimensional ramp bank, as described in Section 3.3. It was found that grounding was most likely to occur at the bow as the vessel passed over the ramp bank. Therefore bow sinkage will be discussed in this section, along with midship sinkage. In Figures 4.5 – 4.10 midship sinkage and bow sinkage are presented for three different water depths at a constant vessel speed. In Figures 4.11 – 4.16 midship sinkage and bow sinkage are presented for three different vessel speeds for the same water depth. The steady-state sinkage measured in an equivalent uniform water depth to that over the bank is also presented in some of these figures.

From Figures 4.5 – 4.16 it can be seen that the general trend of the unsteady sinkage over the bank was predicted reasonably well. As expected, the differences between measurements and predicted midship and bow sinkages in uniform water depth leading up to the ramp were similar to those identified at a water depth to draught ratio of 4.3 in the first stage of validation. As can be seen from Figures 4.5 – 4.16 the midship sinkage was generally under predicted when the origin travelled over the ramp. The prediction of bow sinkage was generally good when the origin passed over the first half of the ramp, however the bow sinkage was generally under predicted when the origin passed over the second half of the ramp. An overshoot of midship and bow sinkage was predicted as the stern of the ship passed into the constant depth of water over the bank. Ferguson *et al.* (1982) measured an overshoot when the bow of a ship model passed onto the level portion of a ramp bank, which had less slope and lower water depth to draught ratios before and over the bank compared to the present study. However, the measured results from the present study exhibit a lag in the midship and bow sinkage reaching the equivalent steady-state sinkage over the bank. Hence, the sinkage was over predicted in this region. Generally, this over prediction was more prominent for bow sinkage than for midship sinkage and was accentuated at lower water depth to draught ratios and higher vessel speeds, as illustrated in Figures 4.5 - 4.16. The heave and pitch oscillations over the level portion of the bank were not predicted as the transient flow phenomena were not considered in the quasi-

steady approach. This resulted in an under prediction of the maximum sinkage over the bank for some cases, as illustrated in Figure 4.8.

The reduction in midship sinkage and bow sinkage as the bow passed the end of the bank occurred early for the prediction. This may be due to the omission of transient flow phenomena in the quasi-steady approach. The first overshoot of midship sinkage after the bow passed the end of the level bank was over predicted. However, the magnitude of the first overshoot of bow sinkage as the bow passed the end of the level bank showed reasonable correlation with the measured values. This may indicate that the transient flow at this stage of the bank transit has a greater influence on the midship sinkage than bow sinkage. Inclusion of dynamic acceleration effects in the present method provided reasonable prediction of bow sinkage when travelling over abrupt changes in water depth, such as passing the end of the bank. This is beneficial when simulating squat behaviour and other phenomena dependent upon instantaneous under keel clearance, such as ship-bank interaction.

As previously mentioned some of the discrepancies between predictions and measurements may be partly attributed to the omission of transient flow effects from the prediction method. In order to further investigate the influence of transient flow on the mathematical model predictions, model scale experiments were conducted to measure the heave force and pitch moment on the model travelling over the same simplified ramp bank using the model set up shown in Figure 3.3. These real-time force and moment measurements include the effects of transient flow and were used as input to the mathematical model to predict vertical plane motions. The predictions using these real-time force and moment input traces are presented in Figures 4.17 and 4.18 for a sample case and the data series are titled 'real time force input'. As expected, the midship and bow sinkages were underestimated as the force and moment were measured with the vessel fixed in the vertical plane; therefore the change in force and moment due to sinkage and trim was neglected. However, it can be seen that, generally, the prediction showed reasonable qualitative agreement with the measured motion in the region where the lag occurred in midship and bow sinkage. This highlights the importance of including the transient phenomena when predicting unsteady sinkage.

Limitations and assumptions

The observed discrepancies between the measured sinkage values and the predicted sinkage using the empirical formulae as input to the mathematical model can be partly attributed to the effects of transient flow as the vessel passed the bank being neglected. Viscous effects may also make a contribution to the flow field around a vessel travelling from deep water to shallow water, where the under keel clearance is relatively low. The presence of the bank may modify the boundary layer growth and wake structure aft of the vessel, which will influence the forces and moments acting on the hull. These effects were also neglected in the quasi-steady prediction. The pitch moment was calculated around the static LCF and the change in LCF location with sinkage and trim was neglected. The water depth to draught ratio was taken as the average of the values at midships, aft perpendicular and forward perpendicular. The heave force and pitch moment were predicted for a zero trim case based on the instantaneous average water depth to draught ratio. The variation of TPC, MCTC, damping and added mass with vessel draught was neglected along with the variation of damping and added mass with under keel clearance. In Section 3.8.3 it was shown that the heave force and pitch moment vary for cases with different draught and constant water depth to draught ratio. The heave force and pitch moment in the empirical equations are only a function of water depth to draught ratio. It should

also be noted that the equations are based on one hull form for vertical surface piercing channel banks with the vessel travelling on the channel centreline.

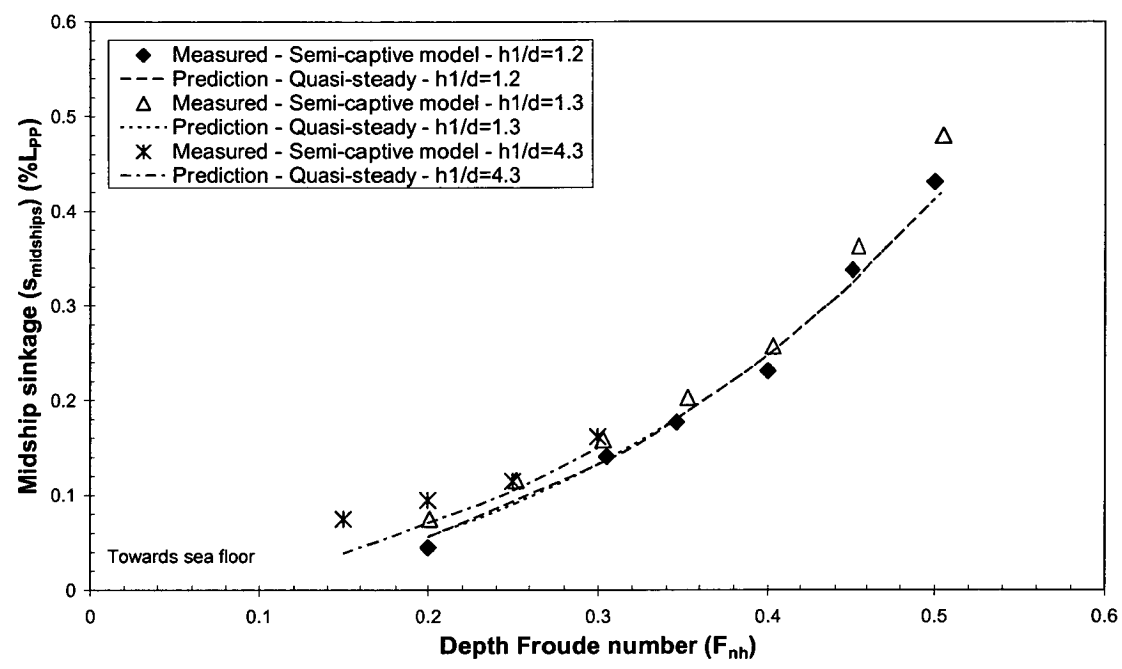


Figure 4.3 Comparison of midship sinkage measured from semi-captive experiments and quasi-steady mathematical model predictions

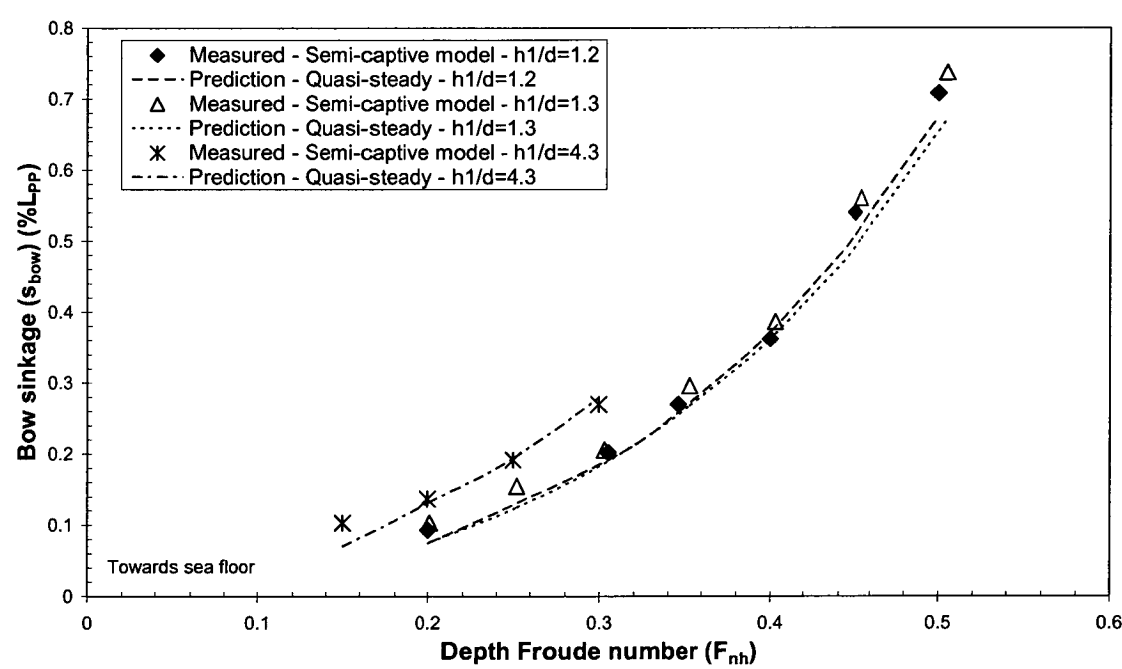


Figure 4.4 Comparison of bow sinkage measured from semi-captive experiments and quasi-steady mathematical model predictions

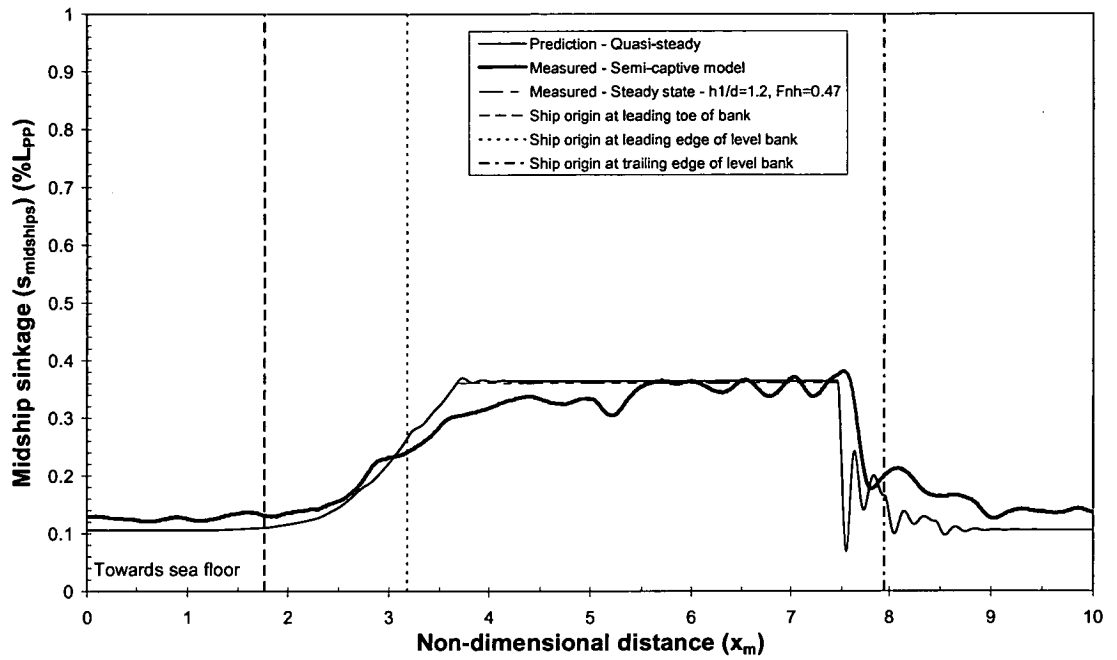


Figure 4.5 Midship sinkage over ramp bank, $F_{nh}=0.25-0.47$, $h_l/d=4.2-1.2$

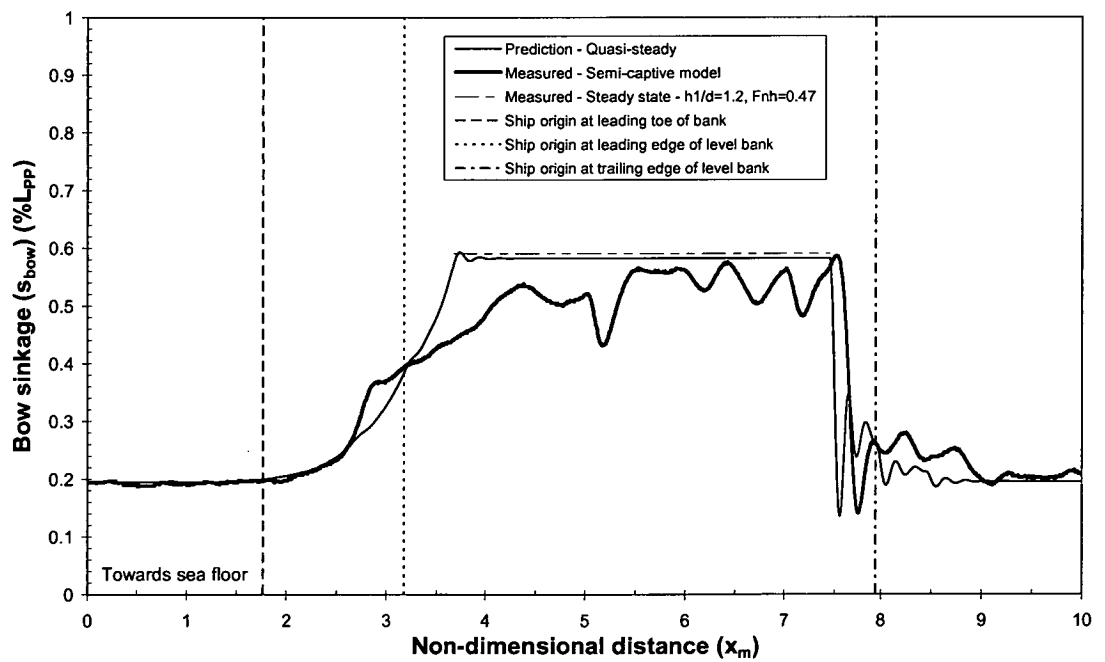


Figure 4.6 Bow sinkage over ramp bank, $F_{nh}=0.25-0.47$, $h_l/d=4.2-1.2$

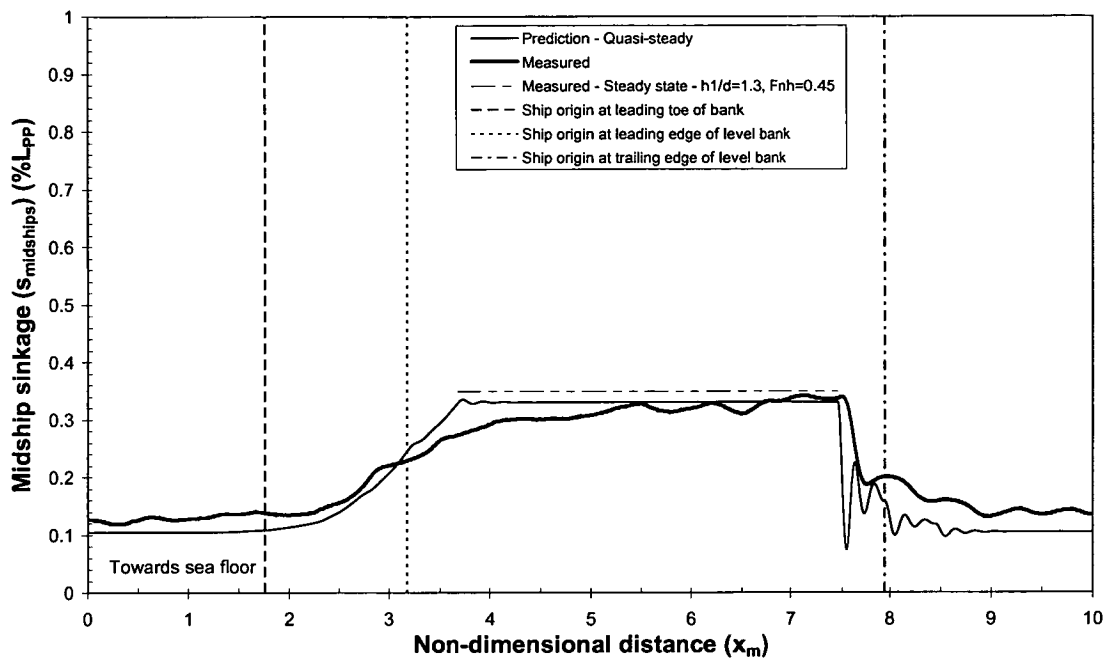


Figure 4.7 Midship sinkage over ramp bank, $F_{nh}=0.25-0.45$, $h_1/d=4.3-1.3$

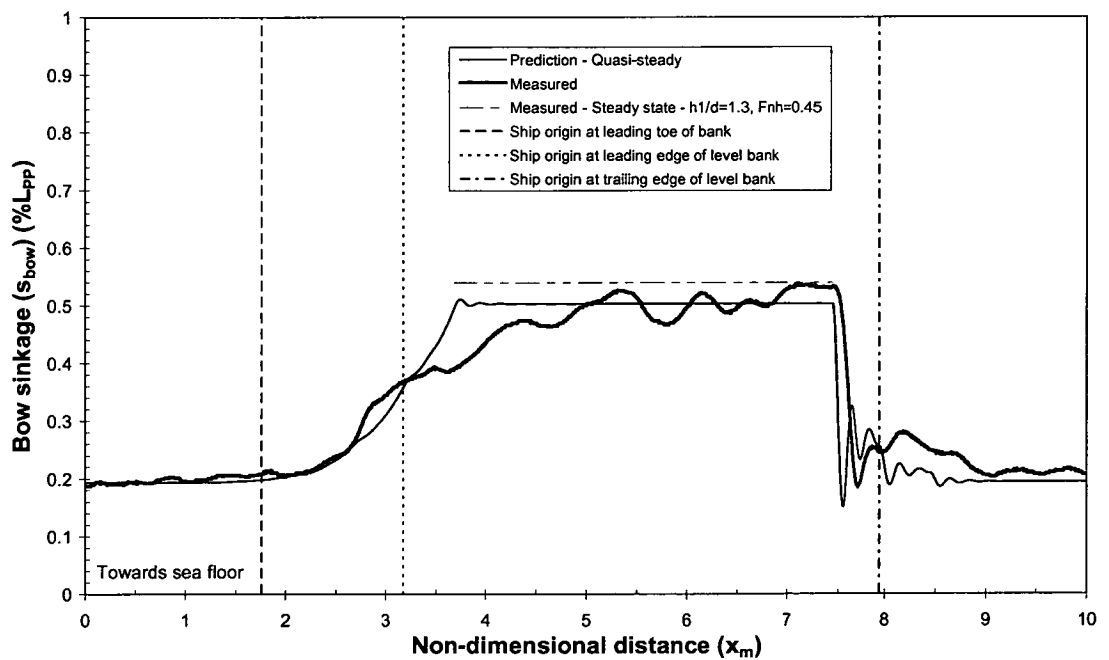


Figure 4.8 Bow sinkage over ramp bank, $F_{nh}=0.25-0.45$, $h_1/d=4.3-1.3$

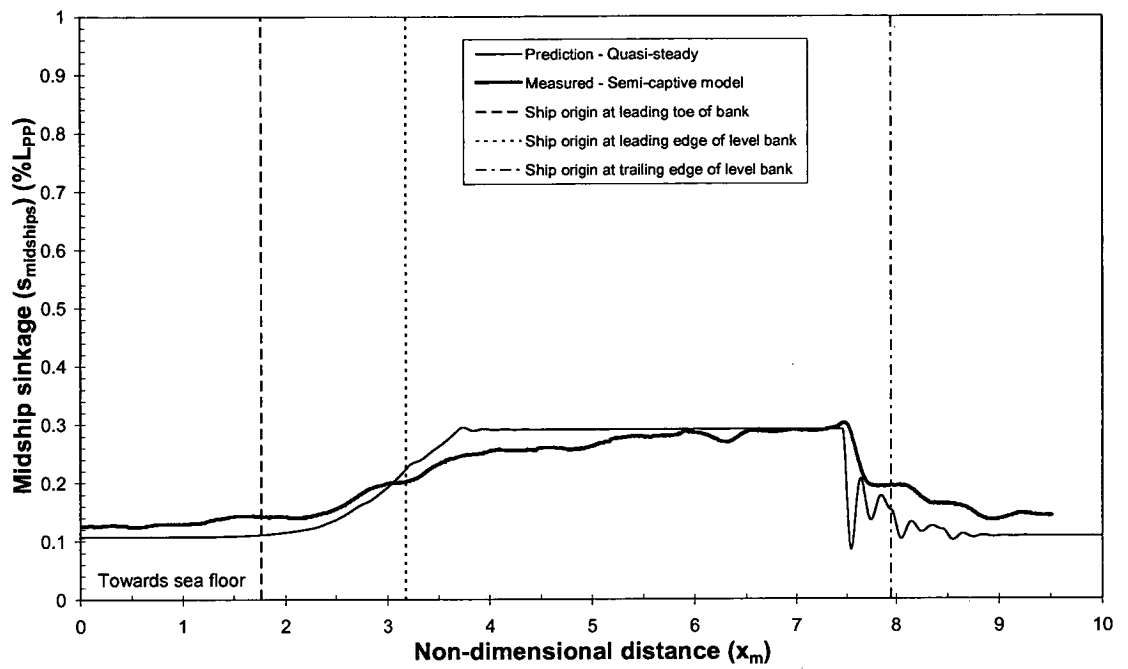


Figure 4.9 Midship sinkage over ramp bank, $F_{nh}=0.25-0.43$, $h_1/d=4.51-1.51$

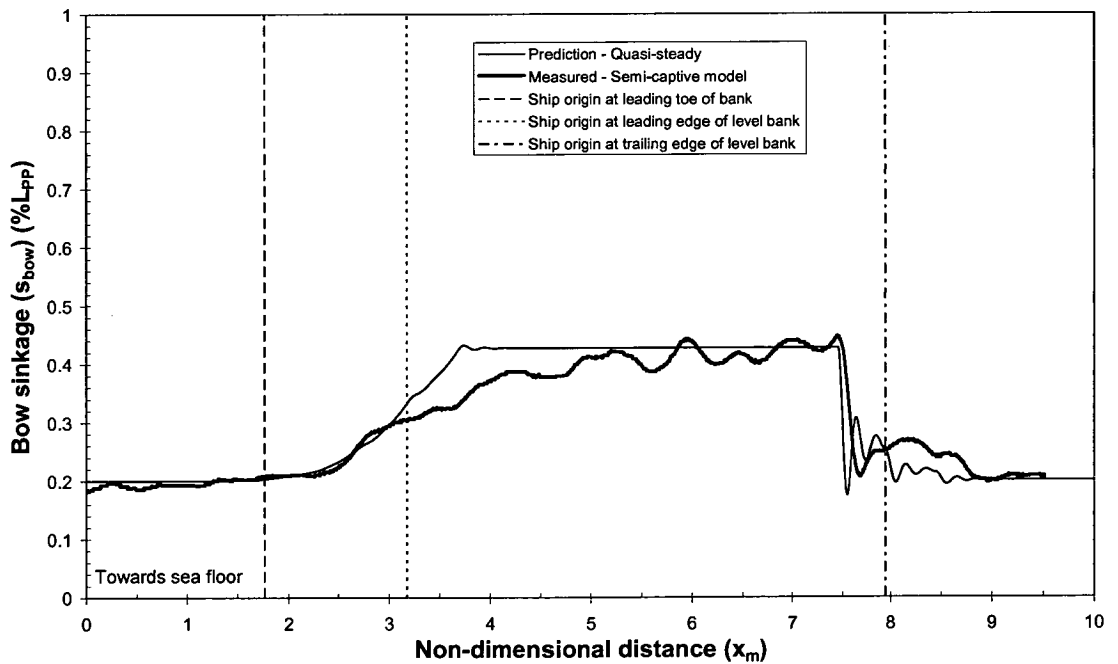


Figure 4.10 Bow sinkage over ramp bank, $F_{nh}=0.25-0.43$, $h_1/d=4.51-1.51$

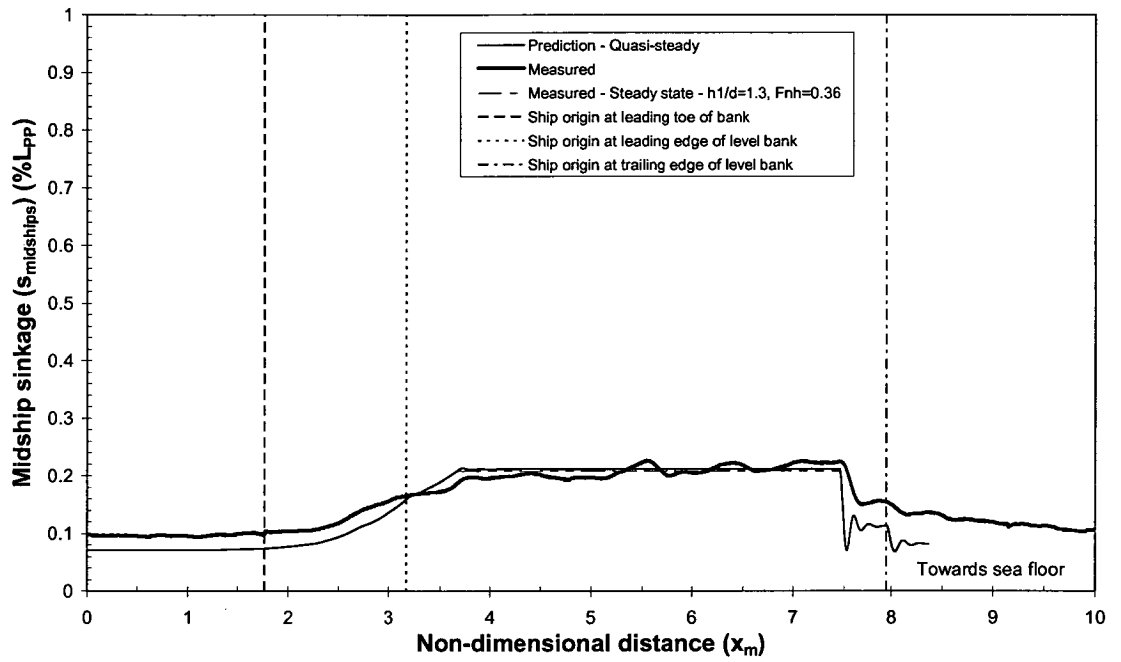


Figure 4.11 Midship sinkage over ramp bank, $F_{nh}=0.20-0.36$, $h_1/d=4.3-1.3$

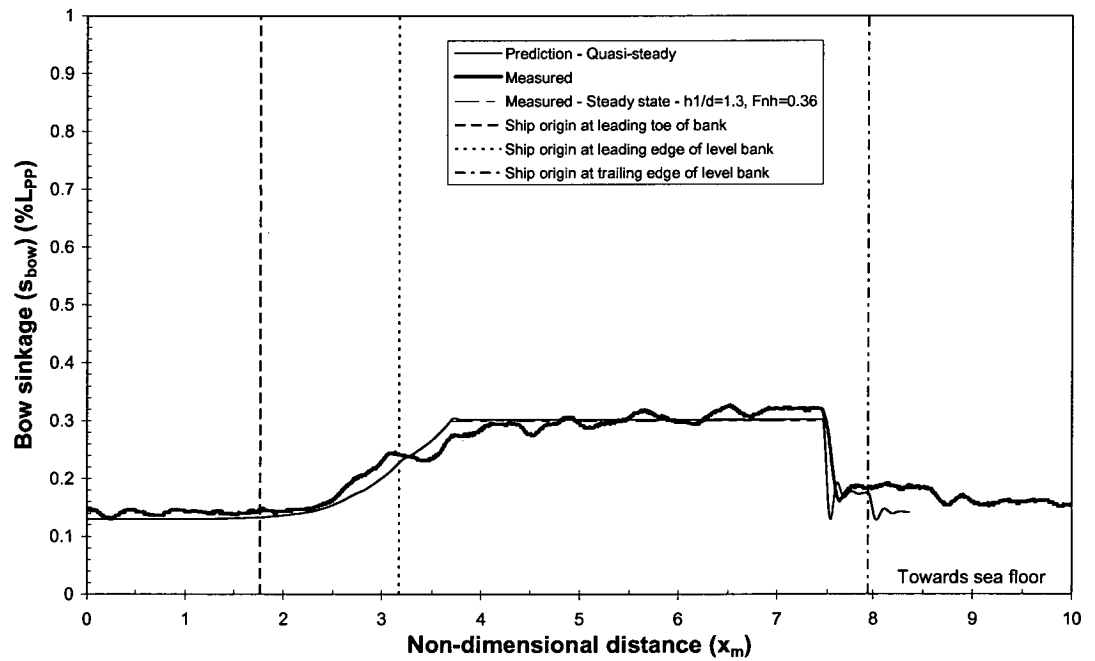


Figure 4.12 Bow sinkage over ramp bank, $F_{nh}=0.20-0.36$, $h_1/d=4.3-1.3$

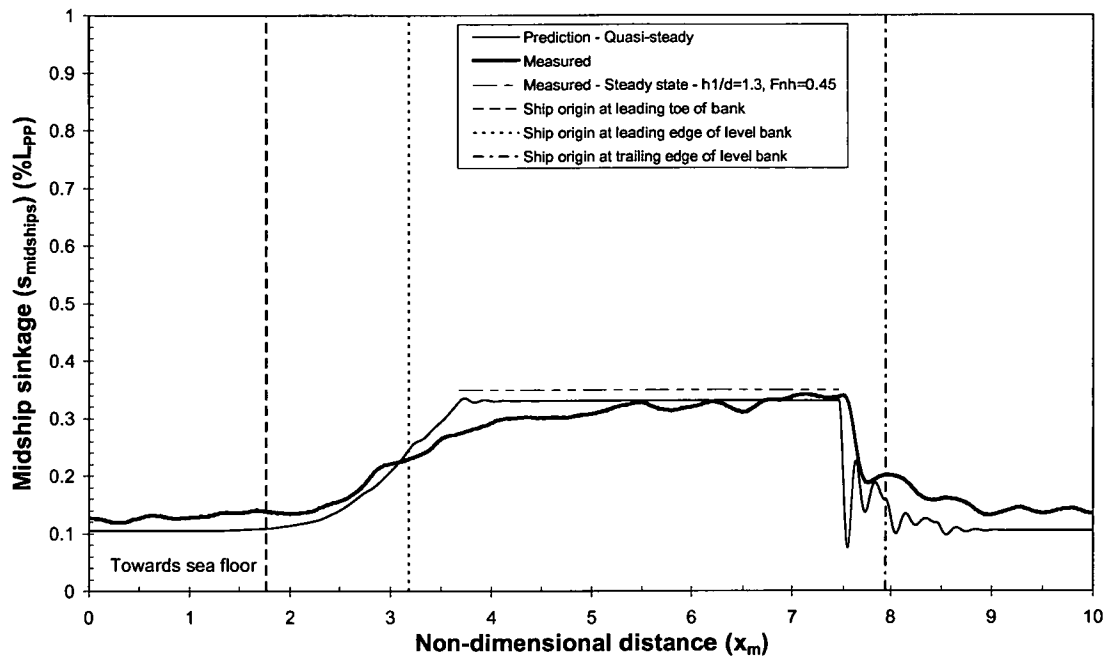


Figure 4.13 Midship sinkage over ramp bank, $F_{rh}=0.25-0.45$, $h_1/d=4.3-1.3$

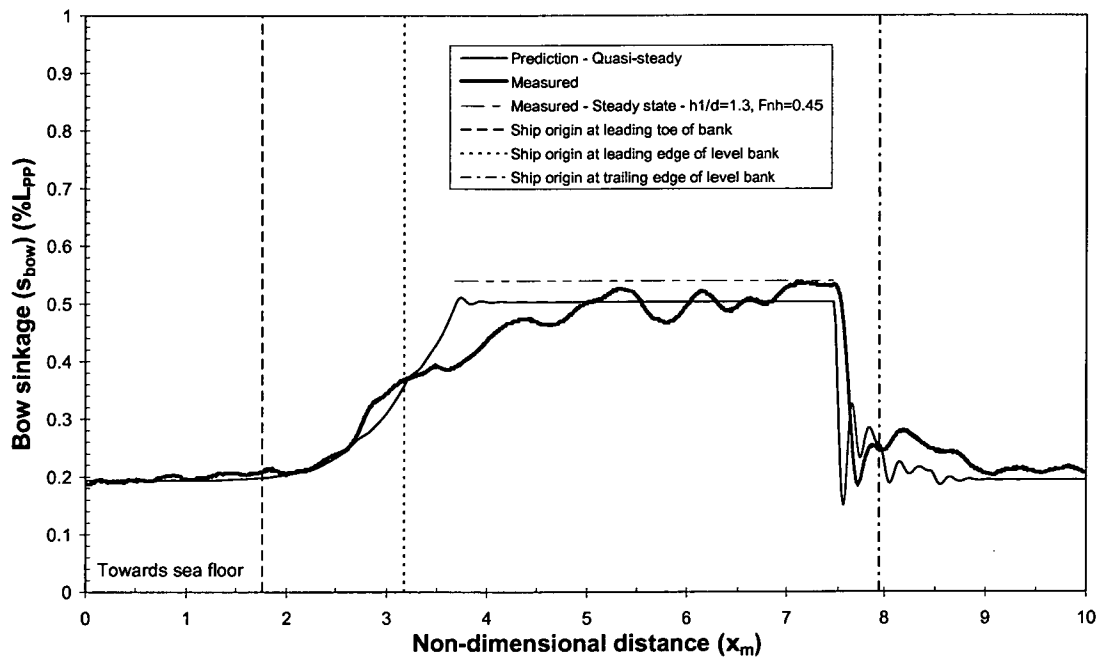


Figure 4.14 Bow sinkage over ramp bank, $F_{rh}=0.25-0.45$, $h_1/d=4.3-1.3$

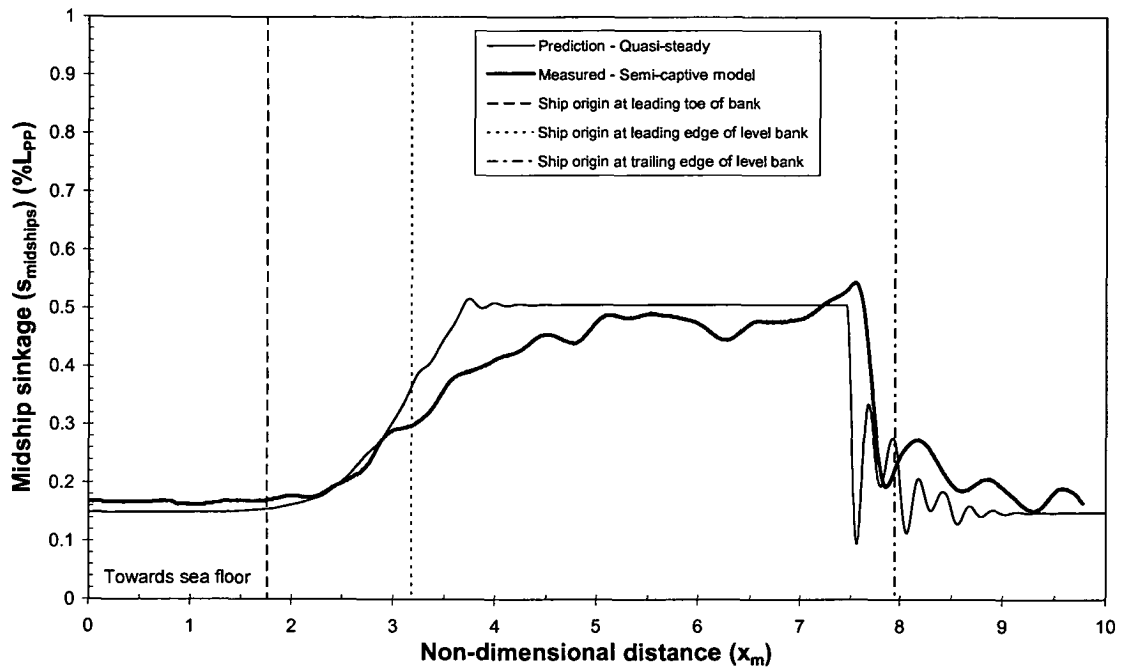


Figure 4.15 Midship sinkage over ramp bank, $F_{nh}=0.30-0.55$, $h_1/d=4.3-1.3$

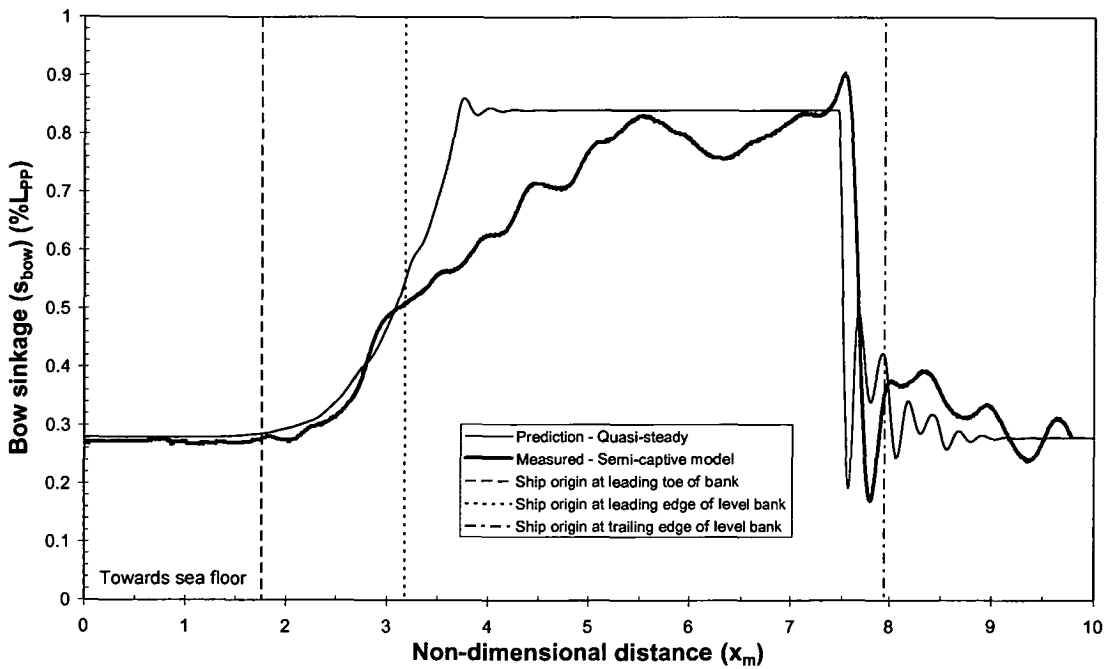


Figure 4.16 Bow sinkage over ramp bank, $F_{nh}=0.30-0.55$, $h_1/d=4.3-1.3$

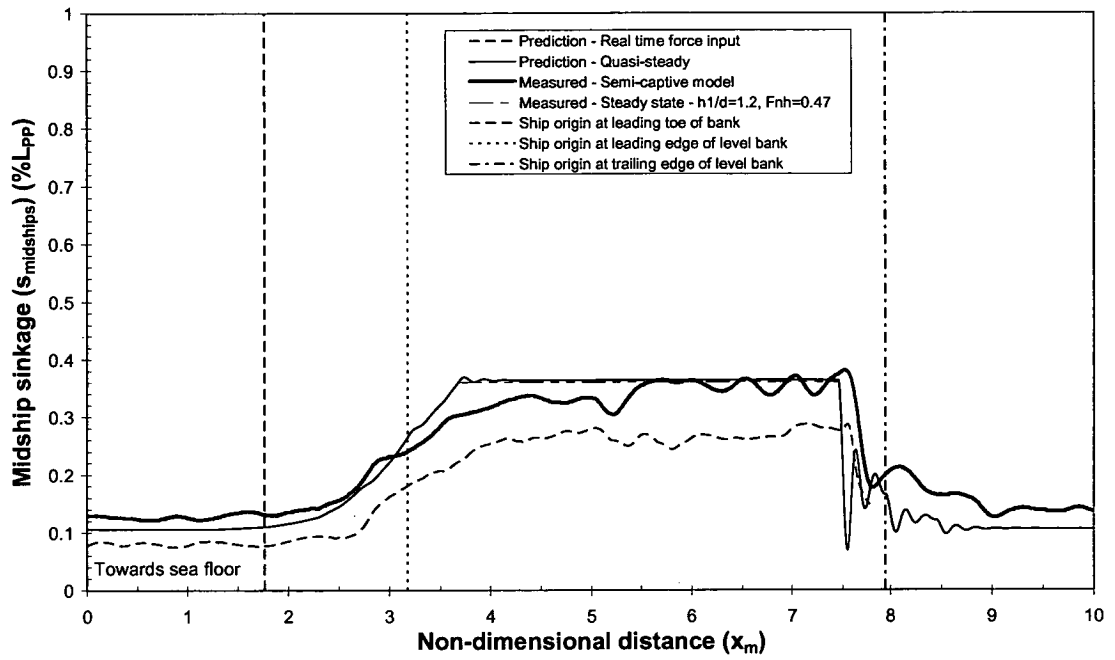


Figure 4.17 Midship sinkage over ramp bank, $F_{nh}=0.25-0.47$, $h_1/d=4.2-1.2$

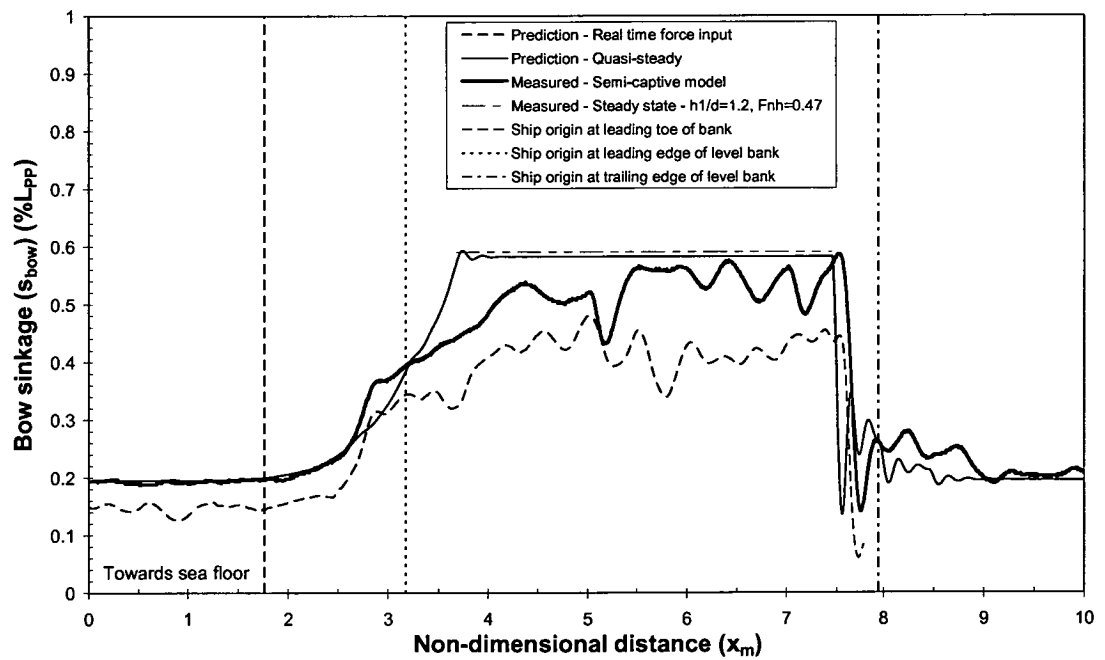


Figure 4.18 Bow sinkage over ramp bank, $F_{nh}=0.25-0.47$, $h_1/d=4.2-1.2$

4.5 Concluding remarks

Empirical equations were developed to predict the heave force and pitch moment due to squat in uniform water depth for an unpropelled full form hull. Empirical corrections were also produced to quantify the influence of propulsion on the unpropelled heave force and pitch moment. The former empirical equations were used as input to a time-domain mathematical model to yield a quasi-steady solution to the problem of unsteady squat in non-uniform water depth, accounting for dynamic acceleration effects in the vertical plane.

Predictions from the mathematical model were compared with model scale measurements of midship sinkage and bow sinkage in uniform water depth. It was found that the predictions were within approximately 15% of the measurements for the majority of depth Froude numbers tested at water depth to draught ratios of 1.2 and 1.3. Similar accuracy was observed for the higher depth Froude numbers tested at a water depth to draught ratio of 4.3. However, the midship sinkage was under predicted by up to approximately 45% and the bow sinkage was under predicted by up to approximately 30% for low depth Froude numbers at a water depth to draught ratio of 4.3. When comparing the mathematical model predictions to independent sinkage measurements for a model travelling over a simplified ramp bank, the general trend of the unsteady sinkage prediction was reasonable. Inclusion of dynamic acceleration effects in the present method provided reasonable prediction of bow sinkage when travelling over abrupt changes in water depth, such as passing the end of the bank. This is beneficial when simulating squat behaviour and other phenomena dependent upon instantaneous under keel clearance, such as ship-bank interaction. However, the maximum unsteady sinkage was not always predicted accurately, which may be attributable to limitations and assumptions associated with the technique.

Chapter 5

Ship-Bank Interaction Experiments

5.1 Introduction

Bank induced sway force and yaw moment can significantly influence the manoeuvring properties of a ship, which may lead to potentially dangerous situations, such as collisions with other ships or waterway boundaries. Knowledge of how vessel and channel particulars influence ship-bank interaction is important to enable realistic real-time simulation of the manoeuvring behaviour of a ship in restricted water. An effective method for determining such influences in previous work has been through the use of model scale experiments.

From previous model scale experiment programs it has been found that bank induced sway force may be either towards or away from the near bank (Norrbin 1971; Dand 1981; Ch'ng 1991; Vantorre 1995; Li 2000). The change in sway force direction was found to be closely dependent on under keel clearance and vessel speed. Ch'ng (1991) found that sway force was towards the near bank for water depth to draught ratios down to 1.3, with the sway force being away from the near bank at a water depth to draught ratio of 1.2. Vantorre (1995) and Li (2000) found that the sway force was towards the near bank for water depth to draught ratios down to around 1.2; the sway force was away from the near bank at a water depth to draught ratio of 1.1.

The yaw moment is typically bow away from the near bank (Dand 1981; Ch'ng 1991; Vantorre 1995; Li 2000). Ch'ng (1991) measured a bow towards the near bank yaw moment for a small number of cases at high water depth to draught ratios, such as 1.8.

Bank induced sway force and yaw moment have been found to generally vary in a quadratic manner for low speed cases (Dand 1981; Fuehrer and Romisch 1983). However, for cases with high blockage at higher vessel speed ranges the sway force and yaw moment vary with vessel speed to a power exceeding 2 (Dand 1981; Li 2000). At higher speeds Koster (1971), Dand (1981) and Renilson and Munro (1989) observed pronounced wave systems between the vessel and the near bank, which may have influenced the observed relationship between sway force/yaw moment and ship speed.

Dand (1981), Ch'ng (1991) and Li (2000) found that at low ship speeds the magnitude of sway force and yaw moment was greater for larger bank slopes. However, at high speeds the magnitude of sway force and yaw moment was greater for smaller bank slopes. Dand (1981) and Renilson and Munro (1989) observed pronounced wave systems between the ship and near banks with small bank slopes at higher speeds, and noted that such wave effects may contribute to the influence of bank slope on bank effect at higher vessel speeds.

Generally, the magnitude of sway force and yaw moment increases for lower lateral ship to bank distances. The sway force and yaw moment are influenced when travelling at different transverse locations within a channel, as measured by Fuehrer and Romisch (1983). Norrbin (1974) and Ch'ng (1991) found that the sway force and yaw moment induced by surface

piercing banks generally varied in a linear manner with the bank distance parameter, y_{Br} . This finding was used to estimate the influence of port and starboard banks in simulation models.

The magnitude of sway force and yaw moment can vary significantly with hull form. Ch'ng (1991) and Li (2000) found that the bank effect experienced by full form vessels, such as bulk carriers and tankers, varied significantly to that experienced by finer form vessels, such as containerhips and ferries. The length Froude number at which the sway force changed from attraction to repulsion from the near bank was found to vary for full form and fine form vessels (Li 2000). Norrbin (1985) noted that bank induced yaw moments are especially sensitive to the fore-end-aft asymmetry of the hull. The aft ward shift of LCB found in fast finer hulls will be reflected in a corresponding shift of the centre of pressure of the lateral force. This may partly explain the difference in yaw moment between the full form and fine form vessels. Laforce *et al.* (1996) found that ship length has a significant influence on the bank induced sway force and yaw moment.

The presence of a working propeller has been found to create an additional suction force to the near bank and an additional yaw moment (Dand 1981; Vantorre 1995; Li 2000). These effects were found to increase with increased propeller loading.

Norrbin (1971), Dand (1981), Chen and Sharma (1994) and Vantorre (1995) found that the bank induced sway force and yaw moment on a vessel travelling alongside channel walls with a drift angle differed from that of a vessel with zero drift angle.

A relatively small depth of water over a bank can have a significant effect on the sway force and yaw moment (Norrbin 1974). Dand (1981) and Li (2000) found that the behaviour of sway force and yaw moment induced by flooded banks varied significantly to that induced by surface piercing banks. Dand (1981) also noted that sway force and yaw moment did not vary with speed in a quadratic manner for flooded banks, with a small depth of water over the bank, at large draught to under keel clearance ratios. Hatch *et al.* (1999) measured the sway force and yaw moment for a specific flooded bank case for an Australian port. Since a practical prediction technique did not exist for the effect of flooded banks, model tests were necessary to determine an optimum dredged channel configuration with respect to ship-bank interaction.

One aim of the present study was to further investigate the influence of vessel and channel particulars on ship-bank interaction. In previous work it was shown that the depth of water over lateral banks significantly influences ship-bank interaction (Norrbin 1974; Dand 1981). However, in comparison to surface piercing banks, there has been little work conducted to investigate the influence of flooded banks. Therefore, model scale experiments were conducted to quantify the bank effect for a vessel travelling parallel to surface piercing and flooded banks for a wide range of cases. The following variables were varied systematically for three hull forms: vessel speed, vessel draught, ship to bank distance, bank slope, bank height and water depth. The results have been used to develop empirical formulae to predict steady-state bank induced sway force and yaw moment for ship-handling simulation as well as to assess the accuracy of a three-dimensional panel code.

5.2 Ship models

The tests were conducted using two models from the MarAd systematic series (Roseman 1987) and an S-175 containerhip (ITTC 1987). No propeller or appendages were fitted to the models.

The principal particulars of the models are presented in Section 3.2. Body plans are given in Appendix B. The hull forms chosen for the present work represent large ships and were selected based on ship types that are most commonly used on ship-handling simulators. A greater emphasis was placed on testing large full form ships because bank effect may have a significant influence on the operation of such ships in restricted water. However, it should be noted that bank effect may influence the handling characteristics of smaller ships with different hull forms operating in close proximity to lateral banks. The effect of ship-bank interaction on the ship handling characteristics will vary, dependent upon the ship form (Li 2000).

5.3 Bank models

Lateral banks were constructed on the port side of the towing tank to investigate the effect of lateral bank geometry on ship-bank interaction. The starboard bank was vertical, pierced the free surface and was located 1.75m from the centreline of the tank. This bank was not varied throughout the test program.

The port surface piercing banks were the same as those used to model the port lateral channel boundary in the squat study, as outlined in Section 3.3.

The flooded banks were constructed from galvanized steel sheet and were supported by a matrix of blocks, whose dimensions were varied to obtain different flooded bank heights. All flooded banks extended laterally to the port wall of the towing tank, i.e. 1.75m from the tank centreline.

To prevent flow into the bank cavity all banks were sealed at the joins and intersections with the towing tank boundaries. Further details concerning the bank models are given in Appendix C.

5.4 Test rig

The test rig was the same as that used to measure heave motion, pitch motion and surge force, as outlined in Section 3.4.1. The only difference being that both vertical posts were fitted with force transducers in this case to measure the forward and aft transverse forces. A schematic of the model setup is shown in Figure 5.1.

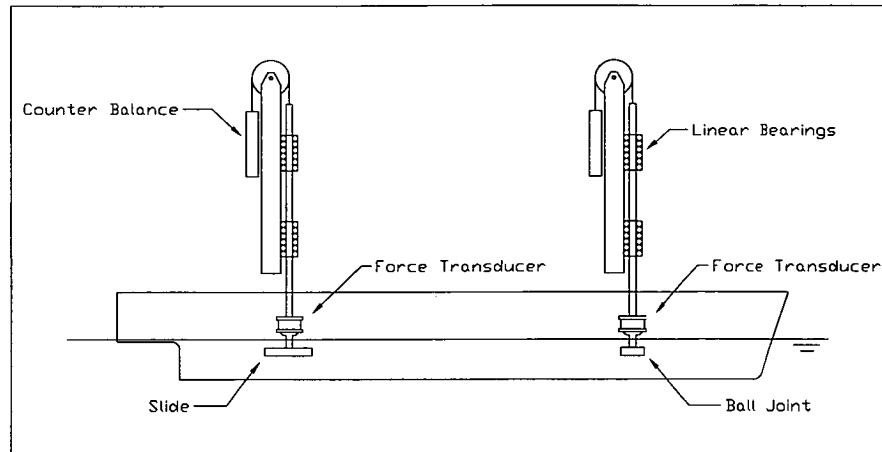


Figure 5.1 Schematic of model set up for sway force and yaw moment tests

5.5 Instrumentation

The sinkage at the forward and aft posts was measured using two Schaevitz 5000 HR linear variable differential transformers (LVDTs). The model resistance, forward and aft sway forces were measured using two AMTI MC3A-X-100 multi-component force transducers.

Details concerning instrument calibration and carriage speed measurement are described in Section 3.5.

5.6 Test procedure and data acquisition

The test procedure and data acquisition techniques were the same as those used for the squat model tests. Details are provided in Section 3.6.

5.7 Test program

A preliminary set of model scale experiments was conducted with ninety degree surface piercing banks, various lateral ship to bank distances at draught to under keel clearance ratios of 9.63 and 5.13 using three different ship models. The purpose of these experiments was to develop and optimise the experimental technique and to extend the work of Ch'ng (1991) by obtaining sway force and yaw moment data for higher draught to under keel clearance ratios.

Vantorre (1995) conducted model scale experiments on two bulk carrier models to investigate sway force and yaw moment induced by surface piercing banks, enabling comparisons with the regression equations developed by Ch'ng (1991). Generally, at low water depth to draught ratios, Vantorre's results exhibited less bow away yaw moment, less repulsive sway force and greater attraction sway force. Initially it was intended to use findings from Ch'ng (1991) for surface piercing cases in the present study. A selection of Ch'ng's test cases was repeated in the present study and differences between these results and Ch'ng's were found to be similar to those observed by Vantorre (1995). This may be due to the fact that the AMC towing tank floor had greater variation in surface flatness when Ch'ng conducted his tests as, generally, Ch'ng's

results matched present study results more closely at small draught to under keel clearance ratios. This is illustrated in Appendix E, where results from the present study are compared to Ch'ng's results for two different draught to under keel clearance ratios. Due to the differences identified between Ch'ng's results and those from the present study a number of surface piercing cases were re-investigated.

The remaining test programs involved systematic variation of the following parameters for the MarAd L series and S-175 containership models: vessel speed, vessel draught, bank slope, bank height, lateral ship to bank distance and water depth.

Initially tests were also conducted using a MarAd F series model. However, since the results were found to be generally similar to those for the MarAd L series model the majority of the tests were conducted using a MarAd L series bulk carrier model and an S-175 containership model.

The range of parameters tested for the tests is as follows:

- $45^\circ < \alpha < 90^\circ$
- $-0.63 < y_{Bt} < 0.63$
- $1.2 < \frac{d}{h_1 - d} < 10$
- $0.44 < 1 - \left(\frac{h_{2p}}{h_1} \right) < 1$
- $0.52 < C_B < 0.85$

A minimum of four speeds was tested for each condition.

5.8 Results and discussion

5.8.1 General

Non-dimensional sway force and yaw moment are given in Equations 5.1 and 5.2 respectively.

$$Y' = \frac{Y}{\frac{1}{2} \rho U^2 L_{pp} d} \quad (5.1)$$

$$N' = \frac{N}{\frac{1}{2} \rho U^2 L_{pp}^2 d} \quad (5.2)$$

It should be noted that, based on the analysis outlined in Appendix D, the uncertainty limits for measurements of sway force and yaw moment are generally in the order of $\pm 5\%$ to $\pm 10\%$.

It should also be noted that the draught to under keel clearance ratios relate to the vessel at zero speed. The zero speed under keel clearance was reduced by the effects of vessel squat.

The variables defining the bank geometry are shown in Figure 5.2. Bank slope is measured from the horizontal plane, i.e. a 90 degree bank is vertical.

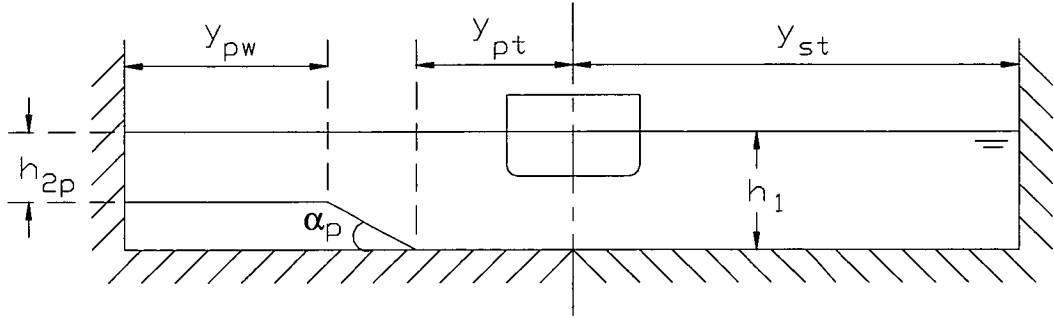


Figure 5.2 Parameters defining bank geometry

5.8.2 Depth Froude number

For the results presented in this section the draught to under keel clearance ratios were varied by changing water depth. Therefore the vessel speed is not constant for a constant depth Froude number for different draught to under keel clearance ratios. It should be noted that non-dimensional sway force and yaw moment have a speed squared term in the denominator.

Three example cases are presented in Figures 5.3 and 5.4 to illustrate the effect of depth Froude number on non-dimensional sway force and yaw moment. As can be seen the sway force is towards the near bank and the yaw moment is bow away from the near bank for cases with relatively low blockage at sub-critical speeds. In each plot the denominator contains a speed squared term; therefore the results will fall onto a horizontal line for a quadratic dependence on vessel speed. For each case the sway force and yaw moment were found to generally vary with vessel speed in a quadratic manner up to a specific depth Froude number. Beyond this depth Froude number the non-dimensional sway force and yaw moment varied with speed to a power greater than 2. This trend occurred for both flooded and surface piercing bank cases, as illustrated by Cases 1 and 3. Case 2 in Figures 5.3 and 5.4 has different bank geometry, lateral ship to bank distance and higher draught to under keel clearance ratio than Cases 1 and 3. It can be seen that for Case 2 the sway force and yaw moment vary with speed to a power greater than 2 from a lower depth Froude number than for Cases 1 and 3. Also, for Case 2 the power with which the yaw moment varied with speed is higher than for the cases with lower draught to under keel clearance ratios (Cases 1 and 3). Dand (1981) found that, for depth Froude numbers greater than 0.3, the yaw moment varied with speed to a power greater than 2. Dand also noted that sway force and yaw moment did not vary with speed in a quadratic manner for flooded banks with a small depth of water over the bank at large draught to under keel clearance ratios.

Further example cases are presented in Figures 5.5 and 5.6 to show the influence of depth Froude number on non-dimensional sway force and yaw moment at draught to under keel clearance ratios of 5.13 and 3.35. For each case the sway force changed sign for both the bulk

carrier and containership models at a specific depth Froude number, as illustrated in Figure 5.5. The depth Froude number value where this occurred was dependent on draught to under keel clearance ratio, and to a lesser extent dependent on ship form, lateral ship to bank distance, bank geometry and the degree of bank flooding. For the MarAd L series model the sway force changed from attraction to the near bank to repulsion from the near bank at high depth Froude numbers for draught to under keel clearance ratios of 5.13 and 3.35 (the sway force was away from the near bank for all depth Froude numbers tested for a few cases at a draught to under keel clearance ratio of 5.13). It was found that the rate of change of bow away yaw moment with vessel speed increased significantly once the sway force changed to away from the near bank, as illustrated in Figure 5.6. This may have serious implications on vessel manoeuvring in a confined waterway. The above trends were found to occur for both surface piercing and flooded banks, as illustrated by Cases 5 and 6. It was found that the rate of increase of non-dimensional yaw moment with vessel speed was generally less for flooded bank cases.

In Figures 5.7 and 5.8 non-dimensional sway force and yaw moment are presented for vertical flooded and surface piercing banks for two different lateral ship to bank distances at a draught to under keel clearance ratio of 9.63. The non-dimensional sway force was found to be away from the near bank for a draught to under keel clearance ratio of 9.63 for all depth Froude numbers tested. For the flooded bank cases it can be seen that the sway force generally varied with speed in a quadratic manner for all depth Froude numbers presented. However, for a constant lateral ship to bank distance, when increasing the blockage (by changing to a surface piercing bank) the sway force varied with vessel speed to a power higher than 2. From Figure 5.8 it can be seen that the bow away yaw moment generally varied with speed to a power higher than 2 for these cases.

During the conduct of the experiments it was observed that for higher model speeds and for cases with higher blockage the influence of the free-surface was more significant. Solitons were observed between the model and near bank for cases where the ship speed and blockage was high, indicating trans-critical flow between the vessel and near bank (Constantine 1961).

An increase in vessel speed and/or propeller loading may increase the squat of the vessel, hence changing the effective under keel clearance of the vessel, which will influence ship-bank interaction.

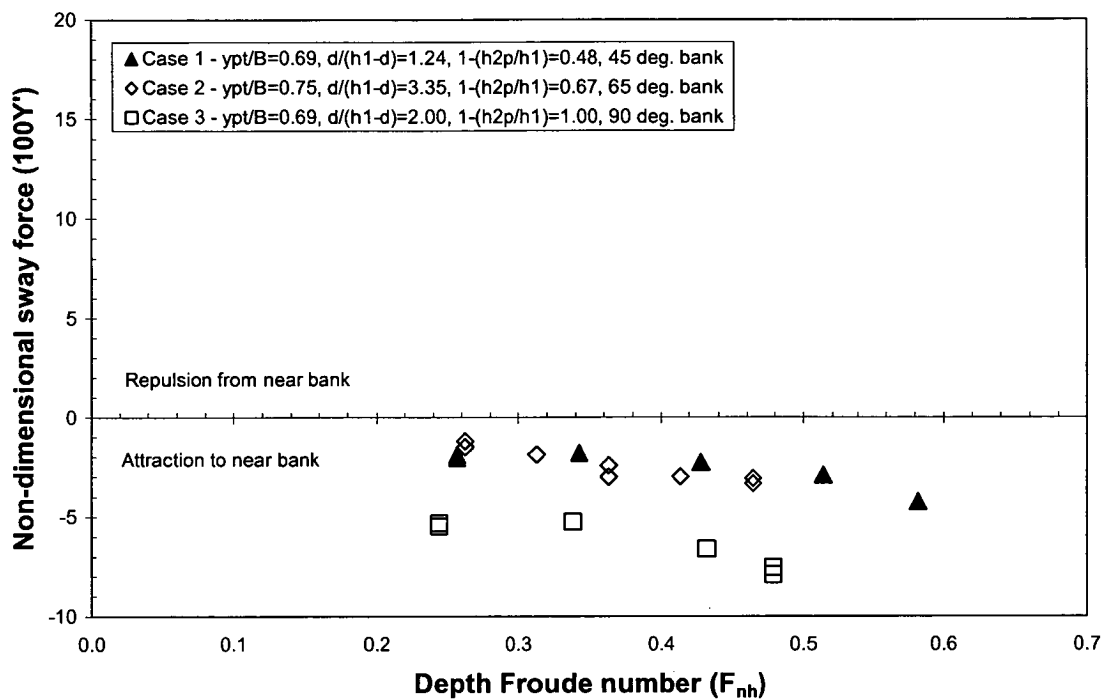


Figure 5.3 Non-dimensional sway force as a function of F_{nh} , MarAd L series model

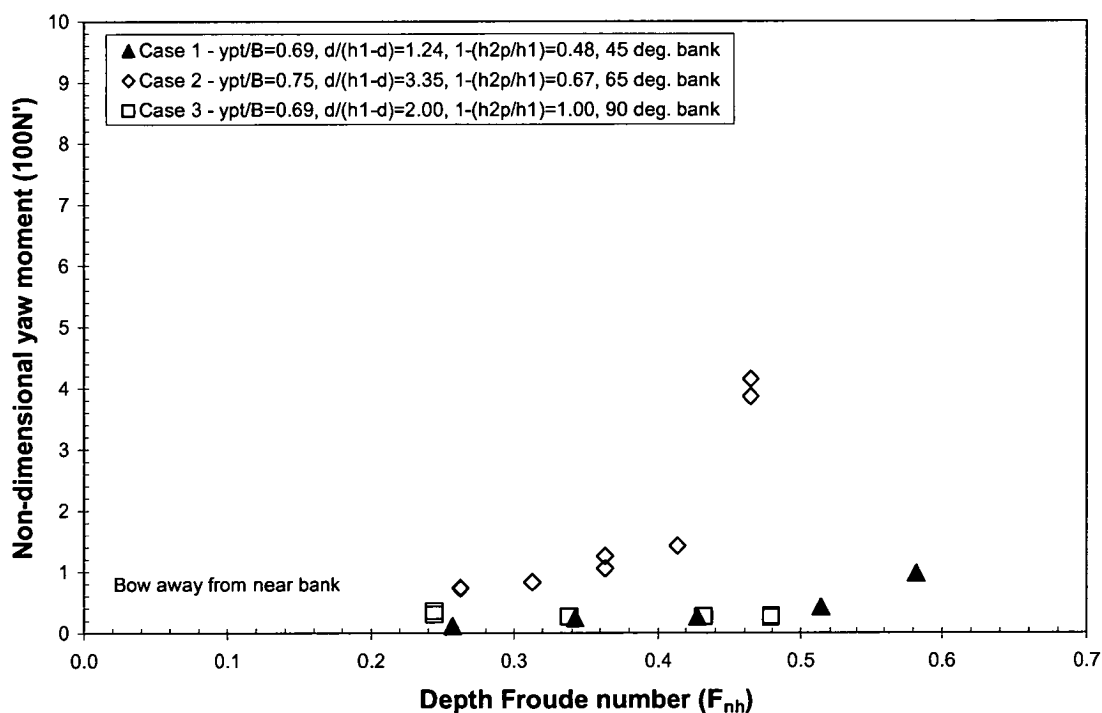


Figure 5.4 Non-dimensional yaw moment as a function of F_{nh} , MarAd L series model

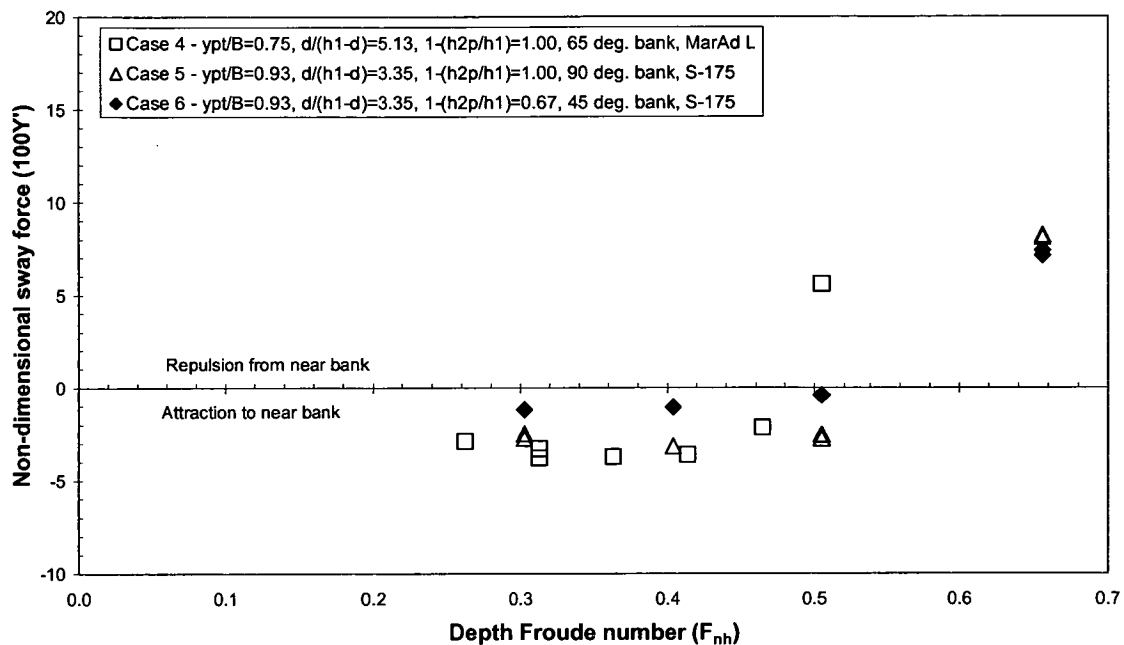


Figure 5.5 Non-dimensional sway force as a function of F_{nh}

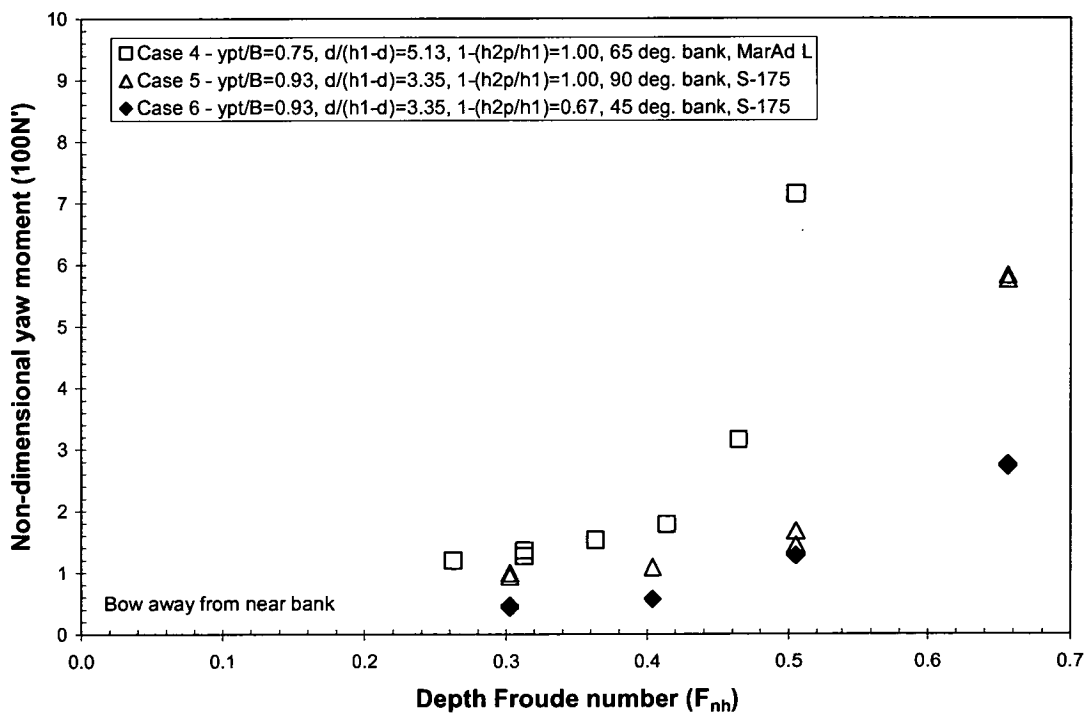


Figure 5.6 Non-dimensional yaw moment as a function of F_{nh}

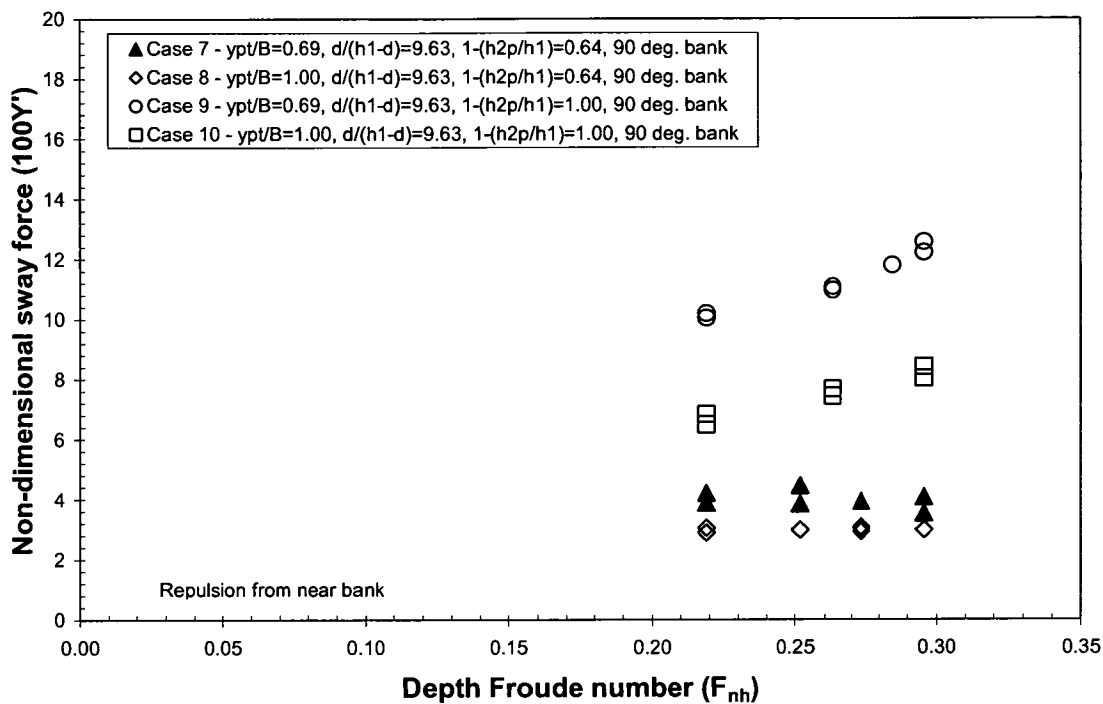


Figure 5.7 Non-dimensional sway force as a function of F_{nh} , MarAd L series model

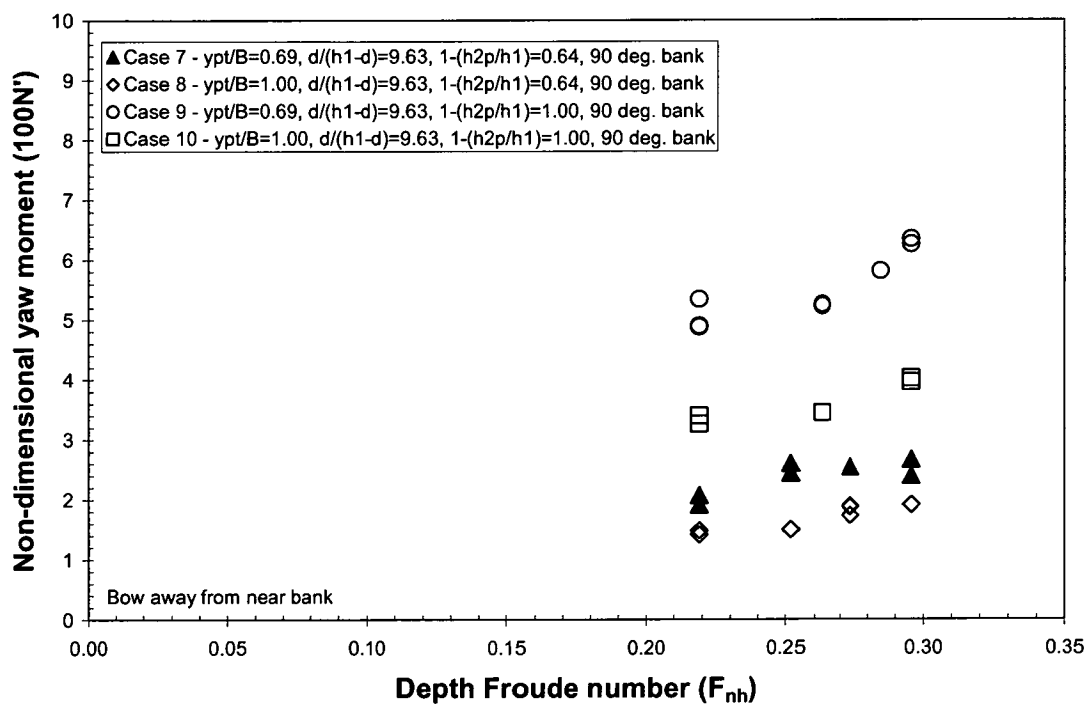


Figure 5.8 Non-dimensional yaw moment as a function of F_{nh} , MarAd L series model

5.8.3 Draught to under keel clearance ratio

The draught to under keel clearance ratio was varied by changing the water depth in the channel for the results presented in this section. Therefore, for each case, the depth Froude number varies at different draught to under keel clearance ratios for a constant vessel speed. To enable a constant non-dimensional speed for each case the following results have been presented in terms of length Froude number.

It was found that there were fundamental differences between the sway force and yaw moment behaviour with small draught to under keel clearance ratios and large draught to under keel clearance ratios, as also measured by Norrbin (1971) and Fuehrer and Romisch (1983).

A selection of cases is presented in Figure 5.9 to illustrate the influence of draught to under keel clearance ratio on non-dimensional sway force. It was found that the sway force was towards the near bank for low draught to under keel clearance ratios and reached a peak at a draught to under keel clearance of approximately 2. Increasing the draught to under keel clearance ratio beyond this value caused a reduction in the attraction sway force until the sway force changed direction to be away from the near bank. This trend occurred for both surface piercing and flooded banks. The non-dimensional yaw moment is presented in Figure 5.10 for the same cases presented in Figure 5.9. It can be seen that the magnitude of the bow away yaw moment was generally greater for the higher draught to under keel clearance ratios tested.

At a draught to under keel clearance ratio of 9.63 the sway force was away from the near bank for the bulk carriers and containership. The sway force was towards the near bank for most cases tested at a draught to under keel clearance ratio of 5.13, however there were a small number of cases where the sway force was away from the near bank for all tested speeds. Also there were some cases where the sway force was away from the near bank at higher vessel speeds at this draught to under keel clearance ratio, as illustrated by Case 12 in Figure 5.9. At a draught to under keel of 3.35 the sway force was towards the near bank for the majority of cases. However, for the closest lateral ship to bank distance and highest speed tested the sway force was away from the near bank for the MarAd L series model at this draught to under keel clearance ratio. Also, the sway force was away from the near bank for the S-175 containership at the highest speed tested for the smallest and intermediate lateral ship to bank distance for the same draught to under keel clearance ratio. The sway force was towards the near bank for all cases tested at draught to under keel clearance ratios of 2.00 and 1.24. The draught to under keel clearance ratio at which the transition from attraction to repulsion occurred was dependent upon vessel speed, and to a lesser extent on vessel form, ship to bank distance, lateral bank geometry and degree of bank flooding (discussed further in following sections).

For flooded banks Dand (1981) found that decreasing the draught to under keel clearance ratio while the height of the bank remained a constant proportion of the water depth reduced the magnitude of both the sway force and yaw moment acting on the ship. This highlights the importance of the draught to under keel clearance parameter; the changes in sway force and yaw moment presumably being due to changes in flow under, as well as around, the model.

It can be seen that draught to under keel clearance ratio has a significant influence on ship-bank interaction. It is therefore important to include the influence of sinkage due to squat when simulating ship-bank interaction.

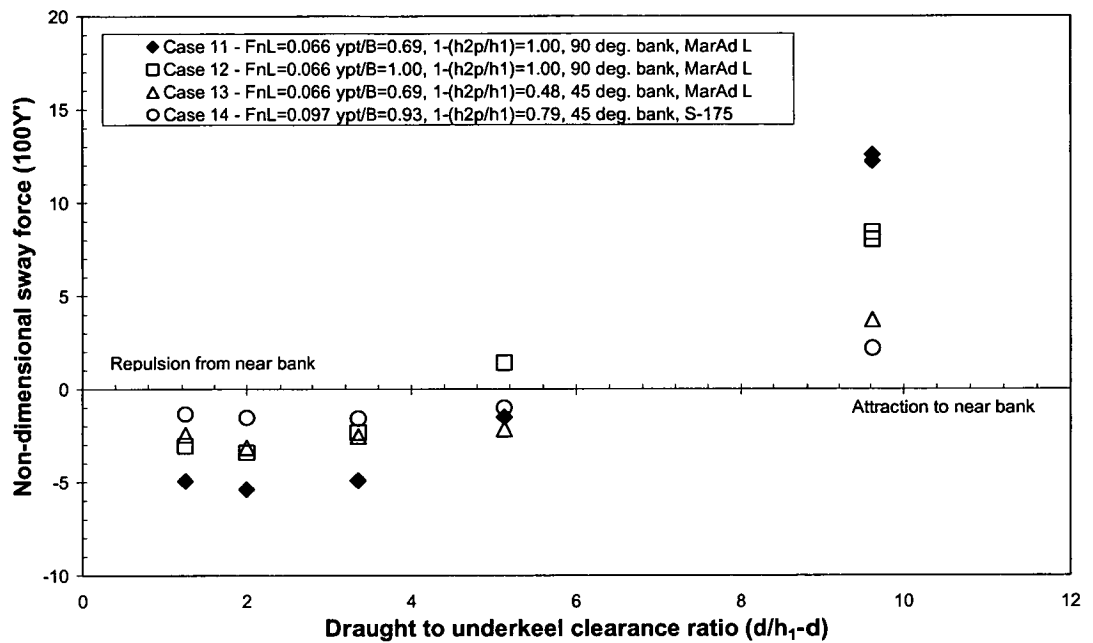


Figure 5.9 Non-dimensional sway force as a function of $d/(h_1-d)$

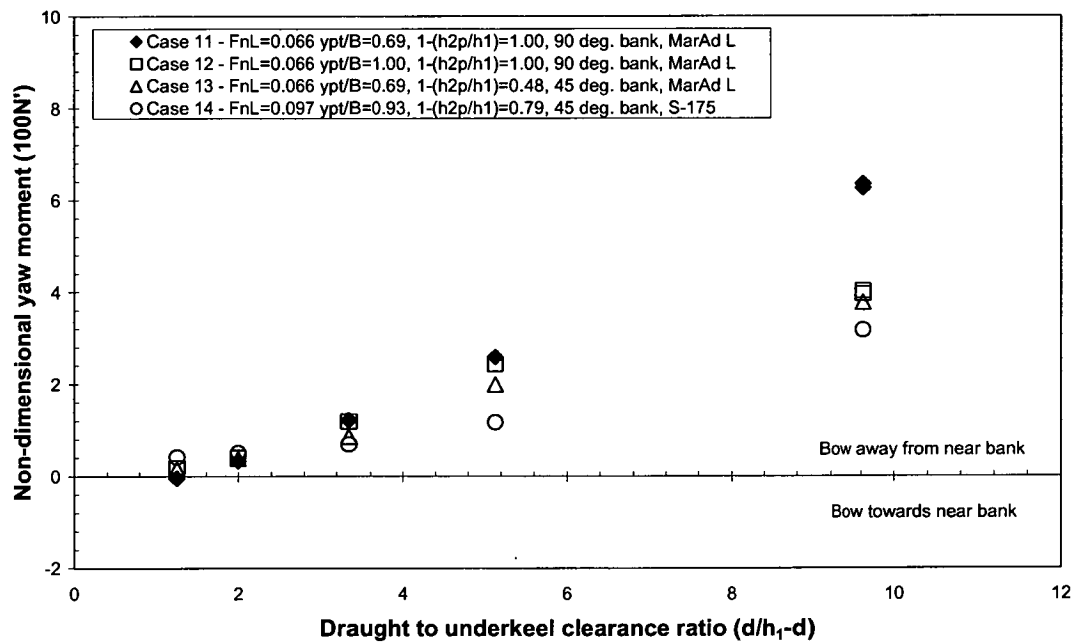


Figure 5.10 Non-dimensional yaw moment as a function of $d/(h_1-d)$

5.8.4 Ship to bank distance

The influence of lateral ship to bank distance on bank induced sway force and yaw moment is illustrated for a selection of surface piercing bank cases in Figures 5.11 and 5.12, whilst results for a selection of flooded bank cases are presented in Figures 5.13 and 5.14. Linear trend lines have been fitted to each data series to highlight trends.

Generally, the magnitude of sway force and yaw moment was larger for small lateral ship to bank distances. Norrbin (1974) and Ch'ng (1991) found that bank induced sway force and yaw moment generally varied in a linear manner with the ship to bank parameter, y_{Bt} , for surface piercing banks. For additional surface piercing bank cases tested in the present study (Figures 5.11 and 5.12) it can be seen that the sway force and yaw moment generally vary in a linear manner with the bank distance parameter, y_{Bt} .

Generally the sway force and yaw moment induced by a port flooded bank varied in a linear manner with the ship to bank distance parameter, y_{Bt} , as illustrated in Figures 5.13 and 5.14.

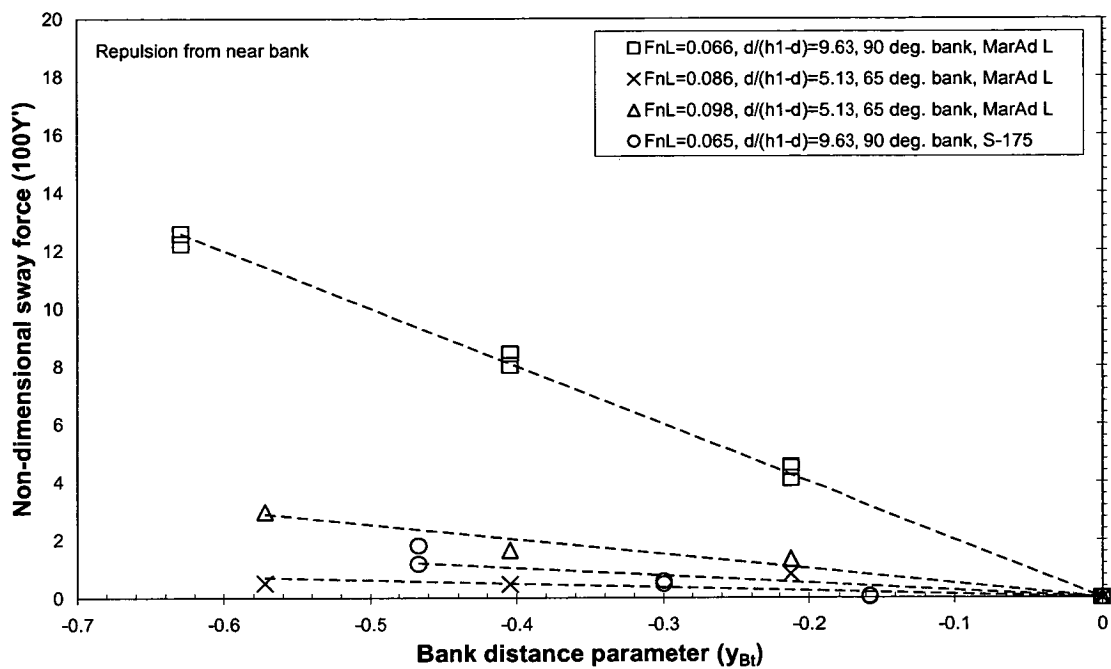


Figure 5.11 Non-dimensional sway force as a function of y_{Bt} for surface piercing banks

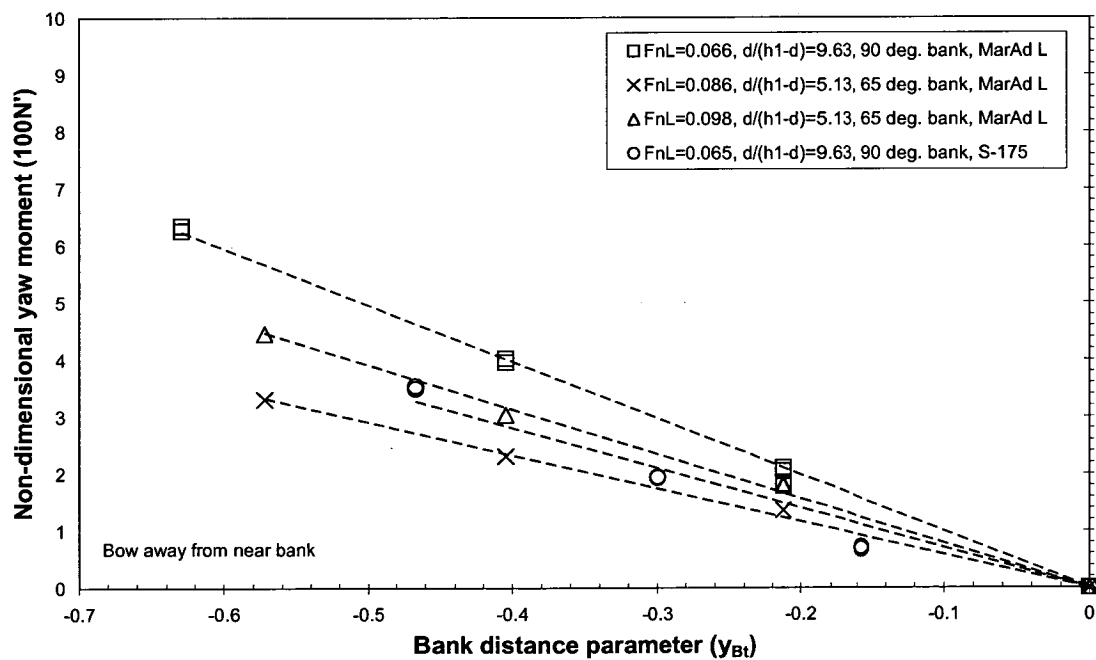


Figure 5.12 Non-dimensional yaw moment as a function of y_{Bt} for surface piercing banks

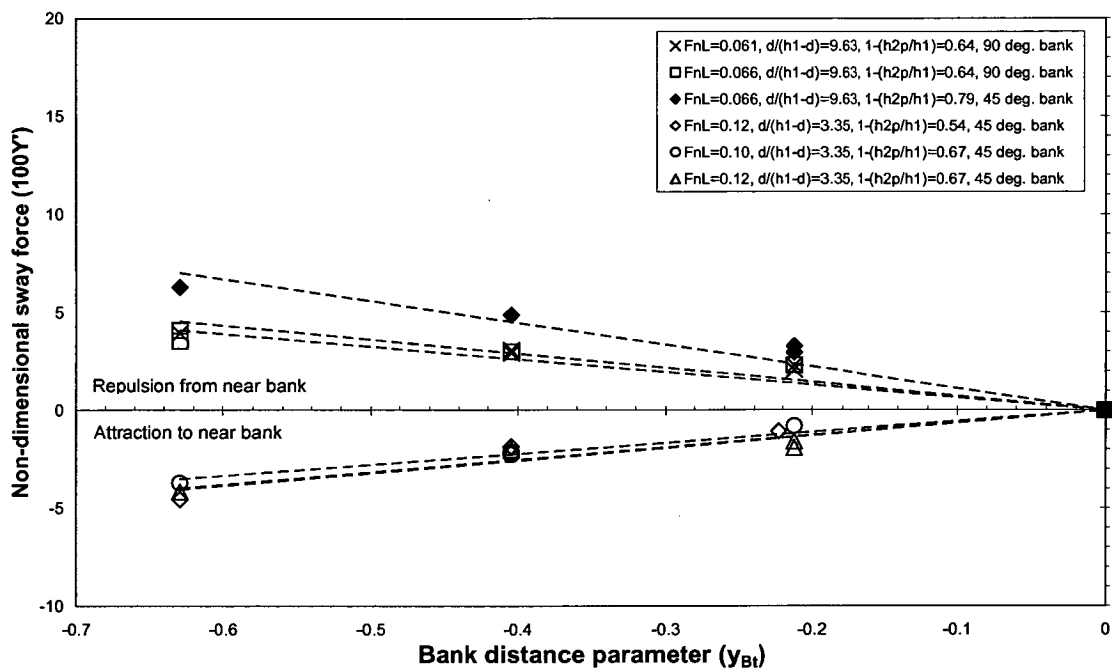


Figure 5.13 Non-dimensional sway force as a function of y_{Bt} for flooded banks, MarAd L series model

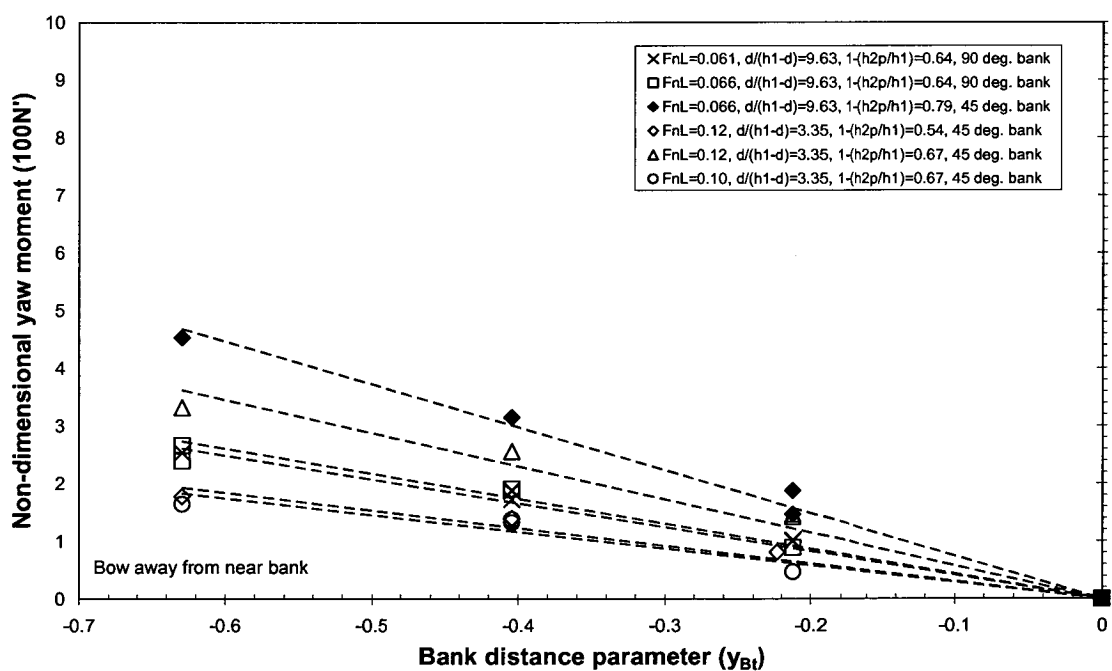


Figure 5.14 Non-dimensional yaw moment as a function of y_{Bt} for flooded banks, MarAd L series model

5.8.5 Bank flooding

For results presented in this section the bank flooding parameter was varied by changing the height of the bank and maintaining constant vessel draught and water depth.

The influence of bank flooding on sway force and yaw moment for a selection of cases is presented in Figures 5.15 and 5.16. The magnitude of the attraction and repulsion sway force was generally smaller for cases with low bank flooding parameter, as illustrated in Figure 5.15. Similarly, it was found for the majority of cases the magnitude of the bow away yaw moment was smaller for cases with a large depth of water over the bank, as shown in Figure 5.16. The rate of change of the sway force and yaw moment with bank flooding parameter was smaller for lower values of bank flooding parameter. Norrbin (1974) found that the presence of a flooded bank with a height equal to up to 40% of the water depth will not significantly influence ship handling. The rate of change of non-dimensional sway force and yaw moment with bank flooding is quantified and discussed in more detail in Chapter 6.

For some cases at length Froude numbers exceeding approximately 0.11, at draught to under keel clearance ratios of 5.13 and 3.35, the sway force and yaw moment for the flooded bank case exceeded that for the corresponding surface piercing case. This is illustrated for an example case in Figure 5.17. This trend also occurred for bow away yaw moment, as illustrated in Figure 5.18. Li (2000) observed a similar trend for a tanker model at a draught to under keel ratio of 5. These cases lie in the region where the sway force changed from attraction to repulsion, which may explain the observed trends.

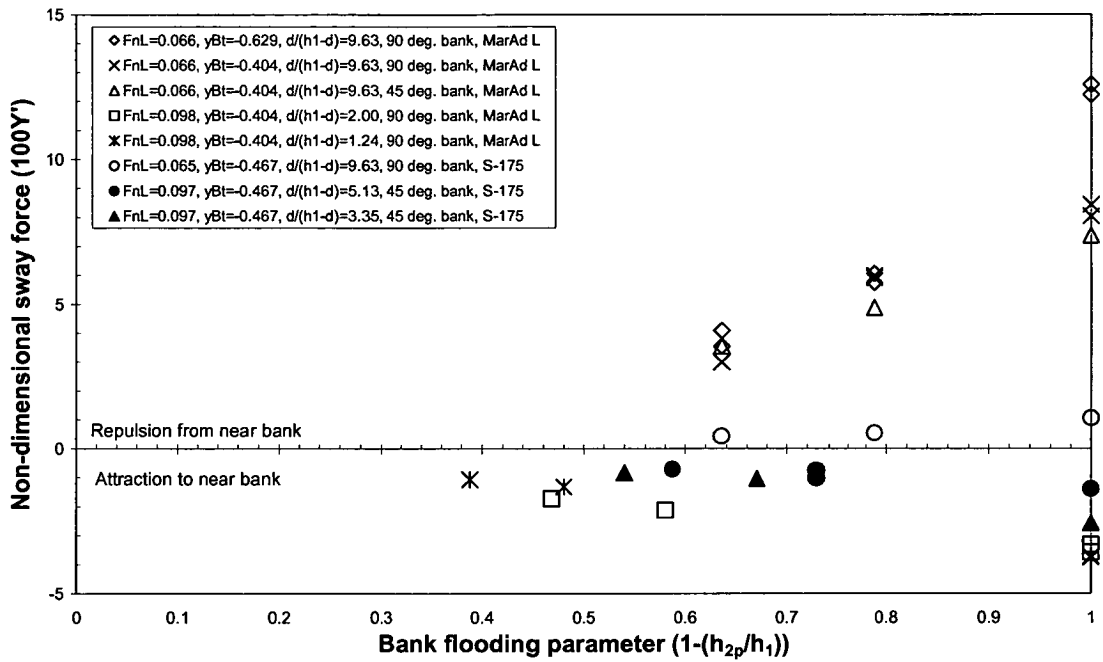


Figure 5.15 Non-dimensional sway force as a function of $1-(h_{2p}/h_1)$

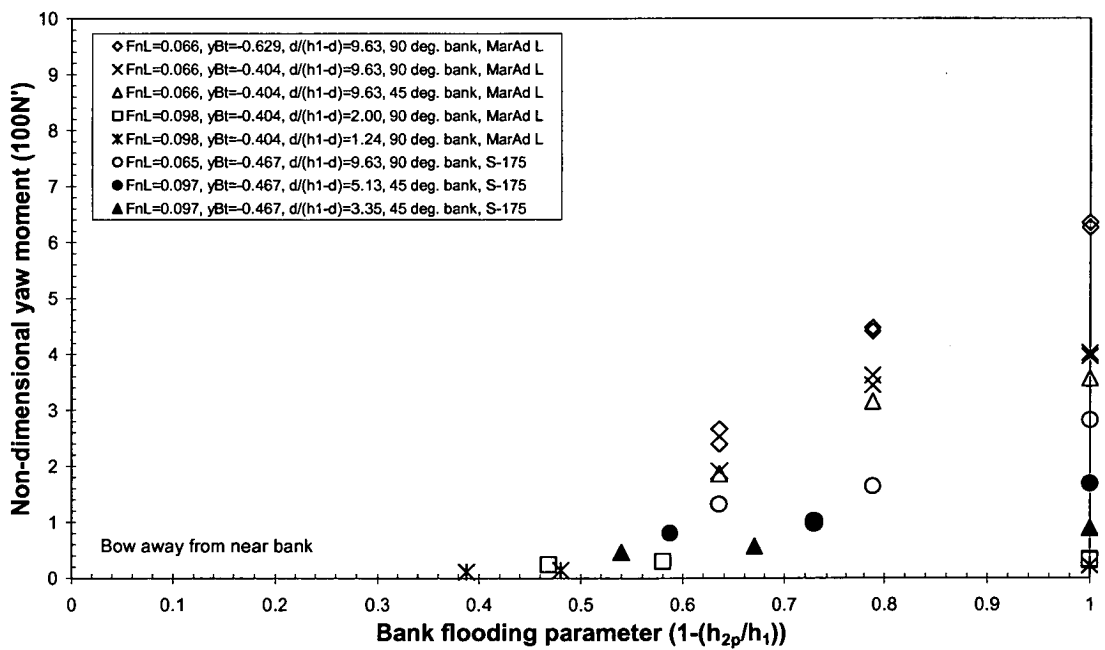


Figure 5.16 Non-dimensional yaw moment as a function of $1-(h_{2p}/h_1)$

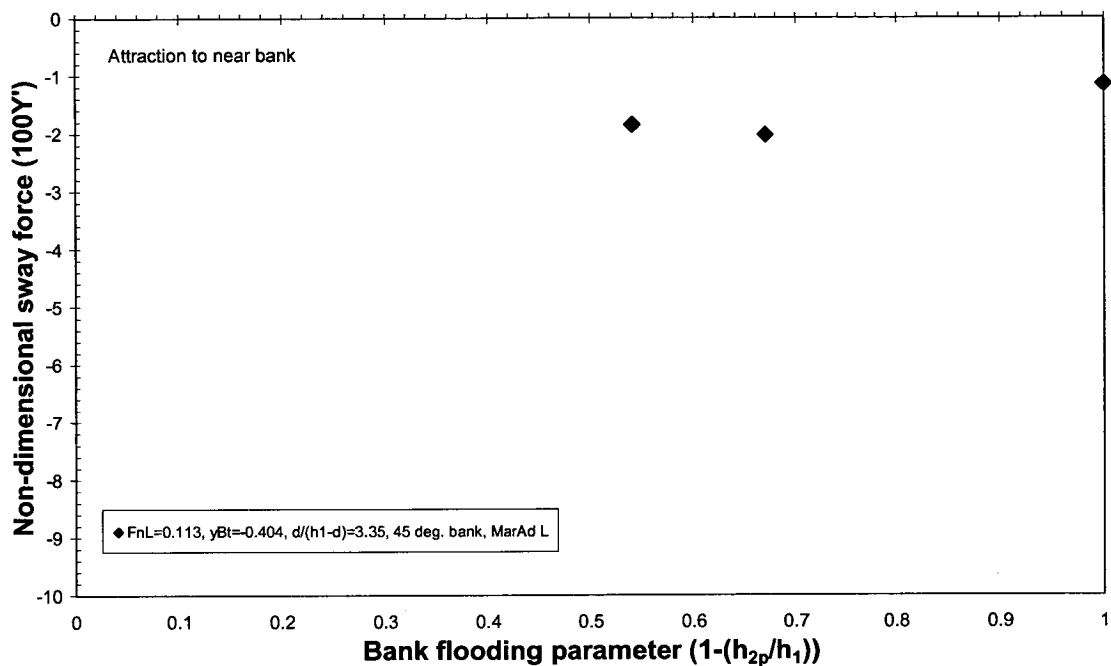


Figure 5.17 Non-dimensional sway force as a function of $1 - (h_{2p}/h_1)$

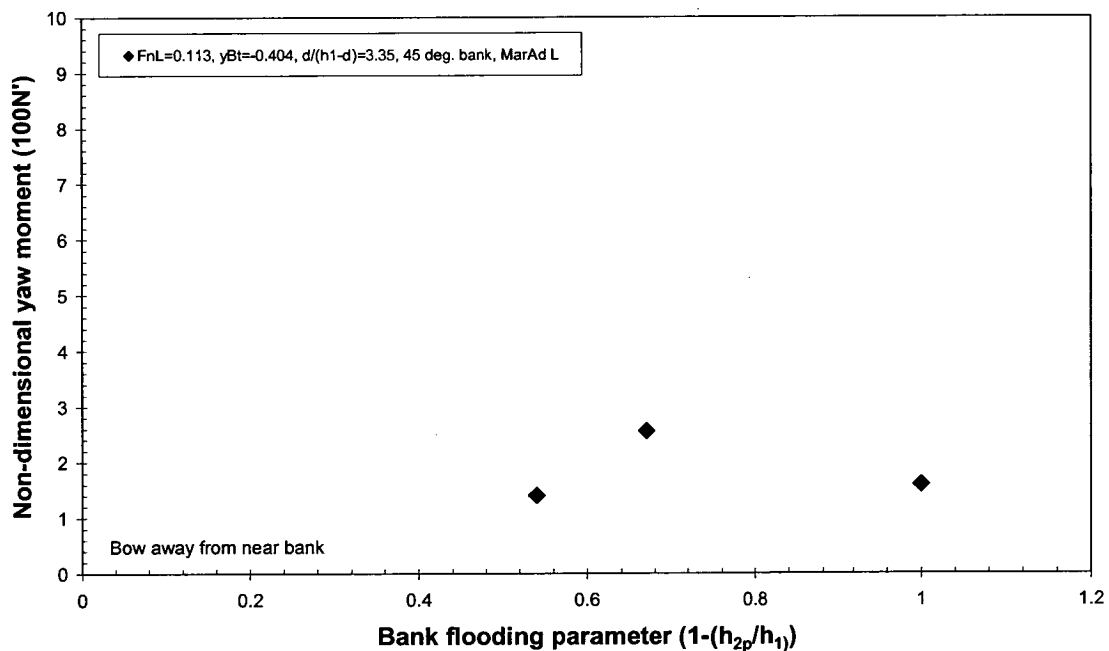


Figure 5.18 Non-dimensional yaw moment as a function of $1 - (h_{2p}/h_1)$

5.8.6 Bank slope

Generally the magnitude of non-dimensional sway force and yaw moment was smaller for lower bank slopes at low length Froude numbers. However, at higher length Froude numbers smaller bank slopes gave rise to larger values of sway force and yaw moment. Similar trends were noted by Dand (1981), Ch'ng (1991) and Li (2000). This trend is illustrated for example cases in Figure 5.19 for sway force and Figure 5.20 for yaw moment.

In the present study bank angles ranging from 45 to 90 degrees to the horizontal were investigated. To examine the influence of lower bank slopes results from Norrbin (1985) and Ch'ng (1991) were used. The magnitude of sway force and yaw moment was generally lower for small bank slopes up to a length Froude number of approximately 0.1 for draught to under keel clearance ratios between 4.17 and 1.24. At a draught to under keel clearance ratio of 5.13, Ch'ng (1991) found that this trend occurred up to a length Froude number of approximately 0.07; at length Froude numbers above this value the yaw moment induced by both 20 and 30 degree surface piercing banks was similar to that for a vertical bank. A selection of cases is presented in Figures 5.21 and 5.22 where the magnitudes of sway force and yaw moment were generally smaller for lower bank slopes.

Since the magnitude of sway force and yaw moment generally reduced with decreasing bank slope for low vessel speeds, an equivalent bank distance parameter can be used to estimate the effect of bank slope (Ch'ng 1991). This is discussed in further detail in Chapter 6.

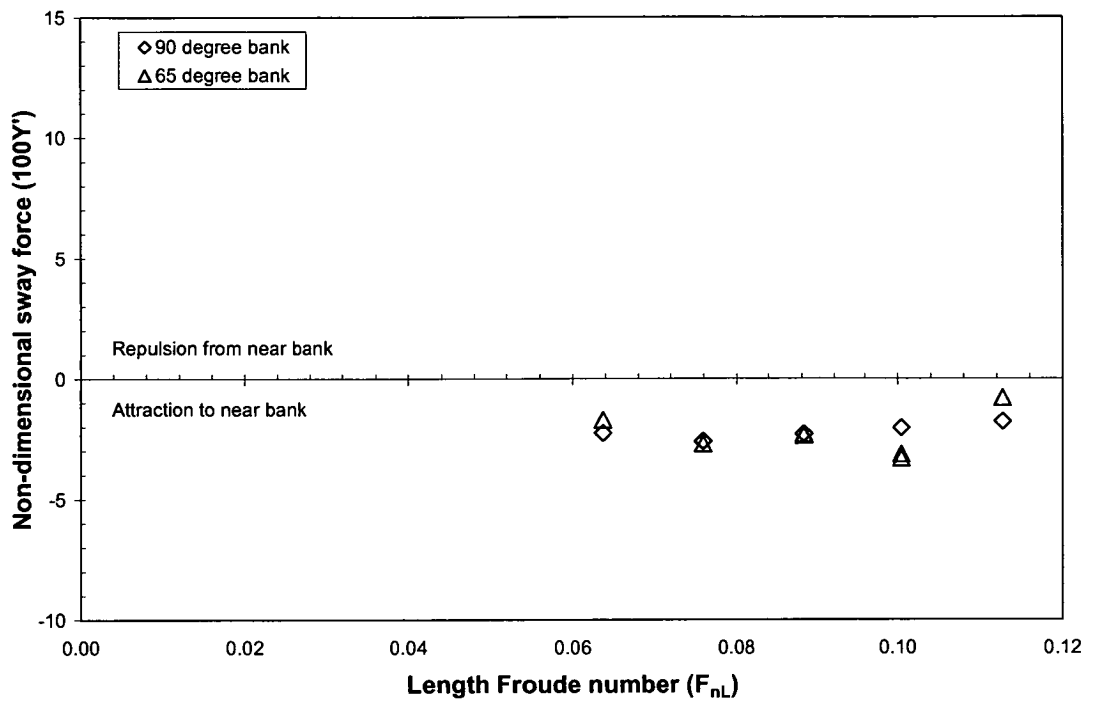


Figure 5.19 Non-dimensional sway force as a function of F_{nL} , varying α_p , $d/(h_1-d)=3.35$, $y_{pt}/B=1.00$, $1-(h_{2p}/h_1)=1.00$, MarAd L series model

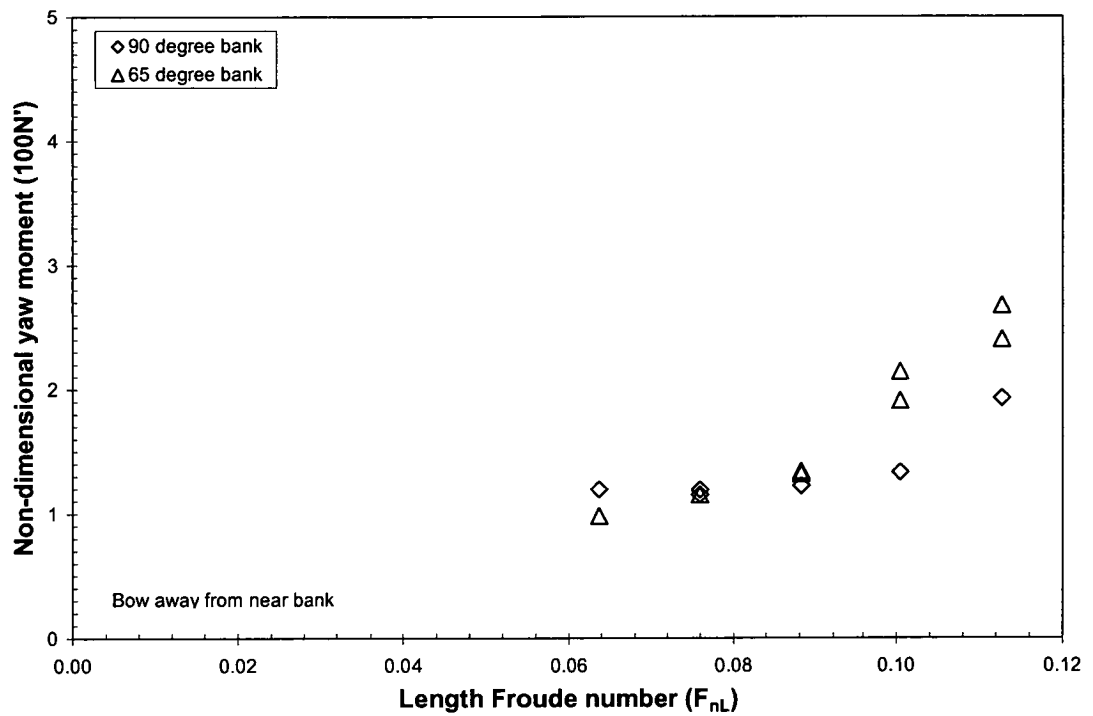


Figure 5.20 Non-dimensional yaw moment as a function of F_{nL} , varying α_p , $d/(h_1-d)=3.35$, $y_{pt}/B=1.00$, $1-(h_{2p}/h_1)=1.00$, MarAd L series model

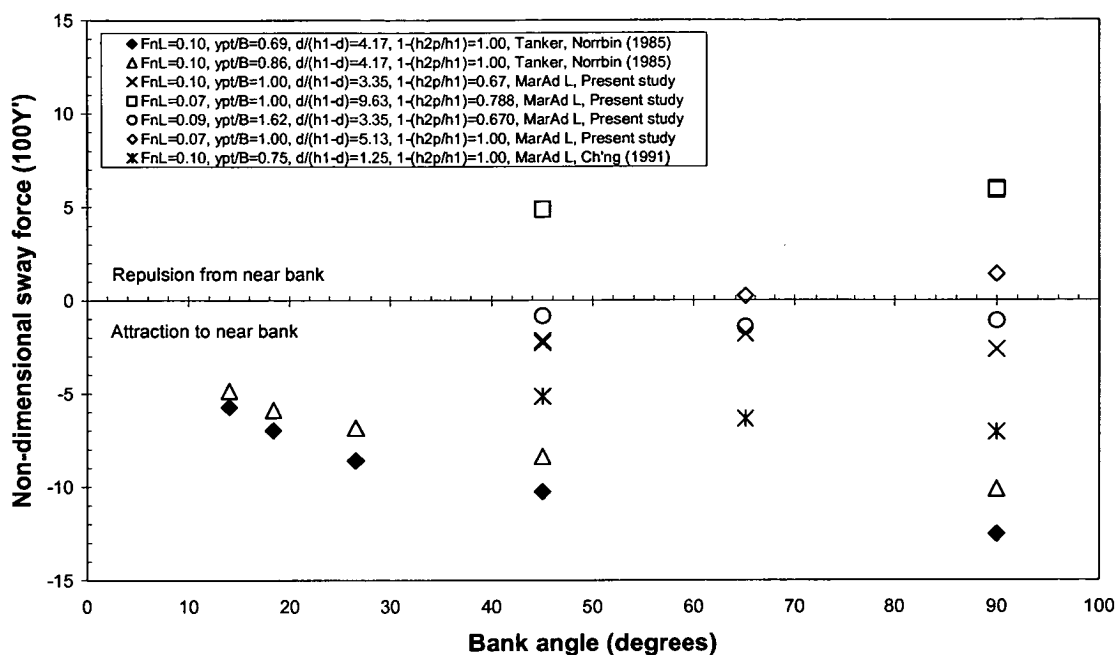


Figure 5.21 Non-dimensional sway force as a function of α_p

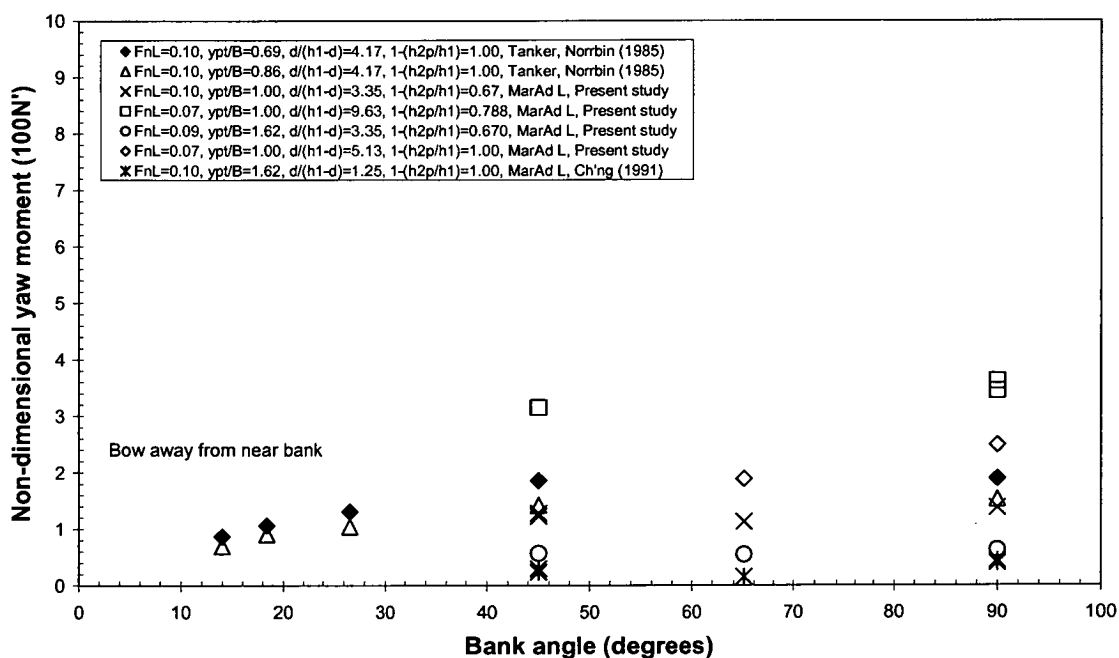


Figure 5.22 Non-dimensional yaw moment as a function of α_p

5.8.7 Hull form

The sway force was away from the near bank for the bulk carrier and containership models at a draught to under keel clearance ratio of 9.63. The magnitude of the repulsion sway force and bow away yaw moment experienced by the bulk carrier hull forms generally exceeded that experienced by the containership hull form. This is illustrated for an example case in Figure 5.23 for sway force and Figure 5.24 for yaw moment for the two bulk carrier models and the S-175 containership for a vertical surface piercing bank at a draught to under keel clearance ratio of 9.63. The magnitude of the repulsion sway force and bow away yaw moment was generally similar for the two bulk carrier hull forms for the cases tested. However, for some cases the MarAd F series model experienced slightly larger non-dimensional sway force and yaw moment, as illustrated in Figures 5.23 and 5.24. The magnitude of the repulsion sway force and bow away yaw moment for the bulk carrier models significantly exceeded that experienced by the containership hull form.

For the majority of cases it was found that the magnitude of the attraction sway force and bow away yaw moment experienced by the bulk carrier hull forms exceeded that experienced by the containership hull form. The sway force and yaw moment are presented for a selection of surface piercing and flooded bank cases for lower draught to under keel clearance ratios in Figures 5.25 and 5.26, respectively. Generally, for these cases where the sway force was towards the near bank at lower speeds, the magnitude of the sway force and yaw moment for the MarAd L series model exceeded that for the S-175 containership. This may be attributed to the additional blockage of the bulk carrier model creating a larger flow velocity between the model and the near bank resulting in a larger pressure drop alongside the vessel. Ch'ng (1991) found similar trends for the MarAd L series and S-175 containership models.

For a small number of cases, at a draught to under keel clearance ratio of 5.13, the attraction sway force for the containership model exceeded that experienced by the bulk carrier hull form, as shown for an example case in Figure 5.27. Li (2000) noted similar trends for sway force at a draught to under keel clearance ratio of 5 with a 30 degree bank when comparing results for a tanker and ferry model. The yaw moment for the case in Figure 5.27 is shown in Figure 5.28. As can be seen the bow away yaw moment for the bulk carrier model was found to exceed that experienced by the containership hull form.

Norrbin (1985) noted that bank induced yaw moments are especially sensitive to the fore-end-aft asymmetry of the hull. The aft ward shift of LCB found in fast finer hulls will be reflected in a corresponding shift of the centre of pressure of the lateral force. This may partly explain why the containership model experienced less bow away yaw moment than the bulk carrier models.

The influences of water depth to draught ratio and ship to bank distance on the non-dimensional sway force and yaw moment had similar tendencies for both the bulk carriers and the containership; i.e. generally, the smaller the ship to bank distance, the greater the non-dimensional sway force and yaw moment and the shallower the water depth, the greater the values of non-dimensional yaw moment.

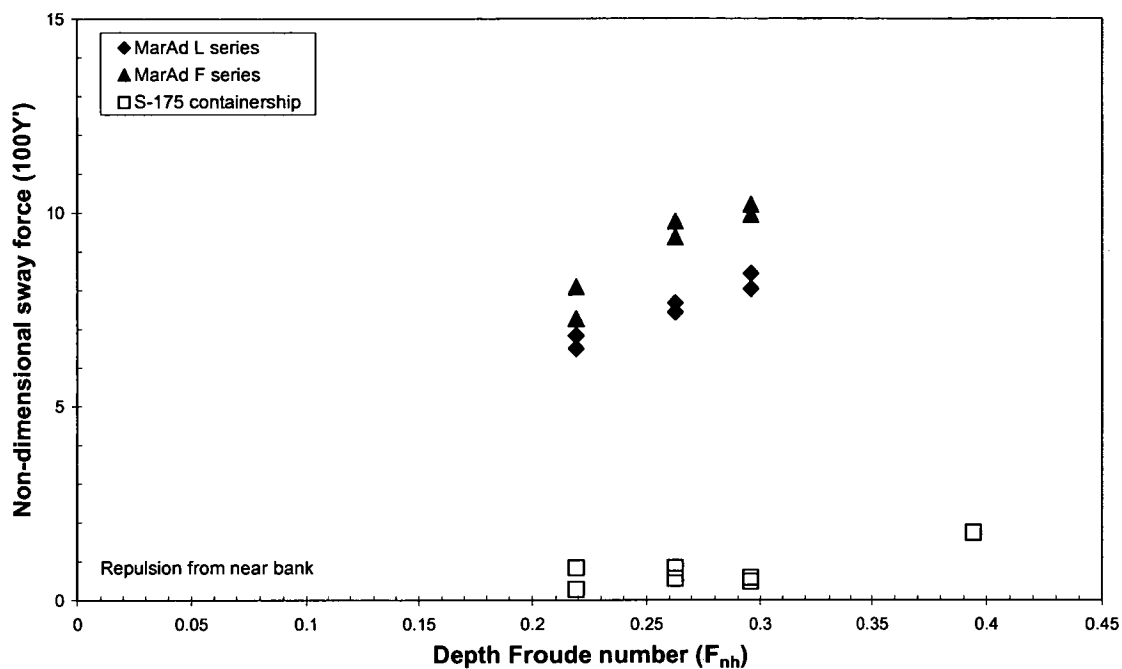


Figure 5.23 Non-dimensional sway force as a function of F_{nh} , $y_{pt}/W=0.162$, $d/(h_1-d)=9.63$, $1-(h_{2p}/h_1)=1.00$, $\alpha_p=90^\circ$

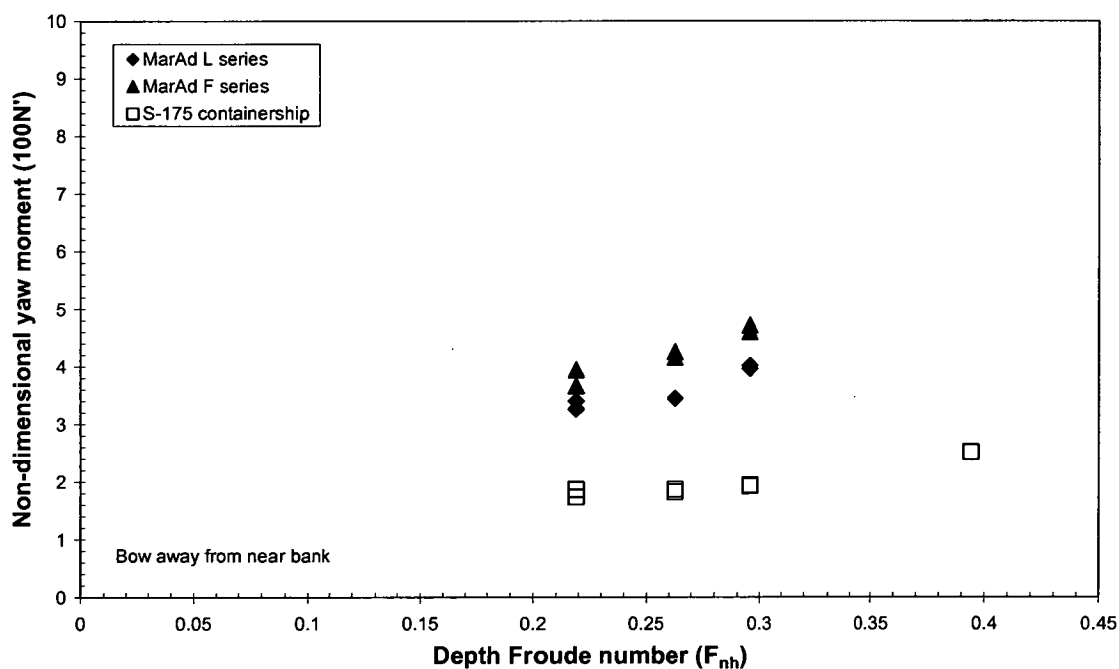


Figure 5.24 Non-dimensional yaw moment as a function of F_{nh} , $y_{pt}/W=0.162$, $d/(h_1-d)=9.63$, $1-(h_{2p}/h_1)=1.00$, $\alpha_p=90^\circ$

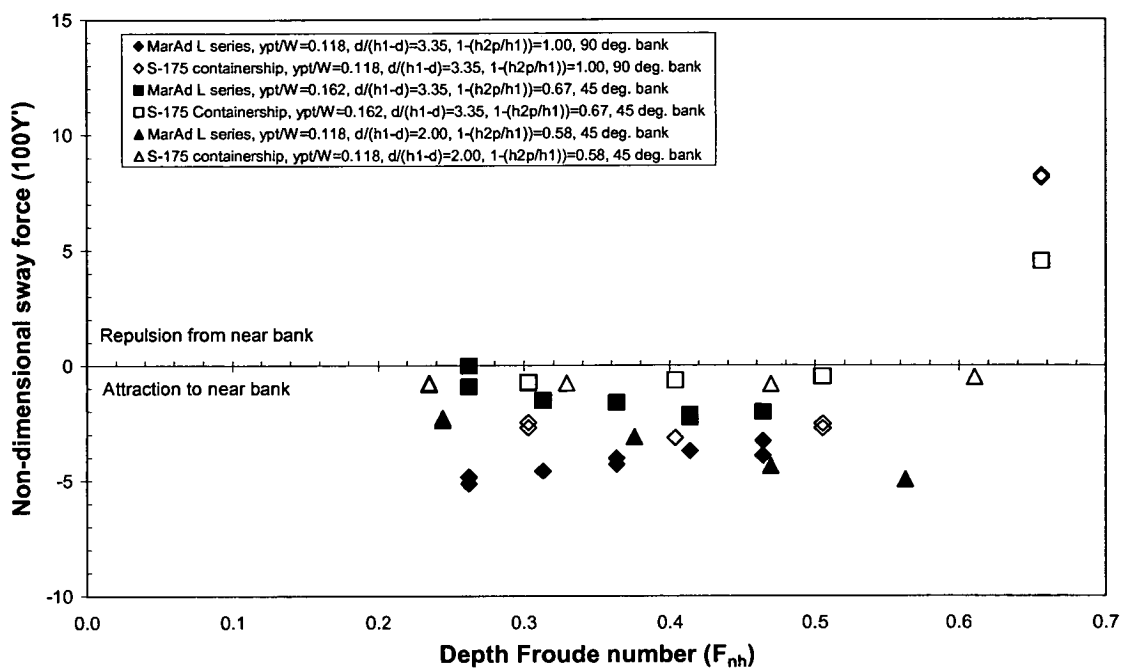


Figure 5.25 Non-dimensional sway force as a function of F_{nh} for bulk carrier and containership models

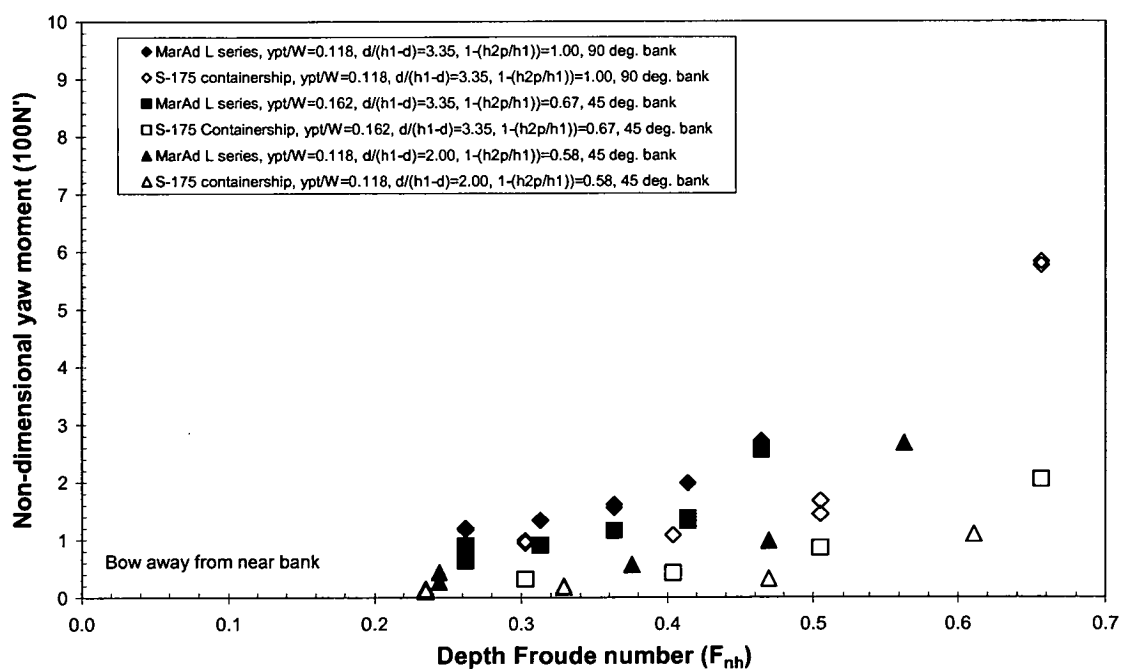


Figure 5.26 Non-dimensional yaw moment as a function of F_{nh} for bulk carrier and containership models

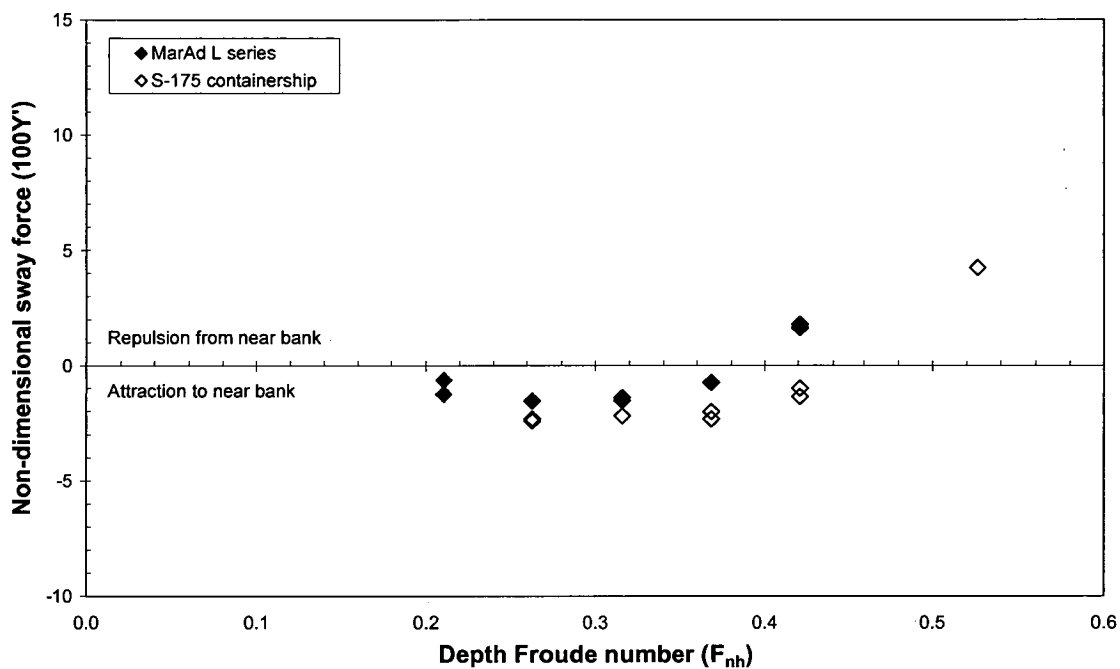


Figure 5.27 Non-dimensional sway force as a function of F_{nh} for bulk carrier and containership models, $y_{pt}/W=0.118$, $d/(h_1-d)=5.13$, $1-(h_{2p}/h_1)=1.00$, $\alpha_p=90^\circ$

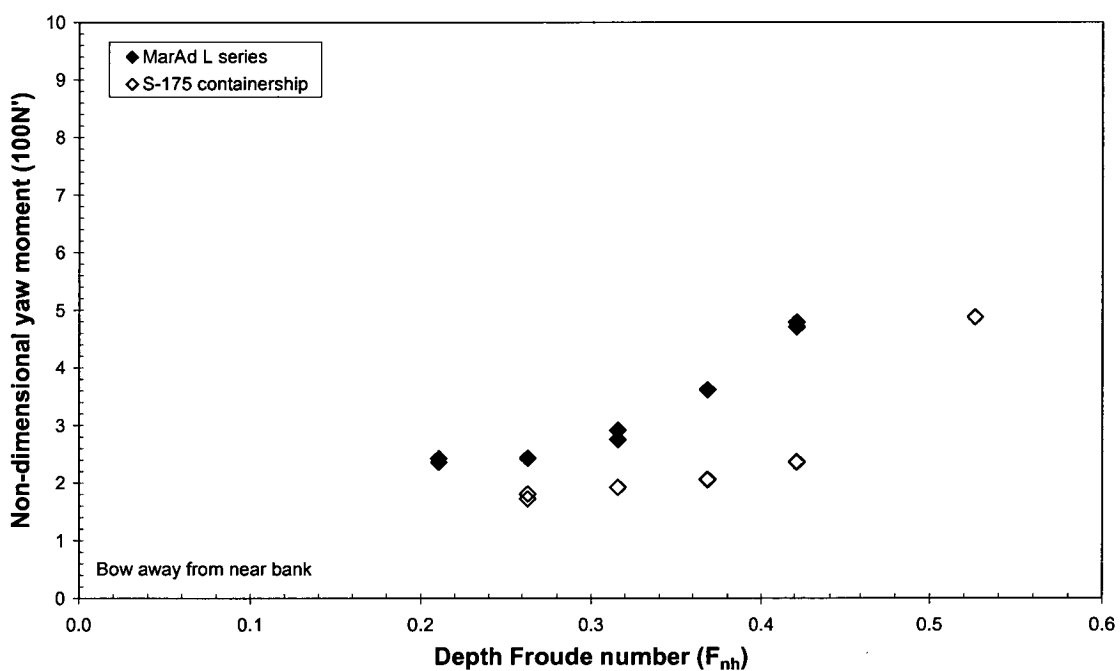


Figure 5.28 Non-dimensional yaw moment as a function of F_{nh} for bulk carrier and containership models, $y_{pt}/W=0.118$, $d/(h_1-d)=5.13$, $1-(h_{2p}/h_1)=1.00$, $\alpha_p=90^\circ$

5.8.8 Discussion

In this chapter it has been shown that the sway force may be towards or away from the near bank. Also, the magnitude of the bow away yaw moment was found to be larger for cases where the ship experienced repulsion from the near bank. In this section, possible causes for this behaviour and other general findings are discussed.

At low under keel clearances the flow beneath the bottom of the hull is restricted. When combined with the relatively small cross sectional area between the hull and the near bank a positive pressure between the fore part of the vessel and the near bank is produced, i.e. a stagnation area. Ch'ng (1991), using flow visualisation tests, found that the free surface stagnation point moved off the vessel's longitudinal centreline towards the near bank for cases with low under keel clearance, causing fluid to be diverted to the open side of the vessel. Li (2000) performed pressure measurements for a model travelling in restricted water and found a large stagnation area between the bow and near bank. This pressure in the bow region, which is much higher than on the open side of the vessel causes a relatively large bow away yaw moment. This positive pressure at the bow can be so dominant that the resultant sway force becomes away from the near bank. Li (2000) found that the magnitude of the positive pressure, and the waves between the bow and near bank, increased for lower under keel clearances. The repulsion phenomenon is similar to wing in ground effect in aerodynamics (Li 2000).

At higher speeds for draught to under keel clearance ratios of 9.63, 5.13 and 3.35, solitons were observed emanating from between the bow and the near bank, whereby the model generates periodic solitary waves in front of itself, with a velocity slightly higher than the model. This implies localised trans-critical flow between the bow of the vessel and the near bank. For these cases the waves on the near bank side of the hull were observed to be much higher than those on the open side, indicating a higher pressure between the near bank and the model than on the open side. The sway force was found to be away from the near bank for these cases, as also predicted by Chen and Sharma (1994). These waves are produced due to a combination of high blockage and high vessel speed (Tuck and Taylor 1970).

The stagnation point at the free surface moves less distance off the vessel's longitudinal centreline (towards the near bank) for cases with attraction sway force compared to those with repulsion sway force. Hence, for cases with attraction sway force more fluid passes between the vessel and the near bank (Ch'ng 1991). The attraction sway force occurs since the flow between the ship and the near bank is faster than on the open side due to the reduced cross sectional area between the ship and the near bank (Norrbin 1978). For such cases the suction force dominates the effect of the positive pressure between the bow and the near bank.

There were some higher speed cases at medium to low draught to under keel clearance ratios where the sway force was towards the near bank and relatively high waves were observed between the bow of the model and the near bank. The effects of such wave patterns may have given rise to some of the counter-intuitive trends identified in the present study; for example, cases where sway force was smaller for larger bank slopes (when the ship to bank distance is measured to the toe of the near bank). Similar reasons for such trends were proposed by Dand (1981).

5.9 Assessment of three-dimensional panel method

The number of model scale experiments that could be conducted was limited by the resources and time required to perform them. The steady-state sway force and yaw moment experienced by a ship travelling alongside a lateral bank of infinite length have been predicted using the potential flow module of Shipflow 2.5. Background concerning the computation technique is provided in Section 2.3.2. In the present section the predictions are compared to steady-state model scale experiment results to assess if the prediction technique is sufficiently accurate to be used to extend the steady-state experimental data matrix for the regression analyses.

In general, as blockage and vessel speed are increased the flow becomes more complicated and the effect of phenomena such as cross flow, ship waves and circulation are usually accentuated. Therefore, in the first instance, sub-critical flow cases were investigated with moderate blockage and moderate vessel speeds. The results presented in this section were computed with a non-linear free surface boundary condition. Computations were performed with both linear and non-linear free surface boundary conditions and the results were found to be similar for both methods, since the effect of waves was small.

Whilst predictions were performed for a large number of cases, only a selection of results that illustrates general trends is presented. Predicted and measured bank induced sway force and yaw moment are presented for a selection of cases in Figures 5.29 and 5.30, respectively. The prediction is within 10% for sway force at a draught to under keel clearance ratio of 1.24. However, the measured and predicted values diverged for lower static under keel clearances with the model scale measurement overestimated by up to approximately 80% at a draught to under keel clearance ratio of 2.5. It was found that the bow away yaw moment was overestimated by up to approximately 80% at a draught to under keel clearance ratio of 1.24 and was underestimated by up to approximately 40% at a draught to under keel clearance ratio of 2.5, as illustrated in Figure 5.30. Tornblom (2000) compared predictions using the potential flow module of Shipflow 2.4 to experimental results for a tanker model at large draught to under keel clearance ratios and found that the under prediction of bow away yaw moment was exacerbated at draught to under keel clearance ratios higher than 2.5. It was also found that the predicted sway force was toward the near bank for a draught to under keel clearance of 16.7, whereas the measured value was actually away from the near bank.

For cases with asymmetrical flow the motion of the ship generates circulation around itself, which produces a lift force. The poor prediction can be partly attributed to the fact that the method does not account for lift effects due to circulation. The effect of separation at the stern due to asymmetrical flow could not be modelled using the potential flow module of Shipflow 2.5 due to the difficulties in defining a Kutta condition for the three-dimensional flow at a transom stern. An alternative approach using Shipflow would be to divide the flow into three zones, as shown in Figure 2.2. The outer flow could be modelled using potential flow theory in Zone I. A momentum integral method could be applied to model the viscous effects in the boundary layer in Zone II and a Reynolds Averaged Navier Stokes solution could be applied over the stern region of the ship in Zone III to account for viscous effects in the stern/wake flow. However, a ship travelling in restricted water can be likened to a very small aspect ratio foil, with separation occurring at locations along the length of the ship; not just at the trailing edge of the stern (Chen and Sharma 1994). Therefore, applying Reynolds Averaged Navier Stokes equations only over the stern of the ship may not provide a sufficiently accurate solution.

Hence, this was not investigated further in the present work. Applying Reynolds Averaged Navier Stokes equations over the entire hull may provide a more accurate prediction (Li 2000).

Due to the poor correlation with model scale measurements, predictions using the Shipflow 2.5 potential flow method were not included in the steady-state data matrix for the regression analyses. There are a number of alternative prediction techniques that could have been investigated, as outlined above and in Section 2.2.1. However, due to the difficulties in accurately predicting the complex nature of the flow around a ship travelling in restricted water, it was decided that empirical equations based on steady-state model scale experimental results would provide the most practical and reliable results for input to the mathematical model.

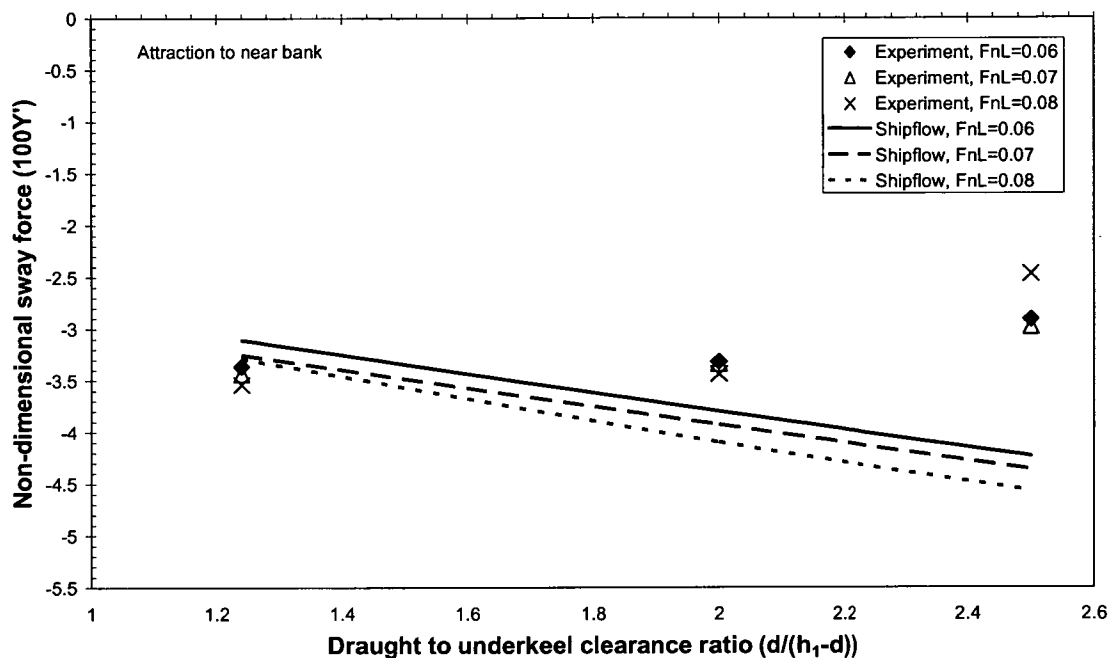


Figure 5.29 Comparison between measured sway force and Shipflow predictions, $y_{Bt} = -0.403$, $1-(h_{2p}/h_1)=1$, $1-(h_{2s}/h_1)=1$, $\alpha_p = 90^\circ$, MarAd L series model

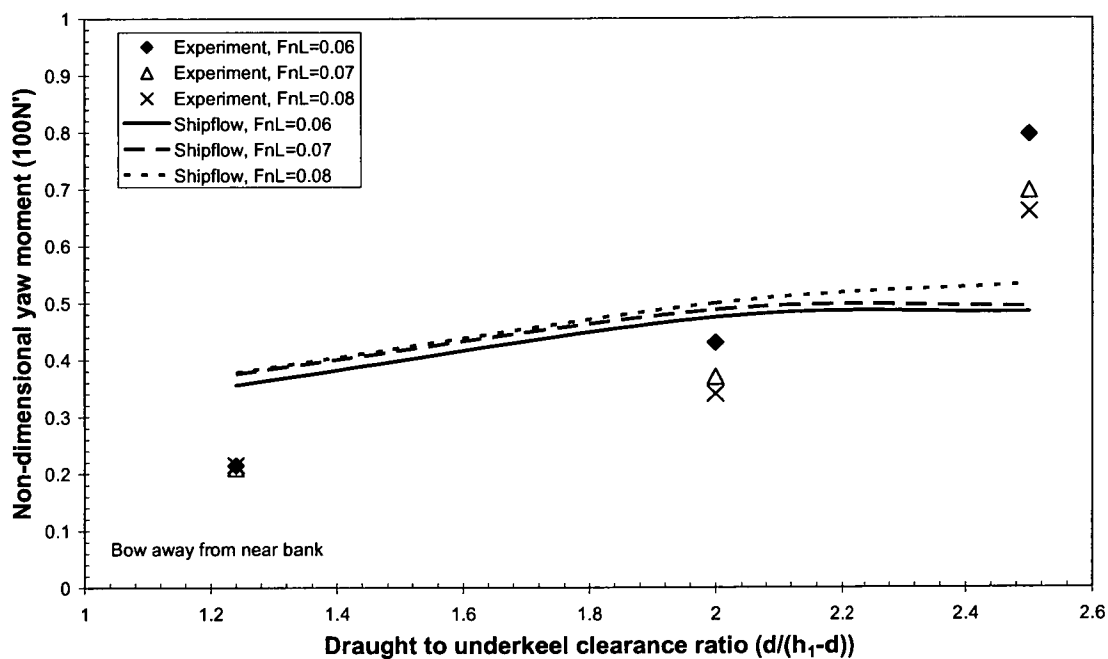


Figure 5.30 Comparison between measured yaw moment and Shipflow predictions, $y_{Bt} = -0.403$, $1-(h_{2p}/h_1)=1$, $1-(h_{2s}/h_1)=1$, $\alpha_p = 90^\circ$, MarAd L series model

5.10 Concluding remarks

Physical model scale experiments were undertaken to investigate sway force and yaw moment induced on a ship travelling alongside infinitely long lateral banks.

There was a significant difference in the magnitude of bank induced sway force and yaw moment experienced by the bulk carrier and containership models tested. The influences of water depth to draught ratio and ship to bank distance on the non-dimensional sway force and yaw moment had similar tendencies for both the bulk carriers and the containership; i.e. generally, the smaller the ship to bank distance, the greater the non-dimensional sway force and yaw moment and the shallower the water depth, the greater the magnitude of non-dimensional yaw moment.

The sway force may be towards or away from the near bank for both the bulk carrier and containership hull forms. The sway force was away from the near bank for all cases tested at a draught to under keel clearance ratio of 9.63. The change in sway force from towards to away from the near bank occurred at a draught to under keel clearance ratio between 9.63 and 5.13 for the majority of cases tested in the present study. There were a few cases with high blockage and high vessel speed where the transition from attraction to repulsion occurred between 5.13 and 3.35, and for a small number of cases with high blockage and high vessel speed the change occurred at a draught to under keel clearance below 3.35. The sway force was towards the near bank at the draught to under keel clearance ratios tested less than 3.35. The point where the sway force changed direction was closely dependent on two variables: draught to under keel clearance ratio and vessel speed, and to a lesser extent dependent on ship form, lateral ship to bank distance, bank geometry and the degree of bank flooding.

The yaw moment was bow away from the near bank, except for a minority of cases at a draught to under keel clearance ratio of 1.24. The bow away yaw moment was found to generally increase significantly for cases where the sway force was away from the near bank.

For cases with low blockage at low vessel speed ranges the sway force and yaw moment varied approximately with the square of vessel speed. However, for cases with high blockage at higher vessel speeds, where free surface effects become significant, the sway force and yaw moment varied with speed raised to a power exceeding 2. The rate of increase of bow away yaw moment with vessel speed was particularly high for cases where the sway force was away from the near bank. The rate of increase of bow away yaw moment with vessel speed for these cases was notably less for flooded banks compared to surface piercing banks.

For the majority of cases the sway force and yaw moment showed a generally linear relationship with the ship to bank distance parameter, y_{Bt} , for surface piercing and flooded bank cases.

Generally, the magnitude of non-dimensional sway force and yaw moment was smaller for low bank slopes at lower length Froude numbers. However, at higher length Froude numbers small bank slopes gave rise to larger values of sway force and yaw moment.

For the majority of cases it was found that the magnitude of the sway force and yaw moment was smaller for cases with greater depth of water over the bank for length Froude numbers less than 0.11. Above this value there was a minority of cases where the magnitudes of the sway

force and yaw moment for flooded banks was equivalent to or exceeded that for the surface piercing case.

Steady-state sway force and yaw moment predictions using the potential flow module of Shipflow 2.5 were compared against model scale measurements to assess if the prediction technique is sufficiently accurate to be used to extend the steady-state experimental data matrix for the regression analyses. It was found that, for some cases, there was a variation of up to approximately 80% between the predicted and measured sway force and bow away yaw moment. This may be partly due to the fact that viscous effects were not modelled. Hence, the Shipflow 2.5 predictions were not included in the steady-state data matrix. Due to the difficulties in accurately predicting the complex nature of the flow around a ship travelling in restricted water, it was decided that empirical equations based on steady-state model scale experimental results would provide the most practical and reliable results for input to the mathematical models.

Chapter 6

Modelling of Ship-Bank Interaction for Ship-Handling Simulation

6.1 Introduction

As discussed in Chapter 5, model scale experiments were conducted to investigate the influence of various parameters on steady-state bank induced sway force and yaw moment. In this chapter multiple linear regression analysis on this experimental data is presented to develop formulae for the prediction of steady-state sway force and yaw moment for surface piercing and flooded banks. Details concerning multiple regression analysis techniques are presented in Section 2.3.1. The formulae have been validated against model scale bank effect measurements made by Dand (1981).

The formulae were used as input to an existing mathematical model, as outlined in Section 2.4.2, to simulate vessel behaviour in restricted water. The behaviour of a vessel in the horizontal plane has been predicted for a real-life manoeuvre where bank effect is utilised to aid a turn. The predictions have been compared to the vessel path known to occur in the real-life manoeuvre.

6.2 Prediction of bank induced sway force and yaw moment

6.2.1 Regression parameters

A number of possible non-dimensional expressions were tested to determine the most suitable regression parameters. The selection of possible parameters was based on the requirement that the net sway force and yaw moment on the vessel must be zero when the vessel is travelling on the centreline of a symmetrical channel with parallel banks or in open water, and each parameter must be easily attainable for input to ship-handling simulator mathematical models. The selection of the regression parameters is discussed in the following sections.

Vessel speed parameter

Length Froude number and depth Froude number were considered as possible non-dimensional vessel speed parameters for the regression analyses. Two regression analyses were performed on all experimental data; one with length Froude number as the vessel speed parameter and the other with depth Froude number as the vessel speed parameter. The equations with each parameter provided a similar fit to the experimental data. Hence, it is reasonable to use either of these parameters in the regression equations. Given that in Chapter 5 it was shown that water depth had a significant influence on the bank induced sway force and yaw moment, depth Froude number has been chosen as the parameter to account for vessel speed.

In Chapter 5 it was shown that non-dimensional sway force and yaw moment varied in a non-linear manner with depth Froude number. A maximum power of 3 was found to be sufficient to account for this non-linearity (up to a length Froude number of 0.1), whilst still providing sufficient accuracy between experimental points.

Under keel clearance parameter

The influence of vessel draught and water depth is represented in the final regression equations by a single parameter. Four possible parameters were selected and are presented in Equations 6.1 – 6.4. Each of the parameters are dependent upon water depth in the channel and vessel draught and satisfy the condition that the parameter approaches zero for the deep water case.

$$e^{(-h_1/d)} \quad (6.1)$$

$$d/h_1 \quad (6.2)$$

$$e^{(-(h_1/d)-1)} \quad (6.3)$$

$$d/(h_1-d) \quad (6.4)$$

Preliminary multiple linear regression analyses were performed to identify the parameter with the best statistical fit for both surface piercing and flooded banks using Equations 6.5 and 6.6. This analysis was restricted to cases where only the under keel clearance parameters were varied; the values of all other independent variables were held constant.

$$100Y' = a_0 + a_1x + a_2x^2 + \dots + a_nx^n \quad (6.5)$$

$$100N' = b_0 + b_1x + b_2x^2 + \dots + b_nx^n \quad (6.6)$$

Where $a_0, a_1, a_n, b_0, b_1, b_n$ are constants and x represents the under keel clearance parameters.

The non-dimensional sway force and yaw moment were found to vary in a non-linear manner with under keel clearance parameters for the bulk carrier and containership hull forms, particularly for sway force for surface piercing bank cases. This was also found by Norrbin (1971). This is illustrated for the draught to under keel clearance ratio parameter for a selection of cases in Figures 6.1 and 6.2. The maximum power of the under keel clearance parameters was increased to 5 to obtain sufficient statistical fit for non-dimensional sway force, whilst a maximum power of 3 was sufficient to account for the non-linearity between non-dimensional yaw moment and under keel clearance parameters.

Results from the preliminary regression analyses are presented in Tables 6.1 and 6.2 for a selection of cases. The parameter $d/(h_1-d)$ can be seen to be the most suitable parameter with the lowest standard error and the largest coefficient of determination. This supports findings from Ch'ng (1991) for the MarAd L series model moving alongside surface piercing banks. The statistical fit for non-dimensional yaw moment was superior to that obtained for non-dimensional sway force.

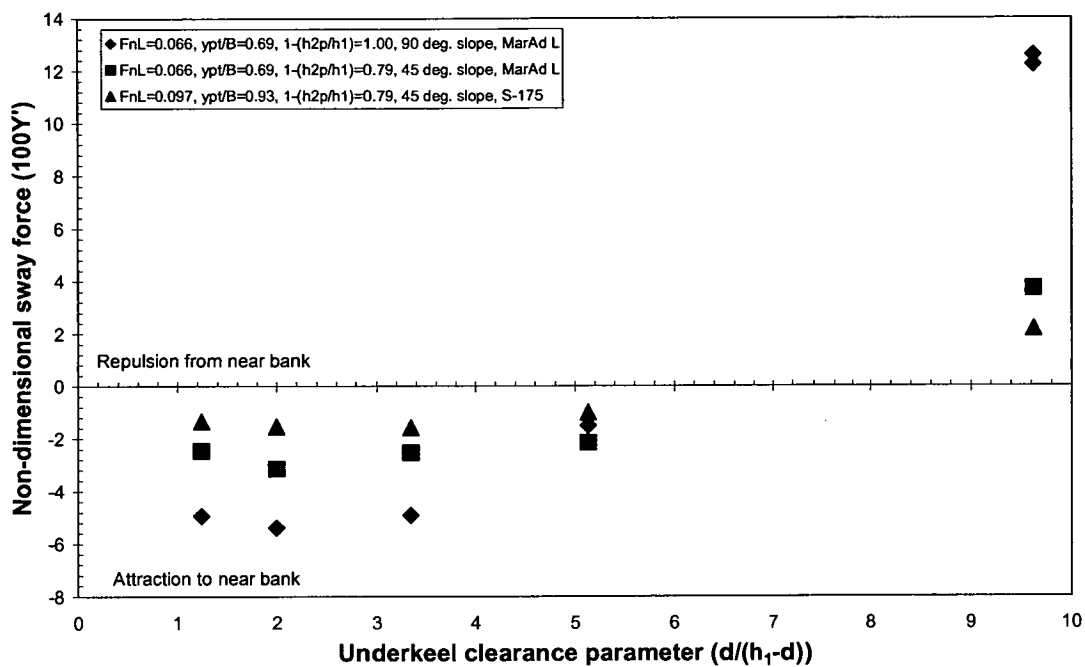


Figure 6.1 Non-dimensional sway force as a function of $d/(h_1-d)$

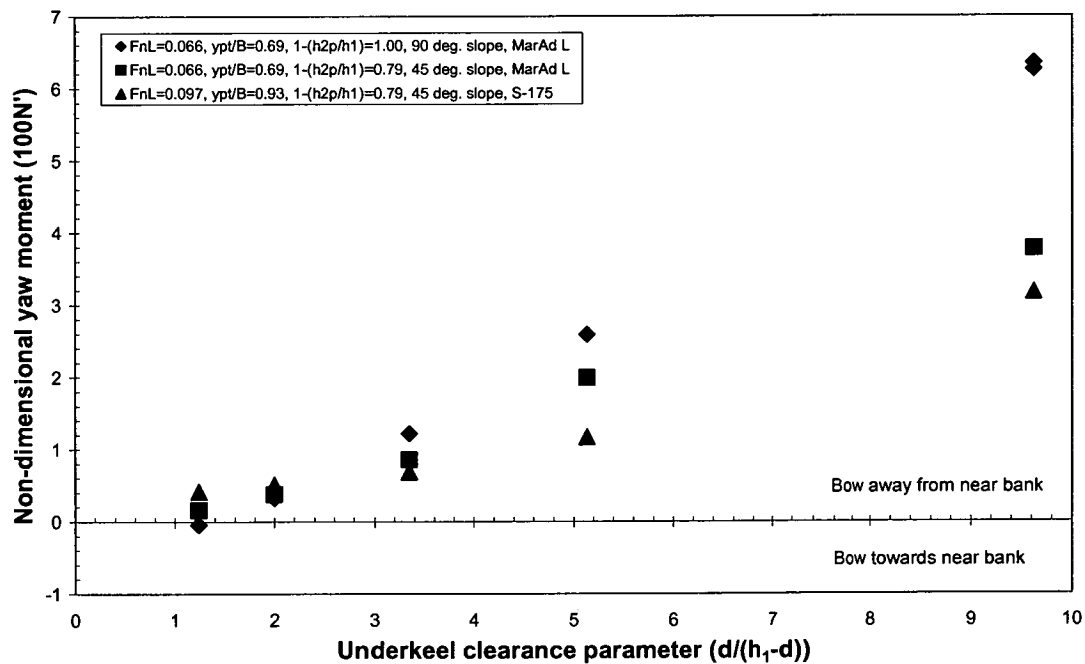


Figure 6.2 Non-dimensional yaw moment as a function of $d/(h_1-d)$

| Param. | F_{nL} | $1-(h_{2p}/h_1)$ | Bank angle (deg.) | y_{pt}/B | Model | Stand. error | Adjusted R^2 | R^2 |
|--------------------|----------|------------------|-------------------|------------|-------|--------------|----------------|--------|
| d/h_1 | 0.066 | 1.00 | 90 | 0.69 | MarAd | 1.6524 | 0.9577 | 0.9788 |
| $e^{(-h_1/d)}$ | | | | | | 0.7760 | 0.9907 | 0.9969 |
| $e^{(-(h_1/d)-1)}$ | | | | | | 0.7760 | 0.9907 | 0.9969 |
| $d/(h_1-d)$ | | | | | | 0.2802 | 0.9988 | 0.9996 |
| d/h_1 | 0.066 | 0.79 | 45 | 0.69 | MarAd | 1.0542 | 0.8632 | 0.9453 |
| $e^{(-h_1/d)}$ | | | | | | 1.0514 | 0.8639 | 0.9728 |
| $e^{(-(h_1/d)-1)}$ | | | | | | 1.0514 | 0.8639 | 0.9728 |
| $d/(h_1-d)$ | | | | | | 0.2544 | 0.9920 | 0.9984 |
| d/h_1 | 0.097 | 0.79 | 45 | 0.93 | S-175 | 0.5113 | 0.8830 | 0.9415 |
| $e^{(-h_1/d)}$ | | | | | | 0.2352 | 0.9752 | 0.9917 |
| $e^{(-(h_1/d)-1)}$ | | | | | | 0.2532 | 0.9752 | 0.9917 |
| $d/(h_1-d)$ | | | | | | 0.0543 | 0.9987 | 0.9996 |

Table 6.1 Statistical fit for under keel clearance parameters for sway force for three sample cases

| Param. | F_{nL} | $1-(h_{2p}/h_1)$ | Bank angle (deg.) | y_{pt}/B | Model | Stand. error | Adjusted R^2 | R^2 |
|--------------------|----------|------------------|-------------------|------------|-------|--------------|----------------|--------|
| d/h_1 | 0.066 | 1.00 | 90 | 0.69 | MarAd | 0.3145 | 0.9932 | 0.9966 |
| $e^{(-h_1/d)}$ | | | | | | 0.1721 | 0.9980 | 0.9993 |
| $e^{(-(h_1/d)-1)}$ | | | | | | 0.1721 | 0.9980 | 0.9993 |
| $d/(h_1-d)$ | | | | | | 0.0467 | 0.9999 | 0.9999 |
| d/h_1 | 0.066 | 0.79 | 45 | 0.69 | MarAd | 0.1155 | 0.9965 | 0.9986 |
| $e^{(-h_1/d)}$ | | | | | | 0.0903 | 0.9979 | 0.9996 |
| $e^{(-(h_1/d)-1)}$ | | | | | | 0.0903 | 0.9979 | 0.9996 |
| $d/(h_1-d)$ | | | | | | 0.0375 | 0.9996 | 0.9999 |
| d/h_1 | 0.097 | 0.79 | 45 | 0.93 | S-175 | 0.2688 | 0.9683 | 0.9842 |
| $e^{(-h_1/d)}$ | | | | | | 0.1369 | 0.9918 | 0.9973 |
| $e^{(-(h_1/d)-1)}$ | | | | | | 0.1369 | 0.9918 | 0.9973 |
| $d/(h_1-d)$ | | | | | | 0.0077 | 0.9999 | 0.9999 |

Table 6.2 Statistical fit for under keel clearance parameters for yaw moment for three sample cases

Ship to bank distance parameter

Norrbin (1971) showed that ship-bank interaction could be modelled through linear superposition of the effects of port and starboard surface piercing banks. Ch'ng (1991) demonstrated that the effects of the starboard and port banks were generally proportional to the parameter y_{B3} for surface piercing banks (see Figure 6.3). Through the use of this bank parameter, Ch'ng was able to linearise the functional model of the bank interference, allowing the general canal problem to be treated satisfactorily by superposition of force interactions originating from banks at varying separation distances. In Section 5.8.4 it was shown that for the majority of cases tested in the present study the non-dimensional sway force and yaw moment generally varied linearly with y_{Bt} for both surface piercing and flooded banks.

Three additional parameters were investigated in an attempt to determine if y_{Bt} is the most suitable ship to bank distance parameter for both surface piercing and flooded banks for a

constant $1-(h_{2p}/h_1)$ value. The proposed bank parameters are based on those that Ch'ng (1991) found to be most suitable for surface piercing banks, as listed below;

$$y_{Bt} = (1/y_{st} + 1/y_{pt})B/2 \quad (6.7)$$

$$y_{BBt} = (1/y_{st}^2 - 1/y_{pt}^2)B^2/2 \quad (6.8)$$

$$y_{EBt} = e^{(-y_{st}/B)} - e^{(y_{pt}/B)} \quad (6.9)$$

$$y_{Et} = e^{(-y_{st}/(B+1/2))} - e^{(y_{pt}/(B+1/2))} \quad (6.10)$$

Preliminary multiple regression analyses were performed to identify the parameter with the best statistical fit for both surface piercing and flooded banks using a linear relationship, Equations 6.11 and 6.12.

$$100Y' = a_1x \quad (6.11)$$

$$100N' = b_1x \quad (6.12)$$

Where a_1 and b_1 are constants and x is the respective ship to bank distance parameter.

The statistical results for a selection of surface piercing bank cases for non-dimensional sway force and yaw moment are given in Tables 6.3 and 6.4. The statistical fit for y_{Et} was similar to that for y_{EBt} and has not been presented. As can be seen there was no single parameter that provided the best fit for all cases for surface piercing banks. The parameter y_{Bt} was generally found to provide the best fit for sway force and yaw moment for the MarAd L series. The parameter y_{EBt} was found to provide a marginally better fit for the containership for sway force, but y_{Bt} was still acceptable explaining greater than 96% of the original variance. In general, y_{Bt} provided the best fit for both sway force and yaw moment for surface piercing banks, as found by Ch'ng (1991), whilst y_{BBt} was found to provide the poorest fit.

The statistical results for a selection of flooded bank cases for non-dimensional sway force and yaw moment is given in Tables 6.5 and 6.6, respectively. As with surface piercing banks, there was not a single bank parameter that provided the best fit for all cases. Generally, y_{EBt} provided the best statistical fit for sway force at a draught to under keel clearance ratio of 9.63 for the MarAd L series and S-175 containership, however, the statistical fit for y_{Bt} was only marginally less than that for y_{EBt} for most cases. Generally, y_{Bt} provided the best fit for sway force for all other draught to under keel clearance ratios. The parameters y_{EBt} and y_{Bt} provided the best fit for yaw moment, with y_{EBt} providing a marginally better fit for the majority of cases.

To simplify the final regression equations it is desirable to use a single bank distance parameter for all cases. Based on the above findings y_{Bt} was considered to be the most suitable parameter to represent the effect of ship to bank distance in the final regression formulae.

The relationship between non-dimensional sway force and yaw moment with y_{Bt} was found to be reasonably linear for the majority of cases. Hence, linear superposition of the effect of port and starboard banks is, in general, a reasonable assumption for the purpose of ship-handling simulation.

| Param. | F_{nL} | $1-(h_{2p}/h_1)$ | Bank angle (deg.) | $d/(h_1-d)$ | Model | Stand. error | Adjusted R^2 | R^2 |
|-----------|----------|------------------|-------------------|-------------|---------|--------------|----------------|--------|
| y_{Bt} | 0.066 | 1.00 | 90 | 9.63 | MarAd L | 0.261 | 0.9991 | 0.9992 |
| y_{BBt} | | | | | | 1.982 | 0.9451 | 0.9529 |
| y_{EBt} | | | | | | 0.476 | 0.9968 | 0.9973 |
| y_{Bt} | 0.098 | 1.00 | 65 | 5.13 | MarAd L | 0.321 | 0.9727 | 0.9796 |
| y_{BBt} | | | | | | 0.599 | 0.9051 | 0.9288 |
| y_{EBt} | | | | | | 0.354 | 0.9669 | 0.9752 |
| y_{Bt} | 0.088 | 1.00 | 65 | 3.35 | MarAd L | 0.210 | 0.9946 | 0.9964 |
| y_{BBt} | | | | | | 0.225 | 0.9938 | 0.9959 |
| y_{EBt} | | | | | | 0.372 | 0.9831 | 0.9888 |
| y_{Bt} | 0.087 | 1.00 | 90 | 9.63 | S-175 | 0.445 | 0.9485 | 0.9614 |
| y_{BBt} | | | | | | 0.075 | 0.9985 | 0.9989 |
| y_{EBt} | | | | | | 0.355 | 0.9672 | 0.9754 |
| y_{Bt} | 0.150 | 1.00 | 90 | 3.35 | S-175 | 0.236 | 0.9990 | 0.9993 |
| y_{BBt} | | | | | | 1.205 | 0.9737 | 0.9824 |
| y_{EBt} | | | | | | 0.155 | 0.9996 | 0.9997 |

Table 6.3 Statistical fit for ship to bank distance parameters for a sample of surface piercing bank cases for sway force

| Param. | F_{nL} | $1-(h_{2p}/h_1)$ | Bank angle (deg.) | $d/(h_1-d)$ | Model | Stand. error | Adjusted R^2 | R^2 |
|-----------|----------|------------------|-------------------|-------------|---------|--------------|----------------|--------|
| y_{Bt} | 0.066 | 1.00 | 90 | 9.63 | MarAd L | 0.130 | 0.9990 | 0.9992 |
| y_{BBt} | | | | | | 0.823 | 0.9616 | 0.9670 |
| y_{EBt} | | | | | | 0.379 | 0.9918 | 0.9930 |
| y_{Bt} | 0.098 | 1.00 | 65 | 5.13 | MarAd L | 0.141 | 0.9978 | 0.9983 |
| y_{BBt} | | | | | | 0.756 | 0.9358 | 0.9518 |
| y_{EBt} | | | | | | 0.199 | 0.9956 | 0.9967 |
| y_{Bt} | 0.088 | 1.00 | 65 | 3.35 | MarAd L | 0.177 | 0.9840 | 0.9883 |
| y_{BBt} | | | | | | 0.384 | 0.9248 | 0.9499 |
| y_{EBt} | | | | | | 0.098 | 0.9951 | 0.9968 |
| y_{Bt} | 0.087 | 1.00 | 90 | 9.63 | S-175 | 0.519 | 0.9628 | 0.9722 |
| y_{BBt} | | | | | | 0.198 | 0.9946 | 0.9959 |
| y_{EBt} | | | | | | 0.385 | 0.9795 | 0.9846 |
| y_{Bt} | 0.150 | 1.00 | 90 | 3.35 | S-175 | 0.275 | 0.9971 | 0.9981 |
| y_{BBt} | | | | | | 0.399 | 0.9939 | 0.9959 |
| y_{EBt} | | | | | | 0.332 | 0.9957 | 0.9972 |

Table 6.4 Statistical fit for ship to bank distance parameters for a sample of surface piercing bank cases for yaw moment

| Param. | F_{nL} | $1-(h_{2p}/h_1)$ | Bank angle (deg.) | $d/(h_1-d)$ | Model | Stand. error | Adjusted R^2 | R^2 |
|-----------|----------|------------------|-------------------|-------------|---------|--------------|----------------|--------|
| y_{Bt} | 0.061 | 0.64 | 90 | 9.63 | MarAd L | 0.498 | 0.9714 | 0.9762 |
| y_{BBt} | | | | | | 1.099 | 0.8606 | 0.8838 |
| y_{EBt} | | | | | | 0.373 | 0.9840 | 0.9866 |
| y_{Bt} | 0.066 | 0.79 | 45 | 9.63 | MarAd L | 0.780 | 0.9706 | 0.9779 |
| y_{BBt} | | | | | | 1.856 | 0.8332 | 0.8749 |
| y_{EBt} | | | | | | 0.496 | 0.9881 | 0.9911 |
| y_{Bt} | 0.076 | 0.67 | 45 | 3.35 | MarAd L | 0.128 | 0.9942 | 0.9956 |
| y_{BBt} | | | | | | 0.359 | 0.9539 | 0.9654 |
| y_{EBt} | | | | | | 0.236 | 0.9801 | 0.9850 |
| y_{Bt} | 0.120 | 0.58 | 45 | 2.00 | MarAd L | 0.236 | 0.9933 | 0.9955 |
| y_{BBt} | | | | | | 0.237 | 0.9932 | 0.9955 |
| y_{EBt} | | | | | | 0.443 | 0.9758 | 0.9839 |
| y_{Bt} | 0.085 | 0.79 | 45 | 9.63 | S-175 | 0.029 | 0.9056 | 0.9370 |
| y_{BBt} | | | | | | 0.043 | 0.7855 | 0.8570 |
| y_{EBt} | | | | | | 0.028 | 0.9136 | 0.9424 |
| y_{Bt} | 0.150 | 0.67 | 45 | 3.35 | S-175 | 0.168 | 0.9993 | 0.9996 |
| y_{BBt} | | | | | | 0.773 | 0.9858 | 0.9905 |
| y_{EBt} | | | | | | 0.217 | 0.9989 | 0.9993 |
| y_{Bt} | 0.085 | 0.58 | 45 | 2.00 | S-175 | 0.109 | 0.9667 | 0.9750 |
| y_{BBt} | | | | | | 0.021 | 0.9988 | 0.9991 |
| y_{EBt} | | | | | | 0.116 | 0.9619 | 0.9714 |

Table 6.5 Statistical fit for ship to bank distance parameters for a sample of flooded bank cases for sway force

| Param. | F_{nL} | $1-(h_{2p}/h_1)$ | Bank angle (deg.) | $d/(h_1-d)$ | Model | Stand. error | Adjusted R^2 | R^2 |
|-----------|----------|------------------|-------------------|-------------|---------|--------------|----------------|--------|
| y_{Bt} | 0.061 | 0.64 | 90 | 9.63 | MarAd L | 0.132 | 0.9944 | 0.9953 |
| y_{BBt} | | | | | | 0.500 | 0.9190 | 0.9324 |
| y_{EBt} | | | | | | 0.060 | 0.9988 | 0.9990 |
| y_{Bt} | 0.066 | 0.79 | 45 | 9.63 | MarAd L | 0.219 | 0.9947 | 0.9960 |
| y_{BBt} | | | | | | 0.885 | 0.9133 | 0.9349 |
| y_{EBt} | | | | | | 0.188 | 0.9961 | 0.9971 |
| y_{Bt} | 0.100 | 0.67 | 65 | 3.35 | MarAd L | 0.035 | 0.9989 | 0.9992 |
| y_{BBt} | | | | | | 0.217 | 0.9577 | 0.9682 |
| y_{EBt} | | | | | | 0.054 | 0.9974 | 0.9981 |
| y_{Bt} | 0.120 | 0.58 | 45 | 2.00 | MarAd L | 0.048 | 0.9953 | 0.9969 |
| y_{BBt} | | | | | | 0.162 | 0.9464 | 0.9643 |
| y_{EBt} | | | | | | 0.004 | 0.9999 | 0.9999 |
| y_{Bt} | 0.085 | 0.79 | 45 | 9.63 | S-175 | 0.141 | 0.9925 | 0.9950 |
| y_{BBt} | | | | | | 0.406 | 0.9380 | 0.9586 |
| y_{EBt} | | | | | | 0.118 | 0.9947 | 0.9965 |
| y_{Bt} | 0.150 | 0.67 | 45 | 3.35 | S-175 | 0.187 | 0.9945 | 0.9963 |
| y_{BBt} | | | | | | 0.516 | 0.9582 | 0.9721 |
| y_{EBt} | | | | | | 0.158 | 0.9961 | 0.9974 |
| y_{Bt} | 0.085 | 0.58 | 45 | 2.00 | S-175 | 0.045 | 0.9404 | 0.9552 |
| y_{BBt} | | | | | | 0.071 | 0.8557 | 0.8918 |
| y_{EBt} | | | | | | 0.043 | 0.9455 | 0.9591 |

Table 6.6 Statistical fit for ship to bank distance parameters for a sample of flooded bank cases for yaw moment

Bank slope parameter

Given the limited data presently available concerning the effect of bank slope, and in order to simplify the final bank effect empirical equations, it is proposed that an equivalent bank distance parameter, similar to that used by Ch'ng (1991), be used to represent the effect of bank slope in the regression equations. In order to introduce such a parameter, the magnitude of sway force and yaw moment must be smaller at low bank slopes. From Chapter 5 it was shown that this condition was satisfied for length Froude numbers up to 0.1 for draught to under keel clearance ratios between 4.17 and 1.24. Ch'ng (1991) found that this trend occurred up to a length Froude number of approximately 0.07 when the draught to under keel clearance ratio was reduced to 5.13. Hence, the effect of bank slope is represented by an equivalent bank distance parameter for these cases.

Ch'ng (1991) investigated four possible equivalent bank distances for surface piercing banks, as presented in Figure 6.3. On plotting non-dimensional sway force and yaw moment as a function of y_{Bi} (using the respective lateral distances from the ship centreline to the port bank) it was found that the most suitable parameter for surface piercing banks was y_{B3} , where the lateral ship to bank distance was measured from the ship's centerline to the bank at half the vessel draught. Ch'ng also discovered that y_{B1} provided a reasonable representation of the effect of bank slope, where the distance from the ship centreline to the bank at half water depth was used (half bank height for surface piercing banks). The representation of bank slope at low water depth to

draught ratios using y_{B1} closely resembled that when using y_{B3} , since the value of y_{B1} approaches the value of y_{B3} as the water depth to draught ratio approaches one.

Four possible ship to bank distance parameters are proposed in the present study that are applicable to both surface piercing and flooded banks, as shown in Figure 6.4. Since Ch'ng found that measuring the lateral distance from the ship centerline to the top of the bank was unsuitable for surface piercing banks, it has not been considered in the present study. Non-dimensional sway force and yaw moment have been plotted as a function of ship to bank distance parameter using each of the proposed ship to port bank distances. Plots for two flooded bank example cases, each with a range of bank slopes, are given in Figures 6.5 – 6.12. Predicted uncertainty limits are presented on these figures. Full details concerning the uncertainty analysis are given in Appendix D. The results will collapse onto two single lines (one for each case) if the bank distance parameter successfully explains the effect of bank slope. It is difficult to identify a parameter that is best for all cases. However, the effect of bank slope was reasonably well approximated (considering experimental scatter) when the lateral distance was measured from the ship centerline to half the height of the bank (y_{B6}).

Ch'ng (1991) showed that it is reasonable to use y_{B6} as an equivalent bank distance to approximate the effect of bank slope for surface piercing cases (y_{B6} is equivalent to y_{B1} for surface piercing cases). From the present study it was found, generally, that y_{B6} is also suitable to approximate the effect of bank slope for flooded bank cases within the specified length Froude number ranges.

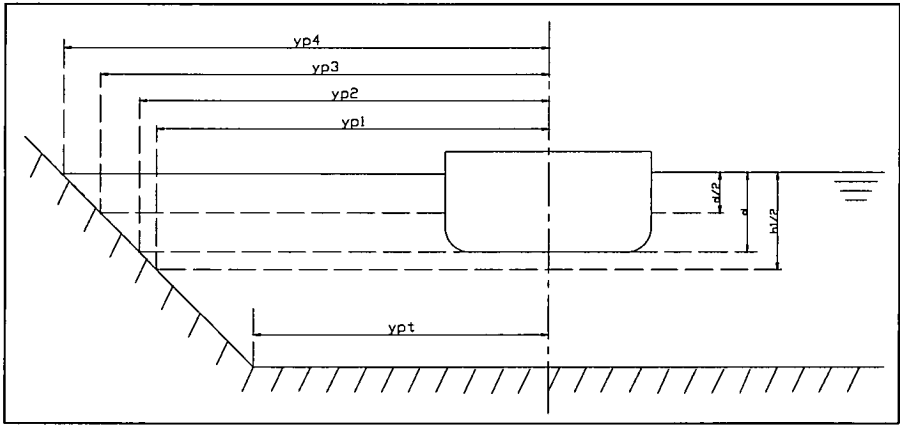


Figure 6.3 Lateral ship to bank distances for surface piercing banks, Ch'ng (1991)

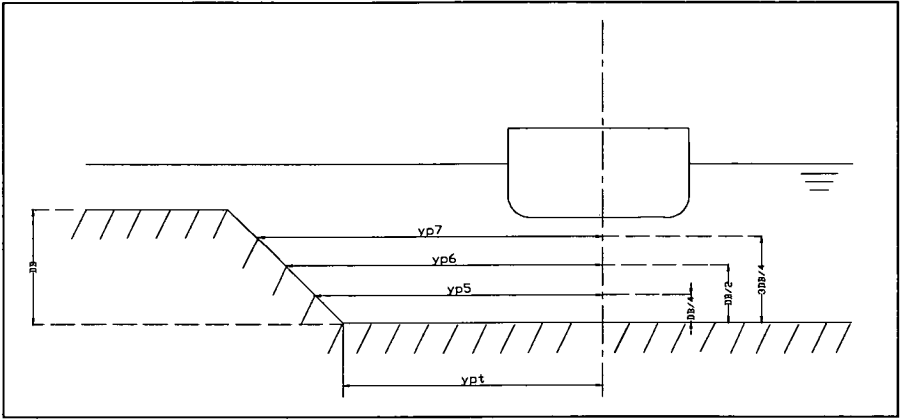


Figure 6.4 Lateral ship to bank distances for flooded and surface piercing banks

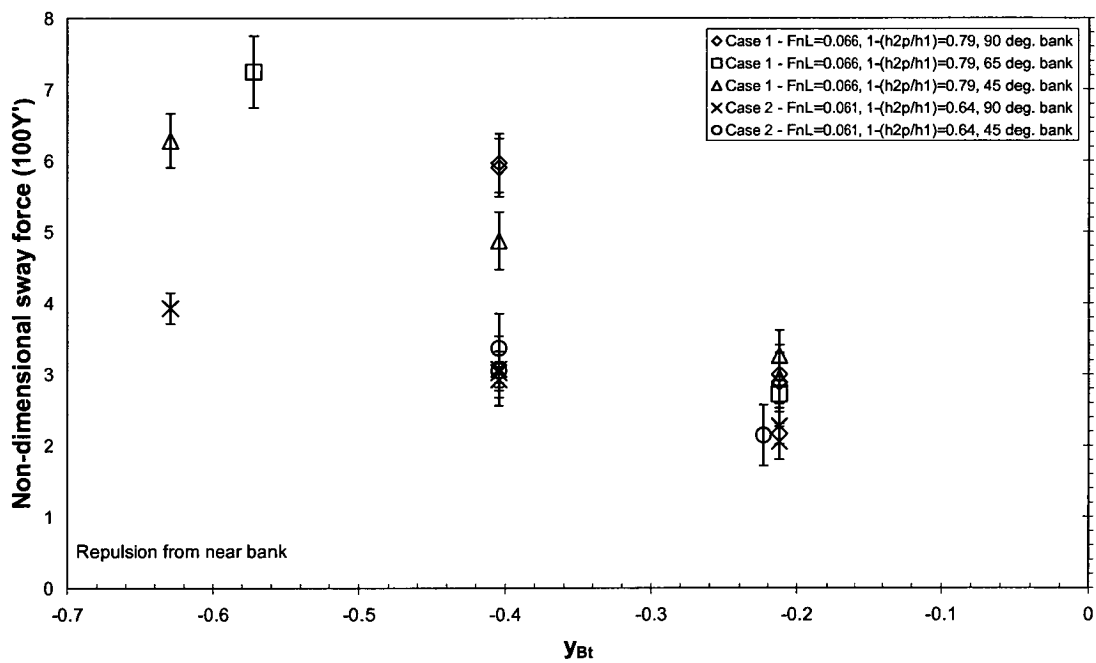


Figure 6.5 Non-dimensional sway force as a function of y_{Bt} , varying α_p , $d/(h_1-d)=9.63$, MarAd L series

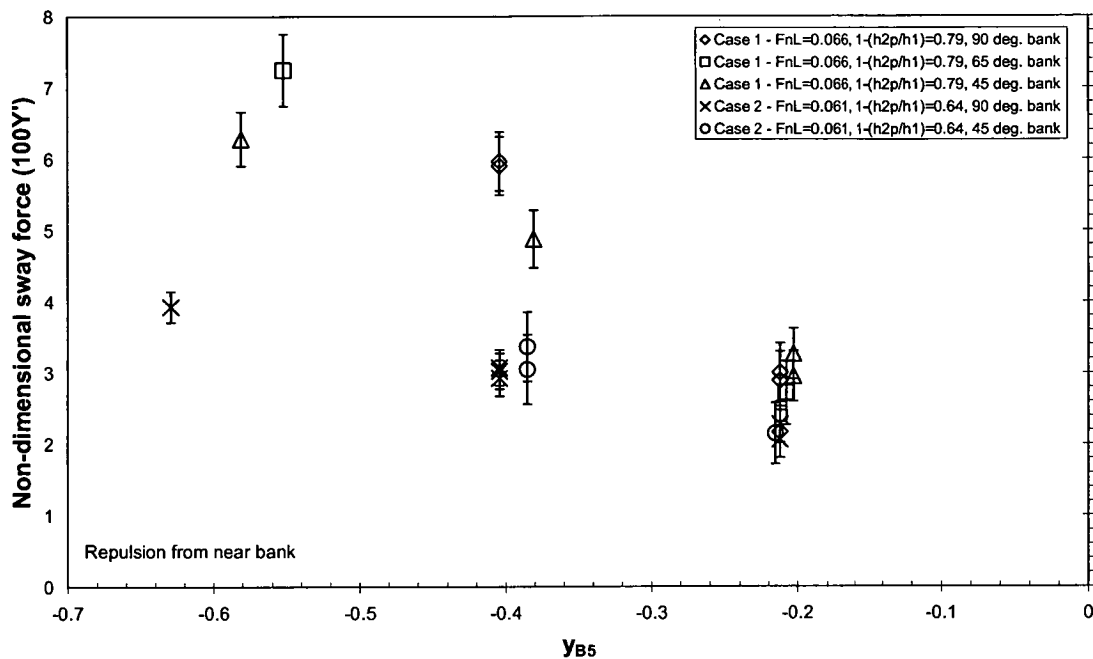


Figure 6.6 Non-dimensional sway force as a function of y_{B5} , varying α_p , $d/(h_1-d)=9.63$, MarAd L series

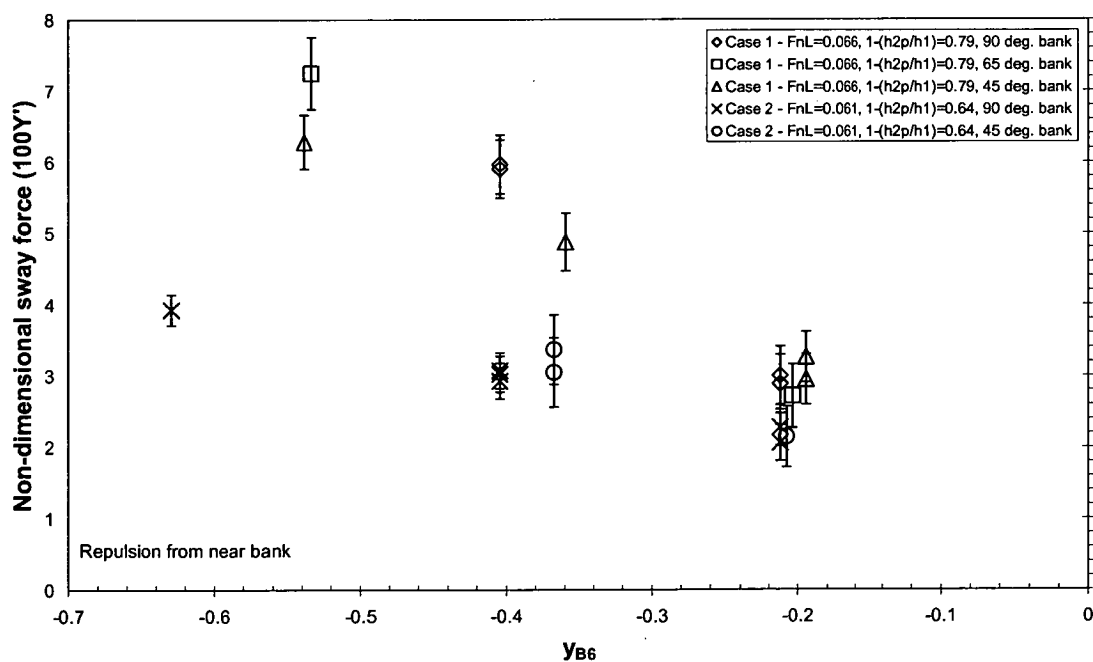


Figure 6.7 Non-dimensional sway force as a function of y_{B6} , varying α_p , $d/(h_1-d)=9.63$, MarAd L series

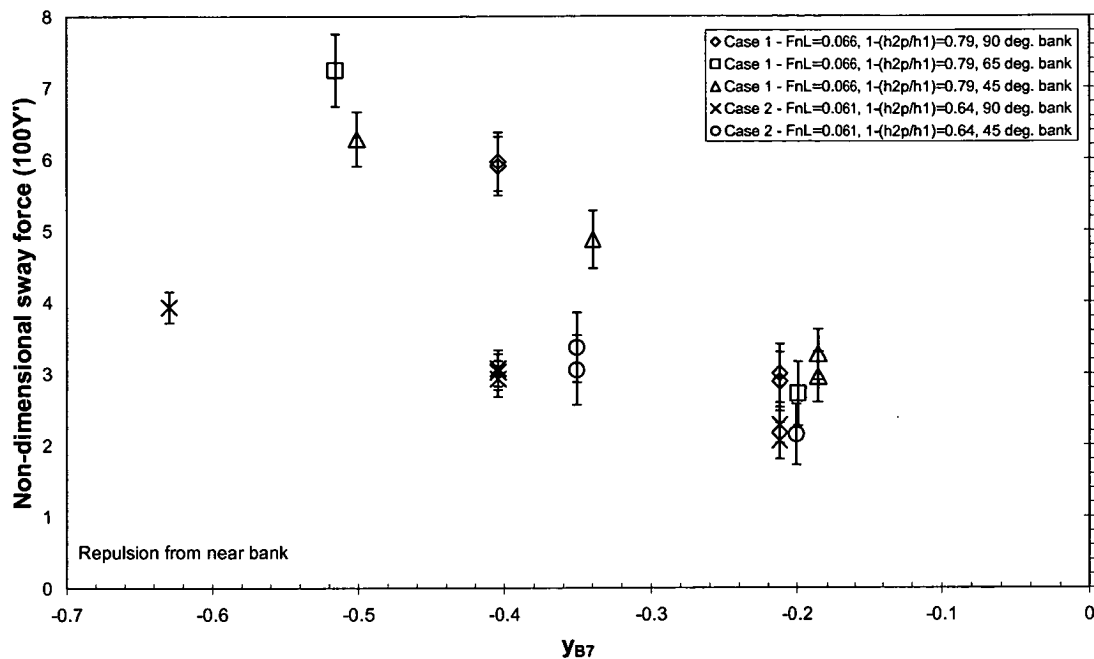


Figure 6.8 Non-dimensional sway force as a function of y_{B7} , varying α_p , $d/(h_1-d)=9.63$, MarAd L series

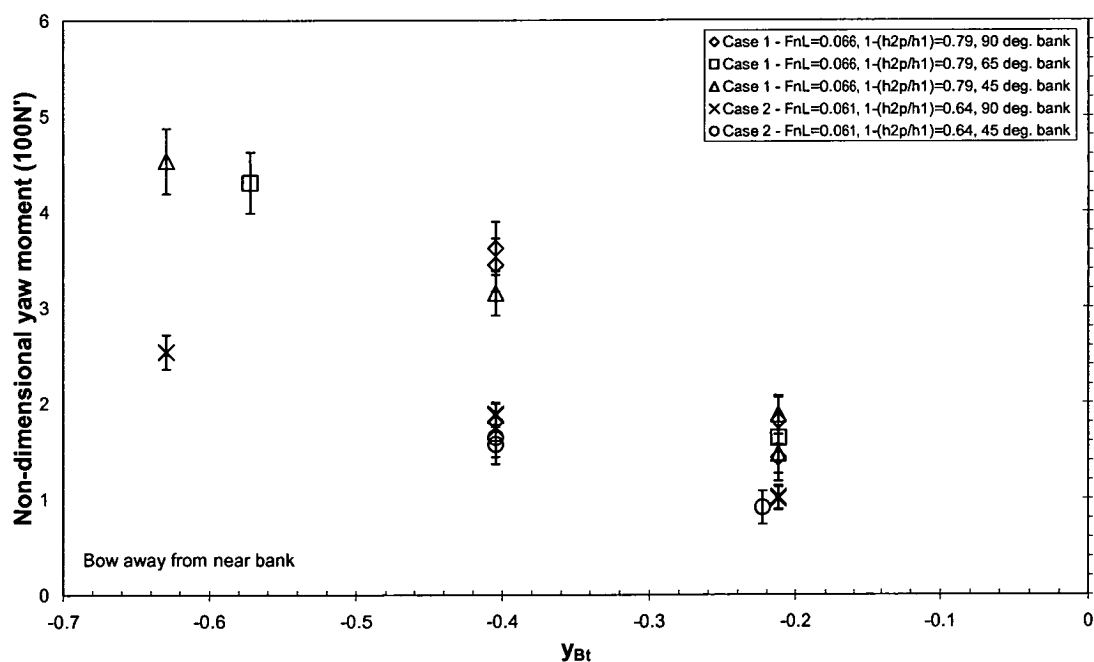


Figure 6.9 Non-dimensional yaw moment as a function of y_{Bt} , varying α_p , $d/(h_1-d)=9.63$, MarAd L series

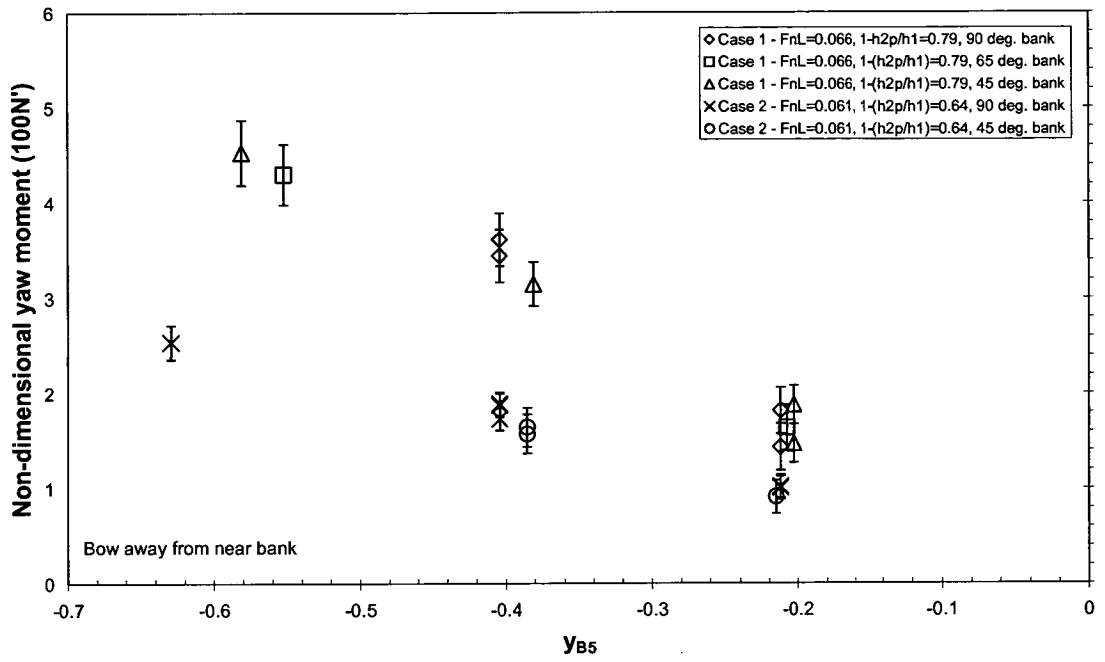


Figure 6.10 Non-dimensional yaw moment as a function of y_{B5} , varying α_p , $d/(h_1-d)=9.63$, MarAd L series

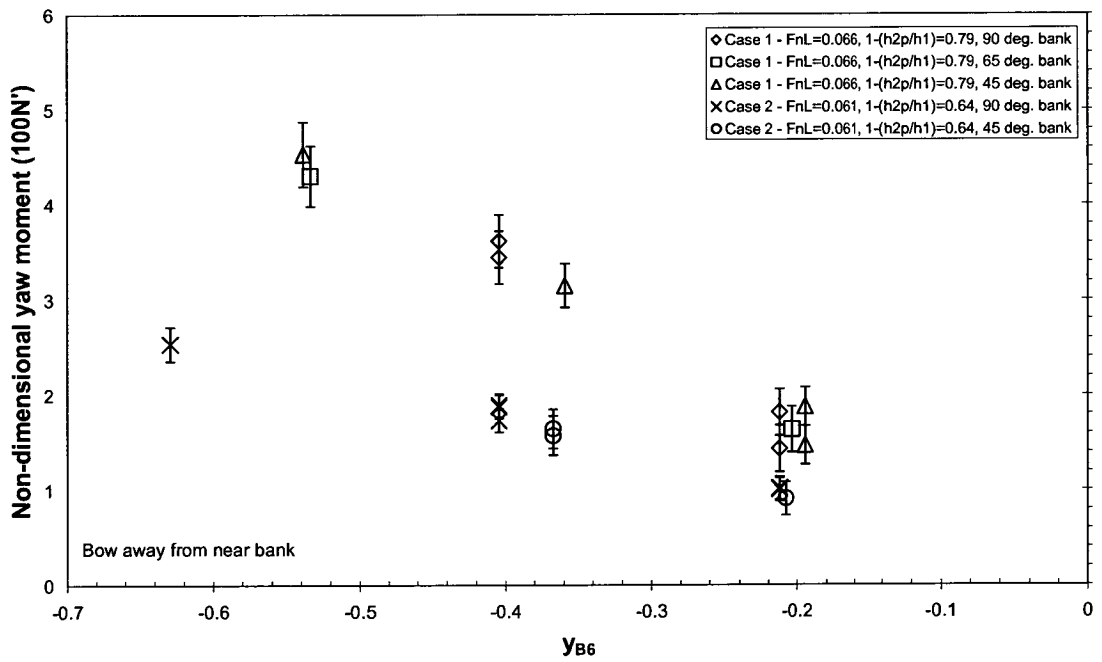


Figure 6.11 Non-dimensional yaw moment as a function of y_{B6} , varying α_p , $d/(h_1-d)=9.63$, MarAd L series

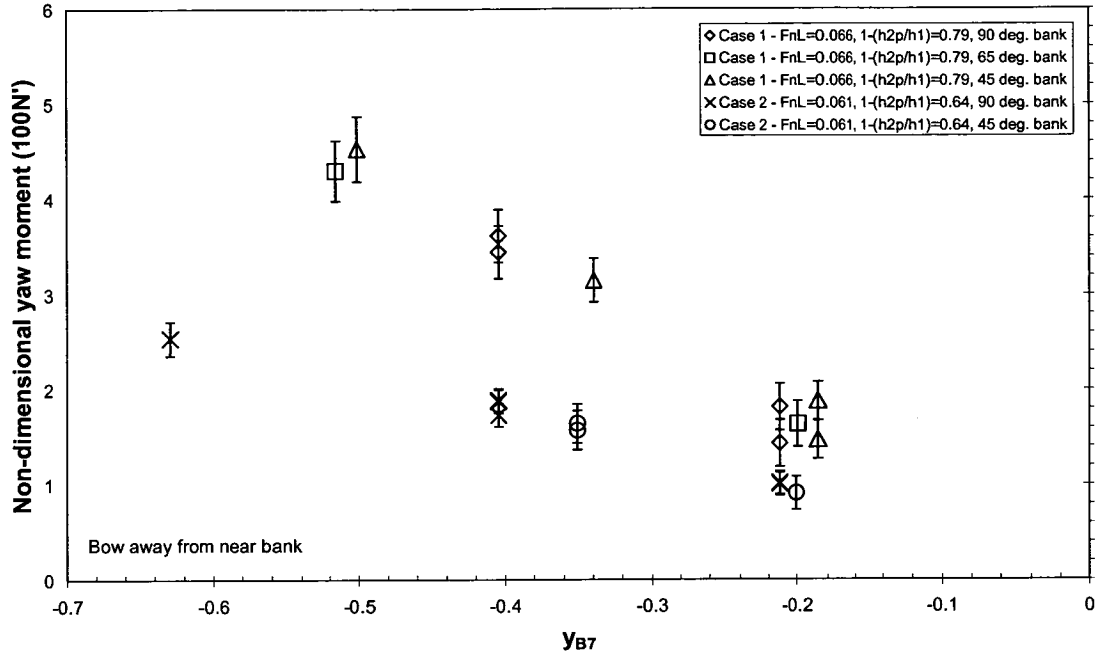


Figure 6.12 Non-dimensional yaw moment as a function of y_{B7} , varying α_p , $d/(h_1-d)=9.63$, MarAd L series

Bank parameter

To simplify the regression equations it is suggested that bank flooding terms are incorporated into the ship to bank distance parameter (y_{B6}) to linearise the effect of ship to bank distance and bank flooding. Such a parameter will enable the general surface piercing and flooded bank problem to be treated by the superposition of force interactions originating from port and starboard banks at varying separation distances and degrees of bank flooding.

In Chapter 5 it was shown that, generally, non-dimensional sway force and yaw moment decreased in a non-linear manner as the depth of water over a bank was increased. Also, the rate of change of non-dimensional sway force and yaw moment was not constant with bank flooding, which can be explained using an exponential expression (Norrbin 1974). Hence, Equations 6.13 and 6.14 have been fitted to the experimental data using non-linear regression techniques and were found to adequately explain the relationships between non-dimensional sway force, yaw moment and bank flooding for most cases.

$$100Y' = a_1 e^{(c_y (h_{2p}/(h_1 - h_{2p})))} \quad (6.13)$$

$$100N' = a_2 e^{(c_n (h_{2p}/(h_1 - h_{2p})))} \quad (6.14)$$

Where a_1 , a_2 , c_y and c_n are constants determined from regression analysis for each case.

To successfully linearise the relationship between sway force, yaw moment and bank flooding it is necessary to determine the influence of other independent variables on c_y and c_n , such as bank

slope, depth Froude number, draught to under keel clearance ratio, ship to bank distance parameter and hull form.

For the majority of cases tested the values of c_y and c_n were similar for the MarAd L series hull and S-175 containership. However, due to the limited number of hull forms tested in the present study it is not possible to identify trends concerning the effect of hull form on c_y and c_n .

In Figures 6.13 and 6.14 c_y and c_n are presented as a function of depth Froude number for a selection of example cases with various bank slopes, lateral ship to bank distances and draught to under keel clearance ratios. It can be seen that, generally, there is no clear trend in the variation of c_y and c_n with depth Froude number and bank slope.

Norrbin (1974) and Li (2000) found that the effect of bank flooding was dramatic at small ship to bank distances at high draught to under keel clearance ratios. In the present study there was a general trend for c_y to be more negative at smaller lateral ship to bank distances at a draught to under keel clearance ratio of 9.63, as illustrated in Figure 6.13. However, at the same draught to under keel clearance ratio the influence of lateral ship to bank distance on c_n was less pronounced, as illustrated in Figure 6.14. At draught to under keel clearance ratios less than 9.63, the influence of lateral ship to bank distance on c_y and c_n was found to be small and a general trend could not be identified, as illustrated in Figures 6.13 and 6.14.

It was found that draught to under keel clearance ratio had the greatest influence on c_y and c_n . In general, it can be seen that the values of c_y and c_n for different depth Froude numbers, bank slopes and lateral ship to bank distances deviated about a distinct mean for each draught to under keel clearance ratio. Therefore it is proposed that average values of c_y and c_n be used with respect to depth Froude number, bank angle, lateral ship to bank distance and hull form at each draught to under keel clearance ratio. In Figures 6.15 and 6.16 these average values are presented and it can be seen that the magnitudes of c_y and c_n are generally less negative for small draught to under keel clearance ratios. To obtain the relationship between both c_y and c_n and draught to under keel clearance ratio, regression equations have been fitted to the experimental data. Logarithm terms were selected to represent the variation in rate of change of c_y and c_n , which are given in Equations 6.15 and 6.16, respectively. The coefficient of determination was 0.8937 for Equation 6.15 and 0.8473 for Equation 6.16, which was deemed to be acceptable given that the aim is to predict a general trend only.

$$c_y = -0.4 \cdot \ln(d/(h_1 - d)) - 0.5 \quad (6.15)$$

$$c_n = -0.5 \cdot \ln(d/(h_1 - d)) - 0.07 \quad (6.16)$$

To assess if Equations 6.15 and 6.16 will provide an adequate representation of c_y and c_n for all cases, predictions using Equations 6.17 and 6.18 were compared to experimental data, where the constants a_1 and a_2 were determined through non-linear regression techniques for each case using Equations 6.13 and 6.14.

$$100Y' = a_1 e^{((-0.4 \ln(d/(h_1 - d)) - 0.5)(h_{2p}/(h_1 - h_{2p})))} \quad (6.17)$$

$$100N' = a_2 e^{((-0.5 \ln(d/(h_1 - d)) - 0.07)(h_{2p}/(h_1 - h_{2p})))} \quad (6.18)$$

Comparison between these predictions and experiments is shown for a selection of example cases with various depth Froude numbers, bank slopes, lateral ship to bank distances and draught to under keel clearance ratios in Figures 6.17 and 6.18. As can be seen the fit with the experimental data was reasonable for the purpose of simulation. Therefore it is proposed that the bank flooding terms identified above be incorporated into the bank distance parameter, y_{B6} , to provide an approximately linear relationship between non-dimensional sway force, yaw moment and bank flooding. The bank parameters for sway force and yaw moment are presented in Equations 6.19 and 6.20.

$$BP_{Y6} = \left[\left(\frac{1}{y_{p6}} \right) e^{c_y \left(h_{2p} / (h_1 - h_{2p}) \right)} + \left(\frac{1}{y_{s6}} \right) e^{c_y \left(h_{2s} / (h_1 - h_{2s}) \right)} \right] \frac{B}{2} \quad (6.19)$$

$$BP_{N6} = \left[\left(\frac{1}{y_{p6}} \right) e^{c_n \left(h_{2p} / (h_1 - h_{2p}) \right)} + \left(\frac{1}{y_{s6}} \right) e^{c_n \left(h_{2s} / (h_1 - h_{2s}) \right)} \right] \frac{B}{2} \quad (6.20)$$

Where c_y and c_n are given in Equations 6.15 and 6.16.

The additional bank flooding terms have been selected such that they take on a value of unity for surface piercing banks. Hence, BP_{Y6} and BP_{N6} reduce to y_{B6} for the case of a surface piercing bank.

Non-dimensional sway force and yaw moment are plotted as a function of bank parameter in Figures 6.19 and 6.20 for various length Froude numbers, draught to under keel clearance ratios and two bank angles. Here the lateral ship to bank distance is held constant and the depth of water over the bank is varied. It can be seen that, for the purpose of simulation, the relationships between non-dimensional sway force, yaw moment and the respective bank parameters are sufficiently linear to allow superposition of the effects of port and starboard flooded banks.

These bank parameters are superior to those presented by Duffy (2002) as they account for increasing and decreasing rates of change of sway force and yaw moment with bank flooding and the variation of this rate of change with draught to under keel clearance is represented.

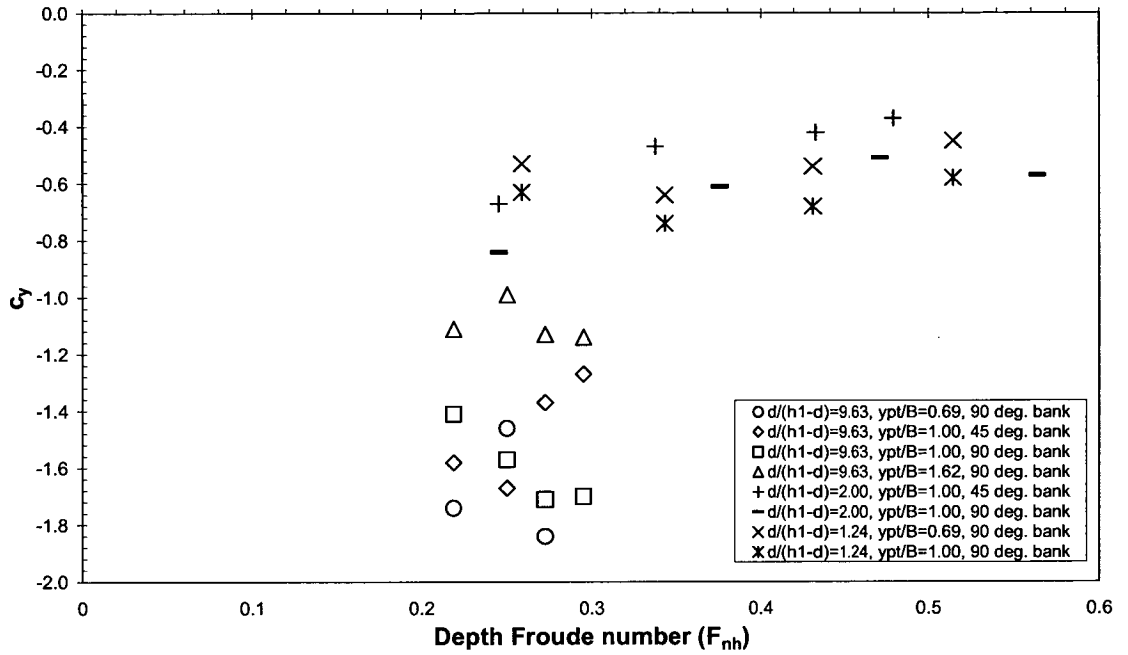


Figure 6.13 c_y as a function of F_{nh} , MarAd L series model

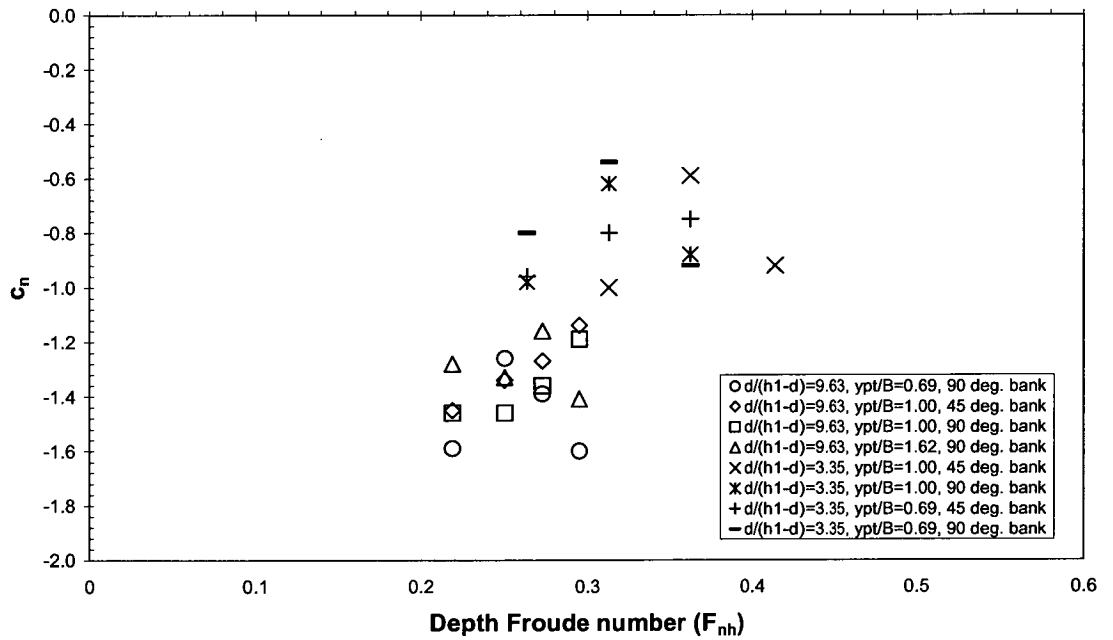


Figure 6.14 c_n as a function of F_{nh} , MarAd L series model

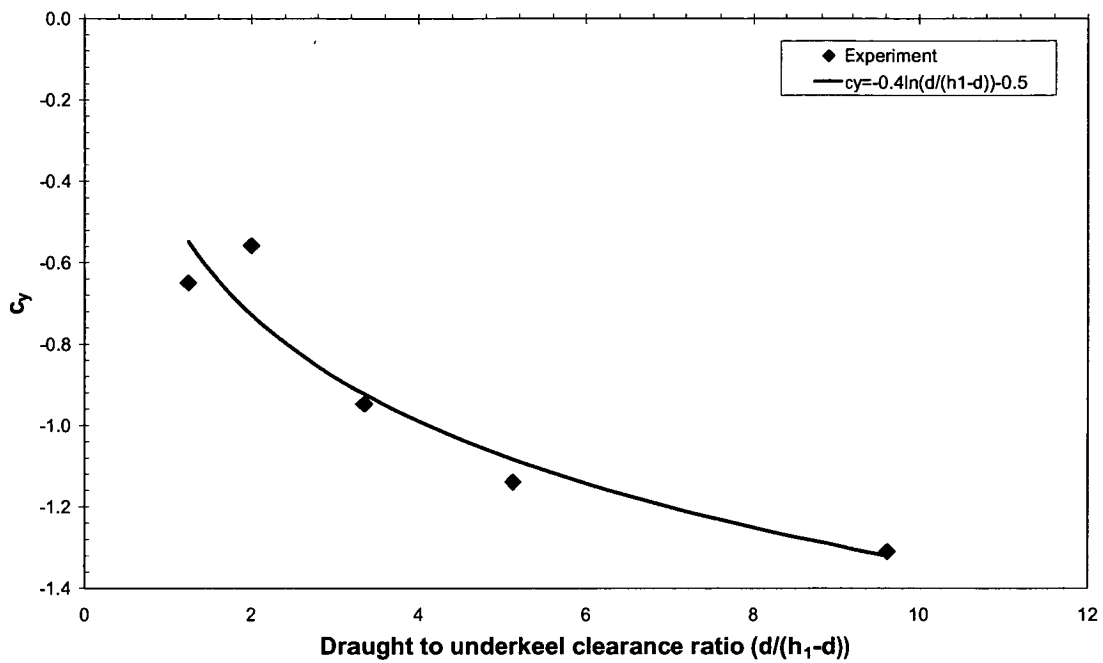


Figure 6.15 c_y as a function of $d/(h_1-d)$

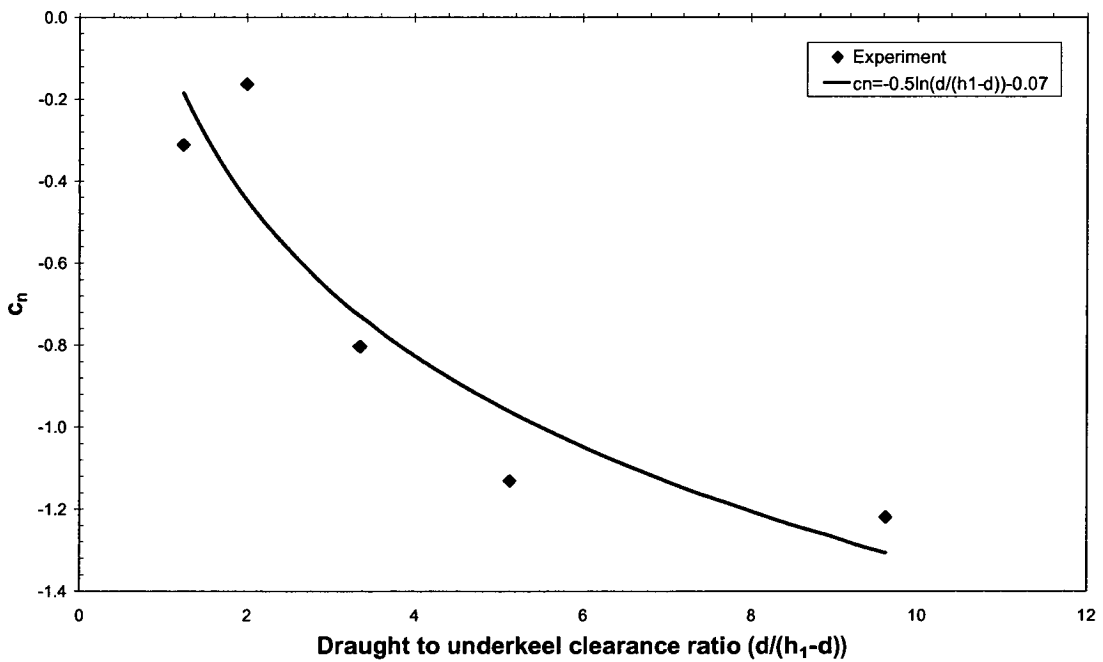


Figure 6.16 c_n as a function of $d/(h_1-d)$

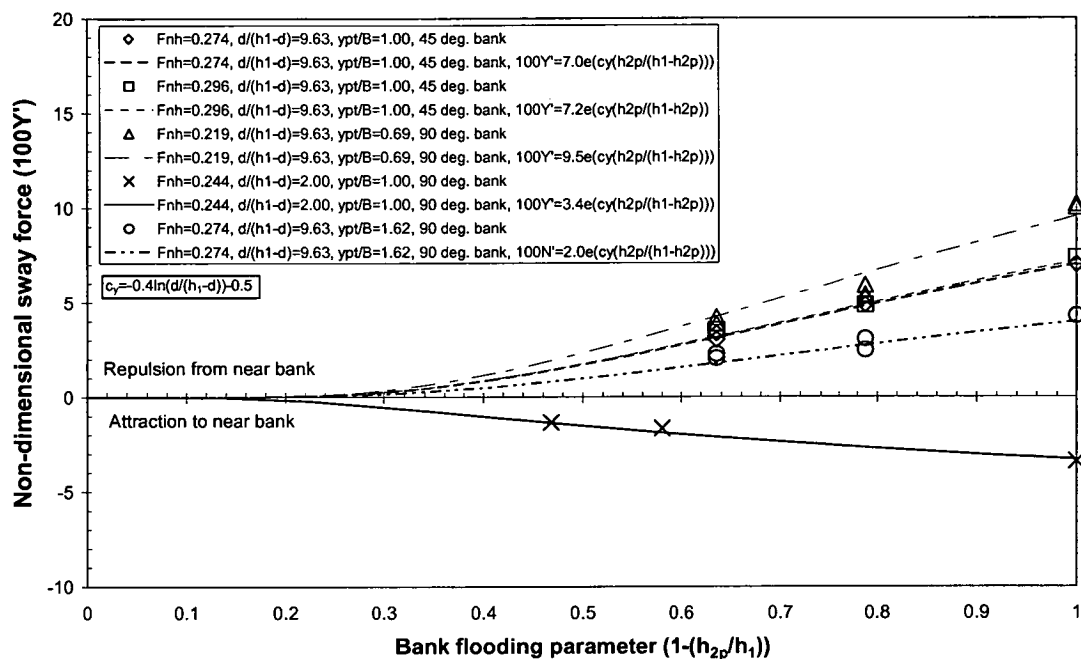


Figure 6.17 Non-dimensional sway force as a function of $1-(h_{2p}/h_1)$, MarAd L series model

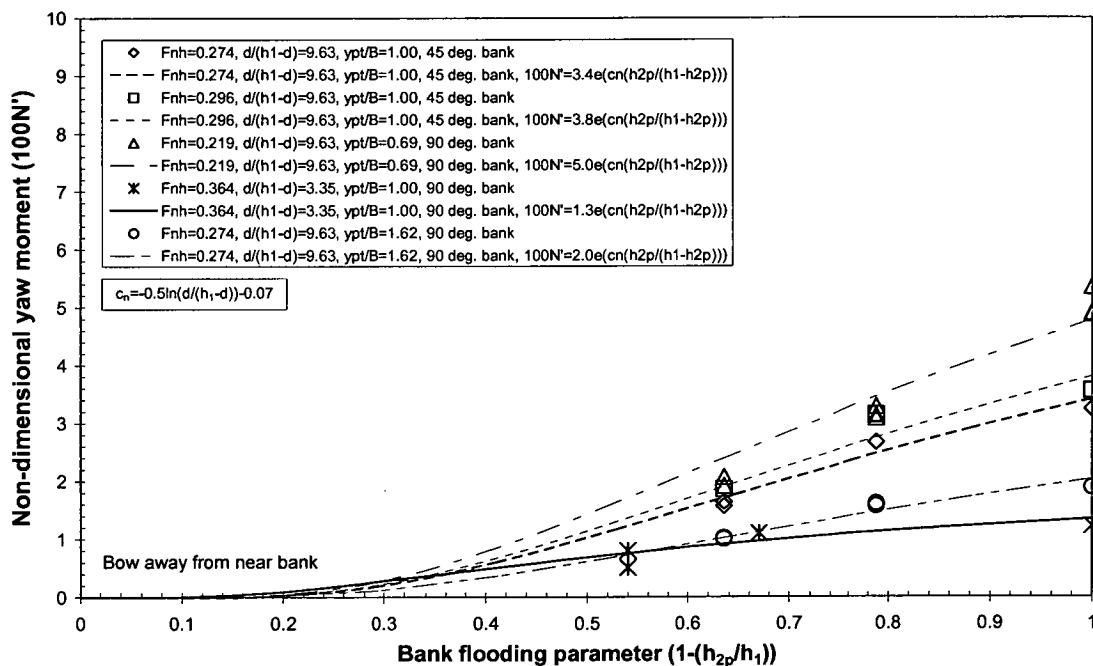


Figure 6.18 Non-dimensional yaw moment as a function of $1-(h_{2p}/h_1)$, MarAd L series model

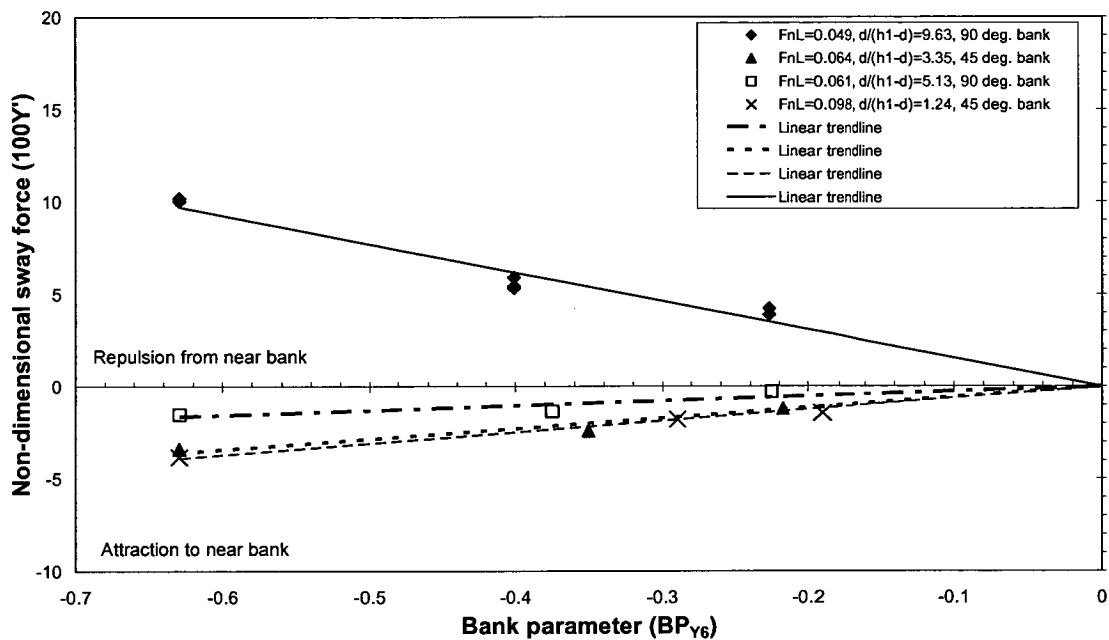


Figure 6.19 Non-dimensional sway force as a function of BP_{Y6} for varying bank submergence, $y_{pt}/B=0.69$, MarAd L series

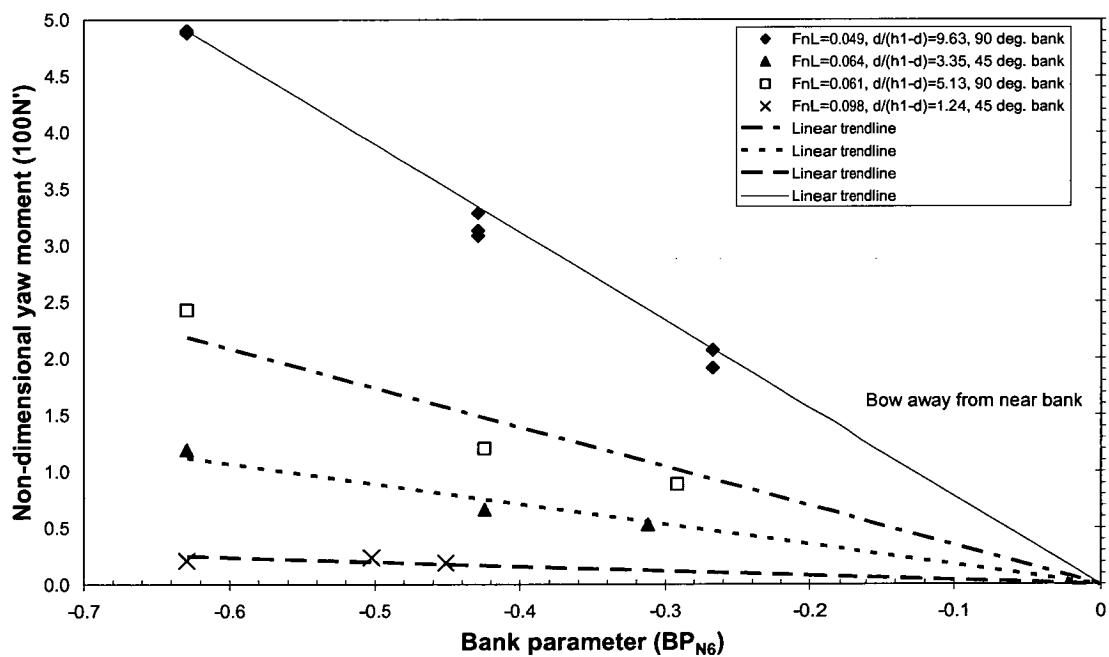


Figure 6.20 Non-dimensional yaw moment as a function of BP_{N6} for varying bank submergence, $y_{pt}/B=0.69$, MarAd L series

Hull form parameter

To quantify the effect of hull form on bank effect three models were tested in the present study; a MarAd L series hull, a MarAd F series hull and an S-175 containership hull. The MarAd L series model was tested at three different level trim draughts to investigate the effect of vessel load condition on bank effect. This allowed investigation into the effect of draught related hull form parameters on bank effect without building a new model with a different design draught. The three load conditions tested corresponded to B/d values of 4.42, 4.00 and 3.62. McDonnell (2003) measured bank induced sway force and yaw moment using the MarAd L series model at B/d values of 3.47 and 2.83. These results were incorporated into the dataset obtained in the present study to increase the size of the data matrix used to derive the empirical equations.

Detailed ship parameters are rarely made available for input to ship-handling simulators. Hence the proposed hull form parameters below are dependent upon principal dimensions of a ship hull that are easily accessible, such as vessel length, vessel beam, vessel draught and block coefficient.

- C_B
- d/B
- d/L_{pp}
- L_{pp}/B
- $d/C_B L_{pp}$
- $B/C_B L_{pp}$
- $d/C_B B$
- $C_B B d / L_{pp}^2$

The inverse of the above parameters were also considered in the analysis, but only results for the most statistically significant parameters are presented.

Preliminary regression analyses were performed to identify the hull form parameter with the best statistical fit for both surface piercing and flooded banks using Equations 6.21 and 6.22. This analysis was restricted to cases where only the hull form parameters are varied; the values of all other independent variables were held constant.

$$100Y' = a_2 x^2 + a_1 x + a_0 \quad (6.21)$$

$$100N' = b_2 x^2 + b_1 x + b_0 \quad (6.22)$$

Where a_0 , a_1 , a_2 , b_0 , b_1 and b_2 are constants and x represents the hull form parameter.

Non-dimensional sway force and yaw moment were found to vary in a non-linear manner with the proposed hull form parameters, as illustrated for one of the parameters in Figure 6.21. A maximum power of 2 was selected to account for the non-linearity between non-dimensional sway force, yaw moment and hull form parameters. A higher maximum power was not justified, given the limited data available for hull form parameter.

Results of the regression analyses for a selection of surface piercing and flooded bank cases are given in Tables 6.7 – 6.10. Results for L_{pp}/B are not presented since these terms do not account for the vessel loading condition, which was shown to influence bank effect in Chapter 5. From

these results C_B is the chosen hull form parameter as it generally provides the best statistical fit for surface piercing and flooded bank cases.

| Parameter | Standard error | Adjusted R^2 | R^2 |
|---------------|----------------|----------------|--------|
| C_B | 2.562 | 0.9287 | 0.9572 |
| d/B | 6.232 | 0.5780 | 0.7468 |
| d/L_{pp} | 5.002 | 0.7281 | 0.8369 |
| $d/C_B L$ | 5.675 | 0.6501 | 0.7900 |
| $B/C_B L$ | 3.322 | 0.8801 | 0.9280 |
| $d/C_B B$ | 3.971 | 0.8286 | 0.8972 |
| $C_B B d/L^2$ | 3.521 | 0.8653 | 0.9192 |

Table 6.7 Analysis of hull form parameters for non-dimensional sway force, $F_{nh}=0.176, 0.194, 0.219$, $d/(h_1-d)=9.63$, $y_{pt}/W=0.097$, $1-(h_{2p}/h_1)=1.00$, $\alpha_p=90^\circ$, MarAd L series, MarAd F series, S-175 containership

| Parameter | Standard error | Adjusted R^2 | R^2 |
|---------------|----------------|----------------|--------|
| C_B | 0.962 | 0.9535 | 0.9721 |
| d/B | 1.989 | 0.8013 | 0.8808 |
| d/L_{pp} | 1.455 | 0.8936 | 0.9362 |
| $d/C_B L$ | 1.972 | 0.8154 | 0.8892 |
| $B/C_B L$ | 1.189 | 0.9290 | 0.9574 |
| $d/C_B B$ | 1.366 | 0.9063 | 0.9438 |
| $C_B B d/L^2$ | 0.913 | 0.9581 | 0.9749 |

Table 6.8 Analysis of hull form parameters for non-dimensional yaw moment, $F_{nh}=0.176, 0.194, 0.219$, $d/(h_1-d)=9.63$, $y_{pt}/W=0.097$, $1-(h_{2p}/h_1)=1.00$, $\alpha_p=90^\circ$, MarAd L series, MarAd F series, S-175 containership

| Parameter | Standard error | Adjusted R^2 | R^2 |
|---------------|----------------|----------------|--------|
| C_B | 0.004 | 0.9999 | 0.9999 |
| d/B | 1.136 | 0.6689 | 0.8897 |
| d/L_{pp} | 1.182 | 0.6419 | 0.8806 |
| $d/C_B L$ | 0.546 | 0.9235 | 0.9745 |
| $B/C_B L$ | 0.126 | 0.9959 | 0.9986 |
| $d/C_B B$ | 0.276 | 0.9805 | 0.9935 |
| $C_B B d/L^2$ | 0.430 | 0.9526 | 0.9842 |

Table 6.9 Analysis of hull form parameters for non-dimensional sway force, $F_{nh}=0.269, 0.296$, $d/(h_1-d)=9.63$, $1-(h_{2p}/h_1)=0.65$, $y_{pt}/W=0.097$, $\alpha_p=90^\circ$, MarAd L series, MarAd F series, S-175 containership

| Parameter | Standard error | Adjusted R^2 | R^2 |
|---------------|----------------|----------------|--------|
| C_B | 0.067 | 0.9983 | 0.9994 |
| d/B | 0.547 | 0.8888 | 0.9629 |
| d/L_{pp} | 0.491 | 0.9104 | 0.9402 |
| $d/C_B L$ | 0.203 | 0.9847 | 0.9949 |
| $B/C_B L$ | 0.145 | 0.9922 | 0.9974 |
| $d/C_B B$ | 0.040 | 0.9987 | 0.9992 |
| $C_B B d/L^2$ | 0.173 | 0.9889 | 0.9960 |

Table 6.10 Analysis of hull form parameters for non-dimensional yaw moment, $F_{nh}=0.269, 0.296, 0.219$, $d/(h_1-d)=9.63$, $y_{pt}/W=0.097$, $1-(h_{2p}/h_1)=0.65$, $\alpha_p=90^\circ$, MarAd L series, MarAd F series, S-175 containership

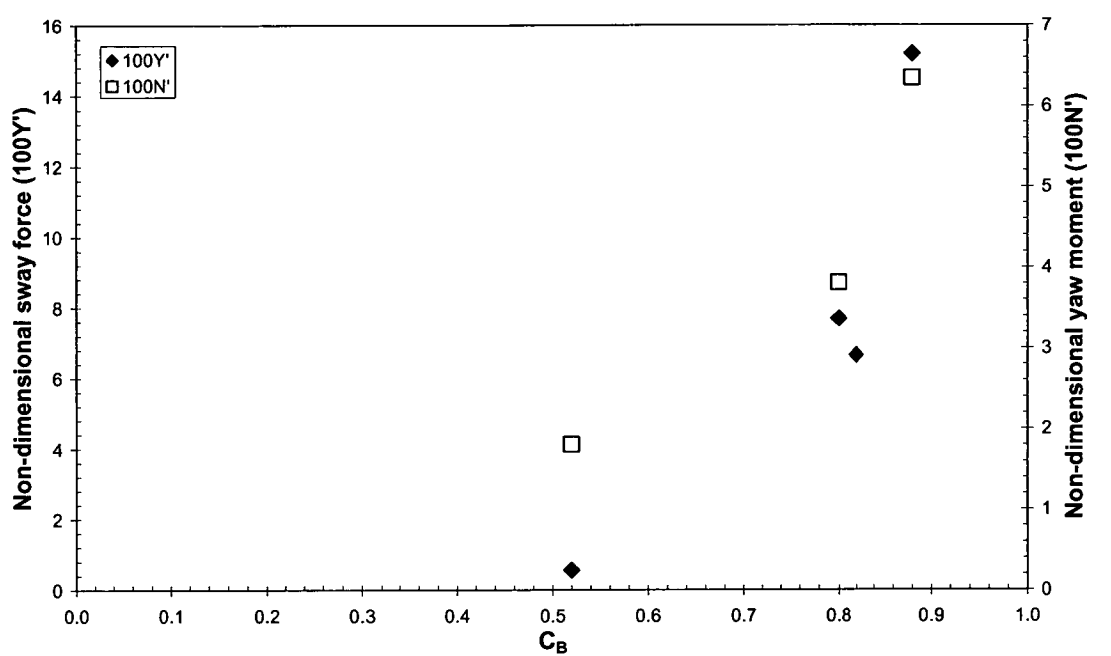


Figure 6.21 Non-linear relationship between non-dimensional sway force and yaw moment with C_B , $d/(h_1-d)=9.63$, $y_{pt}/W=0.097$, $1-(h_{2p}/h_1)=1.00$, $\alpha_p=90^\circ$, MarAd L series, MarAd F series, S-175 containership

6.2.2 Regression formulae for bank induced sway force and yaw moment

Having selected suitable parameters multiple linear regression analyses were conducted on the experimental data to develop equations to predict steady-state bank induced sway force and yaw moment.

The selected parameters are depth Froude number (F_{nh}), bank parameter for sway force (BP_{Y6}), bank parameter for yaw moment (BP_{N6}), draught to under keel clearance ratio ($d/(h_1-d)$) and the hull form parameter (C_B). The general form of the regression equations for sway force and yaw moment is shown in Equations 6.23 and 6.24 respectively. The independent variables were created as functions of the chosen parameters.

$$100Y' = \sum_{i=0}^3 \sum_{j=0}^5 \sum_{k=0}^2 F_{nh}^i \left(\frac{d}{(h_1 - d)} \right)^j \cdot C_B^k \cdot BP_{Y6} \quad (6.23)$$

$$100N' = \sum_{i=0}^3 \sum_{j=0}^3 \sum_{k=0}^2 F_{nh}^i \left(\frac{d}{(h_1 - d)} \right)^j \cdot C_B^k \cdot BP_{N6} \quad (6.24)$$

The maximum power of independent variables was dictated primarily by the non-linearity of sway force and yaw moment with depth Froude number and draught to under keel clearance ratio. The maximum power of draught to under keel clearance ratio for the sway force equation was increased to 5 to account for the high degree of non-linearity. As expected, the coefficient of determination was greater for a higher maximum power. However, the maximum power was only increased provided there was a statistically significant decrease in variance. Tests were conducted to ensure the accuracy of the predictions was sufficient for cases between experimental points within the range of experimental data. This was achieved by comparing the regression predictions with the experiment measurements used in the regression analysis and also with experiment measurements that were omitted from the regression analysis. This is illustrated for a sample case in Figure 6.22.

The final equation for sway force experienced by a ship travelling parallel to a lateral bank is given in Equation 6.25.

$$100Y' = A_Y \left(\begin{aligned} & - (6.6E - 2) (1/F_{nh}) (d/(h_1 - d))^3 (C_B) + 3.41 ((h_1 - d)/d) (1/C_B) \\ & + (5.1E - 3) (1/F_{nh}) (d/(h_1 - d))^4 (C_B) + 1.44 (1/F_{nh}) \\ & + 0.32 (F_{nh}) (d/(h_1 - d)) (1/C_B) + 5.58 (1/F_{nh}) ((h_1 - d)/d) \\ & - (1.0E - 2) (F_{nh}) (d/(h_1 - d))^3 + 0.11 (1/F_{nh}) (d/(h_1 - d))^2 (C_B) \end{aligned} \right) \quad (6.25)$$

Where $A_Y = (F_{nh}) (BP_{Y6}) (d/(h_1 - d)) (C_B)$

The coefficient of determination (R^2) for the sway force equation was 0.934. This indicates that 93.4% of the original variability has been explained with the variables specified in the model. The standard error of estimate was 0.81.

The final equation for yaw moment experienced by a ship travelling parallel to a lateral bank is given in Equation 6.26.

$$100N' = A_N \left(\begin{aligned} & - 6.14 + 14.26 ((h_1 - d)/d) (C_B) + (3.2E - 2) (F_{nh}) (d/(h_1 - d))^2 (1/C_B) \\ & - 30.67 (F_{nh})^2 ((h_1 - d)/d) (C_B) - (1.6E - 2) (1/F_{nh}) (d/(h_1 - d)) (1/C_B) \end{aligned} \right) \quad (6.26)$$

Where $A_N = (F_{nh}) (BP_{N6}) (d/(h_1 - d)) (C_B)$

The coefficient of determination (R^2) was 0.955, which indicates that 95.5% of the original variability has been explained with the variables specified in the model. The standard error of estimate is 0.40.

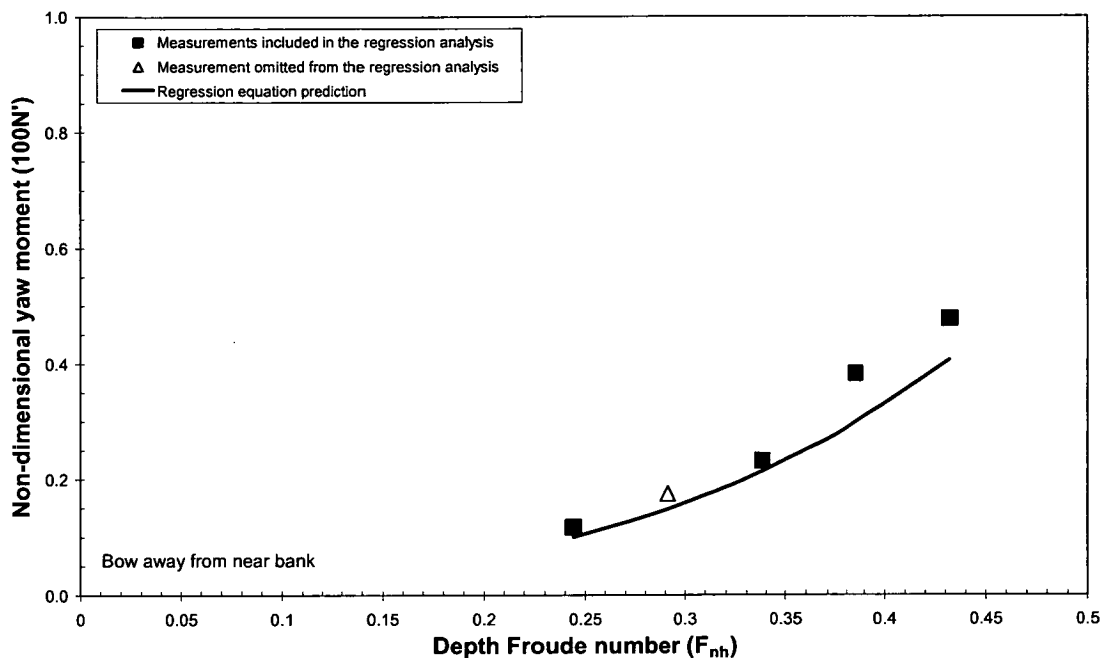


Figure 6.22 Sample of a test conducted to assess the accuracy of regression equations, $y_{pt}/B=1.00$, $y_{st}/B=5.15$, $d/(h_1-d)=2.00$, $1-(h_{2p}/h_1)=0.47$, $1-(h_{2s}/h_1)=1.00$, $\alpha_p=90^\circ$, $\alpha_s=90^\circ$, MarAd L

Limitations and assumptions

A common problem with such equations is that they may not represent the effect of independent variables properly when extrapolated beyond the range of experimental data, particularly when high maximum powers are used. Hence, it is important to highlight the limiting conditions, or boundaries of application, of the developed mathematical expressions for bank induced sway force and yaw moment. The boundaries of application for the above formulae, in terms of extreme values of the varied parameters, are as follows:

- $0.20 < F_{nh} < 0.30$ for $1.1 < h_1/d < 1.2$
- $0.20 < F_{nh} < 0.41$ for $h_1/d = 1.3$
- $0.18 < F_{nh} < 0.38$ for $h_1/d = 1.5$
- $0.17 < F_{nh} < 0.35$ for $h_1/d = 1.8$
- $-0.63 < y_{Bt} < 0.63$
- $0 < (1 - (h_2/h_1)) < 1$
- $1.24 < d/(h_1 - d) < 10.44$
- $0.52 < C_B < 0.85$
- $0 < \alpha < 90$ degrees

The maximum vessel speed was dictated by the range of applicability of the equivalent bank distance parameter for bank slope and the bank flooding component of the bank parameter, BP_{Y6} . The equivalent bank distance parameter is valid up to a length Froude number of approximately 0.07 for draught to under keel clearance ratios less than or equal to 5.13 and is valid up to a length Froude number of 0.1 for draught to under keel clearance ratios between 4.17 and 1.24. The parameter BP_{Y6} is not valid for a small number of cases where the sway

force for flooded banks exceeded that for surface piercing banks. This was found to occur at length Froude numbers above approximately 0.11 for draught to under keel clearance ratios of 5.13 and 3.35.

Since the proposed equations are based on model scale measurements, experimental error will influence the accuracy of the prediction technique. This may be more pronounced for cases where the magnitude of the sway forces and yaw moments were small. The error in the fit of the regression equations to the experimental data will also affect the accuracy of the prediction. The maximum power of some parameters was relatively high for the sway force equations to provide adequate playback. Hence, the accuracy of the sway force equation will be uncertain when used to extrapolate to values beyond the bounds of applicability.

Since there are many variables that influence ship-bank interaction, it was necessary to simplify the test matrix in order to incorporate the influence of as many important variables as possible. For example, the influence of flooded bank width (y_{pw}) for a constant channel width was shown by Li (2000) to influence bank induced sway force and yaw moment, however, this was not considered in the present study. Dand (1981), Ch'ng (1991) and Li (2000) found that an operating propeller influenced bank induced sway force and yaw moment. However, the influence of an operating propeller was neglected in the present empirical equations. The experimental data was limited to three hull forms and thus it is not advised that the equations be used to quantify the changes in bank effect due to small changes in hull form.

A number of approximations have been made to simplify the regression equations, which may introduce error in some instances. For example, the effect of bank slope was estimated through the use of an equivalent bank distance parameter, which may not be accurate for all cases. The linear relationship of the non-dimensional sway force and yaw moment with the respective bank parameters, BP_{Y6} and BP_{N6} , is valid for the majority of cases. However, there were cases for which the linear superposition approach was violated due to non-linearity, particularly for the sway force at draught to under keel clearance ratios around 5.13, in the region where the sway force changed from attraction to the near bank to repulsion from the near bank. Hence, the relationship of non-dimensional sway force and yaw moment with the bank flooding parameter was designed to account for general trends only.

It is possible to have the same value of y_{B6} for different channel width to vessel length ratios. Linear superposition of the effects from surface piercing port and starboard banks can only be adopted if the sway force and yaw moment are similar for a constant y_{B6} with different channel width to vessel length ratios. Ch'ng (1991) showed that the parameter, y_{B3} , can be used to represent the lateral position of a vessel relative to the canal walls, regardless of canal width. Similarly, for flooded banks it needs to be confirmed if the sway force and yaw moment are similar for cases with the same bank parameters, BP_{Y6} and BP_{N6} , but different values of y_{B6} , $1-(h_{2p}/h_1)$ and $1-(h_{2s}/h_1)$. Throughout the model scale experiments in the present study the starboard bank remained at 5.1B from the channel centreline and the transverse location of the port bank was varied to provide different channel widths. Therefore measurements from the present study could not be used to verify this directly for flooded banks. This issue has been addressed indirectly through comparison between predictions and independent measurements with different channel width to vessel length ratios and different $1-(h_{2p}/h_1)$ values to those tested in the present study. The reasonable correlation with the independent results is encouraging; however, further work should be conducted to confirm the validity of this assumption.

Dand (1981) and Chen and Sharma (1994) found that the bank induced sway force and yaw moment on a vessel travelling alongside channel walls with a drift angle may differ from that of a vessel with zero drift angle. This effect is neglected in the proposed prediction technique, as the empirical formulae are based on steady-state cases where a ship is travelling parallel to lateral banks of infinite length with zero drift angle.

The proposed quasi-steady approach should be sufficiently accurate to predict bank induced sway force and yaw moment for cases where the ship speed and lateral ship to bank distance vary slowly with time. However, when the lateral ship to bank distance varies more quickly with time, transient effects may significantly influence the bank induced sway force and yaw moment (Norrbin 1974; Norrbin 1978; Dand 1981). For such cases the quasi-steady assumption may be inadequate, as the effects of the time-dependent flow are neglected.

Due to restrictions on the size of scale models the experiments were conducted at significantly lower Reynolds numbers than full scale. Therefore the flow fields at model-scale and full-scale may be dissimilar due to after-body separation, cross-flow separation and different boundary layer thicknesses. These scale effects should be borne in mind when using the empirical formulae to predict full-scale ship-bank interaction.

6.3 Validation of prediction technique

The empirical formulae developed to predict bank induced sway force and yaw moment were validated using two different approaches. The first involved comparison of the predicted non-dimensional sway force and yaw moment with independent measurements made on scale models by Dand (1981). For the second approach the empirical formulae were incorporated into the existing mathematical model outlined in Section 2.4.2. Then the path of a ship was predicted in real-time for a manoeuvre, within an Australian port, where ship operators use ship-bank interaction to aid turns. The predicted ship path has been compared to the actual ship path known to occur in the real-life manoeuvre.

6.3.1 Comparison with experimental data - sway force and yaw moment

In Figures 6.23 – 6.26 the predicted non-dimensional sway force and yaw moment are compared to a selection of independent model scale measurements for tanker hull forms made by Dand (1981). The starboard bank was vertical and pierced the free surface for all cases presented. The predictions, in general, follow the trends in the measured data and are reasonable when considering experimental error and that the bank slope, some W/B ratios and y_{Bt} values for Dand's tests lie outside the range of test parameters for the present study. Also, the vessel speed for some of Dand's cases exceeds the maximum limit of the regression equations.

The correlation between sway force predictions and measurements was found to be reasonable for a number of cases at draught to under keel clearance ratios below 4. For example, the predictions were generally within 20% of the measured data for Cases 5, 6 and 8. However, there were some instances where the correlation was poor, as can be seen for Case 3 where the sway force was under predicted by up to approximately 70%. The large discrepancy for Case 3 may be partly due to the fact that this combination of draught to under keel clearance ratio and channel geometry was in the region where the sway force changed from attraction to repulsion

from the near bank. The magnitude of the sway force was found to be erratic for such cases and the linearity assumption for the bank parameters may not be valid. The correlation between yaw moment predictions and measurements was reasonable for a number of cases at draught to under keel clearance ratios above 4. For example, the predictions were generally within 20% of the measured data for Cases 1, 2 and 3. However, the yaw moment was under predicted by up to approximately 70% for some instances, as illustrated by Case 8. The discrepancies between predictions and independent measurements may be attributable to the fact that some of Dand's cases lie outside the maximum speed limit of the regression equations and the limitations/assumptions associated with the regression formulae.

On comparing predictions to independent measured values it can be seen that the empirical formulae provide a means to approximate the sway force and yaw moment induced by lateral surface piercing and flooded banks for a wide range of cases. This provides a new method for estimating the sway force and yaw moment induced by flooded lateral banks with confidence, provided the limits of applicability are adhered to.

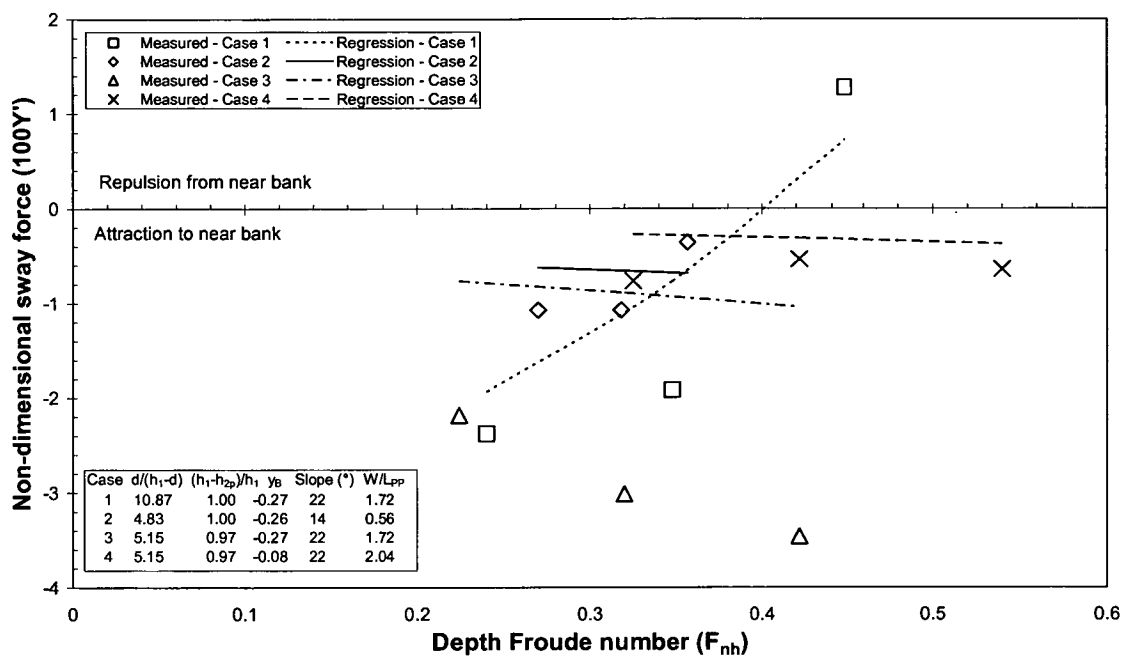


Figure 6.23 Comparison between regression prediction and non-dimensional sway force measured by Dand (1981), Cases 1 – 4

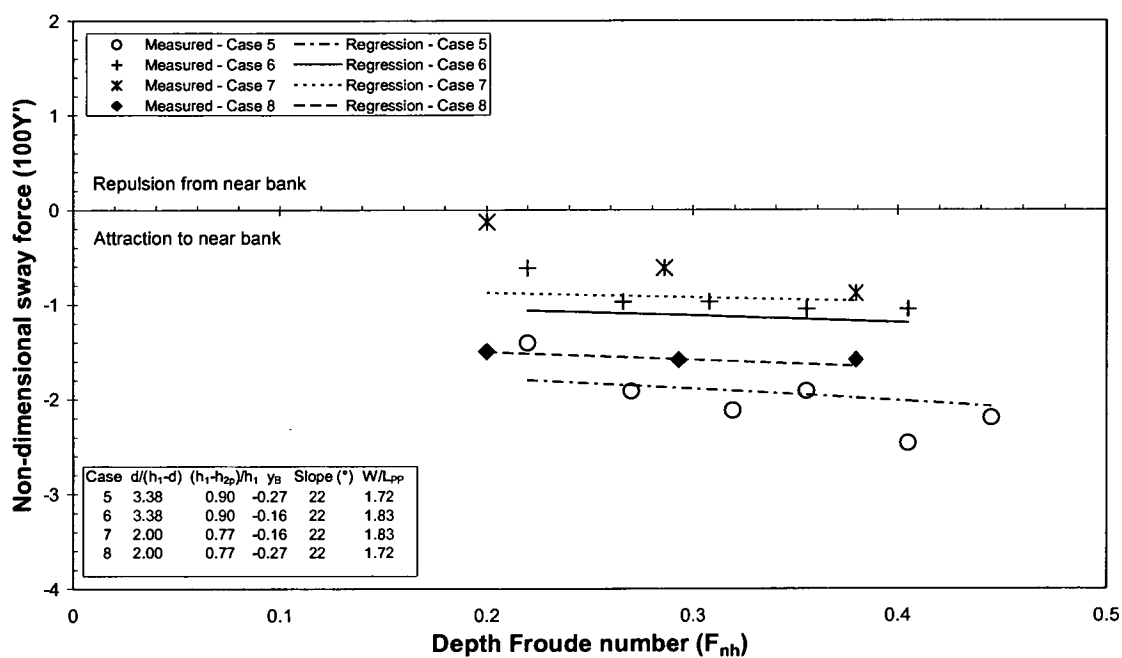


Figure 6.24 Comparison between regression prediction and non-dimensional sway force measured by Dand (1981), Cases 5 – 8

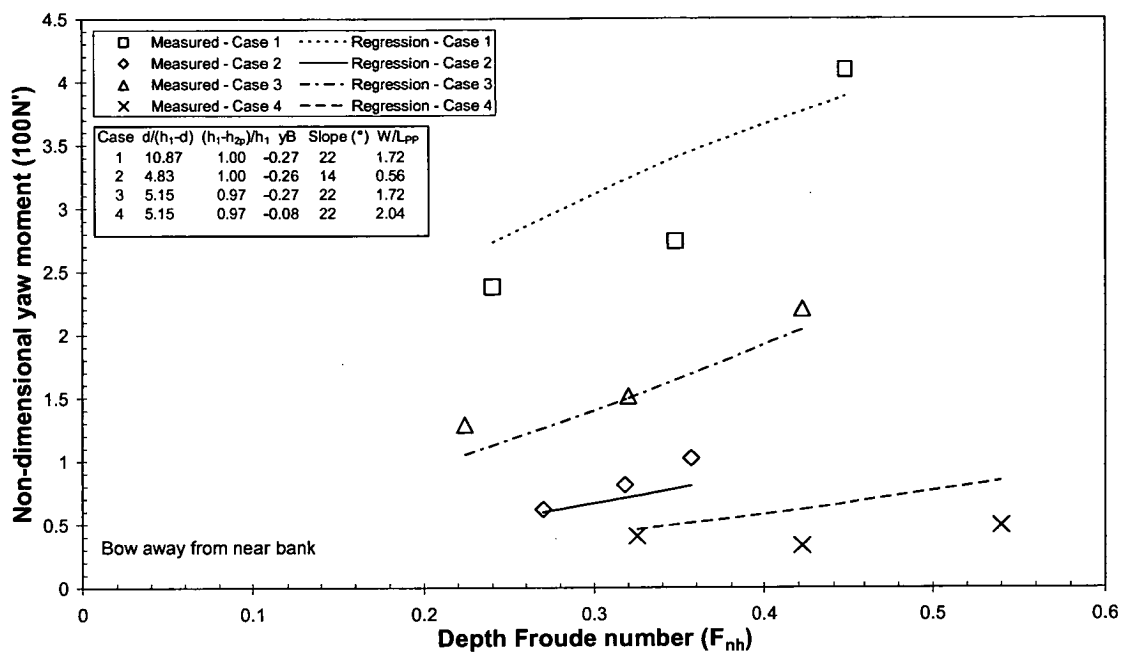


Figure 6.25 Comparison between regression prediction and non-dimensional yaw moment measured by Dand (1981), Cases 1 – 4

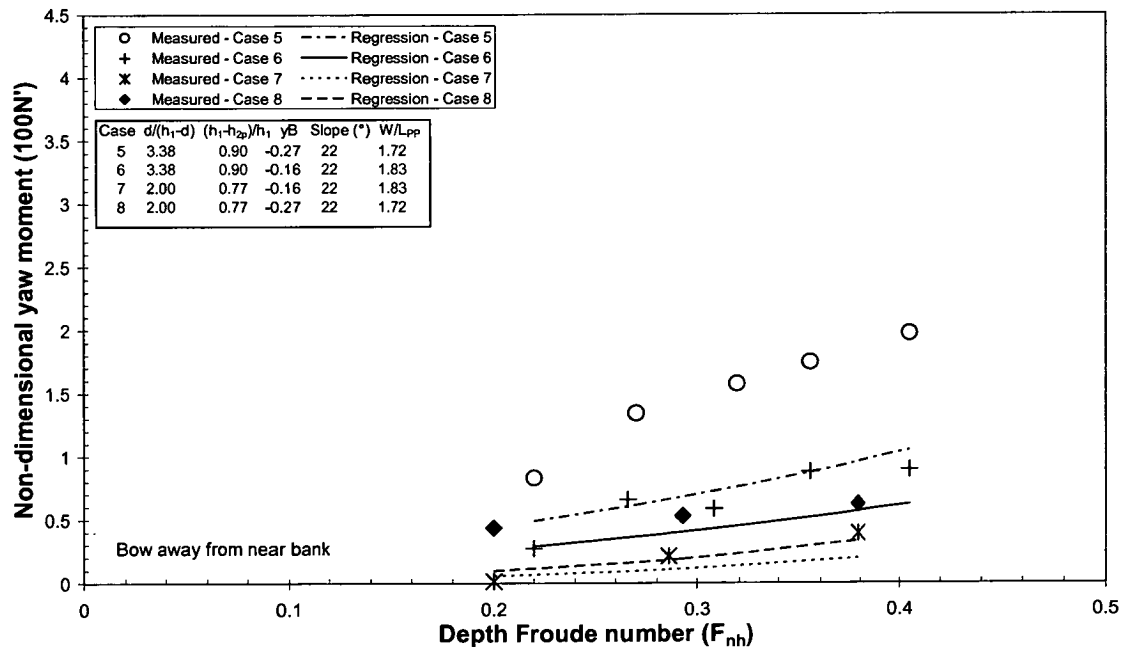


Figure 6.26 Comparison between regression prediction and non-dimensional yaw moment measured by Dand (1981), Cases 5 – 8

6.3.2 Comparison with known real-life manoeuvre - sway and yaw motion

The existing mathematical model in the AMC ship-handling simulator, outlined in Section 2.4.2, is based on work presented by Norrbín (1971). The balance of all forces and moments acting on a ship’s hull at each time instant is used to calculate the appropriate accelerations of a ship in the horizontal plane. The differential equation system is numerically integrated in steps (Euler-Cauchy), until the track of the ship over the ground is determined. The empirical formulae to predict steady-state bank induced sway force and yaw moment have been incorporated into this mathematical model. The instantaneous vessel draught was calculated at each time step, accounting for the influence of vessel squat. The instantaneous ship-bank interaction was calculated based on the instantaneous water depth and ship draught. This quasi-steady technique has been used to predict the motion of a vessel manoeuvring in restricted water.

In some ports bank induced yaw moment is used to assist in negotiating tight bends in approach channels; an example is at the port of Weipa, Queensland, Australia. The path of the bulk carrier, Kumasachi Maru, has been predicted for a standard manoeuvre performed at the port, where the effects of flooded lateral banks are used to aid turns. The aim was to assess the accuracy of the ship-bank interaction model by comparing the predicted ship path with that known to occur in the real-life case. The principal particulars of the Kumasachi Maru are provided in Table 6.11.

| L _{PP} (m) | Beam (m) | Draught (m) | C _B |
|------------------------|-------------|----------------|----------------|
| 215 | 32.2 | 12.2 | 0.84 |

Table 6.11 Principal particulars of the bulk carrier, Kumasachi Maru

The plan view of a section of the port of Weipa and the predicted path of the Kumasachi Maru leaving the port is shown in Figure 6.27. The effects of current were modelled for the simulation and were based on comprehensive measurements made at the port. The maintained channel is marked out by the starboard and port beacons and is shown by the dotted lines. The speed of the ship as it approached beacon 38 was 6 knots. The rudder was held at midships until beacon 36 was abeam the bridge, when a port helm of 5 degrees was applied. The rudder angle was held constant at 5 degrees until just prior to the bow passed beacon 27. It can be seen that the vessel makes a relatively tight port turn with only 5 degrees of port helm. This can be explained by viewing the predicted bank induced sway force and yaw moment for this manoeuvre as a function of time, which is output from the AMC ship-handling simulator and given in Figure 6.28. When the ship is in position 0 (position represented by the red ship shape) there is a steep starboard flooded bank approximately 8.5m high with 3.7m of water over the bank at low tide. In Figure 6.28 the red vertical line corresponds to the point where the vessel is in position 0. It can be seen that the starboard bank caused a counter clockwise yaw moment pushing the bow away from the starboard bank. The rate of turn induced by this bank is used to aid the port turn, reducing the amount of helm required. When the vessel was adjacent to beacon 27 (represented by the blue vertical line on the graph) it experienced a relatively large clockwise moment induced by a steep flooded bank on the port side of the ship. Just prior to the bow reaching beacon 27 the port helm was increased to reduce the clockwise rate of turn, which set up the ship for the starboard turn that occurs after beacon 25.

According to practicing pilots from the port of Weipa, this manoeuvre could not be accurately simulated using the previous bank effect model on the AMC ship-handling simulator, which was designed for surface piercing banks. Using the previous model, the simulated rudder angle required to make the turn did not match reality. However, it was found that the bank effect model developed in the present study provided sufficient accuracy to satisfy their simulation requirements. It should be noted that many simulation runs were conducted for the Port of Weipa to evaluate the bank effect model. The bank effect model has subsequently been assessed for several other ports by practicing pilots. Ideally, the predicted path of the ship would be validated against the measured path of the real-life ship. However, full-scale path measurements are difficult to achieve and were outside the scope of the present work.

The form of the equations means they are ideally suited for use on a real-time ship-handling simulator. The proposed real-time simulation method provides a good solution to the complicated problem of ship-bank interaction simulation and enables the prediction of the effect of flooded banks on ship manoeuvring; a topic which has received little attention in the past.

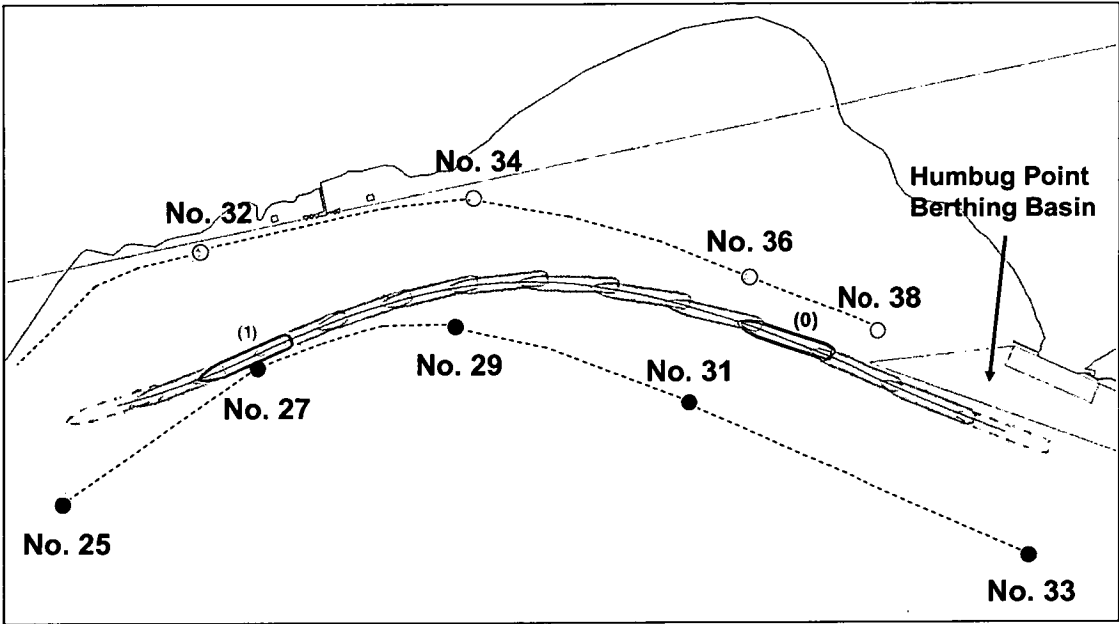


Figure 6.27 Predicted ship path using empirical equations from the present study in the AMC ship-handling simulator for the Port of Weipa

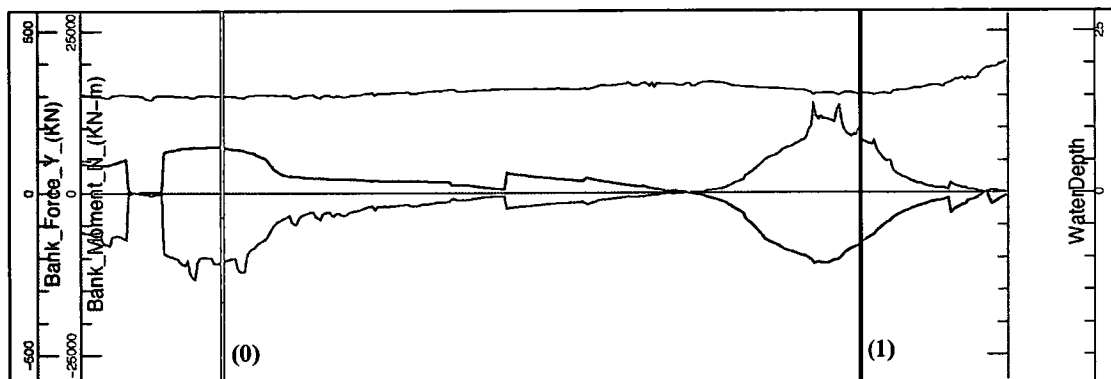


Figure 6.28 Predicted bank induced sway force and yaw moment for the simulation of a manoeuvre at the Port of Weipa (output from AMC ship-handling simulator)

Chapter 7

Concluding Remarks and Recommendations

7.1 Concluding remarks

An investigation has been undertaken into the simulation of ship behaviour in restricted waters. Two aspects have been considered, ship squat and ship-bank interaction. Techniques have been presented to model each phenomenon, which can be used to improve the realism of ship-handling simulation.

A mathematical model was developed to predict unsteady squat and dynamic acceleration effects for a vessel travelling in water of non-uniform depth. The model provides a quasi-steady solution; the vertical plane motion at each time step being predicted from the steady-state heave force and pitch moment due to squat in water of uniform depth. A comprehensive set of model scale experiments was conducted in water of uniform depth and non-uniform depth, providing a greater understanding of steady-state and unsteady squat. Steady-state heave force and pitch moment were predicted using a three-dimensional panel method to establish if the results could be used to extend the experimental data matrix. For some cases it was found that steady-state heave force was underestimated by up to approximately 35%, whilst the pitch moment was underestimated by up to approximately 80%. This may be partly due to the fact that viscous effects were not modelled. Hence, physical model scale measurements were used to develop empirical formulae using regression analysis techniques to predict steady-state heave force and pitch moment experienced by a full form vessel, which were used as input to the mathematical model. These equations are dependent on under keel clearance parameters, channel width parameters and depth Froude number. Empirical correction factors were also developed to estimate the effect of propulsion on squat.

Predictions from the quasi-steady mathematical model were initially validated against model scale steady-state sinkage measurements at water depth to draught ratios of 1.2, 1.3 and 4.3. The predictions were found to be within approximately 15% of the measurements for the majority of depth Froude numbers tested at water depth to draught ratios of 1.2 and 1.3. Similar accuracy was observed for the higher depth Froude numbers tested at a water depth to draught ratio of 4.3. However, the midship sinkage was under predicted by up to approximately 45% and the bow sinkage was under predicted by up to approximately 30% for low depth Froude numbers at this water depth to draught ratio. Predictions were then compared against unsteady sinkage measurements on a vessel travelling over a simplified ramp bank. The general trend of the unsteady sinkage prediction was reasonable. Inclusion of dynamic acceleration effects provided satisfactory prediction of bow sinkage when travelling over abrupt changes in water depth, such as passing the end of the bank, which is beneficial when simulating squat behaviour and other phenomena dependent upon instantaneous under keel clearance, such as ship-bank interaction. However, the maximum unsteady sinkage was not always predicted accurately, which may be attributable to the limitations and assumptions associated with the technique. In summary, the quasi-steady squat mathematical model provided a solution to the problem of unsteady squat in non-uniform water depth.

A comprehensive series of model scale experiments was conducted to measure the sway force and yaw moment induced by lateral banks, providing valuable information to enhance the understanding of ship-bank interaction. The following parameters were systematically varied for three different hull forms: flooded bank height, water depth, bank slope, lateral ship to bank distance, vessel speed, and vessel draught. The results from these experiments were used to develop a bank parameter to estimate the effects of lateral surface piercing and flooded banks. This parameter was utilised in regression analyses to develop empirical formulae for the prediction of steady-state bank induced sway force and yaw moment. A three-dimensional panel method was used to predict steady-state sway force and yaw moment to establish if the results could be used to extend the experimental data matrix. For some cases there was a variation of up to approximately 80% between the predicted and measured sway force and bow away yaw moment. This may be partly due to the fact that viscous effects were not modelled. Therefore, the empirical equations were derived using measurements from the physical model scale experiments.

The empirical formulae were validated against independent model scale measurements from literature. In general, the sway force predictions were found to be within 20% of measurements for a number of cases at draught to under keel clearance ratios below 4. The yaw moment predictions were generally found to be within 20% of measurements for a number of cases at draught to under keel clearance ratios above 4. However, there were some instances where the sway force and yaw moment were under predicted by up to approximately 70%. The cases where the sway force prediction was less accurate were primarily in the region where sway force changed from attraction to repulsion from the near bank. The empirical formulae provide a new practical method for estimating the sway force and yaw moment induced by flooded lateral banks, provided the limits of applicability are adhered to. The form of the equations means they are ideally suited for use on a real-time ship-handling simulator.

In some ports the effects of ship-bank interaction are used to aid vessel turns, for example in the Port of Weipa, Australia. According to practicing pilots from this port, a certain manoeuvre that utilises bank effect could not be accurately simulated using the previous bank effect model on the AMC ship-handling simulator, which was designed for surface piercing banks. Using the previous model, the simulated rudder angle required to make the turn did not match the real-life case. The formulae from the present study were incorporated into the existing mathematical model on the AMC ship-handling simulator. The quasi-steady technique was used to predict the path of a vessel in the Port of Weipa for a manoeuvre where bank induced yaw moment is used to aid a turn. The predicted path was compared to that known to occur in the real-life manoeuvre and it was found that the new bank effect model provided sufficient accuracy to adequately perform the manoeuvre. The new quasi-steady bank effect simulation method therefore provides a good solution to the problem of ship-bank interaction simulation.

The objectives outlined at the beginning of the project have therefore been achieved;

- A practical prediction technique has been developed to simulate squat and dynamic acceleration effects for a vessel travelling in water of non-uniform depth.
- The squat prediction technique has been successfully validated against model scale measurements for cases where a vessel is travelling in uniform water depth and over a simplified ramp bank.
- Empirical formulae have been developed to predict the sway force and yaw moment induced on a ship by surface piercing and/or flooded lateral banks.

- Empirical formulae to predict bank induced sway force and yaw moment have been successfully validated against independent model scale measurements and when incorporated into the existing AMC ship-handling simulator realistic paths were predicted for a ship manoeuvre in close proximity to lateral banks.

7.2 Recommendations for future research

Whilst new methods have been developed to simulate the effects of squat and ship-bank interaction, further work may be conducted to extend knowledge in the area and improve the proposed techniques.

With respect to the steady-state squat prediction technique, further model scale experiments should be conducted with different hull forms, level keel draughts, initial trims, bank geometries and lateral ship positions in the channel. The results would enable additional terms to be incorporated into the empirical equations to account for the effect of hull form, draught, trim, bank geometry and lateral ship position in the channel.

Further model experiments should be carried out to measure unsteady squat for a wider range of sea-bed profiles, bank heights, water depth to draught ratios and lateral bank configurations. This may clarify why different trends were observed between results from the present study and previous studies for a vessel travelling over a ramp bank. These results could be used to perform further validation of the mathematical model.

There are many variables that influence ship-bank interaction; in the present study the experimental test matrix was simplified to address the most important variables. Further experimental investigation should be conducted to gain a clearer understanding of the effect of hull form on bank induced sway force and yaw moment. A more detailed experimental study into the effect of bank slope should be carried out to assess the validity of the equivalent bank distance parameter for a wider range of cases. In particular, data is required for flooded bank slopes less than 45 degrees. A bank slope term should be incorporated into the equations to enable predictions for higher length Froude numbers. Further cases with different bank flooding parameters should be examined using model experiments. This will enable a more accurate representation of the influence of the bank flooding parameter in the regression equations. Further physical scale model tests should be conducted to investigate the effect of vessel draught, flooded bank width, drift angle and propulsion. These results could be used to extend the empirical formulae to include terms to account for these effects.

Linear superposition of the effects from port and starboard banks can only be adopted if the sway force and yaw moment are similar for constant values of BP_{Y6} and BP_{N6} for different combinations of y_{B6} , $1-(h_{2p}/h_1)$ and $1-(h_{2s}/h_1)$. For all of the model scale experiments conducted the starboard bank remained at 5.1B from the channel centreline and the transverse location of the port bank was varied to provide different channel widths. Therefore measurements from the present study could not be used to verify this issue directly for flooded banks. It was addressed indirectly through comparison between predictions and independent measurements with different values of channel width to vessel length ratios and $1-(h_{2p}/h_1)$ to those tested in the present study. The reasonable correlation with the independent results was encouraging; however, further model scale experiment work should be conducted to confirm if the sway force and yaw moment are similar for cases with the same value of bank parameters, BP_{Y6} and BP_{N6} , but different values of y_{B6} , $1-(h_{2p}/h_1)$ and $1-(h_{2s}/h_1)$.

Further experiments should be undertaken to gain a clearer understanding of the flow properties for the case of a vessel operating in restricted water. For example, the free surface elevation should be measured between the ship and lateral banks, along with the pressure acting on the surface of the ship hull, sea floor and lateral banks. Also the boundary layer properties should be measured. This would be particularly useful to investigate the physical mechanism causing the sway force to change from attraction to the near bank to repulsion from the near bank. It would also be useful, for example, to explain why the bow down pitch moment reduced for low channel width to beam ratios for sub-critical cases.

Predictions from the computational fluid dynamics approach using potential flow provided poor correlation with model experiment results. This may be partly due to the fact that viscous effects were not modelled. More advanced computational fluid dynamics may be used to investigate flow properties for a vessel operating in restricted water. For example, to extend the approach used in the present study, for cases with a ship travelling in an asymmetrical channel, a Kutta condition could be applied at the stern to model lift due to circulation. For cases with very low under keel clearance and small channel width to vessel beam ratios, where separation may occur along the length of the ship, applying Reynolds Averaged Navier Stokes equations over the entire hull may provide a more accurate solution.

The effect of varying vessel hydrostatics with changes in draught in the squat mathematical model should be examined; for example the change in position of LCF and change in magnitude of TPC and MCTC with vessel draught. The change in damping and added mass with water depth to draught ratio should be investigated.

Both the squat and ship-bank interaction prediction techniques were based on a quasi-steady assumption. This is reasonably accurate when vessel speed and channel geometry vary sufficiently slowly with time. However, for higher speeds and/or rapidly changing channel geometry, the quasi-steady assumption may break down due to the effect of transient phenomena (Norrbín 1974 & 1978; Dand 1981; Ferguson *et al.* 1982). For both ship squat and ship-bank interaction a prediction method needs developing to account for transient effects.

Full-scale measurements of vessel motions should also be conducted for a range of cases in restricted water where squat and ship-bank interaction influence vessel behaviour. Using advanced measurement systems, such as DGPS, the motions in six degrees of freedom could be obtained during typical ship manoeuvres. Such results could be used to further validate the prediction techniques and to quantify the effect of scale when using model scale experiment results to predict full-scale squat and ship-bank interaction.

References

- Abbott, S. 1998, An investigation into shallow water effects on high speed craft, Bachelor of Engineering (Nav. Arch.) Thesis, Australian Maritime College.
- Ankudinov, V.K. & Jacobsen, B.K. 1996, 'Squat predictions at an early design stage', *Proceedings of Workshop on Ship Squat in Restricted Waters*, The Society of Naval Architects and Marine Engineers, pp. 48-70.
- Balanin, V.V. & Bykov, L.S. 1965, 'Selection of leading dimensions of navigation canal sections and modern methods of bank protection', *Proceedings of the 21st International Navigation Congress*, Permanent International Association of Navigation Congresses (PIANC), Stockholm, SI-4, pp. 151-169.
- Barlow, J.B., Rae, W.H. & Pope, A. 1999, *Low-Speed Wind Tunnel Testing*, 3rd edn, John Wiley & Sons, New York.
- Barrass, C.B. 1979, 'The phenomena of ship squat', *International Shipbuilding Progress*, vol. 26, pp. 44-47.
- Barrass, C.B. 1989, 'Squatting of ships crossing in a confined channel', *Seaways*, November, pp. 16-18.
- Barrass, C.B. 1995, 'Ship squat', *Proceedings of Squat Interaction Manoeuvring: Humberside Branch Seminar*, The Nautical Institute, London, pp. 21-33.
- Beck, R., Newman, J. & Tuck, E. 1975, 'Hydrodynamic forces on ships in dredged channels', *Journal of Ship Research*, vol. 19, no. 3, pp. 166-171.
- Beck, R.F. 1977, 'Forces and moments on a ship moving in a shallow channel', *Journal of ship Research*, vol. 21, no. 2, pp. 107-120.
- Blaauw, H., & Van Der Knaap, F. 1983, 'Prediction of squat of ships sailing in restricted water', *Proceedings of the 8th International Harbour Congress*, Antwerp, Belgium.
- Bouwmeester, J. 1977, 'Calculation return flow and water level depressions; new method', *Proceedings of the 24th International Navigation Congress*, Permanent International Association of Navigation Congresses (PIANC), Leningrad, SI-3, pp. 148-151.
- Bojovic, P. 1999, Resistance prediction of high speed round bilge hull forms, Master of Philosophy Thesis, Australian Maritime College.
- Chen, X. & Sharma, S. 1994, 'Nonlinear theory of asymmetric motion of a slender ship in a shallow channel', *Twentieth Symposium on Naval Hydrodynamics*, Santa Barbara, California, pp. 386 - 407.

Ch'ng, P.W. 1991, An investigation into the influence of bank effect on ship manoeuvring and its mathematical modelling for a ship-handling simulator, Master of Engineering Thesis, School of Mechanical and Manufacturing Engineering, Univ. of New South Wales.

Ch'ng, P.W., Doctors, L.J. & Renilson, M.R. 1993, 'A method of calculating the ship-bank interaction forces and moments in restricted water', *International Shipbuilding Progress*, vol. 40, no. 421, pp. 7-23.

Collinson, R.G. 1994, A review of methods of predicting the squat of a ship in shallow water, Masters Thesis, University of Liverpool.

Constantine, T. 1961, 'On the movement of ships in restricted waterways', *Journal of Fluid Mechanics*, vol. 9, pp. 247-256.

Dand, I.W. & Ferguson, A.M. 1973, 'The squat of full ships in shallow water', *Trans. RINA*, vol. 115, pp. 237-255.

Dand, I.W. 1981, 'Some measurements of interaction induced by surface-piercing and flooded banks', *National Maritime Institute*, Report NMI R110.

Dand, I.W. 1996, 'Prediction of squat at sub-, trans-, and supercritical speeds for displacement ships in shallow water', *Proceedings of Workshop on Ship Squat in Restricted Waters*, The Society of Naval Architects and Marine Engineers, pp. 11-29.

Dawson, C.W. 1977, 'A practical computer method for solving ship-wave problems', *Proceedings of 2nd International Conference on Numerical Ship Hydrodynamics*, Berkeley, pp. 30-38.

Drobyshevskiy, Y.E. 2000, 'Ship squat over a stepped bottom: theoretical model', *Trans. RINA*.

Duffield, R. 1997, Investigation into steady and unsteady state squat, Bachelor of Engineering (Nav. Arch.) Thesis, Australian Maritime College.

Duffy, J.T. & Renilson, M.R. 2000, 'An investigation into the effect of propulsion on ship squat', *Oceanic Engineering International*, vol. 4, no. 1, pp.1-12.

Duffy, J.T., Renilson, M.R. & Smith I. 2000, 'The effect of bank geometry on the simulation of ship manoeuvring in restricted water', *Proceedings of Safe Navigation Beyond 2000*, Gdynia, Poland.

Duffy, J.T. & Renilson, M.R. 2001, 'The effect of channel design on ship operation in a port', *Proceedings of Coasts and Ports 2001*, Queensland, Australia.

Duffy, J.T. 2002, 'The effect of channel geometry on ship operation in a port', *Proceedings of 30th International Navigation Congress*, Permanent International Association of Navigation Congresses (PIANC), Sydney, Australia.

Duffy, J.T. 2005, 'Prediction of bank induced sway force and yaw moment for ship-handling simulation', *Proceedings of SimTecT 2005*, Sydney, Australia.

Duffy, J.T. 2007, 'Investigation into the influence of channel geometry on ship squat', *Australian Maritime College Towing Tank/Model Test Basin*, Report 07-01.

Duncan, H. 1968, 'Harbour entrances, channels and turning basins', *The Dock and Harbour Authority*.

Edstrand, H. & Norrbin, N. H. 1978, 'Shallow water phenomena and scale model research – some first experience from the SSPA Maritime Dynamics Laboratory', *Publications of the Swedish State Shipbuilding Experimental Tank*, Report no. 81, Goteborg, Sweden.

Eryuzlu, N. & Hausser, R. 1978, 'Experimental investigation into some aspects of large vessel navigation in restricted waterways', *Proceedings of the Symposium of Aspects of Navigability*, Delft, The Netherlands, vol. 2, pp. 1-15.

Eryuzlu, N., Cao, Y. & d'Agnolo, F. 1994, 'Underkeel requirements for large vessels in shallow waterways', *Proceedings of the 28th International Navigation Congress*, Permanent International Association of Navigation Congresses (PIANC), Seville, Spain, Paper S II-2, pp 17-25.

Fuehrer, M. and Romisch, K. 1977, 'Effects of modern ship traffic on inland- and ocean-waterways and their structures', *Proceedings of the 24th International Navigation Congress*, Permanent International Association of Navigation Congresses (PIANC), Leningrad, SI-3, pp. 79-93.

Fuehrer, M., & Romisch, I. K. 1983, 'The effects of hydrodynamic forces on ships navigating through canals: a contribution to an estimation of the manoeuvrability of ships in a restricted channel', *PIANC Bulletin*, vol. 57, no. 43, pp. 10-22.

Ferguson, A., Seren, D. & McGregor, R. 1982, 'Experimental investigation of a grounding on a shoaling sandbank', *Trans. RINA*, vol. 124, pp. 303-324.

Ferguson, A., Seren, D., & McGregor, R. 1983, 'The prediction and practical measurement of ship squat in shallow water', *Proceedings of Marine Safety Conference 1983*, University of Glasgow, United Kingdom, Paper 12, pp. 12/1-12/19.

Fujino, M. 1972, 'New experimental results of forced yaw tests in shallow water', *University of Tokyo Department of Naval Architecture*, Report no. 5001.

Gates, E.T. & Herbich, J.B. 1977, 'The squat phenomenon and related effects of channel geometry', *Proceedings of 25th Annual Hydraulics Specialty Conference*, Texas, pp. 236-244.

Gertler, M. 1969, 'Final analysis of first phase of ITTC standard captive-model-test programme', *Proceedings of the 12th International Towing Tank Conference (ITTC)*, Appendix III, part 2, Rome.

- Gourlay, T.P. & Tuck, E.O. 1998, 'One-dimensional theory for flow past a ship in a channel of variable depth', *Australian Mathematical Society Gazette*, vol. 25, no. 4, pp. 206-211.
- Gourlay, T.P. 2000, Mathematical and computational techniques for predicting the squat of ships, PhD thesis, University of Adelaide.
- Gourlay, T.P. 2003, 'Ship squat in water of varying depth', *International Journal of Maritime Engineering*, vol. 145, Part A1, pp. 1-12.
- Gourlay, T.P. 2006, 'Flow beneath a ship at small underkeel clearance', *Journal of Ship Research*, vol. 50, no. 3, pp.250-258.
- Graff, W., Kracht, A. & Weinblum, G. 1964, 'Some extensions of D.W. Taylor's standard series', *Trans. SNAME*, vol. 72, no. 374.
- Hatch, T.L. 1996, Squat of a full form vessel over an undulating sea floor, Bachelor of Engineering (Nav. Arch.) Thesis, Australian Maritime College.
- Hatch, T. 1999, 'Experience measuring full scale squat of full form vessels at Australian ports', *Proceedings of Coasts and Ports '99*, Perth, Australia.
- Hatch, T., O'Brien, T., Berwick, B., Woods, I., Duffy, J.T. & Renilson, M.R. 1999, 'Ship – bank interaction effects: A case study – Port of Townsville.', *Proceedings of Coasts & Ports '99*, Perth, Western Australia.
- Haatainen, P., Lund, J. & Kostilainen, V. 1978, 'Experimental investigation on the squat in changing water depth conditions', *Helsinki University of Technology Ship Hydrodynamics Laboratory*, Report no. 14.
- Hess, J.L. & Smith, A.M.O. 1962, 'Calculation of nonlifting potential flow about arbitrary three-dimensional bodies', *Douglas Aircraft Company*, Report no. E.S. 40622.
- Hess, F. 1978, 'Bank suction cancelled by rudder deflection: a theoretical model', *International Shipbuilding Progress*, vol. 25, no. 281, pp. 7-13.
- Hooft, J.P. 1974, 'The behaviour of a ship in head waves at restricted water depth', *International Shipbuilding Progress*, vol. 21, no. 244, pp. 367-390.
- Hsiung, C.C. & Gui, Q. 1988, 'Computing interaction forces and moments on a ship in restricted waterways', *International Shipbuilding Progress*, vol. 35, no. 403, pp. 219-254.
- Huuska, O. 1976, 'On the evaluation of underkeel clearances in Finnish waters', *Helsinki University of Technology Ship Hydrodynamics Laboratory*, Report no. 9.
- ITTC 1987, 'Report of the seakeeping committee, S-175 comparative model experiments', *Proceedings of the 18th International Towing Tank Conference (ITTC)*, vol. 1, Kobe, Japan.
- ITTC 1999, 'Report of the manoeuvring committee', *Proceedings of the 22nd International Towing Tank Conference (ITTC)*, vol. 1, Seoul, Korea & Shanghai, China.

- ITTC 2002, 'ITTC recommended procedures', *Approved by the 23rd International Towing Tank Conference (ITTC)*, Venice, Italy.
- Kijima, K. & Higashi, E. 1996, 'The simple prediction method for squat', *Proceedings of Workshop on Ship Squat in Restricted Waters*, The Society of Naval Architects and Marine Engineers, pp. 30-39.
- Koster, J. 1971, 'Suction effects of canal banks on ship behaviour', *Delft Hydraulics Laboratory*, Report no. 91.
- Laforce, E., Claeysens, P. & Vantorre, M. 1996, 'Influence of the ship's length on the manoeuvrability in a canal', *Proceedings of the 11th International Harbour Congress*, Antwerp, Belgium, pp. 523-534.
- Larsson, L., Broberg, L., Kim, K.-J. & Zhang, D.H. 1989, 'New viscous and inviscid CFD techniques for Shipflow', *Proceedings of 5th International Conference on Numerical Ship Hydrodynamics*, Hiroshima.
- Larsson, L., 1993, 'Resistance and flow predictions using the Shipflow Code', *19th WEGEMT School*.
- Li, D.-Q. 2000, 'Experiments on bank effects under extreme conditions', *SSPA Research*, Report no. 113, Sweden.
- Longo, J. & Stern, F. 2005, 'Uncertainty assessment for towing tank tests with example for surface combatant DTMB model 5415', *Journal of Ship Research*, vol. 49, no. 1, pp. 55-68.
- McDonnell, S. 2003, An investigation into vessel squat and ship-bank interaction for full form vessels, Bachelor of Engineering (Nav. Arch.) Thesis, Australian Maritime College.
- Mei, C.C. & Choi, H.S. 1987, 'Forces on a slender ship advancing near the critical speed in a wide canal', *Journal of Fluid Mechanics*, vol. 179, pp. 59-76.
- Miao, Q., Chwang, A.T., Xia, J. & Duffy, J.T. 2003, 'Numerical study of bank effects on a ship travelling in a channel', *Proceedings of 8th International Conference on Numerical Ship Hydrodynamics*, Busan, Korea.
- Millward, A. 1990, 'A preliminary design method for the prediction of squat in shallow water', *Marine Technology*, vol. 27, no.1, pp. 10-19.
- Millward, A. 1992, 'A comparison of the theoretical and empirical prediction of squat in shallow water', *International Shipbuilding Progress*, vol. 39, no. 417, pp. 69-78.
- Millward, A. & Bevan, M.G. 1986, 'The behaviour of high speed ships forms when operating in water restricted by a solid boundary', *Trans. RINA*, vol. 128, pp. 189-204.
- McNown, J.S. 1976, 'Sinkage and resistance for ships in channels', *Journal of the Waterways, Harbours and Coastal Engineering Division*, pp. 287-298.

Naghdi, P., & Rubin, M. 1984, 'On the squat of a ship', *Journal of Ship Research*, vol. 28, no.2, pp. 107-117.

National Transportation Safety Board (NTSB) 1993, 'Grounding of the United Kingdom passenger vessel RMS Queen Elizabeth II near Cuttyhunk Island', Vineyard South, Massachusetts on August 7, 1992, *Marine Accident Report* PB93-916201, March 1993.

Newman, N.J. 1965, 'The force and moment on a slender body of revolution moving near a wall', *David Taylor Model Basin*, DTMB Report 2127.

Newman, J.N. 1972, 'Some theories for ship manoeuvring', *Proceedings of IUTAM/ITTC Symposium on Directional Stability and Control of Bodies in Water*, University College, London.

Norrbin, N.H. 1971, 'Theory and observations on the use of a mathematical model for ship manoeuvring in deep and confined waters', *Publications of the Swedish State Shipbuilding Experimental Tank*, Report no. 68, Goteborg, Sweden.

Norrbin, N.H. 1974, 'Bank effects on a ship moving through a short dredged channel', *Proceedings of 10th Symposium on Naval Hydrodynamics*, Office of Ship Research.

Norrbin, N.H. 1978, 'A method for the prediction of the manoeuvring lane of a ship in a channel of varying width', *Proceedings of Symposium: Aspects of Navigability of Constraint Waterways, Including Harbour Entrances*, vol. 3, Delft.

Norrbin, N.H. 1985, 'Bank clearance and optimal section shape for ship canals', *Proceedings of 26th International Navigation Congress*, Permanent International Association of Navigation Congresses (PIANC), Brussels, Belgium.

Pettersen, B. 1982, 'Calculation of potential flow about three-dimensional bodies in shallow water with particular application to ship manoeuvring', *Journal of Ship Research*, vol. 26, no. 3, pp. 149-165.

Plotkin, A. 1976a, 'The flow due to a slender ship moving over a wavy wall in shallow water', *Journal of Engineering Mathematics*, vol. 10, no. 3, pp. 207-218.

Plotkin, A. 1976b, 'Hydrodynamic pressure field on a slender ship moving over a high frequency wavy shallow bottom', *Journal of Applied Mechanics*, vol. 43, no. 2, pp. 232-236.

Queensland Transport 1996, 'Squat measurements in the Port of Cairns', *Transport Technology Division, Maritime Division*, Document no. R-007.

Renilson, M.R. & Hatch, T. 1998, 'A preliminary investigation into squat over an undulating bottom', *The Naval Architect*, February, pp. 36-37.

Renilson, M.R. & Munro, A. 1989, 'The effect of slope and angle on bank interaction', *The Naval Architect*, March, pp. E111-E112.

- Roseman, D.P. (ed.) 1987, *The MarAd systematic series of full form ship models*, Society of Naval Architects and Marine Engineers Publications.
- Schoenherr, K.E. 1960, 'Bank suction effects on merchant ship hulls in restricted waters', *David Taylor Model Basin*, DTMB Report 1461.
- Seren, D.B., Ferguson, A.M. & McGregor, R.C. 1981, 'Squat – an examination of two practical prediction methods', *The Naval Architect*, September, pp. E228-E230.
- Sharp, B.B. & Fenton, J. D. 1968, 'Report of investigation of a proposed dock at Yarraville', *University of Melbourne*.
- Soukhomel, G.I. & Zass, V.M. 1958, 'Abaissement du navire en marche', *Navires, Ports et Chantiers*, pp. 18-23.
- StatSoft™ 1994, *STATISTICA™ for windows (vol. I): General conventions & statistics I*, Software Manuals, StatSoft.
- Tornblom, O. 2000, Calculation of bank effects and wash waves with Shipflow, Master of Science Thesis, Department of Mechanical Engineering, Lulea University of Technology.
- Tothill, J.T. 1967, 'Ships in restricted channels - a correlation of model tests, field measurements, and theory', *Marine Technology*, pp. 111-128.
- Tuck, E.O. 1966, 'Shallow water flows past slender bodies', *Journal of Fluid Mechanics*, vol. 26, part 1, pp. 81-95.
- Tuck, E.O. 1967, 'Sinkage and trim in shallow water of finite width', *Schiffstechnik*, vol. 14, pp. 92-94.
- Tuck, E.O. & Taylor, P.J. 1970, 'Shallow-water problems in ship hydrodynamics', *Proceedings of 8th Symposium on Naval Hydrodynamics*, Washington DC, pp. 627-659.
- Tuck, E.O. & Newman, N.J. 1974, 'Hydrodynamic interactions between ships', *Proceedings of 10th Symposium on Naval Hydrodynamics*, Cambridge, pp. 35-38.
- Tuck, E.O. 1976, 'Some classical water-wave problems in varying depth', *Proceedings of IUTAM Symposium on Waves on Water of Varying Depth*, Australian Academy of Science, Canberra.
- United States Coast Guard (USCG) 1993, 'Grounding of the passenger liner Queen Elizabeth II near Cuttyhunk Island, Vineyard Sound, Massachusetts on August 7, 1992', *Marine Casualty Report*.
- Vantorre, M., 1995, 'Experimental study of bank effects of full form ship models', *Mini Symposium on Ship Manoeuvrability*, Fukuoka, Japan, pp. 85-102.
- Vermeer, H. 1977, 'The behaviour of a ship in restricted water', *International Shipbuilding Progress*, vol. 24.

Vugts, J.H. 1968, 'The hydrodynamic coefficients for swaying, heaving and rolling cylinders in a free surface', *Laboratorium voor Schepsboukunde*, Technische Hogeschool Delft, Report no. 194.

Xiong, X.M., Wu, X.H. 1996, 'A study on manoeuvring hydrodynamic forces acting on 3D ship hulls with free surface effect in restricted water', *International Shipbuilding Progress*, vol. 43, no. 433, pp. 48-69.

Yeung, R.W. & Tan, W.T. 1980, 'Hydrodynamic interactions of ships with fixed obstacles', *Journal of Ship Research*, vol. 24, no. 1, pp. 50-59.

Zhang, X. & Wu, X, 1998, 'Calculation of hydrodynamic forces of ships in restricted water', *Proceedings of 2nd Conference for New Ship & Marine Technology into the 21st Century*, Hong Kong, pp.93-101.

Appendix A

Australian Maritime College towing tank details

Model experiments were conducted using the towing tank facility situated on the Australian Maritime College campus in Launceston, Tasmania, Australia. The tank is 100m long by 3.5m wide and has a standard water depth of 1.5m. It is filled with fresh water at a temperature of approximately 17 degrees Centigrade. The building is well insulated from temperature changes and allows minimal natural light to avoid algal growth within the body of water.

Two carriages are available for use in the tank. One is motorised for towing tests and has onboard power and is fitted with a computer for data acquisition. The other carriage is unpowered and can be fitted with motion measuring equipment and stationed immediately over the model.

Appendix B

Ship model details

Three different hull forms were used in the study; two bulk carrier models and a containership model. The bulk carrier models were based on the L and F hull forms from the MarAd systematic series (Roseman 1987). The containership hull form was an S-175 containership (ITTC 1987). Body plans for each of the models are given in Figures B1 – B3. A propeller was fitted to the MarAd L series hull to investigate the influence of propulsion on vessel squat. The propeller model is shown in Figure B4.

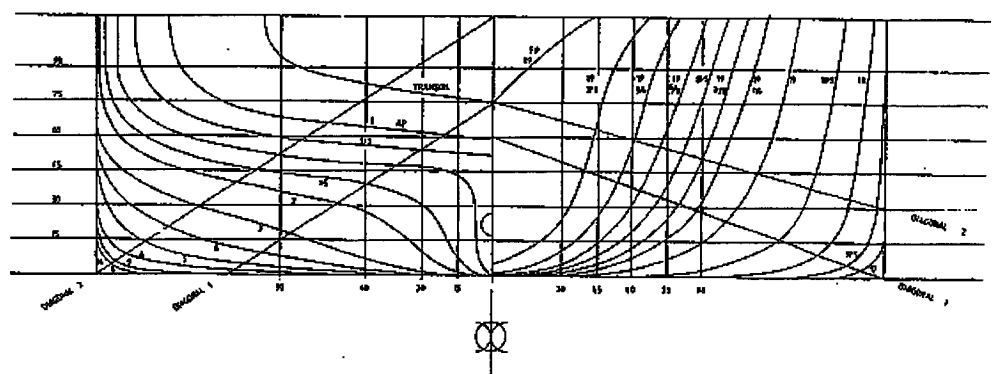


Figure B1 Body plan of MarAd L series model (Roseman 1987)

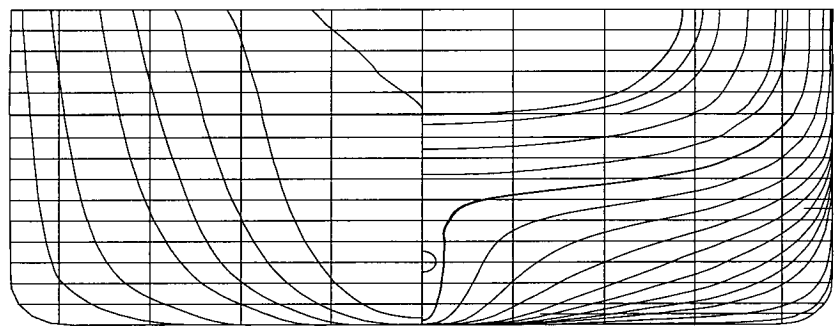


Figure B2 Body plan of MarAd F series model (Roseman 1987)

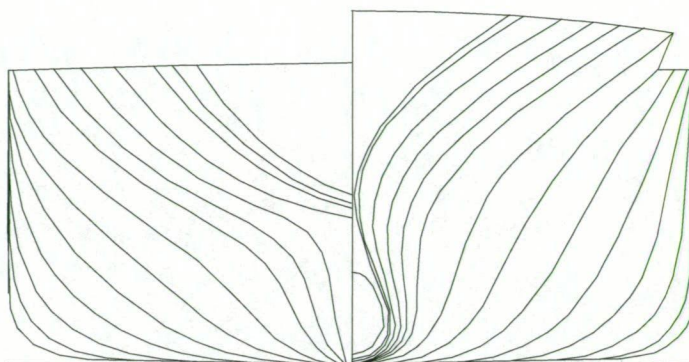


Figure B3 Body plan of S-175 containership (ITTC 1987)

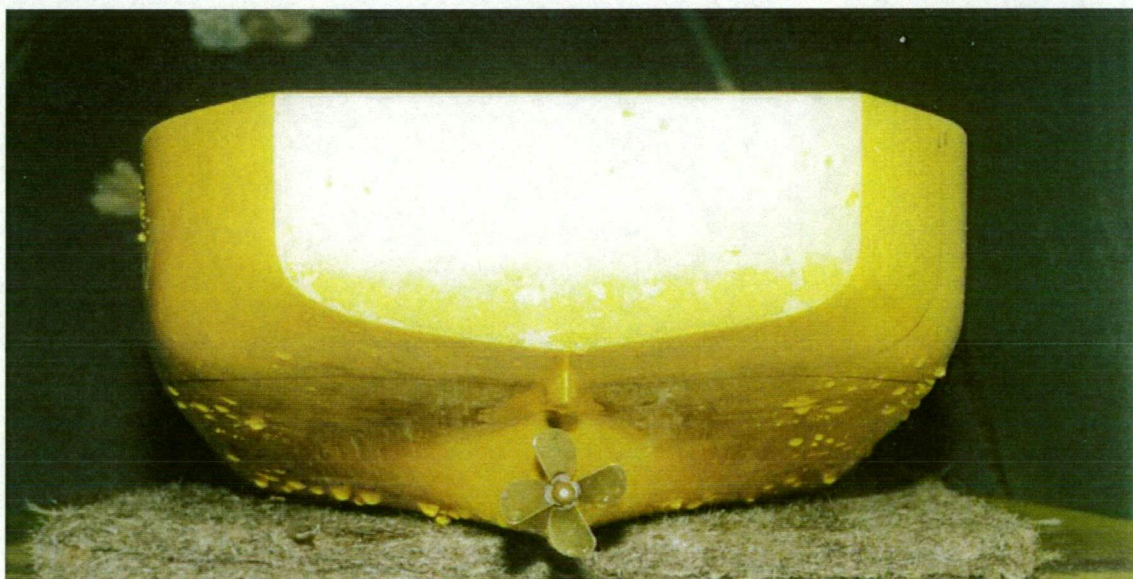


Figure B4 MarAd L series model with propeller fitted

Appendix C

Model bank set up

Squat

A series of physical model scale tests were conducted to measure the squat of a vessel in channels of varying width. Port and starboard vertical, surface piercing channel walls were constructed in the towing tank as shown in Figure C1. These walls were made from galvanised steel and were stiffened with Dexion supports. The bank was sealed along its length to prevent pressure leakage.



Figure C1 Channel walls constructed in towing tank for squat tests

Ship-bank interaction

Lateral banks were constructed on the port side of the AMC towing tank to investigate the effect of lateral bank geometry on ship-bank interaction. Both surface piercing and flooded bank geometries were modelled on the port side of the model.

The port surface piercing banks were constructed using the same walls that were used in the squat study. An example of a channel model for the ship-bank interaction study is given in Figure C2. The bank slope could be varied by adjusting the Dexion support frames.

The flooded banks were constructed from galvanized steel sheet and were supported by a matrix of blocks whose dimensions were varied to obtain different flooded bank heights. All flooded

banks extended laterally to the port wall of the towing tank, i.e. 1.75m from the tank centreline. An example of a flooded bank model is shown in Figure C3.

To prevent flow into the bank cavity, all banks were sealed at joins and intersections with the towing tank boundaries.

For the ship-bank interaction study the starboard bank was vertical, pierced the free surface and was located 1.75m from the centreline of the tank. This bank was not varied throughout the test program.



Figure C2 Photograph showing steel port wall set up in the towing tank

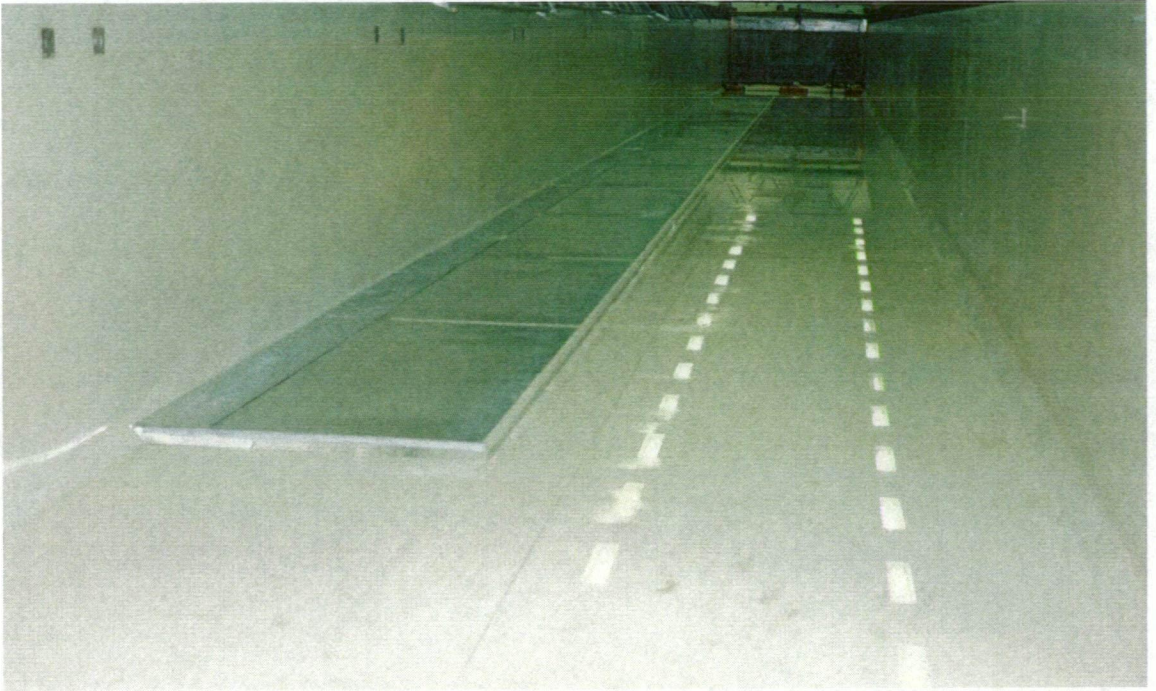


Figure C3 Flooded bank assembly prior to water fill

Appendix D

Uncertainty analysis

Measurement of vertical displacement

Vertical displacements were measured at the forward and aft posts. For these cases the midship and bow sinkage were calculated using Equations D1 and D2 respectively.

$$S_{\text{midships}} = \left(\left(\frac{Z_{\text{fwdpost}} - Z_{\text{aftpost}}}{X_{\text{posts}}} \right) \times X_{\text{aftmid}} \right) + Z_{\text{aftpost}} \quad (\text{D1})$$

$$S_{\text{bow}} = \left(\left(\frac{Z_{\text{fwdpost}} - Z_{\text{aftpost}}}{X_{\text{posts}}} \right) \times X_{\text{aftfp}} \right) + Z_{\text{aftpost}} \quad (\text{D2})$$

Where:

Z_{fwdpost} = sinkage measurement at the forward post.

Z_{aftpost} = sinkage measurement at the aft post.

X_{posts} = distance between forward and aft posts along the x axis.

X_{aftmid} = distance between aft post and midships along the x axis.

X_{aftfp} = distance between aft post and forward perpendicular along the x axis.

The midship and bow sinkage coefficients are given by Equations D3 and D4 respectively.

$$SC_{\text{midships}} = \frac{100 \cdot S_{\text{midships}}}{F_{\text{nh}}^2 L_{\text{pp}}} = \frac{100gh_1 (C_{\text{fwd}} V_{\text{fwd}} X_{\text{aftmid}} - C_{\text{aft}} V_{\text{aft}} X_{\text{aftmid}} + C_{\text{aft}} V_{\text{aft}} X_{\text{posts}})}{X_{\text{posts}} U^2 L_{\text{pp}}} \quad (\text{D3})$$

$$SC_{\text{bow}} = \frac{100 \cdot S_{\text{bow}}}{F_{\text{nh}}^2 L_{\text{pp}}} = \frac{100gh_1 (C_{\text{fwd}} V_{\text{fwd}} X_{\text{aftfp}} - C_{\text{aft}} V_{\text{aft}} X_{\text{aftfp}} + C_{\text{aft}} V_{\text{aft}} X_{\text{posts}})}{X_{\text{posts}} U^2 L_{\text{pp}}} \quad (\text{D4})$$

Where:

C_{fwd} = forward LVDT calibration factor.

V_{fwd} = forward LVDT voltage.

C_{aft} = aft LVDT calibration factor.

V_{aft} = aft LVDT voltage.

For estimation purposes it was assumed that the uncertainty on the forward and aft vertical displacement measurements arose from four sources: LVDT calibration factor; voltage measurement; water depth measurement and speed measurement. Appropriate uncertainty estimates for each of these sources were used to find the uncertainty in each vertical displacement measurement. In turn, these estimates were used to find the uncertainty on the midship sinkage and bow sinkage.

Uncertainty sources that were smaller than 1/4th or 1/5th of the largest sources were considered negligible (Longo and Stern 2005). Therefore the uncertainty due to the following parameters was considered negligible:

- Acceleration due to gravity.
- Accuracy of model geometry.
- Distance between forward and aft posts.
- Distance between aft post and midships.
- Distance between aft post and forward perpendicular.

The standard uncertainty in a typical midship sinkage and bow sinkage measurement is calculated using Equations D5 and D6 (Barlow *et al.* 1999).

$$\sigma_{sc_{midships}}^2 = \left(\frac{\partial sc_{midships}}{\partial C_{fwd}} \cdot \sigma_{C_{fwd}} \right)^2 + \left(\frac{\partial sc_{midships}}{\partial V_{fwd}} \cdot \sigma_{V_{fwd}} \right)^2 + \left(\frac{\partial sc_{midships}}{\partial C_{aft}} \cdot \sigma_{C_{aft}} \right)^2 + \left(\frac{\partial sc_{midships}}{\partial V_{aft}} \cdot \sigma_{V_{aft}} \right)^2 + \left(\frac{\partial sc_{midships}}{\partial h_1} \cdot \sigma_{h_1} \right)^2 + \left(\frac{\partial sc_{midships}}{\partial U} \cdot \sigma_U \right)^2 \quad (D5)$$

$$\sigma_{sc_{bow}}^2 = \left(\frac{\partial sc_{bow}}{\partial C_{fwd}} \cdot \sigma_{C_{fwd}} \right)^2 + \left(\frac{\partial sc_{bow}}{\partial V_{fwd}} \cdot \sigma_{V_{fwd}} \right)^2 + \left(\frac{\partial sc_{bow}}{\partial C_{aft}} \cdot \sigma_{C_{aft}} \right)^2 + \left(\frac{\partial sc_{bow}}{\partial V_{aft}} \cdot \sigma_{V_{aft}} \right)^2 + \left(\frac{\partial sc_{bow}}{\partial h_1} \cdot \sigma_{h_1} \right)^2 + \left(\frac{\partial sc_{bow}}{\partial U} \cdot \sigma_U \right)^2 \quad (D6)$$

Where:

$$\frac{\partial sc_{midships}}{\partial C_{fwd}} = \frac{100gh_1 V_{fwd} x_{aftmid}}{x_{posts} U^2 L_{PP}}$$

$$\frac{\partial sc_{midships}}{\partial V_{fwd}} = \frac{100gh_1 C_{fwd} x_{aftmid}}{x_{posts} U^2 L_{PP}}$$

$$\frac{\partial sc_{midships}}{\partial C_{aft}} = -\frac{100gh_1 V_{aft} x_{aftmid}}{x_{posts} U^2 L_{PP}}$$

$$\frac{\partial sc_{midships}}{\partial V_{aft}} = -\frac{100gh_1 C_{aft} x_{aftmid}}{x_{posts} U^2 L_{PP}} + \frac{100gh_1 C_{aft}}{U^2 L_{PP}}$$

$$\frac{\partial sc_{midships}}{\partial h_1} = \frac{100gC_{fwd} V_{fwd} x_{aftmid}}{x_{posts} U^2 L_{PP}} - \frac{100gC_{aft} V_{aft} x_{aftmid}}{x_{posts} U^2 L_{PP}} + \frac{100gC_{aft} V_{aft}}{U^2 L_{PP}}$$

$$\frac{\partial sc_{midships}}{\partial U} = -\frac{200gh_1 C_{fwd} V_{fwd} x_{aftmid}}{x_{posts} U^3 L_{PP}} + \frac{200gh_1 C_{aft} V_{aft} x_{aftmid}}{x_{posts} U^3 L_{PP}} - \frac{200gh_1 C_{aft} V_{aft}}{U^3 L_{PP}}$$

$$\frac{\partial sc_{\text{bow}}}{\partial C_{\text{fwd}}} = \frac{100gh_1 V_{\text{fwd}} x_{\text{aftfp}}}{x_{\text{posts}} U^2 L_{\text{PP}}}$$

$$\frac{\partial sc_{\text{bow}}}{\partial V_{\text{fwd}}} = \frac{100gh_1 C_{\text{fwd}} x_{\text{aftfp}}}{x_{\text{posts}} U^2 L_{\text{PP}}}$$

$$\frac{\partial sc_{\text{bow}}}{\partial C_{\text{aft}}} = -\frac{100gh_1 V_{\text{aft}} x_{\text{aftfp}}}{x_{\text{posts}} U^2 L_{\text{PP}}}$$

$$\frac{\partial sc_{\text{bow}}}{\partial V_{\text{aft}}} = -\frac{100gh_1 C_{\text{aft}} x_{\text{aftfp}}}{x_{\text{posts}} U^2 L_{\text{PP}}} + \frac{100gh_1 C_{\text{aft}}}{U^2 L_{\text{PP}}}$$

$$\frac{\partial sc_{\text{bow}}}{\partial h_1} = \frac{100gC_{\text{fwd}} V_{\text{fwd}} x_{\text{aftfp}}}{x_{\text{posts}} U^2 L_{\text{PP}}} - \frac{100gC_{\text{aft}} V_{\text{aft}} x_{\text{aftfp}}}{x_{\text{posts}} U^2 L_{\text{PP}}} + \frac{100gC_{\text{aft}} V_{\text{aft}}}{U^2 L_{\text{PP}}}$$

$$\frac{\partial sc_{\text{bow}}}{\partial U} = -\frac{200gh_1 C_{\text{fwd}} V_{\text{fwd}} x_{\text{aftfp}}}{x_{\text{posts}} U^3 L_{\text{PP}}} + \frac{200gh_1 C_{\text{aft}} V_{\text{aft}} x_{\text{aftfp}}}{x_{\text{posts}} U^3 L_{\text{PP}}} - \frac{200gh_1 C_{\text{aft}} V_{\text{aft}}}{U^3 L_{\text{PP}}}$$

Typical uncertainties for each variable are:

- $\sigma_{C_{\text{fwd}}} = 0.5\%$ of the calibration factor.
- $\sigma_{C_{\text{aft}}} = 0.5\%$ of the calibration factor.
- $\sigma_{V_{\text{fwd}}} = 3.94\text{mV}$, based on accuracy of the A/D board where typical range of measurement was 0 - 3.5V for the 4m model.
- $\sigma_{V_{\text{aft}}} = 3.94\text{mV}$, based on accuracy of the A/D board where typical range of measurement was 0 - 3.5V for the 4m model.
- $\sigma_{V_{\text{fwd}}} = 2.00\text{mV}$, based on accuracy of the A/D board where typical range of measurement was approximately 0 - 2V for the 2m model.
- $\sigma_{V_{\text{aft}}} = 2.00\text{mV}$, based on accuracy of the A/D board where typical range of measurement was approximately 0 - 2V for 2m model.
- $\sigma_h = 0.005\text{m}$.
- $\sigma_U = 0.01\text{m/s}$.

Other examples of error sources include friction in the bearings and post bending due to loads exerted by the models.

Measurement of sway force and yaw moment

It was assumed that the uncertainty of the forward and aft sway force measurements were due to five sources; voltage measurement, speed measurement, force calibration factor, vessel draught, and water density. Appropriate uncertainty estimates for each of these sources were used to find the uncertainty in each sway force and yaw moment measurement.

The non-dimensional sway force and yaw moment are given by;

$$100Y' = \frac{100.V_{fwd}.C_{fwd}}{\frac{1}{2}.\rho.U^2.L_{pp}.d} + \frac{100.V_{aft}.C_{aft}}{\frac{1}{2}.\rho.U^2.L_{pp}.d} \quad (D7)$$

$$100N' = \frac{100.V_{fwd}.C_{fwd}.x_{fwdmid}}{\frac{1}{2}.\rho.U^2.L_{pp}^2.d} - \frac{100.V_{aft}.C_{aft}.x_{aftmid}}{\frac{1}{2}.\rho.U^2.L_{pp}^2.d} \quad (D8)$$

Where:

C_{fwd} = forward force transducer calibration factor.

V_{fwd} = forward force transducer voltage.

C_{aft} = aft force transducer calibration factor.

V_{aft} = aft force transducer voltage.

x_{fwdmid} = distance between midships and the forward post.

x_{aftmid} = distance between midships and the aft post.

Uncertainty sources that were smaller than 1/4th or 1/5th of the largest sources were considered negligible (Longo and Stern 2005). Therefore the uncertainty due to the following parameters was considered negligible:

- Accuracy of model geometry.
- Acceleration due to gravity.
- Distance between midships and forward post.
- Distance between midships and aft post.

The standard uncertainty in a typical sway force and yaw moment measurement was calculated using Equations D9 and D10 (Barlow *et al.* 1999).

$$\begin{aligned} \sigma^2_{100Y'} = & \left(\frac{\partial 100Y'}{\partial V_{fwd}} . \sigma_{V_{fwd}} \right)^2 + \left(\frac{\partial 100Y'}{\partial V_{aft}} . \sigma_{V_{aft}} \right)^2 + \left(\frac{\partial 100Y'}{\partial C_{fwd}} . \sigma_{C_{fwd}} \right)^2 + \left(\frac{\partial 100Y'}{\partial C_{aft}} . \sigma_{C_{aft}} \right)^2 \\ & + \left(\frac{\partial 100Y'}{\partial \rho} . \sigma_{\rho} \right)^2 + \left(\frac{\partial 100Y'}{\partial U} . \sigma_U \right)^2 + \left(\frac{\partial 100Y'}{\partial d} . \sigma_d \right)^2 \end{aligned} \quad (D9)$$

$$\begin{aligned} \sigma^2_{100N'} = & \left(\frac{\partial 100N'}{\partial V_{fwd}} . \sigma_{V_{fwd}} \right)^2 + \left(\frac{\partial 100N'}{\partial V_{aft}} . \sigma_{V_{aft}} \right)^2 + \left(\frac{\partial 100N'}{\partial C_{fwd}} . \sigma_{C_{fwd}} \right)^2 + \left(\frac{\partial 100N'}{\partial C_{aft}} . \sigma_{C_{aft}} \right)^2 \\ & + \left(\frac{\partial 100N'}{\partial \rho} . \sigma_{\rho} \right)^2 + \left(\frac{\partial 100N'}{\partial U} . \sigma_U \right)^2 + \left(\frac{\partial 100N'}{\partial d} . \sigma_d \right)^2 \end{aligned} \quad (D10)$$

Where;

$$\frac{\partial 100Y'}{\partial V_{fwd}} = \frac{100.C_{fwd}}{\frac{1}{2}.\rho.U^2.L_{pp}.d}$$

$$\begin{aligned}
\frac{\partial 100Y'}{\partial V_{\text{aft}}} &= \frac{100.C_{\text{aft}}}{\frac{1}{2} \cdot \rho \cdot U^2 \cdot L_{\text{PP}} \cdot d} \\
\frac{\partial 100Y'}{\partial C_{\text{fwd}}} &= \frac{100.V_{\text{fwd}}}{\frac{1}{2} \cdot \rho \cdot U^2 \cdot L_{\text{PP}} \cdot d} \\
\frac{\partial 100Y'}{\partial C_{\text{aft}}} &= \frac{100.V_{\text{aft}}}{\frac{1}{2} \cdot \rho \cdot U^2 \cdot L_{\text{PP}} \cdot d} \\
\frac{\partial 100Y'}{\partial \rho} &= -\frac{100.V_{\text{fwd}} \cdot C_{\text{fwd}}}{\frac{1}{2} \cdot \rho^2 \cdot U^2 \cdot L_{\text{PP}} \cdot d} - \frac{100.V_{\text{aft}} \cdot C_{\text{aft}}}{\frac{1}{2} \cdot \rho^2 \cdot U^2 \cdot L_{\text{PP}} \cdot d} \\
\frac{\partial 100Y'}{\partial U} &= -\frac{200.V_{\text{fwd}} \cdot C_{\text{fwd}}}{\frac{1}{2} \cdot \rho \cdot U^3 \cdot L_{\text{PP}} \cdot d} - \frac{200.V_{\text{aft}} \cdot C_{\text{aft}}}{\frac{1}{2} \cdot \rho \cdot U^3 \cdot L_{\text{PP}} \cdot d} \\
\frac{\partial 100Y'}{\partial d} &= -\frac{100.V_{\text{fwd}} \cdot C_{\text{fwd}}}{\frac{1}{2} \cdot \rho \cdot U^2 \cdot L_{\text{PP}} \cdot d^2} - \frac{100.V_{\text{aft}} \cdot C_{\text{aft}}}{\frac{1}{2} \cdot \rho \cdot U^2 \cdot L_{\text{PP}} \cdot d^2}
\end{aligned}$$

$$\begin{aligned}
\frac{\partial 100N'}{\partial V_{\text{fwd}}} &= \frac{100.C_{\text{fwd}} \cdot x_{\text{fwdmid}}}{\frac{1}{2} \cdot \rho \cdot U^2 \cdot L_{\text{PP}}^2 \cdot d} \\
\frac{\partial 100N'}{\partial V_{\text{aft}}} &= -\frac{100.C_{\text{aft}} \cdot x_{\text{aftmid}}}{\frac{1}{2} \cdot \rho \cdot U^2 \cdot L_{\text{PP}}^2 \cdot d} \\
\frac{\partial 100N'}{\partial C_{\text{fwd}}} &= \frac{100.V_{\text{fwd}} \cdot x_{\text{fwdmid}}}{\frac{1}{2} \cdot \rho \cdot U^2 \cdot L_{\text{PP}}^2 \cdot d} \\
\frac{\partial 100N'}{\partial C_{\text{aft}}} &= -\frac{100.V_{\text{aft}} \cdot x_{\text{aftmid}}}{\frac{1}{2} \cdot \rho \cdot U^2 \cdot L_{\text{PP}}^2 \cdot d} \\
\frac{\partial 100N'}{\partial \rho} &= -\frac{100.V_{\text{fwd}} \cdot C_{\text{fwd}} \cdot x_{\text{fwdmid}}}{\frac{1}{2} \cdot \rho^2 \cdot U^2 \cdot L_{\text{PP}}^2 \cdot d} + \frac{100.V_{\text{aft}} \cdot C_{\text{aft}} \cdot x_{\text{aftmid}}}{\frac{1}{2} \cdot \rho^2 \cdot U^2 \cdot L_{\text{PP}}^2 \cdot d} \\
\frac{\partial 100N'}{\partial U} &= -\frac{200.V_{\text{fwd}} \cdot C_{\text{fwd}} \cdot x_{\text{fwdmid}}}{\frac{1}{2} \cdot \rho \cdot U^3 \cdot L_{\text{PP}}^2 \cdot d} + \frac{200.V_{\text{aft}} \cdot C_{\text{aft}} \cdot x_{\text{aftmid}}}{\frac{1}{2} \cdot \rho \cdot U^3 \cdot L_{\text{PP}}^2 \cdot d} \\
\frac{\partial 100N'}{\partial d} &= -\frac{100.V_{\text{fwd}} \cdot C_{\text{fwd}} \cdot x_{\text{fwdmid}}}{\frac{1}{2} \cdot \rho \cdot U^2 \cdot L_{\text{PP}}^2 \cdot d^2} + \frac{100.V_{\text{aft}} \cdot C_{\text{aft}} \cdot x_{\text{aftmid}}}{\frac{1}{2} \cdot \rho \cdot U^2 \cdot L_{\text{PP}}^2 \cdot d^2}
\end{aligned}$$

Typical uncertainties for each variable are:

- $\sigma_{V_{\text{fwd}}} = 3.45\text{mV}$, based on accuracy of the A/D board where typical range of measurement was approximately 0 - 5V.

- $\sigma_{V_{aft}} = 3.45\text{mV}$, based on accuracy of the A/D board where typical range of measurement was approximately 0 – 5V.
- $\sigma_{C_{fwd}} = 0.5\%$ of the forward calibration factor.
- $\sigma_{C_{aft}} = 0.5\%$ of the aft calibration factor.
- $\sigma_{\rho} = 2\text{kg/m}^3$ for water density variations due to temperature.
- $\sigma_U = 0.01\text{m/s}$.
- $\sigma_d = 0.002\text{m}$.

Appendix E

Comparison between sway force and yaw moment measurements from the present study and Ch'ng (1991)

Ch'ng (1991) conducted model scale experiments to measure the sway force and yaw moment experienced by a ship model due to surface piercing banks. A selection of Ch'ng's tests was repeated to assess if they could be used to complement the data matrix in the present study. In this section a selection of results from the present study are compared to those measured by Ch'ng and the correlation is briefly discussed.

Non-dimensional sway force and yaw moment are compared for a case with a ship model travelling off the centreline of a channel with vertical surface piercing banks in Figures E1 – E4. In Figures E1 and E2 non-dimensional sway force and yaw moment are presented as a function of length Froude number for a draught to under keel clearance ratio of 5.13, whilst the non-dimensional sway force and yaw moment results in Figures E3 and E4 correspond to a draught to under keel clearance ratio of 2.00. As can be seen from Figures E1 and E2 the correlation between Ch'ng's results and those from the present study is poor at a draught to under keel clearance ratio of 5.13. At this draught to under keel clearance ratio Ch'ng measured a sway force away from the near bank, whilst, in the same length Froude number range, a sway force towards the near bank was measured in the present study. The non-dimensional yaw moment measured in the present study at a draught to under keel clearance ratio of 5.13 is less than that measured by Ch'ng. Vantorre (1995) found similar differences when comparing measurements on a bulk carrier with predictions from regression equations developed by Ch'ng. Generally, it was found that the correlation between Ch'ng's results and those from the present study improved at low draught to under keel clearance ratios. This is illustrated by comparing Figure E1 with Figure E3 and Figure E2 with Figure E4. This may be due to the fact that the AMC towing tank floor had greater variation in surface flatness when Ch'ng conducted testing.

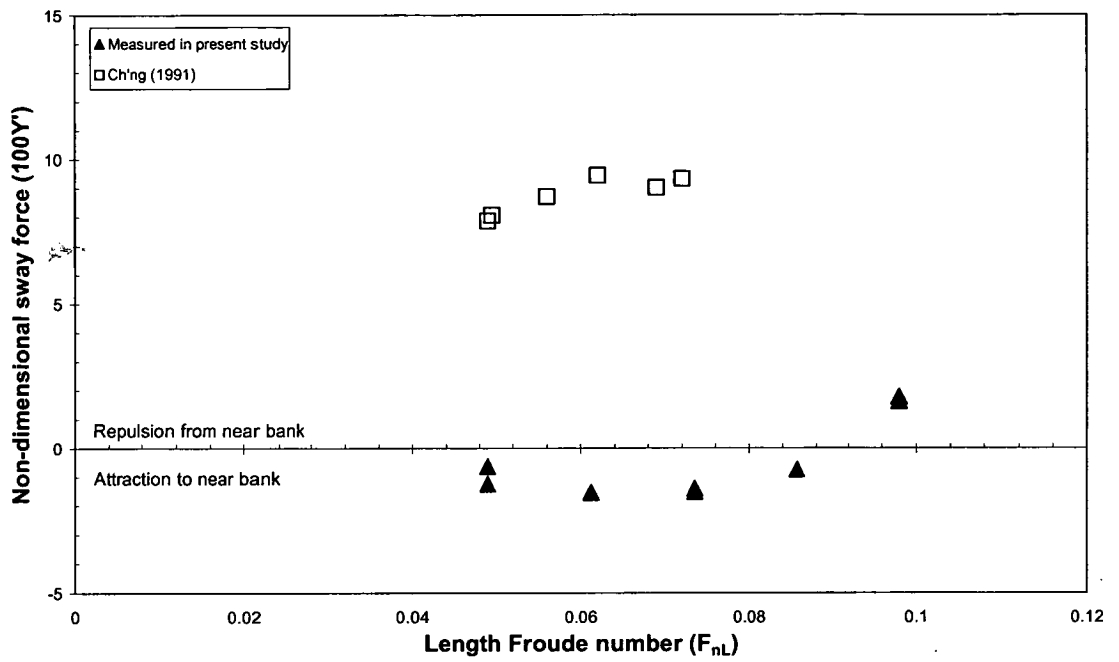


Figure E1 Non-dimensional sway force as a function of F_{nL} , $y_{Bt}=-0.629$, $d/(h_1-d)=5.13$, $1-(h_{2p}/h_1)=1.00$, $1-(h_{2s}/h_1)=1.00$, $\alpha_p=90^\circ$, $\alpha_s=90^\circ$, MarAd L

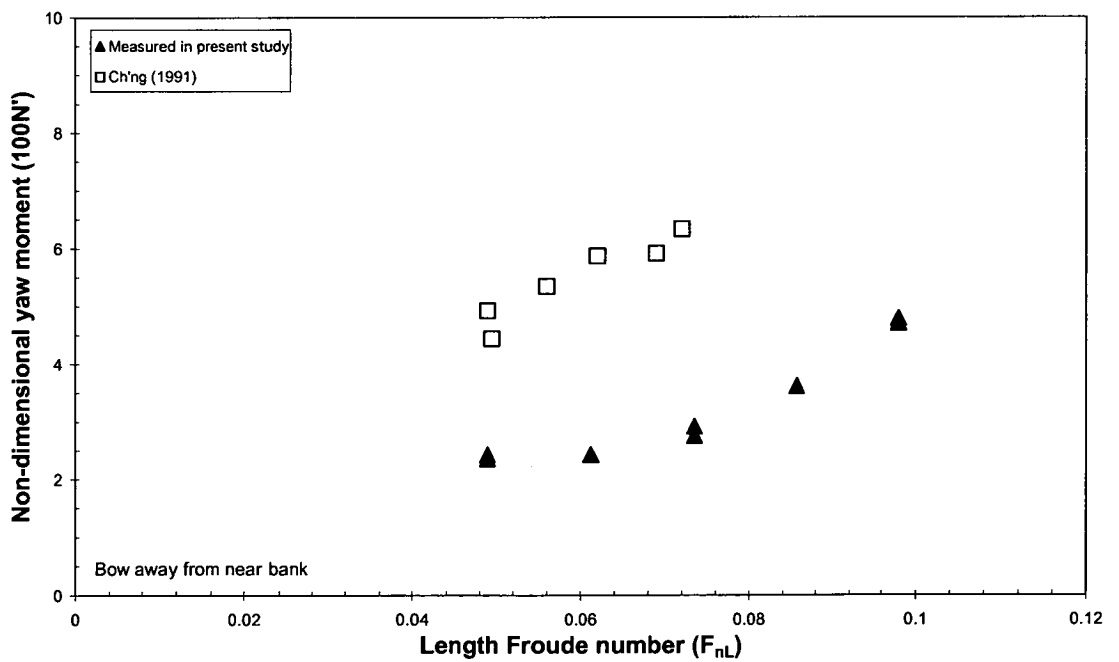


Figure E2 Non-dimensional yaw moment as a function of F_{nL} , $y_{Bt}=-0.629$, $d/(h_1-d)=5.13$, $1-(h_{2p}/h_1)=1.00$, $1-(h_{2s}/h_1)=1.00$, $\alpha_p=90^\circ$, $\alpha_s=90^\circ$, MarAd L

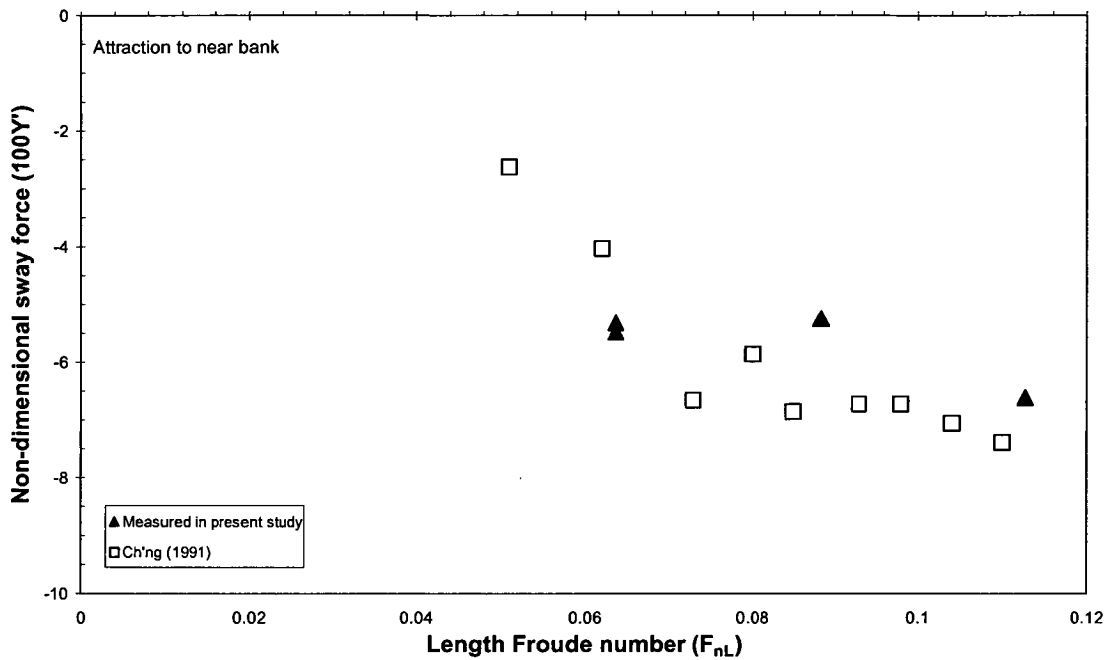


Figure E3 Non-dimensional sway force as a function of F_{nL} , $y_{Bt}=-0.629$, $d/(h_1-d)=2.00$, $1-(h_{2p}/h_1)=1.00$, $1-(h_{2s}/h_1)=1.00$, $\alpha_p=90^\circ$, $\alpha_s=90^\circ$, MarAd L

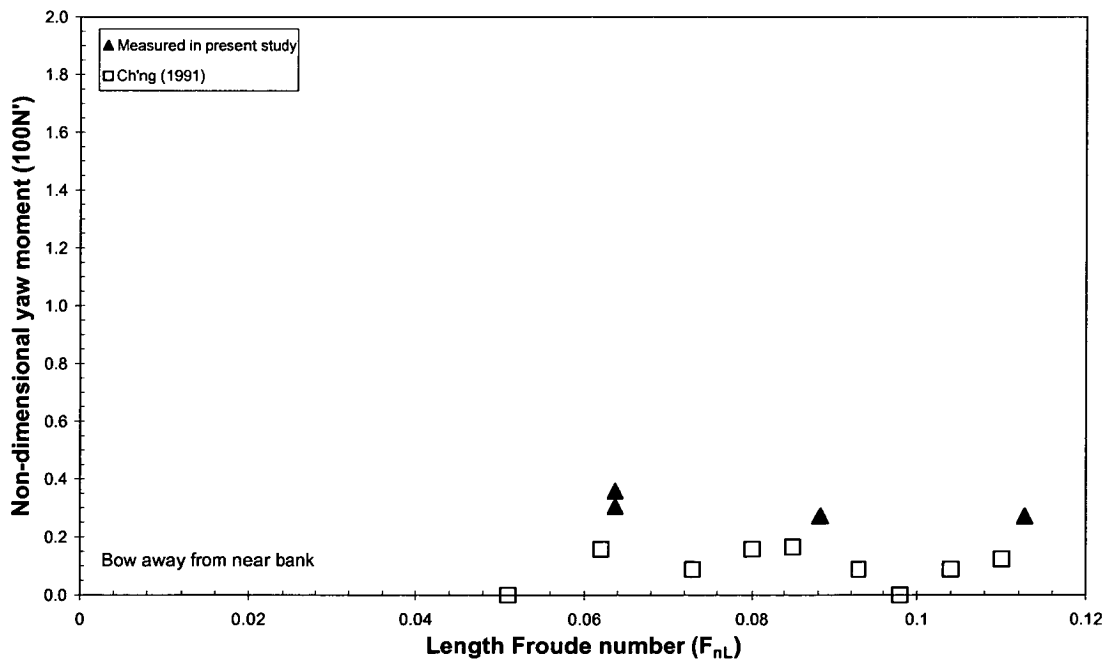


Figure E4 Non-dimensional yaw moment as a function of F_{nL} , $y_{Bt}=-0.629$, $d/(h_1-d)=2.00$, $1-(h_{2p}/h_1)=1.00$, $1-(h_{2s}/h_1)=1.00$, $\alpha_p=90^\circ$, $\alpha_s=90^\circ$, MarAd L